GEORGIA INSTITUTE OF TECHNOLOGY
OFFICE OF CONTRACT ADMINISTRATION
SPONSORED PROJECT INITIATION

Date: July 29, 1976

Project Title: Submillimeter Wave Spectroscopy and Technology

Project No: A-1861

Project Director: Dr. M. D. Blue/Mr. James J. Gallagher, Co-Principal Investigators

Sponsor: U.S. Army Research Office; Research Triangle Park, N.C. 27709

Agreement Period: From June 15, 1976 Until June 14, 1979 (Grant Period)

Type Agreement: Grant No. DAAG29-76-G-0280

Amount: $226,653 ARO ($75,551 for first funding increment)
12,372 GIT Cost Sharing ($3,925 for first funding increment)
$239,025 Total ($79,476 for first funding increment)

Reports Required: Progress Reports; Interim Technical; Reprint; Final Technical

Sponsor Contact Person (s):

Technical Matters

U.S. Army Research Office
Attention: Physics Division
P.O. Box 12211
Research Triangle Park, North Carolina 27709

Contractual Matters
(thru OCA)

U. S. Army Research Office
Attn: DRXRO-PR (Jack L. Harless)
P.O. Box 12211
Research Triangle Park, N.C. 27709

Property Admin. & Closeout only:
ONR Resident Representative
325 Hinman Research Building
Campus

Defense Priority Rating: None

Assigned to: Electromagnetics (School/Laboratory)

COPIES TO:

Project Director
Division Chief (EES)
School/Laboratory Director
Dean/Director—EES
Accounting Office
Procurement Office
Security Coordinator (OCA)
Reports Coordinator (OCA)

Library, Technical Reports Section
Office of Computing Services
Director, Physical Plant
EES Information Office
Project File (OCA)
Project Code (GTRI)
Other

3 (3/76)

GEORGIA INSTITUTE OF TECHNOLOGY
OFFICE OF CONTRACT ADMINISTRATION

SPONSORED PROJECT TERMINATION

Date: 12/11/79

Project Title: Submillimeter Wave Spectroscopy and Technology

Project No: A-1861

Project Director: Blue/Gallagher

Sponsor: U.S. Army

Effective Termination Date: 6/14/79

Clearance of Accounting Charges: 6/14/79

Grant/Contract Closeout Actions Remaining:

- X Final Invoice and Closing Documents
- X Final Fiscal Report
- X Final Report of Inventions
- X Govt. Property Inventory & Related Certificate
- __ Classified Material Certificate
- __ Other _____

Assigned to: EML/EOD (School/Laboratory)

COPIES TO:

Project Director
Division Chief (EES)
School/Laboratory Director
Dean/Director–EES
Accounting Office
Procurement Office
Security Coordinator (OCA)
Reports Coordinator (OCA)

Library, Technical Reports Section
EES Information Office
Project File (OCA)
Project Code (GTRI)
Other _____

CA–4 (1/79)

SUBMILLIMETER WAVE SPECTROSCOPY AND TECHNOLOGY FIRST SEMI-ANNUAL TECHNICAL REPORT

J. J. Gallagher
M. D. Blue

February 4, 1977

U.S. ARMY RESEARCH OFFICE

Grant No. DAAG29-76-G-0280

Electromagnetics Laboratory
Engineering Experiment Station
Georgia Institute of Technology
Atlanta, Georgia 30332

SECURITY CLASSIFICATION OF THIS PAGE (When Data Entered)

REPORT DOCUMENTATION PAGE

READ INSTRUCTIONS BEFORE COMPLETING FORM

1. REPORT NUMBER: First Semi-Annual Technical	2. GOVT ACCESSION NO.
3. RECIPIENT'S CATALOG NUMBER	
4. TITLE (and Subtitle): Submillimeter Wave Spectroscopy and Technology	5. TYPE OF REPORT & PERIOD COVERED: Semi-Annual, June 15 - Dec. 31, 1976
	6. PERFORMING ORG. REPORT NUMBER
7. AUTHOR(s): J. J. Gallagher & M. D. Blue	8. CONTRACT OR GRANT NUMBER(s): DAAG29-76-G-0280
9. PERFORMING ORGANIZATION NAME AND ADDRESS: Engineering Experiment Station, Georgia Institute of Technology, Atlanta, Georgia 30332	10. PROGRAM ELEMENT, PROJECT, TASK AREA & WORK UNIT NUMBERS
11. CONTROLLING OFFICE NAME AND ADDRESS: U. S. Army Research Office, Post Office Box 12211, Research Triangle Park, NC 27709	12. REPORT DATE: February 4, 1977
	13. NUMBER OF PAGES: 10
14. MONITORING AGENCY NAME & ADDRESS (if different from Controlling Office)	15. SECURITY CLASS. (of this report): Unclassified
	15a. DECLASSIFICATION/DOWNGRADING SCHEDULE: NA

16. DISTRIBUTION STATEMENT (of this Report)

Approved for public release; distribution unlimited.

17. DISTRIBUTION STATEMENT (of the abstract entered in Block 20, if different from Report)

NA

18. SUPPLEMENTARY NOTES

The findings in this report are not to be construed as an official Department of the Army position, unless so designated by other authorized documents.

19. KEY WORDS (Continue on reverse side if necessary and identify by block number)

Submillimeter Waves; Schottky Barrier Diodes; Spectroscopy; Water Molecules; Fabry-Perot Interferometers; Electron Beam Sources Heterodyne Receivers; Atmospheric Absorption.

20. ABSTRACT (Continue on reverse side if necessary and identify by block number)

Spectroscopic investigations in waveguide cells and Fabry-Perot interferometers have been started on the water molecule. Pressure broadening, line width parameters and dipole moments are phenomena currently being studied. Reflectivity measurements have been performed on natural and man-made materials in the wavelength region from 0.050 millimeters to 0.500 millimeters. Receiver work has been initialed on superheterodyne receivers with Schottky barrier mixers. Gyroton studies are beginning.

DD FORM 1 JAN 73 1473 EDITION OF 1 NOV 65 IS OBSOLETE

Unclassified

SECURITY CLASSIFICATION OF THIS PAGE (When Data Entered)

PROGRESS REPORT

1. ARO PROPOSAL NUMBER: P-14104-PX

2. PERIOD COVERED BY REPORT: 15 June, 1976 - 31 December, 1976

3. TITLE OF PROPOSAL: Submillimeter Wave Spectroscopy and Technology

4. CONTRACT OR GRANT NUMBER: DAAG29-76-G-0280

5. NAME OF INSTITUTION: Engineering Experiment Station, Georgia Institute of Technology

6. AUTHOR(S) OF REPORT: J. J. Gallagher, M. D. Blue

7. LIST OF MANUSCRIPTS SUBMITTED OR PUBLISHED UNDER ARO SPONSORSHIP DURING THIS PERIOD, INCLUDING JOURNAL REFERENCES: See attached list of Papers Presented at Second International Conference and Winter School on Submillimeter Waves and Their Applications, Dec. 6-11, 1976, San Juan, Puerto Rico.

8. SCIENTIFIC PERSONNEL SUPPORTED BY THIS PROJECT AND DEGREES AWARDED DURING THIS REPORTING PERIOD:
   J. J. Gallagher
   M. D. Blue
   R. W. McMillan
   J. H. Rainwater
   P. B. Reinhart
   A. M. Cook, Student
   C. H. Branch, Student
   N. K. O'Rourke, Student
   J. A. Keahey, Student
   W. M. Penn, Student

14104F

DR. M. D. BLUE
MR. JAMES J. GALLAGHER
GEORGIA INSTITUTE OF TECHNOLOGY
ENGINEERING EXPERIMENT STATION
ATLANTA, GA 30332

BRIEF OUTLINE OF RESEARCH FINDINGS

During the first six months of this grant, spectroscopic measurements of atmospheric constituents have been initiated. These measurements are being performed in a waveguide cell to obtain data on the linewidth parameter of molecules and in a semi-confocal Fabry-Perot interferometer to obtain data in the the transmission windows of atmospheric water vapor. Procedures have been established to compute the line shape of individual molecules with theoretical line shapes. During this initial period, computer programs have been prepared to compare experimental line shapes with theoretical line shapes. The program can employ one or more lines for computation of pressure broadening effects. For transmission in the atmospheric windows, computer programs have been prepared to use 16 or more lines up to the total tabulated by AFCRL.

Papers have been presented at the San Juan Submillimeter Wave Conference on the spectroscopic studies.

Submillimeter receiver work has been started during this initial 6-months. Observations have been performed with an optically-pumped laser as local oscillator. Severe local oscillator power limitations have been experienced in attempts to achieve good receiver sensitivity. Work is currently under way to improve the local oscillator output power. Quasi-optical techniques for coupling local oscillator and input signals to the receiver are being developed. Open structure mixers and Fabry-Perot resonator schemes are being employed to improve coupling mechanisms. Subharmonic mixing which can provide improvement in noise over fundamental mixing is being investigated. This technique allows the use of low frequency klystrons as local oscillators.

Reflectivity measurements have been performed on materials of importance to background clutter in military systems. These preliminary measurements, using a Fourier spectrometer, will be continued and extended to longer wavelengths.

A bibliography has been assembled on relativistic electron beam sources. Design of a small gyrotron is now being started.

Abstracts of papers presented at the Second International Conference and Winter School on Submillimeter Waves and Their Applications are listed below.

Papers Presented at Second International Conference and Winter School on Submillimeter Waves and Their Applications, December 6-11, 1976, San Juan, Puerto Rico.

1. G. T. Wrixon and M. D. Blue, "Materials for Low Noise Schottky-Barrier Converters at Submillimeter Wavelengths," Paper Tu-2-3.

2. R. W. McMillan, J. J. Gallagher and G. T. Wrixon, "Fabry-Perot Spectroscopy of the Water Molecule in Submillimeter Atmospheric Windows," Paper W-1-3.

3. R. W. McMillan, J. J. Gallagher and A. M. Cook, "Calculations of Antenna Temperature and Horizontal Path Attenuation Due to the 320 GHz Absorption Line of Water Vapor," Paper W-1-6.

4. B. Bean, S. Perkowitz, M. D. Blue and J. J. Gallagher, "Characteristics of a Submillimeter Optically Pumped Laser-Receiver System," Paper Th-4-6.

5. J. J. Gallagher, W. M. Penn and G. T. Wrixon, "Submillimeter Pressure Broadening Measurements," Paper F-1-3.

6. M. D. Blue and S. Perkowitz, "Reflectivity of Common Materials in the Submillimeter Region," Paper S-3-4.

7. R. W. McMillan, R. G. Shackelford, M. D. Blue and J. J. Gallagher, "Submillimeter Wave Propagation Studies - A Comparison with Other Spectral Regions," Paper S-3-5.

Papers 3 and 6 have been submitted and accepted for publication in a Conference issue of the June Transactions of the S-MTT.

Related papers presented by EES/Georgia Tech Staff but not sponsored by ARO:

1. J. J. Gallagher and W. M. Penn, "Extension of Electric Resonance Spectroscopy to the Submillimeter Wavelength Region," Paper F-1-6.

2. R. E. Cupp and J. J. Gallagher, "Stark Measurements of H_2S in the Millimeter/Submillimeter Wavelength Region," Paper F-1-9.

3. G. T. Wrixon (consultant), "Submillimeter Mixers," Paper Th-4-1.

4. R. W. McMillan and J. B. Langley, "Analysis of Submillimeter Wave Fabry-Perot Interferometers Made of Four Wire Grids," Paper Tu-1-6.

5. R. W. McMillan, R. G. Shackelford and J. J. Gallagher, "Application of Submillimeter Wave Techniques to Isotope Separation," Paper M-2-4.

SUBMILLIMETER WAVE PROPAGATION STUDIES - A COMPARISON WITH OTHER SPECTRAL REGIONS

R. W. McMillan, R. G. Shackelford
M. D. Blue and J. J. Gallagher
Georgia Institute of Technology
Atlanta, Georgia

Simultaneous propagation measurements at visible, IR, submm and mm wavelengths provide important information for operation in inclement weather. A program performing these measurements and the meteorologically instrumented range which is used are described. Initial measurement results are presented.

FABRY-PEROT SPECTROSCOPY OF THE WATER MOLECULE IN SUBMILLIMETER ATMOSPHERIC WINDOWS

R. W. McMillan and J. J. Gallagher
Georgia Institute of Technology
Atlanta, Georgia

and

G. T. Wrixon
University College
Cork, Ireland

A description is given of measurements being performed on water molecule in the submillimeter atmospheric transmission windows at 0.75 mm, 0.85 mm and 1.3 mm by the use of a high Q Fabry-Perot interferometer. Comparison is made with theory and existing related measurements.

STARK MEASUREMENTS OF H_2S IN THE MILLIMETER/SUBMILLIMETER WAVELENGTH REGION

R. E. Cupp
Atmospheric Spectroscopy Laboratory
National Oceanic and Atmospheric Administration
Boulder, Colorado

and

J. J. Gallagher
Georgia Institute of Technology
Atlanta, Georgia

A parallel plate Stark cell has been used for measurements on millimeter and submillimeter wave transitions of the hydrogen sulfide molecule. With this cell and phase locked sources, high precision values for molecular dipole moments are achieved.

EXTENSION OF ELECTRIC RESONANCE SPECTROSCOPY TO THE SUBMILLIMETER WAVELENGTH REGION

J. J. Gallagher
and
W. M. Penn
Georgia Institute of Technology
Atlanta, Georgia

The requirements for the performance of molecular beam electric resonance experiments at wavelengths shorter than one millimeter are discussed. Examples relevant to current experiments are presented, and comparisons made with millimeter and near IR experiments.

CHARACTERISTICS OF A SUBMILLIMETER OPTICALLY PUMPED LASER-RECEIVER SYSTEM

B. Bean and S. Perkowitz
Emory University
Atlanta, Georgia

and

M. D. Blue and J. J. Gallagher
Georgia Institute of Technology
Atlanta, Georgia

The characteristics of a superheterodyne receiver with an optically pumped laser local oscillator and Schottky barrier diode mixer are presented. Noise figure measurements for receivers in the 0.5 mm wavelength region and comparison with klystron harmonical mixer receivers are discussed.

APPLICATION OF SUBMILLIMETER WAVE TECHNIQUES TO ISOTOPE SEPARATION

R. W. McMillan, R. G. Shackelford
and J. J. Gallagher
Georgia Institute of Technology
Atlanta, Georgia

Techniques for the use of high energy submillimeter oscillators in isotope separation experiments are discussed. Frequency up-conversion of submillimeter signals to the spectral regions of interest by resonance enhanced mixing in molecular gases is described.

CALCULATIONS OF ANTENNA TEMPERATURE AND HORIZONTAL PATH ATTENUATION DUE TO THE 320 GHz ABSORPTION LINE OF WATER VAPOR

R. W. McMillan
J. J. Gallagher
A. M. Cook

Engineering Experiment Station
Georgia Institute of Technology
Atlanta, Georgia 30332

Abstract

The results of calculations of antenna temperatures due to emission, and due to the sun as a source, for the 320 GHz line of water vapor are given, along with results of horizontal path attenuation calculations.

ANALYSIS OF SUBMILLIMETER WAVE FABRY-PEROT INTERFEROMETERS MADE OF FOUR WIRE GRIDS

R. W. McMillan
J. B. Langley

Engineering Experiment Station
Georgia Institute of Technology
Atlanta, Georgia 30332

Abstract

Matrix equations for phase and polarization dependent transmission and reflection of microwaves of arbitrary polarization by Fabry-Perot interferometers, made of two identical pairs of wire grids, oriented at arbitrary angles, are derived.

SUBMILLIMETER PRESSURE BROADENING MEASUREMENTS

J. J. Gallagher
W. M. Penn
Georgia Institute of Technology
Atlanta, Georgia

and

G. T. Wrixon
University College
Cork, Ireland

Abstract

Pressure broadening measurements on symmetric, asymmetric, and linear polyatomic molecules in the 0.5-1.0 mm wavelength region are described. Both self-broadening and foreign gas broadening effects are discussed. Comparison with longer and shorter wavelength measurements is treated.

SUBMILLIMETER MIXERS

G. T. Wrixon
University College
Cork, Ireland

Abstract

Mixer performance at submillimeter wavelengths is currently limited by insufficient LO pump power. The use of subharmonically pumped mixers incorporating low capacitance diodes appears to offer a solution.

REFLECTIVITY OF COMMON MATERIALS IN THE SUBMILLIMETER REGION

M. D. Blue
Georgia Institute of Technology
Atlanta, Georgia

and

S. Perkowitz
Emory University
Atlanta, Georgia

Abstract

The appearance of an illuminated scene at submillimeter wavelengths is determined by surface reflectivity. Reflectivities of some man-made and natural materials have been measured. The results provide some insight for evaluating possible applications of submillimeter radiation.

MATERIALS FOR LOW NOISE SCHOTTKY BARRIER CONVERTERS AT SUBMILLIMETER WAVELENGTHS

G. T. Wrixon
University College
Cork, Ireland

and

M. D. Blue
Georgia Institute of Technology
Atlanta, Georgia

Abstract

The prospects for realization of low noise coherent detectors in the 25 μm - 100 μm region are critically assessed. Use of high efficiency Schottky-barrier converters can be extended to the submillimeter region through the use of appropriate diode materials.

A-1861

SUBMILLIMETER WAVE SPECTROSCOPY AND TECHNOLOGY

SECOND SEMI-ANNUAL TECHNICAL REPORT

J. J. Gallagher
M. D. Blue

September 13, 1977

U. S. ARMY RESEARCH OFFICE
Grant No. DAAG29-76-G-0280

Electromagnetics Laboratory
Engineering Experiment Station
Georgia Institute of Technology
Atlanta, Georgia 30332

REPORT DOCUMENTATION PAGE

READ INSTRUCTIONS BEFORE COMPLETING FORM

1. REPORT NUMBER: Second Semi-Annual Technical	2. GOVT ACCESSION NO.
3. RECIPIENT'S CATALOG NUMBER	
4. TITLE (and Subtitle): Submillimeter Wave Spectroscopy and Technology	5. TYPE OF REPORT & PERIOD COVERED: SEMI-ANNUAL 1 January-June 30, 1977
6. PERFORMING ORG. REPORT NUMBER	
7. AUTHOR(s): J. J. Gallagher & M. D. Blue	8. CONTRACT OR GRANT NUMBER(s): DAAG29-76-G-0280
9. PERFORMING ORGANIZATION NAME AND ADDRESS: Engineering Experiment Station, Georgia Institute of Technology, Atlanta, Georgia 30332	10. PROGRAM ELEMENT, PROJECT, TASK AREA & WORK UNIT NUMBERS
11. CONTROLLING OFFICE NAME AND ADDRESS: U. S. Army Research Office, Post Office Box 12211, Research Triangle Park, N.C. 27709	12. REPORT DATE: September 13, 1977
	13. NUMBER OF PAGES
14. MONITORING AGENCY NAME & ADDRESS(if different from Controlling Office)	15. SECURITY CLASS. (of this report): Unclassified
	15a. DECLASSIFICATION/DOWNGRADING SCHEDULE: N/A

16. DISTRIBUTION STATEMENT (of this Report)

Approved for public release; distribution unlimited.

17. DISTRIBUTION STATEMENT (of the abstract entered in Block 20, if different from Report)

N/A

18. SUPPLEMENTARY NOTES

The findings in this report are not to be construed as an official Department of the Army position, unless so designated by other authorized documents.

19. KEY WORDS (Continue on reverse side if necessary and identify by block number)

Submillimeter Waves; Schottky Barrier Diodes; Spectroscopy; Water Molecules; Fabry-Perot Interferometers; Electron Beam Sources; Heterodyne Receivers; Atmospheric Absorption.

20. ABSTRACT (Continue on reverse side if necessary and identify by block number)

Spectroscopic investigations have continued on atmospheric molecules in a large Fabry-Perot interferometer, a waveguide cell and a parallel plate Stark cell. Computer programs have been prepared with the capability for determining low pressure spectroscopic absorption, atmospheric absorption (horizontal) or vertical propagation characteristics. Work continues on receiver and mixer technology for the submillimeter wavelength region. Studies are being performed on the gyrotron; lack of information on the electron gun is currently the draw-back to initiating a design for construction of an experimental device.

DD FORM 1 JAN 73 1473 EDITION OF 1 NOV 65 IS OBSOLETE

ABSTRACT (Continued)

Work on optically pumped lasers as receiver L.O.'s, quasi-optical devices and waveguide filters are continuing efforts.

PROGRESS REPORT

1. ARO PROPOSAL NUMBER: P-14104-PX

2. PERIOD COVERED BY REPORT: 1 January, 1977 - 30 June, 1977

3. TITLE OF PROPOSAL: Submillimeter Wave Spectroscopy and Technology

4. CONTRACT OR GRANT NUMBER: DAAG29-76-G-0280

5. NAME OF INSTITUTION: Engineering Experiment Station, Georgia Institute of Technology

6. AUTHOR(S) OF REPORT: J. J. Gallagher, M. D. Glue

7. LIST OF MANUSCRIPTS SUBMITTED OR PUBLISHED UNDER ARO SPONSORSHIP DURING THIS PERIOD, INCLUDING JOURNAL REFERENCES:
   1) M. D. Blue and S. Perkowitz, IEEE Trans. MTT, MTT-25, #6, 491 (1977);
   2) R. W. McMillan, J. J. Gallagher and A. M. Cook, IEEE Trans. MTT, MTT-25, #6, 484 (1977).

8. SCIENTIFIC PERSONNEL SUPPORTED BY THIS PROJECT AND DEGREES AWARDED DURING THIS REPORTING PERIOD:
   J. J. Gallagher
   M. D. Blue
   R. W. McMillan
   J. H. Rainwater
   P. B. Reinhart
   R. Rogers
   A. M. Cook, Student
   C. H. Branch, Student
   N. K. O'Rourke, Student
   W. M. Penn, Student
   O. Simpson, Student

14104P

DR. M. D. BLUE
MR. JAMES J. GALLAGHER
GEORGIA INSTITUTE OF TECHNOLOGY
ENGINEERING EXPERIMENT STATION
ATLANTA, GA 30332

BRIEF OUTLINE OF RESEARCH FINDINGS

Investigations on atmospheric constituents have continued, mainly in a semi-confocal Fabry-Perot interferometer. The experimental apparatus has been assembled for both the Fabry-Perot interferometer and the waveguide cell systems. Measurements with the waveguide cell have been delayed owing to failure of millimeter wave klystrons. Two klystrons are currently on order to allow measurements to continue.

Receiver/mixer investigations have continued. An optically pumped laser has been assembled and operated. This device will serve as a local oscillator. A quasi-optical mixer, diplexer and associated components have been constructed. The quasi-optical mixer is an open structure device with the L.O. and signal fed to the device at right angles. The diplexer is a polarization interferometer scheme employing linear grids and corner reflectors.

The appendices of this report outline in greater detail the tasks currently being performed, planned future work and Army technology which this program is supporting.

APPENDICES

I. Introduction

The appendices which are given here outline the various tasks which are being performed on this grant or present information relevant to the performance of these tasks. The following briefly states the subjects, with related notes, that constitute the Appendices:

I. Calculations of Antenna Temperature, Horizontal Attenuation, and Zenith Attenuation Due to Water Vapor in the Frequency Band 150 - 700 GHz, R. W. McMillan, J. J. Gallagher and A. M. Cook, IEEE Trans. MTT, MTT-25, No. 6, pp. 484-488, June 1977. This paper was presented at the Second International Conference and Winter School on Submillimeter Waves and Their Applications, December 6 - 10, 1976 and was published in the June, 1977 issue of the Transactions of Microwave Theory and Techniques. The calculations are based on the monomer water vapor and have not included the continuum term which is necessary for agreement with measurements. This continuum absorption is analytically expressed by the term given by Gaut and Reifenstein:

$$\Delta k_\nu = 1.08 \times 10^{-11} \rho \left(\frac{300}{T}\right)^{2.1} \left(\frac{P}{1000}\right) \nu^2 \text{ cm}^{-1}$$

where ν is the frequency, ρ is the water-vapor density in grams per meter cubed, P the total pressure (millibars) and T is the temperature.

Variations of the computer program exist and are briefly described after the paper in Appendix I. It is necessary, as emphasized above, to add the continuum to the results of the paper, and this has been done in the programs which currently exist. The programs are being used for radiometric and propagation studies.

II. "Reflectivity of Common Materials in the Submillimeter Region", M. D. Blue and S. Perkowitz, IEEE Trans. MTT, MTT-25, No. 6, pp. 491-493 (June, 1977). This paper was also presented at the Submm Conference. As part of this program, it is planned to extend the reflectivity measurements to longer wavelengths beyond 1 mm. A comparison of these measurements

should be made with monochromatic source reflectivity measurements as a function of angle of incidence to provide information relevant to systems applications.

III. The third appendix describes a computer program for atmospheric vapors which has been prepared to handle the spectroscopic data which is being gathered on this grant. The program allows the use of any line shape at all pressures up to atmospheric pressure. It can be employed with both the interferometric measurements and the waveguide cell measurements. The latter will assist in line-shape/line width determinations, and the large interferometer will provide data in the window regions. The computer program has been modeled after the near-IR AFCRL programs.

IV. An important part of this program is research on mixer and receiver technology which is important for Army systems applications in the submillimeter wavelength region. This work includes investigation of suitable materials for extending Schottky-barrier mixers to shorter wavelengths. A paper was presented by M. D. Blue and G. T. Wrixon at the Second Submm Conference. The material presented is given as Appendix IV. This work can be summarized by the following abstract:

ABSTRACT

The potential for extending efficient low noise Schottky-barrier converter operation into the submillimeter region is examined. Operating temperatures in the 20°K to 60°K region are desired for minimum noise. High mobility semiconductors with a reduced carrier concentration in the metal-semiconductor barrier depletion region are desired in order to minimize parasitic loss. An excellent choice appears to be InSb with a potential cut-off frequency of 20 THz.

V. Submillimeter wave components which are being investigated include mixers, receivers, local oscillators, filters and various quasi-optical components. A brief description is given of this work in Appendix V.

VI. The apparatus employed for spectroscopic investigations is described in Appendix VI. The experiments consist of Fabry-Perot interferometer observations, waveguide cell studies and Stark effect measurements.

APPENDIX I

Calculations of Antenna Temperature, Horizontal Path Attenuation, and Zenith Attenuation Due to Water Vapor in the Frequency Band 150–700 GHz

R. W. McMILLAN, J. J. GALLAGHER, SENIOR MEMBER, IEEE, AND A. M. COOK, JR., STUDENT MEMBER, IEEE

Abstract—**The results of calculations of antenna temperature at zenith, both with and without the sun viewed as a source, are given. Horizontal path and total zenith attenuation are also calculated. Each of these calculations was made over the frequency band 150–700 GHz, using data from the 24 water-absorption lines between 150 and 1000 GHz.**

I. Introduction

MOLECULAR RESONANCES of atmospheric water vapor have been studied for many years because this gas makes the major contribution to attenuation of microwaves and infrared radiation by the atmosphere. Many of these lines are very strong, with horizontal-path attenuations that exceed 10^4 dB/km, and exhibit strong pressure-broadening effects, so that attenuation is appreciable at frequencies several gigahertz removed from the center frequencies of the lines. The effects of these lines extend generally through the millimeter/submillimeter portion of the microwave spectrum, being most pronounced between about 2000 and 10 μm. These absorptions make large portions of the submillimeter spectrum useless for communications or astronomical observations. However, the usefulness of these strong lines for remote sensing of the atmosphere from airborne, satellite, and ground-based stations is just beginning to be realized.

This paper presents the results of calculations of radiometric antenna temperatures at zenith, both with and without the sun viewed as a source. Calculations of horizontal path and total zenith attenuation are also given. The range of frequencies covered by these calculations is 150–700 GHz. Since the skirts of the water-vapor absorption lines extend to frequencies far removed from their center frequencies, all 24 lines in the frequency range 150–1000 GHz were considered in the calculations. The effects of oxygen and ozone were not included because the contributions of these molecules are considered to be negligible over the frequency range of interest for ground-based observations. Furthermore, absorptions due to the water dimer and the continuum were not treated because there exists no firm analytical basis for their inclusion in a calculation of this sort. For these reasons, more detailed calculations are required for specific system applications over limited wavelength ranges. The calculations of horizontal attenuation show good agreement with the results of Zhevakin and Naumov [1].

Manuscript received December 21, 1976; revised January 17, 1977. This work was supported by NASA Grant NSG-5012 and by the U.S. Army Research Office under Grant DAAG29-76-G-0280.

The authors are with the Engineering Experiment Station, Georgia Institute of Technology, Atlanta, GA 30332.

II. Absorption Calculations

Van Vleck and Weisskopf [2] have shown that the attenuation coefficient α, at frequency ν, for a collision-broadened absorption line centered at frequency ν_0, with linewidth parameter $\Delta\nu$, is given by

$$\alpha = \frac{8\pi^2 N n|\mu|^2\nu^2 \exp(-E_i/kT)}{3ckTG} F(\nu) \tag{1}$$

where the other parameters are determined as discussed below. The parameter N is the number of molecules per unit volume and is

$$N = \frac{N_A \rho}{M} \tag{2}$$

in which N_A is Avogadro's number, ρ is the density of molecules, and M is the number of grams in a gram molecular weight. For water, this number is $N = 3.346 \times 10^{16}\ \rho$, where ρ is measured in grams/cubic meter. The factor $|\mu|^2$ is the square of the dipole matrix element between transition states and is equal to $\Sigma|\phi|^2\mu_0^2$, where μ_0^2 is the electric dipole moment. The factor $\Sigma|\phi|^2$ is the line-strength parameter determined by King *et al.* [3], and μ_0^2 is 3.39×10^{-36} ESU from Van Vleck [4]. The statistical weighting factor n which accounts for nuclear spin is unity [5] for even rotational states and 3 for odd rotational states. In the exponential term, E_i is the energy of the lower transition state, k is Boltzmann's constant, and T is the absolute temperature at which the attenuation is measured. The partition function G has been calculated by Van Vleck [4] to be 170 at 293 K and varies with temperature as

$$G = KT^{3/2}. \tag{3}$$

Evaluation of the constant K from the previous values gives $G = 0.0339T^{3/2}$.

For these calculations, the line-shape factor $F(\nu)$ was replaced by a factor calculated by Gross [6], which has been found to give better agreement with absorption-cell measurements

$$F(\nu) = \frac{4\nu\nu_0\Delta\nu}{(\nu_0^2 - \nu^2)^2 + 4\nu^2\Delta\nu^2} \tag{4}$$

in which the parameters are defined as before.

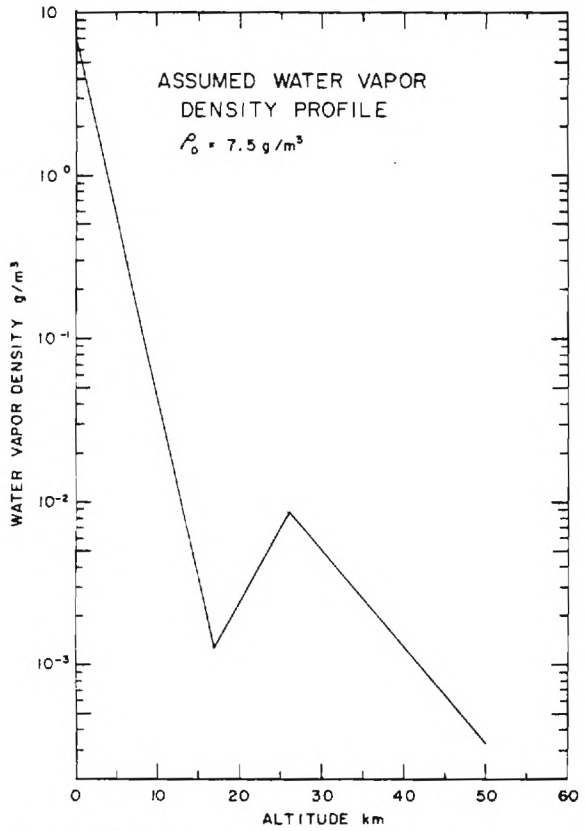

Fig. 1. Altitude dependence of water-vapor density for sea-level density of 7.5 g/m³.

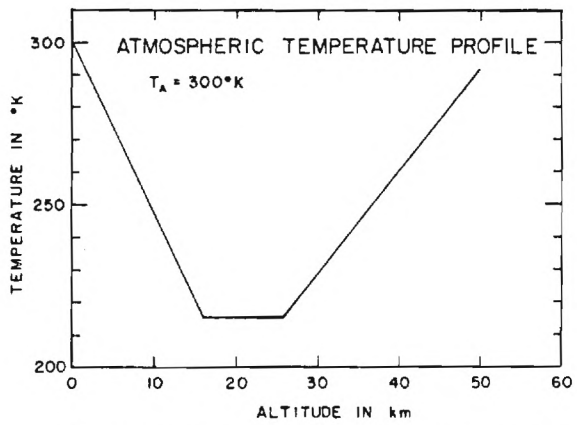

Fig. 2. Altitude dependence of air temperature for sea-level temperature of 300 K.

Since radiometric calculations must include the effects of altitude, the altitude dependence of terms in (1) must be considered. The density varies with altitude according to a relation given by Croom [7], [8], who based his altitude dependence on U.S. Weather Bureau data. This dependence is shown plotted in Fig. 1.

Barrett and Chung [9], based on U.S. Air Force data, give the altitude-dependent temperature profile shown in Fig. 2, and the pressure dependence as

$$P = 760[10^{-3.05Z/50}]. \tag{5}$$

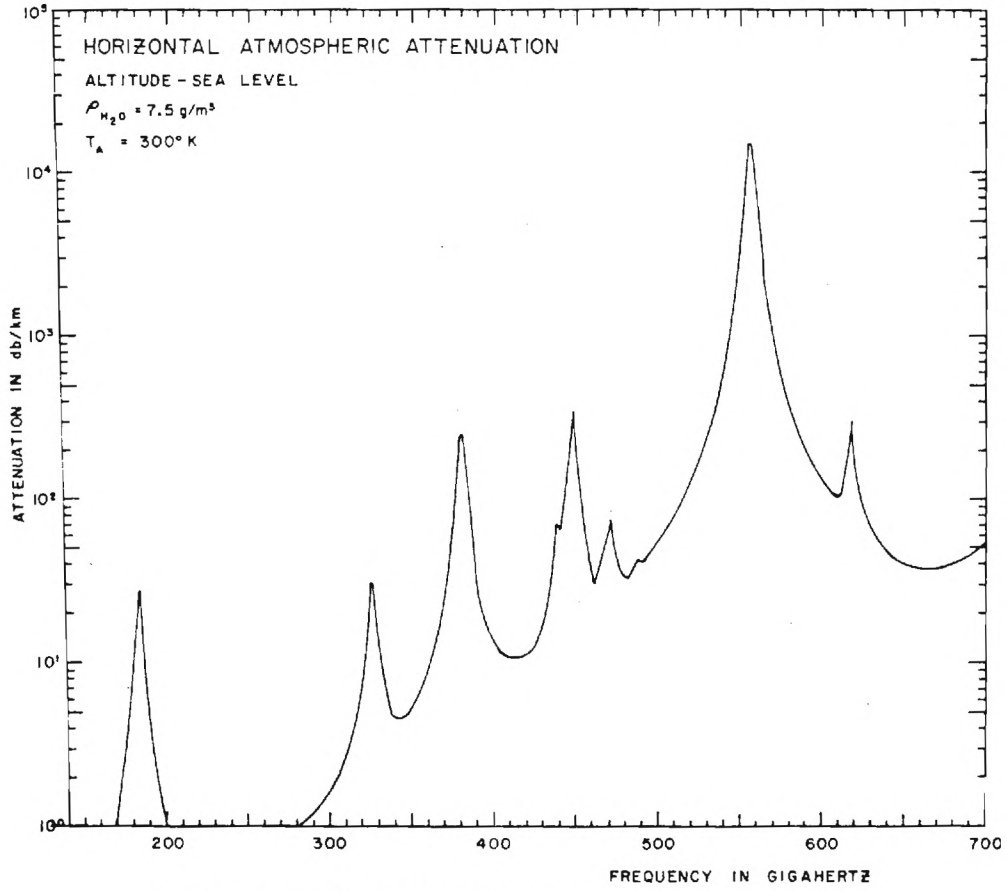

Fig. 3. Horizontal-path attenuation versus frequency at sea level.

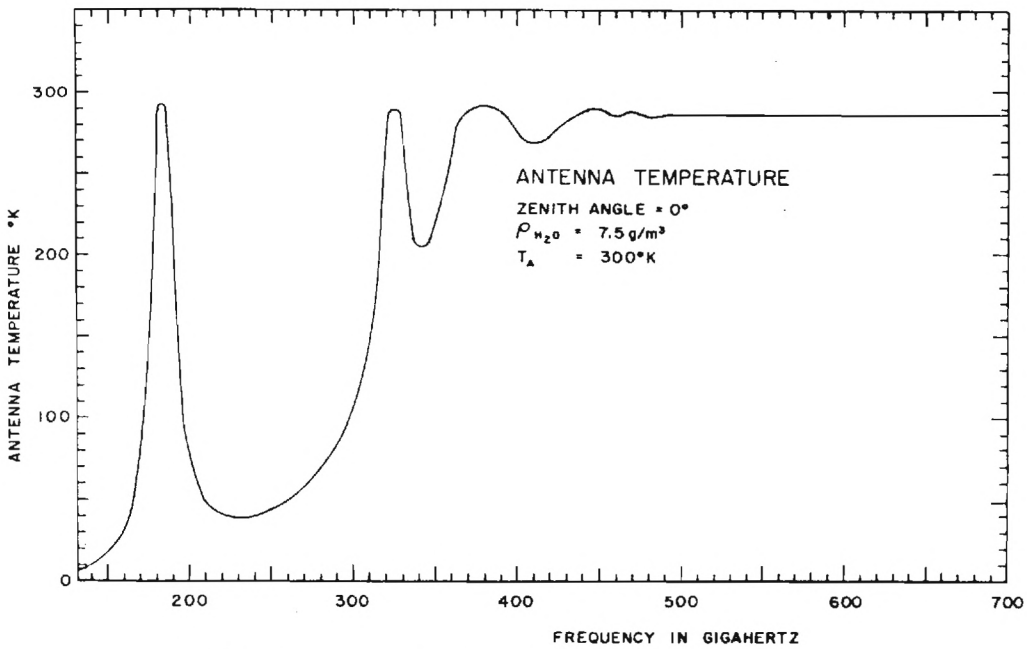

Fig. 4. Antenna temperature at zenith for sea-level altitude.

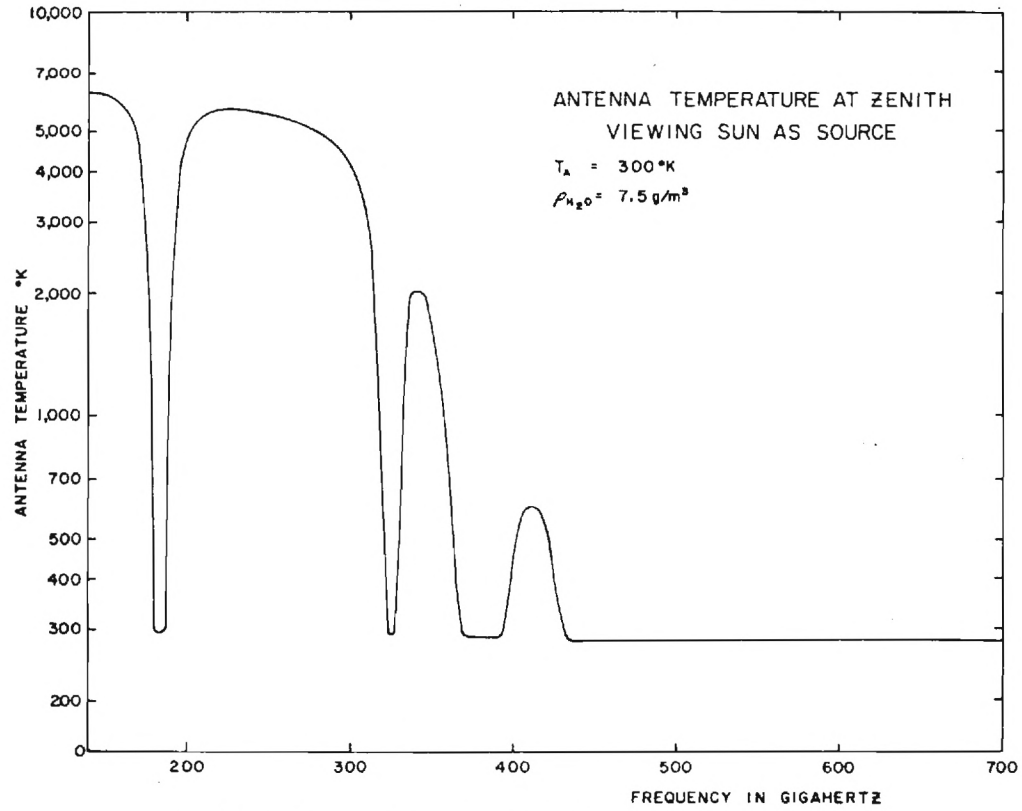

Fig. 5. Antenna temperature viewing the sun as a source at zenith from sea level.

Also from Barrett and Chung, the linewidth parameter is

$$\Delta\nu = \frac{\Delta\nu_0 \dfrac{P}{760}(1 + 0.0046\rho)}{\left(\dfrac{T}{318}\right)^{0.625}} \tag{6}$$

where $\Delta\nu_0$ is the linewidth parameter at $P = 760$ mm and $T = 318$ K for small ρ.

Using these parameters with the indicated altitude, density, and temperature dependence, the attenuation in decibels/kilometer due to contributions from all of the water absorption lines below 1000 GHz was calculated in

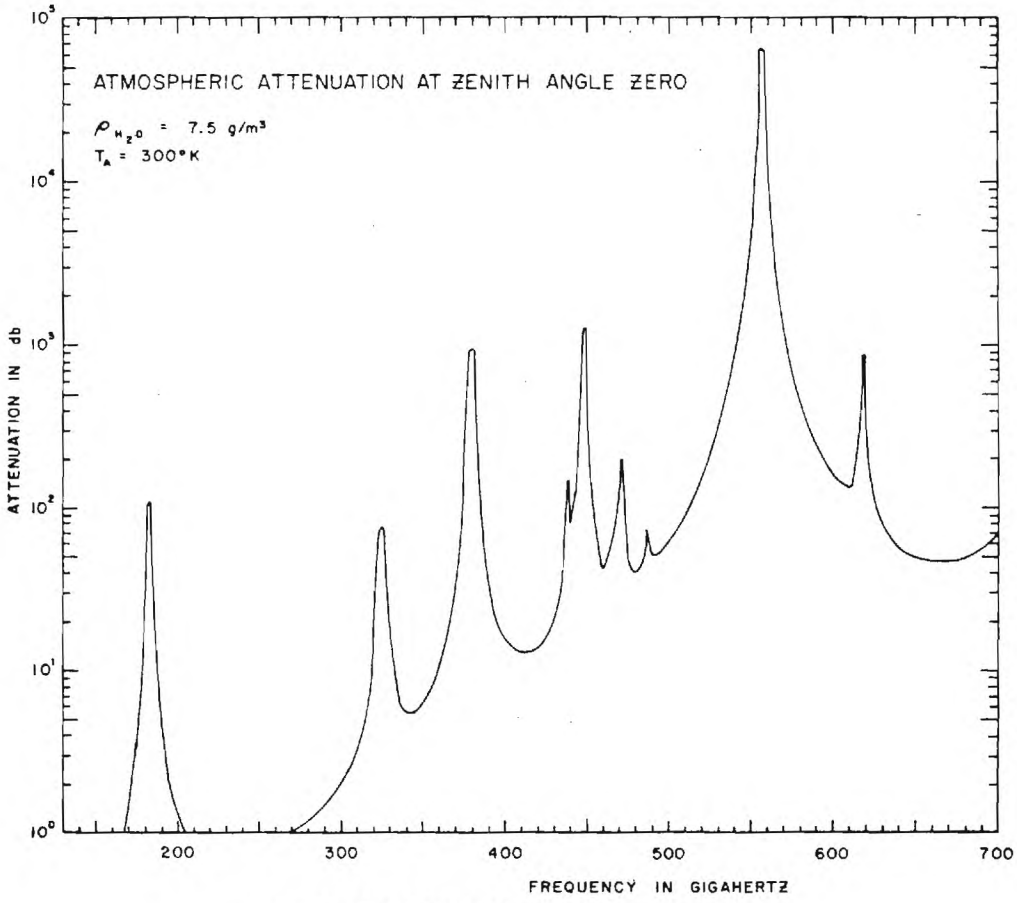

Fig. 6. Total zenith attenuation from sea level.

the frequency range from 150 to 700 GHz. The result of this calculation at sea level is shown in Fig. 3.

III. Sky-Temperature Calculations

The background sky temperature T_b, measured by a radiometer at altitude h with an infinitesimally narrow beamwidth looking upward at zenith angle θ, is [6]–[8]

$$T_b = T_s \exp\left(-\int_h^\infty \alpha(Z)\sec\theta\, dZ\right) + \int_h^\infty \alpha(Z)T(Z) \cdot \exp\left(-\int_h^Z (Z')\sec\theta\, dZ'\right)\sec\theta\, d\theta \quad (7)$$

in which T_s is the sun temperature, and $T(Z)$ is the temperature of a stratum of atmosphere of thickness dZ located at altitude Z. In this equation, the first term is seen to be the brightness of the sun as viewed through the atmosphere, and the second term is the emission of the atmosphere. The sum of these two terms is the temperature that would be measured if the sun were viewed as a source through the atmosphere. Using the value of α given by (1), this equation was integrated numerically up to an altitude of 50 km. In order to get good accuracy and minimize computer time, the stratum width was varied as follows:

$Z <$ 1.0 km	$\Delta Z =$ 2.5 m
1.0 km $< Z <$ 4.0 km	$\Delta Z =$ 5.0 m
4.0 km $< Z <$ 8.0 km	$\Delta Z =$ 10.0 m
8.0 km $< Z <$ 16.0 km	$\Delta Z =$ 20.0 m
16.0 km $< Z <$ 50.0 km	$\Delta Z =$ 50.0 m.

The computer was programmed to read out emission temperature of the atmosphere, which is the temperature that would be measured by a radiometer pointing away from the sun; sky temperature, measured when the sun is viewed as a source; and zenith attenuation. The contributions of all of the water absorption lines between 150 and 1000 GHz to these temperatures were included in the calculations. The result of calculating emission temperature with the antenna pointing to the zenith is shown in Fig. 4. Emission temperature calculated with the sun viewed as a source is shown in Fig. 5, and total zenith attenuation is shown in Fig. 6.

IV. Conclusions

Calculations of attenuation and emission temperatures due to water vapor in the atmosphere have been made between 150 and 700 GHz. Attenuation curves show windows at 230 and 400 GHz, and strong absorption elsewhere within this frequency band. Antenna temperature curves show no structure above 450 GHz, but strong structure due to the 183- and 325-GHz lines is evident at the lower frequencies. This result shows that the atmosphere appears to be a black body at near-ambient temperature at the peaks of the strong absorption lines and at frequencies greater than 450 GHz.

Acknowledgment

The authors wish to thank Dr. G. Schaerer of the NASA/Goddard Space Flight Center for calling the work of

Dr. J. W. Waters [10] in this area to their attention and for furnishing data obtained from Dr. Waters.

REFERENCES

[1] S. A. Zhevakin and A. P. Naumov, "The absorption coefficient of water vapor for electromagnetic waves in the range 2 cm–10 μm," *Radiophys. Quantum Electron.*, vol. 6, p. 675, 1963.

[2] J. H. Van Vleck and V. F. Weisskopf, "On the shape of collision-broadened lines," *Rev. Mod. Phys.*, vol. 17, pp. 227–236, Apr.–July 1945.

[3] G. W. King, R. M. Hainer, and P. C. Cross, "Expected microwave absorption coefficients of water and related molecules," *Phys. Rev.*, vol. 71, pp. 433–443, Apr. 1947.

[4] J. H. Van Vleck, "The absorption of microwaves by uncondensed water vapor," *Phys. Rev.*, vol. 71, pp. 425–433, Apr. 1947.

[5] C. H. Townes and A. L. Schawlow, *Microwave Spectroscopy*. New York: McGraw-Hill, 1955, p. 104.

[6] E. P. Gross, "Shape of collision-broadened spectral lines," *Phys. Rev.*, vol. 97, pp. 395–403, Jan. 1955.

[7] D. L. Croom, "Stratospheric thermal emission and absorption near the 22.235 Gc/s (1.35 cm) rotational line of water-vapor," *J. Atmos. Terrest. Phys.*, vol. 27, pp. 217–233, 1965.

[8] ——, "Stratospheric thermal emission and absorption near the 183.311 Gc/s (1.64 mm) rotational line of water-vapor," *J. Atmos. Terrest. Phys.*, vol. 27, pp. 235–243, 1965.

[9] A. H. Barrett and V. K. Chung, "A method for the determination of high-altitude water-vapor abundance from ground-based microwave observations," *J. Geophys. Res.*, vol. 67, pp. 4259–4266, Oct. 1962.

[10] J. W. Waters in *Methods of Experimental Physics*, vol. 12, part B, M. L. Meeks, Ed. New York: Academic, 1976, pp. 142–176.

Program 2HORZA

Description: This program calculates horizontal atmospheric attenuation in db/km for up to 25 lines (of a single species) at 1000 points. The attenuation at each point is the composite attenuation of all lines at that point. The program uses a Gross line shape, and additional points and lines may be added with slight modification, if desired. The 1000 points are spaced 5 GHz apart away from the line peaks and 1 GHz near line peaks. An optional mode allows the selection of 0.1 GHz spacing if desired.

Inputs: The program is designed to prompt the user for the desired input when used on a terminal. Inputs required are begin frequency, end frequency, water vapor density in gm/m^3 (RHO 0), altitude (Z), and ambient temperature in degrees kelvin (AMBT). Additional inputs required for each line are lower state energy (ergs) divided by Boltzmann's constant in ergs/deg K, the line strength parameter multiplied by the statistical weighting factor (1 or 3 for water), the line width parameter, and the center frequency.

Program MULTI

Description: This program calculates sun temperature viewed through atmospheric attenuation, (no atmospheric emission), zenith antenna temperature both with and without the sun as a source, and total zenith attenuation. The program integrates contributions from 2500 layers of progressively increasing thickness to obtain these values. Other features are the same as 2HORZA above.

Program MULTI (cont'd)

Inputs: Inputs are the same as 2HORZA except that zenith angle (THET) and initial layer number or altitude (INIT) are also required.

```
*ED,ZHURZA.
/G,MULTI
/ED,MULTI
ED 1.1.    77/04/25. 16.24.58.
0 ? LNP*
      1        PROGRAM MAIN (INPUT,OUTPUT,TAPE5 = INPUT,TAPE6 = OUTPUT)
      2        DIMENSION GNU(1000),TEMP(2500),ANTP(1000),
      3       &LNWIDTH(25),CENTERV(25),IENERGY(25),ASUM(1000)
      4       &,STRNTH(25),TB183(1000)
      5        REAL IENERGY,LNWIDTH
      6        LOGICAL TENTH
      7  C
      8  C
      9  C     PREDICTED ANTENNA TEMPERATURE CALCULATIONS
     10  C       CONSIDERING MULTIPLE ABSORPTION LINES
     11  C                    VERSION 1.1
     12  C
     13  C          R. W. MCMILLAN AND A. M. COOK, JR.
     14  C            ENGINEERING EXPERIMENT STATION
     15  C          GEORGIA  INSTITUTE  OF  TECHNOLOGY
     16  C
     17        CONTINUE
     18  C     >>>READ IN PARAMETERS<<<
     19        PRINT*,"ENTER NUMBER OF LINES:",
     20        READ(5,*) NLINES
     21        PRINT*,".1 GHZ SPACING AROUND CENTER FREQUENCIES",
     22     88 READ(5,1006) ANS
     23   1006 FORMAT(A10)
     24        IF (ANS.EQ.3HYES.OR.ANS.EQ.2HYE.OR.ANS.EQ.1HY) GO TO 85
     25        IF(ANS.EQ.2HNO.OR.ANS.EQ.1HN) GO TO 86
     26        PRINT*,"PLEASE ENTER YES OR NO!  ",
     27        GO TO 88
     28     85 TENTH=.TRUE.
     29        GO TO 87
     30     86 TENTH=.FALSE.
     31     87 PRINT*,"BEGIN FREQUENCY",
     32        READ(5,1007) BEGINV
     33   1007 FORMAT(F6.1)
     34        PRINT*,"END FREQUENCY",
     35        READ(5,1007) ENDV
     36        PRINT*,"ENTER THET,RHOO,INIT,AMBT",
     37        READ (5,*) THET,RHOO,INIT,AMBT
     38        IF (EOF(5)) 200,3
     39      3 DO 105 L=1,NLINES
     40        PRINT*,"LINE ",L
     41        PRINT*,"ENTER LINEWIDTH:",
     42        READ(5,1000) LNWIDTH(L)
     43   1000 FORMAT(F6.3)
     44        PRINT*,"ENTER CENTER FREQUENCY:",
     45        READ(5,1001) CENTERV(L)
     46   1001 FORMAT(F5.1)
     47        PRINT*,"ENTER INITIAL STATE ENERGY / K :",
     48        READ(5,1002) IENERGY(L)
     49   1002 FORMAT(F8.2)
     50        PRINT*,"ENTER LINE STRENGTH:",
     51        READ(5,1008) STRNTH(L)
     52   1008 FORMAT(F6.4)
     53    105 CONTINUE
     54  C     DETERMINE FREQUENCY POINTS
     55        CALL VARRAY(NLINES,BEGINV,ENDV,II,CENTERV,GNU,TENTH)
     56        PMU=7.18E-8
     57        DO 10 J=INIT,2500
     58        IF (J-400) 31,31,32
     59     31 Z=J*0.0025
     60        GO TO 33
     61     32 IF (J-1000) 34,34,35
```

```
      34 Z=J*0.005-1.0
         GO TO 33
      35 IF (J-1400) 36,36,37
      36 Z=J*0.01-6.0
         GO TO 33
      37 IF (J-1800) 38,38,39
      38 Z=J*0.02-20.0
         GO TO 33
      39 Z=J*0.05-75.0
      33 CONTINUE
         SPAC=.05556*(1.0-EXP(-0.046*Z))
C        DETERMINATION OF DELTA NU
         PRES = 760.0*10.0**(-3.05*Z/50)
         IF (Z-12) 4,4,6
       4 TEMP(J) = AMBT - 5.83*Z
         GO TO 17
       6 IF (Z-25.0) 12,12,14
      12 TEMP(J) = 216.0
         GO TO 17
      14 TEMP(J) = 3.08*Z + 139.0
   17    IF(Z-17) 18,19,19
   18    RHO=RH00*(10**(-0.2286*Z))
         GO TO 21
   19    IF (Z-26) 22,23,23
   22    RHO=3.611E-5*(10**(0.09155*Z))
         GO TO 21
   23    RHO=0.3*(10**(-0.05914*Z))
      21 FRHO = 1.0 + 0.0046*RHO
         FPRE = PRES/760.0
         FTEM = (TEMP(J)/318.0)**0.625
         PARF = 3.390E-2*(TEMP(J)**2.5)
         DO 20 L=1,NLINES
         DGNU = LNWIDTH(L)*1.0E9*FPRE*FRHO/FTEM
         CENF = CENTERV(L)*1.0E9
         FRAC = EXP(-IENERGY(L)/TEMP(J))
         A183 = RHO*PMU*STRNTH(L)
         DO 30 I=1,II
         DEN1=(CENF**2-GNU(I)**2)**2+4.0*(GNU(I)**2)*DGNU**2
         ARG1=4.0*DGNU*CENF*GNU(I)/DEN1
         B183 = (A183*FRAC*ARG1/PARF)*(GNU(I)**2)
         COEF=B183*TEMP(J)*SPAC/COS(THET)
         K=J-1
         IF(K) 55,55,56
      56 AEXP=TB183(I)*SPAC/COS(THET)
         ASUM(I)=ASUM(I)+AEXP
         GO TO 121
      55 ASUM(I)=0
     121 IF (ASUM(I)-200.0) 123,122,122
     122 ATTN=0.0
         GO TO 124
     123 ATTN=EXP(-ASUM(I))
     124 CONTINUE
         TAX=ATTN*COEF
         ANTP(I)=ANTP(I)+TAX
         TB183(I)=B183
      30 CONTINUE
      20 CONTINUE
      10 CONTINUE
         WRITE (6,1)
       1 FORMAT (//" FREQ GHZ",5X,"SUN TEMP",5X,"EMIT TEMP",
        &5X,"ANT TEMP",5X,"ZENITH ATTN")
         DO 199 I=1,II
     131 IF (ASUM(I)-200.0) 133,132,132
     132 SUN=0.0
         GO TO 134
     133 SUN = ASUM(I)*EXP(-ASUM(I))
```

```
      134 CONTINUE
          TANT = ANTP(I) + SUN
          ZAT = 4.3429*ASUM(I)
          FREQ=GNU(I)/1.0E9
          WRITE (6,2) FREQ,SUN,ANTP(I),TANT,ZAT
        2 FORMAT (1X,F7.2,5X,E9.3,5X,F8.3,5X,F8.3,5X,E9.4)
      199 CONTINUE
      200 STOP
          END
C
C     >>>> SUBROUTINE VARRAY <<<<
C
          SUBROUTINE VARRAY(NLINES,BEGINV,ENDV,II,CENTERV,GNU,TENTH
          DIMENSION CENTERV(25),GNU(1000)
          LOGICAL PTFIVE,TENTH,FIVE
C
          FIVE=.FALSE.
          PTFIVE=.FALSE.
          II=1
          VINC=5.0
          GNU(I)=BEGINV*1.0E9
          CURENTV=BEGINV
      600 II=II+1
          TESTV=CURENTV+VINC
          IF(TESTV.GT.ENDV) GO TO 699
          CALL CHECKV(FIVE,PTFIVE,CENTERV,JJ,TESTV,NLINES,TENTH)
          IF(PTFIVE) GO TO 610
          IF(FIVE) GO TO 620
          IF(VINC.EQ.1.0) GO TO 607
          CURENTV=TESTV
          GNU(II)=CURENTV*1.0E9
          GO TO 600
      607 TEMPV=TEMPV+5.0
          CALL CHECKV(FIVE,PTFIVE,CENTERV,JJ,TEMPV,NLINES,TENTH)
          IF((FIVE.OR.PTFIVE).AND.(JJT.LE.JJ)) GO TO 607
          TESTV=TEMPV
          CALL CHECKV(FIVE,PTFIVE,CENTERV,JJ,TESTV,NLINES,TENTH)
          IF(PTFIVE.OR.FIVE) GO TO 608
          VINC=5.0
          CURENTV=TESTV
          GNU(II)=CURENTV*1.0E9
          GO TO 600
      608 VINC=5.0
      610 IF(VINC-1.0) 612,615,618
      612 CURENTV=TESTV
          GNU(II)=CURENTV*1.0E9
          GO TO 600
      615 CURENTV=CENTERV(JJ)-0.5
          VINC=0.1
          GNU(II)=CURENTV*1.0E9
          GO TO 600
      618 TEMPV=CURENTV
          JJT=JJ
          CURENTV=CENTERV(JJ)-5.0
          VINC=1.0
          GNU(II)=CURENTV*1.0E9
          GO TO 600
      620 IF(VINC-1.0) 622,612,618
      622 VINC=1.0
          CURENTV=CURENTV+VINC-0.5
          GNU(II)=CURENTV*1.0E9
          GO TO 600
      699 II=II-1
          RETURN
          END
```

```
      191           RETURN
      192           END
      193   C
      194   C       > > > SUBROUTINE CHECKV < < <
      195   C
      196           SUBROUTINE CHECKV(FIVE,PTFIVE,CENTERV,JJ,TV,NLINES,TENTH)
      197           DIMENSION CENTERV(25)
      198           LOGICAL FIVE,TENTH,PTFIVE
      199           FIVE=.FALSE.
      200           PTFIVE=.FALSE.
      201           IF(.NOT.TENTH) GO TO 712
      202           DO 710 L=1,NLINES
      203           JJ=L
      204           IF(ABS(CENTERV(L)-TV).LE.0.5)GO TO 720
      205       710 CONTINUE
      206       712 DO 711 L=1,NLINES
      207           JJ=L
      208           IF(ABS(CENTERV(L)-TV).LE.5.0)GO TO 730
      209       711 CONTINUE
      210           GO TO 700
      211       720 PTFIVE=.TRUE.
      212           GO TO 700
      213       730 FIVE=.TRUE.
      214       700 RETURN
      215           END
SCAN  215 EOR  215
0 ? END
LINES  215
$ED,MULTI.
/PURGE REVSHF,NREVSHF,CARDS,ZZZZZEM,HORZAT,MODSHP,LINSHP
 FORMAT ERROR ON CONTROL CARD.
/HELLO

QF642RM   LOG OFF     16.33.10.
QF642RM   SRU       1.111 UNTS.



 77/04/25. 16.33.16.
PLEASE PURGE ALL UNNECESSARY FILES.
USER NUMBER:
```

APPENDIX II

Reflectivity of Common Materials in the Submillimeter Region

M. D. BLUE AND S. PERKOWITZ

Abstract—**The appearance of an illuminated scene at submillimeter wavelengths is determined by surface reflectivity. Reflectivities of some man-made and natural materials have been measured. The results provide some insight for evaluating possible applications of submillimeter radiation.**

INTRODUCTION

THE gradual realization of practical submillimeter-wave sources, including optically pumped lasers throughout the submillimeter region [1], and relativistic electron-beam devices [2], gives rise to the possibility of practical terrestial systems operating within the atmospheric windows [1]. Systems calculations are handicapped by a lack of data concerning dielectric properties of common materials in this spectral region. Recent transmission data and active imaging experiments indicate the potential utility of this technology [3]. The work reported here represents an initial attempt to characterize the far-infrared submillimeter reflectivity of common materials, and can be used as a guide for initial estimates of system performance. The contrast expected in imaging systems in this wavelength region between man-made and natural objects is of interest and is difficult to predict. In addition to military applications, several applications for civil systems might be envisioned, such as a system for locating and identifying aircraft on remote airport taxiways and runways during periods of severe weather.

Manuscript received January 17, 1977. This work was supported by the Army Research Office.

M. D. Blue is with the Georgia Institute of Technology, Atlanta, GA 30332.

S. Perkowitz is with Emory University, Atlanta, GA 30322.

EXPERIMENTAL METHODS

The room-temperature reflectivity measurements employed a modified Grubb Parsons Mark II Fourier-transform spectrometer [4]. Light-pipe optics carried the radiation to a sample holder which was open to the atmosphere so that the sample could be studied under natural conditions. Conventional disiccant and a constant flow of dry nitrogen gas were used to eliminate water-vapor absorption from the sample light pipe and holder and the remainder of the spectrometer was evacuated. The radiation impinged on the samples at an angle of 12°, negligibly different from normal incidence. The sample holder was mounted horizontally to accomodate loose samples such as sand. The detector was a Unicam quartz-window Golay cell with the usual polyethylene filtering. All data were taken at a resolution of 8 cm^{-1}. A sample in/sample out

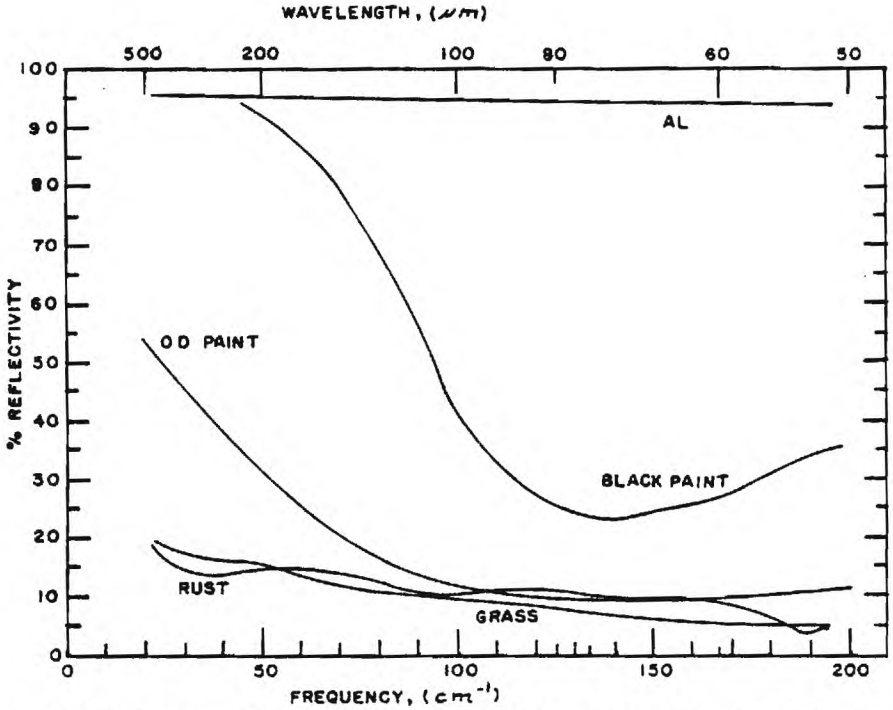

Fig. 1. Normal reflectivity in percent for common materials. Included are a normally oxidized aluminum surface (Al), aluminum sprayed flat-black paint (Black Paint), olive-drab paint on brass (OD Paint), a freshly cut blade of grass (Grass), and a rusty iron surface (Rust).

TABLE I
FAR-INFRARED REFLECTIVITY OF SOME COMMON MATERIALS

Natural Materials	
Sand	2% (overall reflectivity 20-200 cm^{-1})
Soil	2% (overall reflectivity 20-200 cm^{-1})
Wood	
Oak, Mahogany, Fir	2% (overall reflectivity 20-200 cm^{-1})
Rosewood	5% (overall reflectivity 20-200 cm^{-1})
Leaf	
Maple - fresh, dry (green)	See text, 20% (at 100 cm^{-1})
Grass - fresh, dry (green)	
Man Made Materials	
Asphalt	5% (overall reflectivity 20-200 cm^{-1})
Painted metal	
Flat black on Al, Army OD on brass, Rusted iron, Oxidised Al	Refer to Fig. 1.
Concrete	Similar to Rusted Iron

method was used to obtain the reflection coefficient, with the reference value supplied by a polished stainless-steel mirror. Such a mirror has a nearly constant far-infrared reflectivity of about 97 percent and so can be treated as a 100-percent reflector with little error.

EXPERIMENTAL RESULTS

A list of materials examined in this study is presented in Table I. Both natural and man-made materials were considered. Natural materials include typical surfaces as seen in earth backgrounds. Man-made materials include asphalt and concrete as well as metal surfaces.

The normal reflectivities for several metal surfaces as well as for grass are shown in Fig. 1. It can be seen that flat-back paint on aluminum reduces the reflectivity to a value below that of a normally oxidized aluminum surface in the submillimeter region. Similarly, flat olive-drab paint reduces the reflectivity of clean brass which, like all high-conductivity materials, has very high reflectivity throughout this region. However, these two paints have quite different spectra.

For many natural surfaces, it is likely that the surface-scattering effects dominate the reflectivity. For example, the reflectivity of concrete closely parallels rusty iron over this spectral region. As these materials are quite different, it is possible that the normal reflectivity is dominated by surface-roughness effects.

Fig. 2 shows the reflectivity spectra for several of the organic materials examined in this study along with the reflectivity of concrete. Fresh grass shows a reflectivity which is typical of several of these materials. Reflectivity of dry grass was similar, both samples showing a decrease in reflectivity from near 20 percent at 20 cm^{-1} to 3 percent at 200 cm^{-1}. As shown in Fig. 2, a dry maple leaf has a modest peak in reflectivity of 16 percent at 100 cm^{-1} dropping to 10 percent at 50 and 150 cm^{-1}. This peak did not appear in the fresh specimen. Reflectivity measurements on the organic materials did not show any obvious correlation with chlorophyll transmission spectra where a strong structure at 200 cm^{-1} has been observed [5].

In general, all organic samples along with sand, mud, asphalt, and concrete have lower reflectivities than the

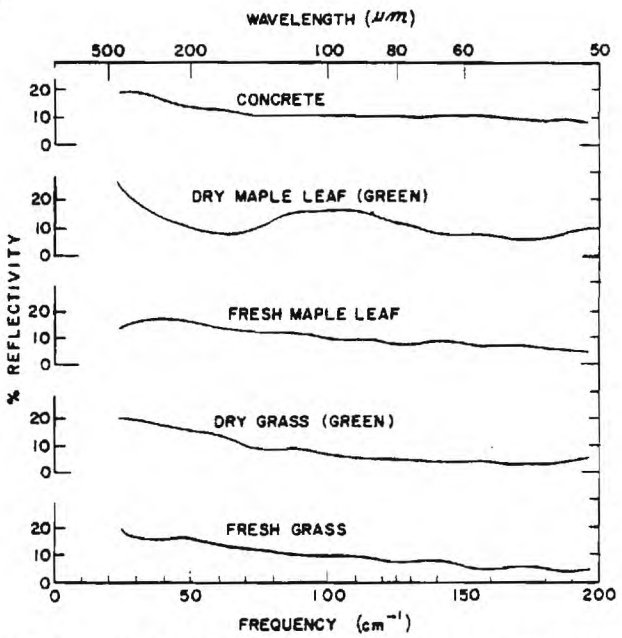

Fig. 2. Normal reflectivity in percent for typical organic materials, and a concrete surface for comparison. Both fresh and dried samples of the same specimens are shown. A rise in reflectivity going toward small wavenumbers was a typical trend for these samples.

metal and painted metal surfaces examined within the limited scope of this study.

Summary and Discussion

This study examined normal reflectivity for a small group of natural and man-made samples from 20 to 200 cm^{-1} at room temperature. Many interesting questions are raised by these data which suggest several directions for further work. Among these are extensions to longer wavelengths, off-axis reflection, temperature effects, and additional samples. The transition between reflectivity related to the metal and reflectivity characteristic of the surface paint takes place in the submillimeter region in our metal samples, and additional data would be helpful. For the painted surfaces shown in Fig. 1, the increase in reflectivity at long wavelengths could be related more closely to paint thickness than dielectric properties. The olive-drab paint layer was much thicker than the layer of black spray paint, and the shift to higher reflectivity occurs at an appropriately longer wavelength.

For more a complete characterization of the optical properties of common materials, it would be helpful to make transmission as well as reflection measurements. A high-power optically pumped laser is especially useful for precise transmission work. Such a laser has been used to measure the transmission of liquid water [6] which plays an important role in our natural samples. Recent preliminary results show that fresh leaf can transmit as much as 7 percent between 39 and 104 cm^{-1} [7].

The most significant result to date appears to be the clear separation in the value of normal reflectivity between metal surfaces and typical natural materials representative of terrestrial backgrounds. This result suggests that detection and imaging systems operating in this wavelength region can distinguish man-made objects from their backgrounds.

References

[1] J. J. Gallagher, M. D. Blue, B. Bean, and S. Perkowitz, "Tabulation of optically pumped far infrared laser lines and applications to atmospheric transmission," *Infrared Phys.*, vol. 17, pp. 43–55, Jan. 1977.

[2] (a) H. H. Fleischmann, "High-current beams," *Phys. Today*, vol. 28, pp. 35–43, May 1975.
(b) V. L. Granastein, M. Herndon, P. Sprangle, Y. Carmel, and J. A. Nation, "Gigawatt microwave emissions from an intense relativistic electron beam," *Plasma Phys.*, vol. 17, pp. 23–28, Jan. 1975.

[3] T. S. Hartwick, D. T. Hodges, D. H. Barker, and F. B. Foote, "Far infrared imagery," *Appl. Opt.*, vol. 15, pp. 1919–1922, Aug. 1976.

[4] S. Perkowitz and J. Breecher, "Characterization of GaAs by far infrared reflectivity," *Infrared Phys.*, vol. 13, pp. 321–326, Feb. 1973.

[5] (a) S. Perkowitz and B. Bean, "Far infrared studies of biological materials: Application to chlorophyll," *Bull. Amer. Phys. Soc.*, vol. 21, p. 371, Mar. 1976.
(b) ——, "Far infrared absorption of chlorophyll in solution," *J. Chem. Phys.*, Feb. 1977, in press.

[6] B. Bean and S. Perkowitz, "Far infrared transmission measurements with an optically pumped FIR laser," *Appl. Opt.*, vol. 15, pp. 2617–2618, Nov. 1976.

[7] ——, unpublished results.

APPENDIX III

-WITS-

The objective of the WITS Program is to compare three theoretical calculations of atmospheric attenuation in the 10-1000 GHz range due to water vapor. Ultimately these three theoretical calculations will be compared with values of atmospheric attenuation measured by several experiments.

Two of the theoretical calculations have already been made. Both of these calculations are based on theory presented in J. Water's article [1]. The parameters used in these calculations are as follows: 1) water vapor density - 7.5 grams/m^3, 2) pressure - 1013 millibars, 3) temperature = 300°K. Twenty-five water lines were used in the calculation. These 25 lines ranged in frequency from 22.23515 GHz to 916.05 GHz and are stored in the 25 element array "FC" in the function sub program named AH20 (P,T,F,RHO, N,M,DOPP). A copy of this sub program and an explanation of its operation is given in Appendix I.

Both calculations use a Gross line shape (eqn. 2.3.12 in Waters'), but the first calculation includes an empirical correction term developed by Gaut & Reifenstein and the second calculation omits this term. (The eqns in Waters' [1] are 2.3.20-2.3.21, 2.3.21). The output of these calculations are plotted on a semilog scale of frequency versus attenuation (in dB/Km). Note that Waters' eqns for K_v and ΔK_v have to be multiplied by 4.34×10^5 to convert from units of cm^{-1} to dB/Km). Hence, calculation 1 consists of

$$Y_{axis} = K_v + \Delta K_v$$

whereas calculation 2 consists of

$$Y_{axis} = K_v$$

The figures at the end of this appendix show the submillimeter program with and without the continuum term, ΔK_v.

The third theoretical calculation is not yet completed. The theory for that calculation is described in this Appendix - entitled WITS. The only difference between what is described in this Appendix and our intended cal-

culation is that we will not be using (in the beginning) any of the calculations involving oxygen lines. In effect this is equivalent to setting the contents of register 2 equal to zero on page 2 of the Flow Chart at the end of the Appendix. We already have a program written to make the necessary calculations; the only major problem remaining is developing a program to read the Clough AFCRL data type which is not in a form easily compatible with our computer.

REFERENCE

1. J. W. Waters, "Absorption and Emission by Atmospheric Gases", Chapter 2.3, Methods of Experimental Physics, Astrophysics, Part B, Academic Press, New York, 1976.

WINDOW IN THE SKY (WITS) PROGRAM

INTRODUCTION

Theoretical calculations and experimental measurements of atmospheric attenuation in the 10-1000 GHz range typically do not agree with each other. These calculations have been made using Van Vleck-Weisskopf or Gross line shapes and considering only transition frequencies within the 10-1000 GHz region.

The purpose of the WITS program is to determine whether a more accurate theoretical prediction results when all the transition frequencies of H_2O and O_2 between 1 μm and the far infrared are included in the calculation. In the paragraphs below, the theory and procedure for calculating the attenuation from the AFCRL tape is discussed. Depending on the results, techniques for evaluating the calculations will occur in another report.

II. THEORY

"If da is the amount of matter per cm^2 along the direction in which the intensity is defined, then, by Lambert's law, the change of intensity in traversing this infinitesimal path is

$$dI_v \text{ (extinction)} = -e_v I_v \, da \tag{1}$$

The constant of proportionality, e_v, is the extinction coefficient "Since all processes are linear, the extinction coefficient can be expressed on the sum of an absorption coefficient (k_v) and a scattering coefficient (s_v):

$$e_v = +k_v + s_v \text{ ."} \tag{2}$$

In the WITS program, we are interested in attenuation due to absorption only. Thus, we have

$$dI_v = -k_v I_v \, da. \tag{3}$$

To calculate the attenuation of energy at frequency v in units of db/km, we must know the number of molecules/cm^2 in a column of air 1 km long having a cross-section 1 cm^2 as shown below

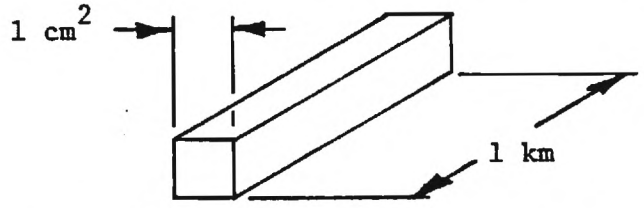

and the absorption coefficient, k_v, at that frequency. Having that data we calculate the attenuation from the equation

$$\text{attenuation (in db/km)} = -10 \log \left| {}^{dI_v}/_{I_v} \right| = -10 \log (k_v \, da). \qquad (4)$$

The absorption coefficient, k_v, is given by

$$k_v = \sum_{lm} (k_v)_{lm} \qquad (5)$$

where $(k_v)_{lm}$ in the absorption coefficient at frequency v due to the (lm) transition. $(k_v)_{lm}$ can be calculated using the Lorentz line shape from the equation

$$(k_v)_{lm} = \frac{1}{\pi} \frac{S \alpha}{(v-v_o)^2 + \alpha^2} \, d\alpha, \qquad (6)$$

where

S = the intensity per absorbing molecules (cm^{-1}/molecule -cm^{-1})
α = the line half-width at half maximum (cm^{-1})
ν_o = transition frequency (in cm^{-1})
ν = frequency at which attenuation is being calculated (in cm^{-1})
da = number of molecules/cm^2 in the air column of interest.

III. PROCEDURE FOR CALCULATING ATTENUATION AT AN ARBITRARY FREQUENCY ν

A. Calculate da for H_2O

Assuming a water vapor content of 7.5 grams/m^3, we ask how many grams/cm^2 exist in a column of air 1 km long x 1 cm^2. The appropriate equation is

$$\text{no. of grams/cm}^2 = \text{no. of grams in the 1 km column}$$
$$= 7.5 \frac{\text{grams}}{\text{m}^3} \times \text{volume of column}$$
$$= \left(7.5 \frac{\text{grams}}{\text{m}^3}\right)\left(.1\ \text{m}^3\right) \tag{7}$$
$$= .75\ \text{grams/cm}^2$$

From p. 5 in the AFCRL pamphlet we have the relation

$$1\ \text{g/cm}^2 \text{ of } H_2O = 3.34 \times 10^{22}\ \text{molecules/cm}^2. \tag{8}$$

Hence, the number of molecules of H_2O per cm^2 in the 1 km column is given by

$$da_{H_2O} = \left(.75 \frac{\text{grams}}{\text{cm}^2}\right)\left(\frac{3.34 \times 10^{22}\ \text{molecules/cm}^2}{1\ \text{g/cm}^2 \text{ of } H_2O}\right) \tag{9}$$

$$= 2.5 \times 10^{22}\ \text{molecules/cm}^2.$$

B. Calculate da for O_2

We need to find da_{O_2} at 296°K and atmospheric pressure. We know that at STP, 1 mole of an ideal gas occupies 22415 cm^3 and that one mole of a substance contains Avogadro's number, 6.02×10^{23}, of molecules. Hence, the number of molecules/m^3 of an ideal gas at STP is given by

$$\text{no. of molecules (STP) per unit volume}$$
$$= \frac{6.02 \times 10^{23}\ \text{molecules}}{22{,}415\ \text{cm}^3}\left(\frac{100\ \text{cm}}{1\ \text{m}}\right)^3$$
$$= 2.686 \times 10^{25}\ \text{molecules/m}^3 \tag{10}$$

However, the mole fraction of O_2 in the atmosphere is .20, so that the number of molecules of O_2 per m^3 is given by

$$\text{no. of molecules (STP) of oxygen per unit volume}$$
$$= (\text{no. of molecules (STP) of air per unit volume}) \times (\text{mole fraction of } O_2)$$
$$= (2.686 \times 10^{25})\ (.2)$$
$$= \frac{5.37 \times 10^{24}\ \text{molecules of } O_2 \text{ (STP)}}{3} \tag{11}$$

We now need to calculate the number of molecules of O_2 at 296°K and atmospheric pressure. To see how this calculation is done, recall the perfect gas law,

$$PV = nRT \tag{12}$$

From which we can see that

$$\frac{n}{v} = \frac{\text{no. of moles}}{\text{volume}} = \frac{P}{RT} \tag{13}$$

However, at constant pressure (atmospheric pressure in our case), the number of molecules per unit volume is given by

$$\frac{\text{no. of molecules}}{\text{volume}} \alpha \frac{n}{v} \alpha \frac{P}{RT}$$

$$= K/T \text{ (for cst. pressure)}, \tag{14}$$

where K is some constant. Thus,

$$\frac{\dfrac{\text{no. of molecules of } O_2 \text{ at 296°K and atmospheric pressure}}{m^3}}{\dfrac{\text{no. of molecules of } O_2 \text{ at STP}}{m^3}} =$$

$$= \frac{K/296}{K/273} = \frac{273}{296}, \tag{15}$$

or

$$\frac{\text{no. of molecules } O_2 \text{ at 296°K and atmospheric pressure}}{m^3}$$

$$= \frac{273}{296} = 5.37 \times 10^{24}$$

$$= 5 \times 10^{24} \; O_2 \text{ molecules/m}^3 \tag{16}$$

From eqns 11 & 15.

Now since a column of air 1 km long by 1 cm^2 has a volume of .1 m^3, therefore

$$da_{O_2} = (.1\ m^3)\ \frac{5.0 \times 10^{24}\ \text{molecules}}{m^3}$$

$$= 5.0 \times 10^{23}\ \frac{\text{molecules}}{cm^2} \qquad (17)$$

C. Read Data from ARCRL Tape

"A standard computer format was adopted for card or card-image input and is outlined below, the number between vertical lines representing the column on an IBM card, and the letter-number combination representing the computer format.* The first four columns are: ν = frequency in wavenumbers, S = line intensity in cm^{-1}/molecule - cm^{-2} at 296°K, α = half-width in cm^{-1} - atm^{-1} at 296°K, E "= energy of the lower state expressed in wavenumbers."[c]

ROTATION AND VIBRATION

ν	S	α	E"	ID	DATE	ISOTOPE	MOLECULE
1-10	11-20	21-25	26-35	36-70	71-73	74-77	78-80
F10.3	E10.3	F5.3	F10.3	5A6, A5	I3	I4	I3

*"In the far infrared (ν < 100 cm^{-1}) a different format (F10.6) was occasionally chosen for frequencies where high accuracy microwave measurements are available."[3]

For our purposes it is sufficient to use the following data from a card: ν, S, α, isotope, molecule. Further, we are interested only in water and O_2 in their most abundant isotopic form. A chart indicating the necessary coding immediately follows:

MOLECULE	MOST ABUNDANT ISOTOPE	CODE FOR ISOTOPE	IDENTIFICATION NUMBER
H_2O	$^1H\ ^{16}O\ ^1H$	161	1
O_2	$^{16}O\ ^{16}O$	66	7

D. Calculating the Attenuation

Recalling eqns 5 & 6, it will be seen that for each frequency at which the attenuation will be calculated each card or card image will have to be read. If the card image refers to $^1H\ ^{16}O\ ^1H$, then (kv)lm for H_2O will have to be calculated and added to other (kv)lm from water lines. A similar procedure will be followed for the $^{16}O\ ^{16}O$ lines.

After all the card images have been read, then (kv)lm for water will be added to (kv)lm for O_2:

$$(kv)_{Total} = (kv)_{H_2O} + (kv)_{O_2}. \tag{18}$$

Finally, using eqn. 4 the attenuation in db/km at freq. v will be determined. The attenuation will be calculated for all frequencies in the range [10,1000] GHz over an approximately fine grid. (See Bob McMillan or Alex Cook.)

E. Flow Chart for Calculating Attenuation (appears on the following two pages).

FLOW CHART

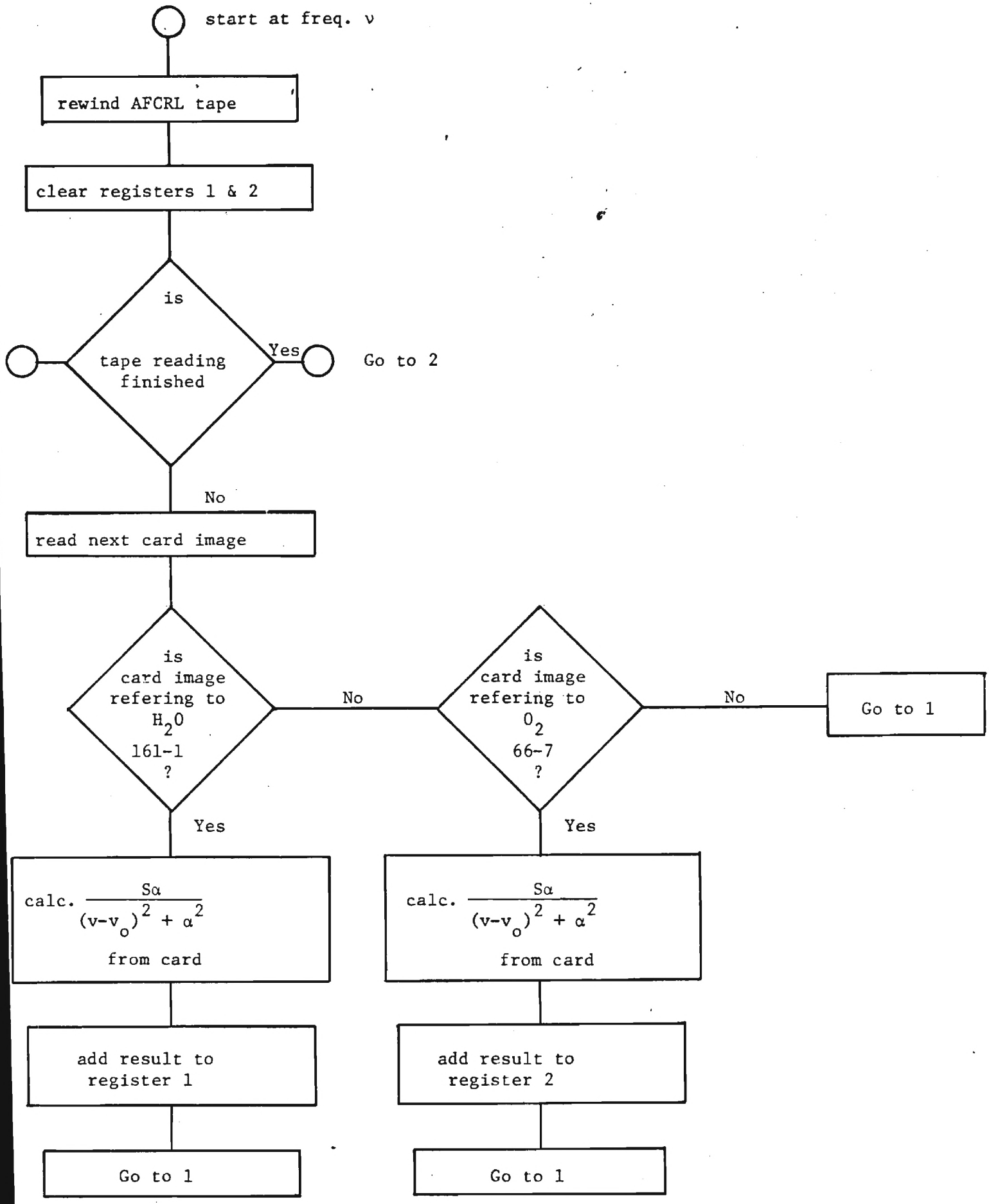
start at freq. ν
rewind AFCRL tape
clear registers 1 & 2
is tape reading finished
Yes
Go to 2
No
read next card image
is card image refering to H_2O 161-1 ?
No
is card image refering to O_2 66-7 ?
No
Go to 1
Yes
Yes
calc. $\frac{S\alpha}{(\nu-\nu_o)^2 + \alpha^2}$ from card
calc. $\frac{S\alpha}{(\nu-\nu_o)^2 + \alpha^2}$ from card
add result to register 1
add result to register 2
Go to 1
Go to 1

FLOW CHART (continued)

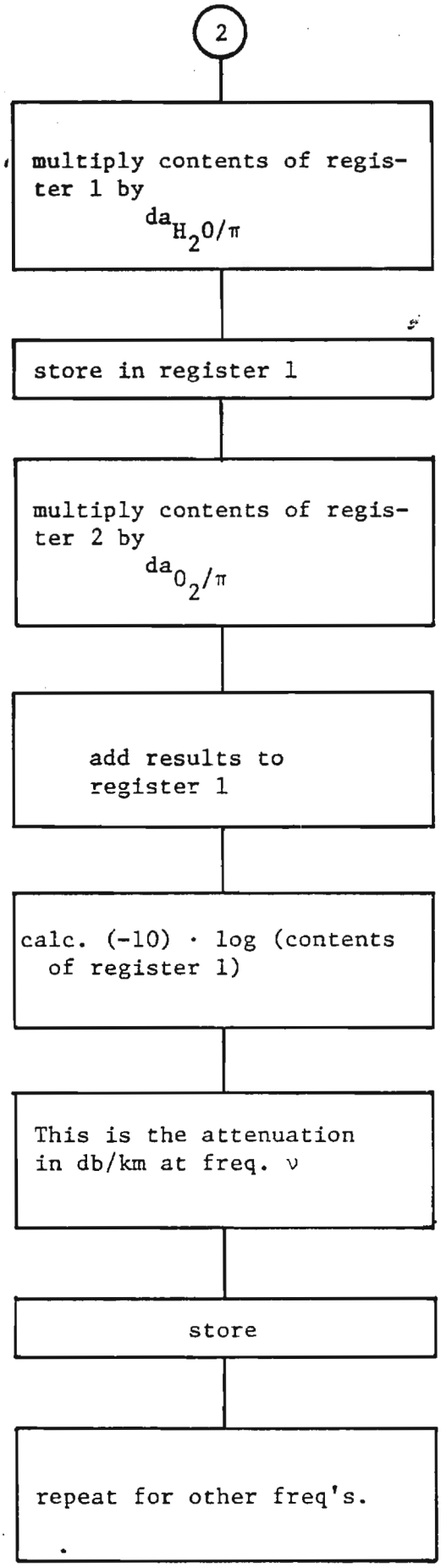

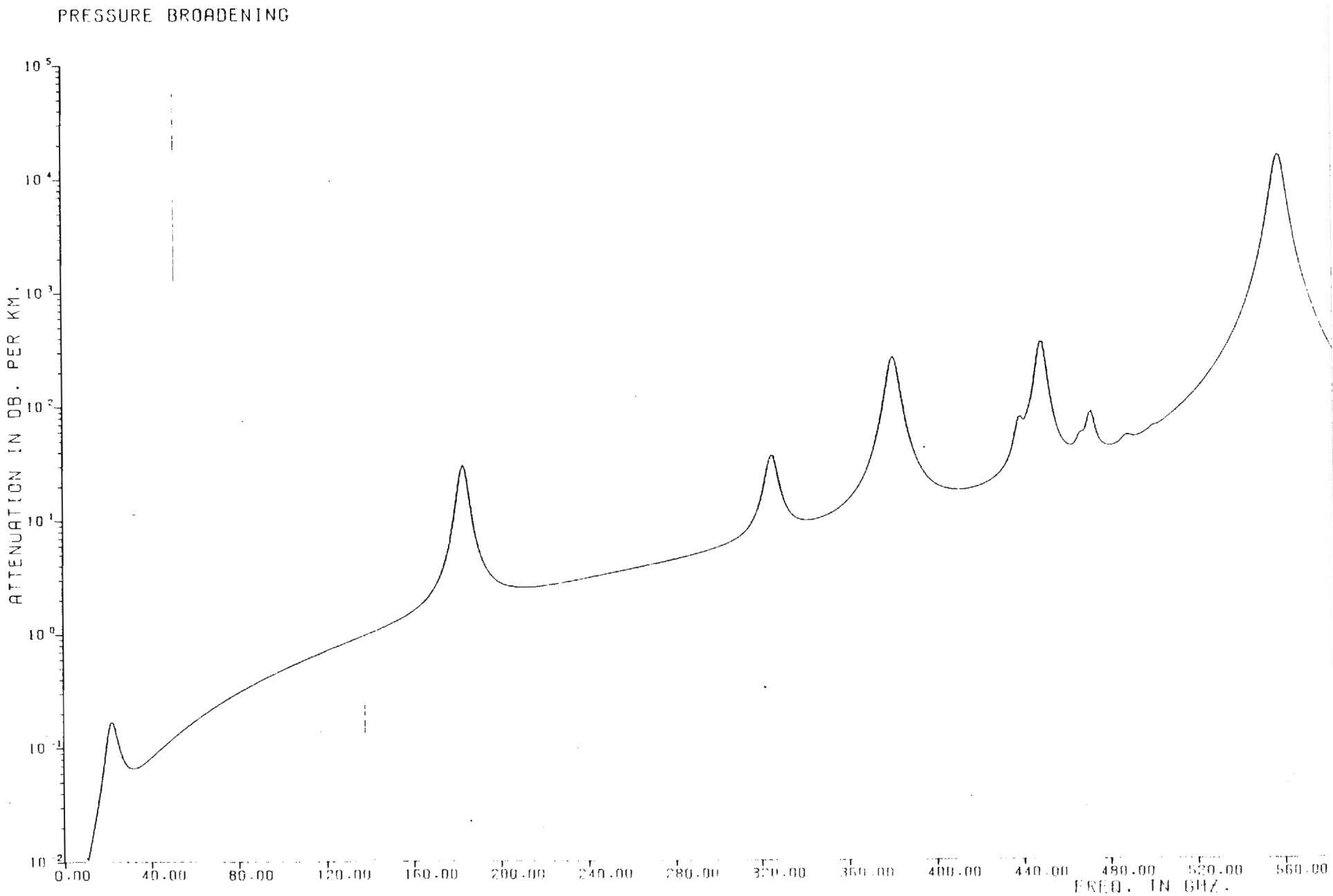
PRESSURE BROADENING
ATTENUATION IN DB. PER KM.
10^{5}
10^{4}
10^{3}
10^{2}
10^{1}
10^{0}
10^{-1}
10^{-2}
0.00
40.00
80.00
120.00
160.00
200.00
240.00
280.00
320.00
360.00
400.00
440.00
480.00
520.00
560.00
FREQ. IN GHZ.

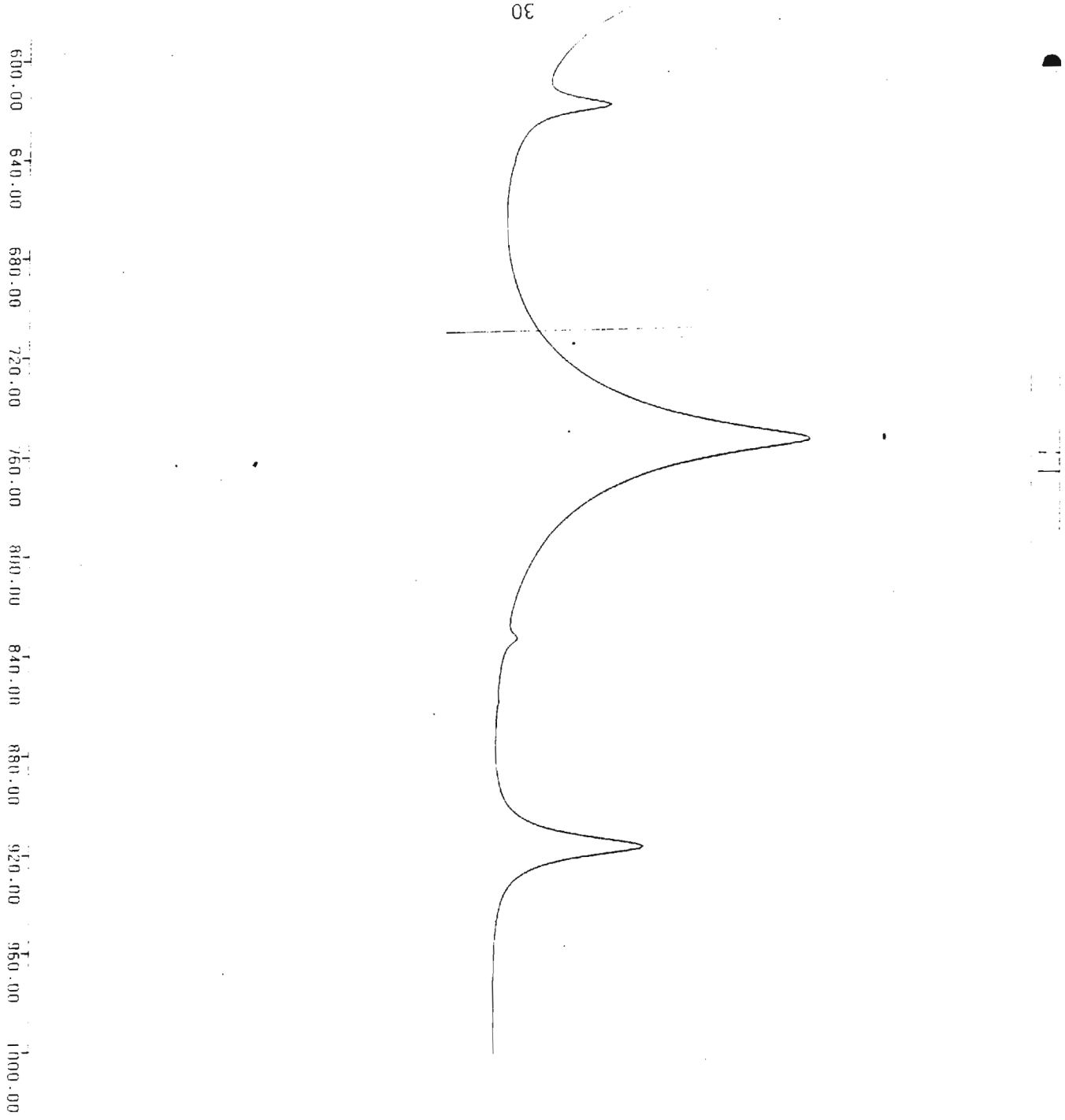

PLOT: 2.882 FEET. 5.053 MIN. 10.23.53 77/05/31

P = 1013 mb
T = 300° K
FL = 10 GHz
FU = 1000 GHz
water calculation with empirical correction term, but without Doppler broadening

PRESSURE BROADENING

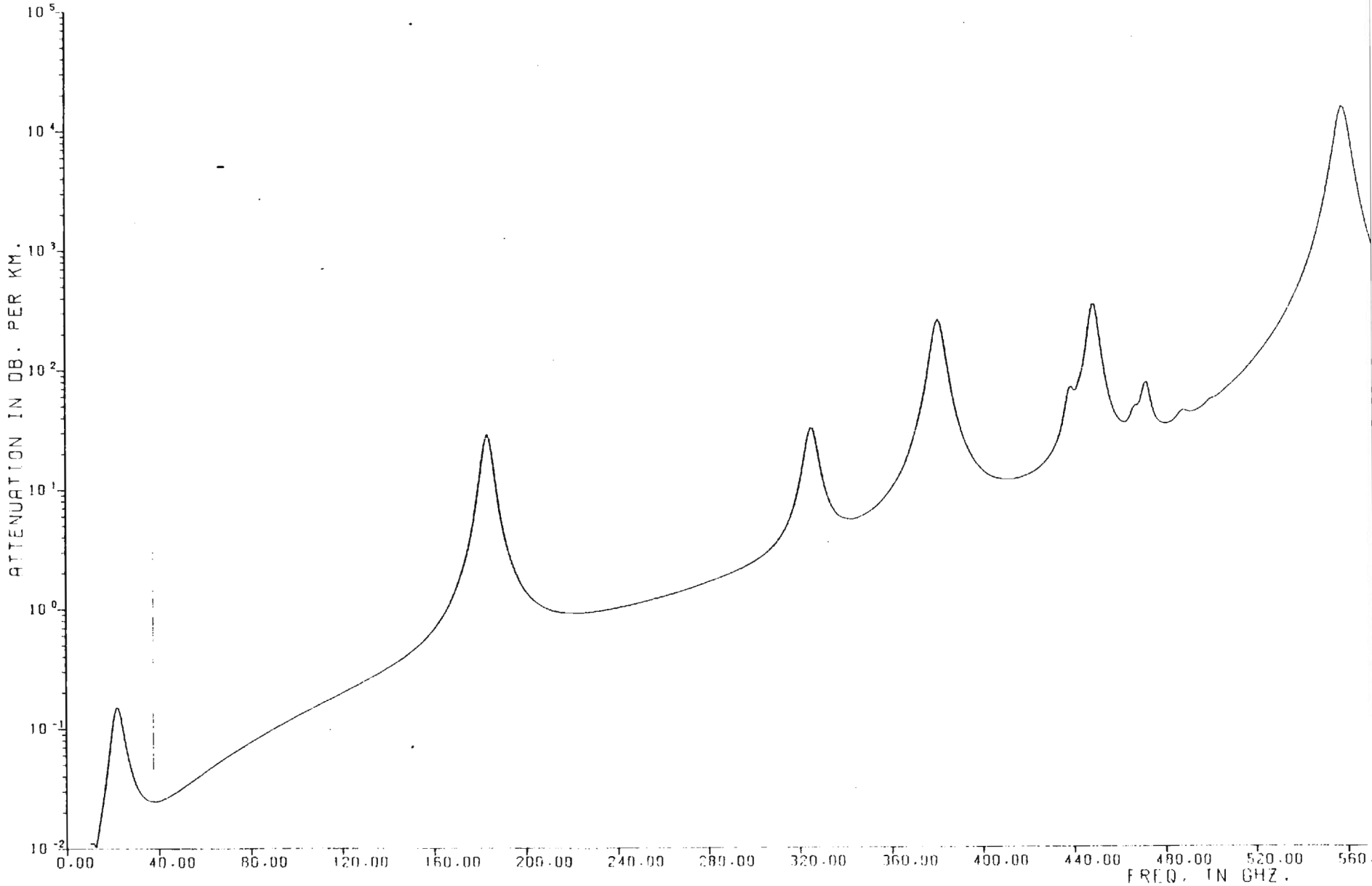

PLOT: 2.882 FEET. 5.053 MIN. 10.03.15 77/06/01

β = 1013 mb
T = 300°K
ρ_w = 10 GHz
ρ_d = 1000 GHz

Waltz's calculation with and empirical correction term A_{ν_0} with and Doppler Broadening.

REFERENCES

1. Goody, R. M., Atmospheric Radiation Oxford, Claredon Press 1964, p. 24.

2. Goody, R. M., Atmospheric Radiation Oxford, Claredon Press 1964, p. 26.

3. McClatchey, R. A. et al, "AFCRL Atmospheric Absorption Line Parameters Compilation", AFCRL-TR-73-0096 (26 January, 1973), p. 6.

APPENDIX IV

MATERIALS FOR LOW NOISE SCHOTTKY BARRIER CONVERTERS AT SUBMILLIMETER WAVELENGTHS

M. D. Blue
Georgia Institute of Technology
Atlanta, Georgia 30332

and

G. T. Wrixon
University College
Cork, Ireland

ABSTRACT

The prospects for realization of low noise coherent detectors in the 25 μm - 100 μm region are critically assessed. Use of high efficiency Schottky-barrier converters can be extended to the submillimeter region through the use of appropriate diode materials.

INTRODUCTION

Possible development of Schottky-barrier diode mixers optimized for operation in the submillimeter-far infrared wavelength region will require improvements in several areas such as material technology and packaging. Provision should be made for cooling the diode in order to minimize noise. We consider here the potential for extending operation to shorter wavelengths through reduction of parasitic loss obtained by the use of alternative semiconducting compounds.

A low noise temperature and a high frequency cut-off are desired. Small diameters have been found to be of limited value because of the deleterious effects of high current density on both noise and conversion loss performance. Therefore, thin layer epitaxial technology will be essential to extract maximum performance and minimize loss for a given material. The performance of a submillimeter wave receiver employing a Schottky-barrier mixer cooled to a temperature near 50°K could be expected to provide a significantly lower NEP than is obtainable from cryogenic bolometers as well as the capability of GHz bandwidth operation.

The high frequency performance of Schottky-barrier diodes is limited by the barrier capacitance, C_j, and the series resistance, R_s. The barrier or depletion-layer capacitance effectively shunts the non-linear diode resistance R_j. In an epitaxial diode, the resistance R_s arises from the undepleted portion of the epilayer under the metal plus the spreading resistance of the bulk material, and is in series with the parallel combination of R_j and C_j. Thus C_j allows current to by-pass R_j, while R_s is a source of signal and LO power dissipation, heat production, and excess diode noise.

For a diode radius r_D, the dependences of C_j and R_s are $C_j \sim r_D^{\,2}$, $R_s \sim r_D^{\,-n}$, where n is typically one for material with uniform properties, but may approach a value of 1.5 for epitaxial material and small diode diameters.

The diode cut-off frequency $f_c = (2\pi R_s C_j)^{-1}$ has been found to be a reliable indicator of high frequency performance if $R_s < 10\ \Omega$. Under this condition, $f_c \sim r_D^{\,-m}$ where typically $0.5 < m < 1$ depending again on material and epilayer properties.

The I-V characteristic of a Schottky diode for $I >> I_s$ may be written [1]

$$I = I_s \exp (V/V_o) \tag{1}$$

$$V_o = (E_{oo}/q) \coth (E_{oo}/kT) \tag{2}$$

$$E_{oo} = qh\,(N/4\varepsilon m^*)^{1/2} \tag{3}$$

where N is the semiconductor carrier concentration, m* is the carrier effective mass, and ε is the dielectric constant.

Under most operating conditions, the principal source of noise from a Schottky diode is shot noise. For this case, the available noise power for bandwidth B is

$$P_N = qIR_jB/2$$

where

$$R_j = (dI/dV)^{-1} \sim V_o/I$$

The equivalent noise temperature of the diode limited by shot noise may be shown to be

$$T_{eq} = qV_o/2k \tag{4}$$

For simplicity we have assumed a nearly perfect trap-free metal semiconductor interface. Under the doping conditions desired, dielectric relaxation effects will not be significant, and full shot noise is possible.

It can be seen from equations (2) and (4) that reducing the diode's physical temperature will reduce T_{eq} until V_o becomes temperature independent at $V_o = E_{oo}/q$. At this temperature field emission dominates the conduction process giving a minimum noise temperature of

$$T_{eq} = E_{oo}/2k = (qh/2k)\ [N/4\varepsilon m^*]^{1/2} \tag{5}$$

SCHOTTKY-BARRIER DIODE PARAMETERS

The parameters of interest are T_{eq} from (5), C_j, R_s, and f_c given by

$$C_j = (\pi r_D^{\,2})\ [q\varepsilon\ N/2V_B]^{1/2} \tag{6}$$

$$R_s = (Nq\mu)^{-1}\ (4r_D)^{-1} \tag{7}$$

$$f_c = (2\pi R_s C_j)^{-1} \tag{8}$$

where V_B is the barrier potential, and μ is the carrier mobility.

In equation (6) we have taken the bias voltage and signal voltage which reduce V_B and increase barrier capacitance under forward bias to be zero, and neglected a contribution from the mobile carriers which will be small for the operating conditions of interest.

Equation (7) is taken from Holm [2] and assumes uniform resistivity in the semiconductor. For epitaxial material, a satisfactory estimate of series resistance across a region of varying resistivity can be obtained by approximating the resistance variation in a stepwise manner, and then summing the resistance between consecutive equipotential surfaces.

As an example, we take a GaAs substrate with an electron concentration of 2.5×10^{18} cm^{-3} and a resistivity of 0.001 Ω cm. The epitaxial layer with electron concentration of 2×10^{17} cm^{-3} and a resistivity of 0.009 Ω cm is taken to be 0.1 μm thick, and only an undepleted layer thickness of 0.05 μm is assumed to contribute to the series resistance. The transition region

between epitaxial layer resistivity and bulk resistivity is assumed to be 0.2 μm, leading to a value of R_s = 6 Ω. The calculated series resistance is weakly dependent on the thickness assumed for the transition region under the epitaxial layer.

Equations (6), (7), and (8) indicate that the most useful material will have the largest value of $N^{1/2}V_B{}^{1/2}/\varepsilon^{1/2}$. For a given material, $\mu N^{1/2}$ can be maximized by doping. The mobility will be a strong function of carrier concentration, temperature, compensation, and crystal perfection. The maximum does not occur at the highest electron concentrations.

For GaAs, an electron concentration of 2 x 10^{17} cm^{-3} is near optimum, giving a value of T_{eq} = 23°K. For a 2 μm diameter diode, we obtain from (6) and (7), C_j = 4 x 10^{-15} F and R_S = 22 Ω. This value of series resistance is unacceptably high, and may be reduced using an epitaxial layer as described above. For an epitaxial layer with an electron concentration of 2 x 10^{17} cm^{-3} on a substrate with an electron concentration of 2 x 10^{18} cm^{-3}, the 6 Ω value calculated previously permits a f_c = 7 THz cut-off frequency or a 45 μm cut-off wavelength.

The diode diameter assumed in these calculations is 2 μm, near optimum as a further reduction in diameter raises the current density, increases the diode junction temperature, and increases R_s. Some improvement can be obtained by increasing the perimeter-to-area ratio of the device [4] in a manner somewhat analogous to emitter configurations in planar silicon power transistors.

However, the potential for improvement in performance through optimized geometry is limited. To reduce parasitic loss and extend operation to shorter wavelengths, other materials can be considered. The combination of small ε and large μ leads to consideration of the III-V and II-VI semiconducting compounds. The interesting compounds have electron mobility increasing as the energy gap decreases while ε remains constant to within a factor near two. The best performance should be obtainable with compound semiconductors having an energy gap near 0.1 - 0.4 eV and low temperature mobilities greater than 10^4 cm^2/V sec.

The calculated parameters for the materials of interest are shown in Table 1. Smaller gap compounds have smaller electron effective masses resulting in a higher value of T_{eq}. The largest uncertainty in these calculated quantities is the appropriate value of electron mobility for the temperature and carrier concentration of interest. We have attempted to choose values of N and μ maximizing $\mu N^{1/2}$ at T_{eq}[5, 6].

In order to compare materials with nearly equivalent fabrication technology, eventual availability of epitaxial technology was assumed for all materials listed in Table 1. An estimate of the series resistance, of epitaxial devices, R_ε, for various materials is made using the approach previously described for GaAs. The results are necessarily approximate, but provide an indication of potential performance. Metal contacts to n-type InAs are found to be ohmic, ruling out an otherwise interesting compound, while the lower mobility of the p-type materials makes their performance inferior to that expected from the n-type Schottky-barrier.

The calculated parameters are in accord with our expectations that improved performance over GaAs devices requires materials with smaller energy gaps. Of the two semiconducting compounds of greatest interest, InSb and HgCdTe, InSb appears to be the most interesting at this time because a sizeable amount of device technology has been developed, and because single crystal material of uniform resistivity is available. The lack of single crystal wafers and absence of data concerning Schottky-barrier performance are limitations to development of HgCdTe devices. For the purpose of this analysis, we have assumed a barrier height of 0.08 ev and electron mobility of 3.5×10^5 cm^2/V sec which corresponds to an energy gap of 0.12 eV. The potential performance of both these materials is superior to that of GaAs.

The continual improvement in heterocrystal technology in III-V compounds offers the possibility of another degree of freedom in material selection. Thus, a thin epitaxial layer of one III-V compound on a high conductivity substrate of a different III-V compound could permit a higher f_c and a lower T_{eq} than would be possible using a single III-V material. For a specific example, a high quality Au-GaAs barrier combined with the high conductivity of InSb could provide reduced parasitic loss and lower noise from cryogenic temperatures to room temperature than a Au-GaAs device with epitaxial construction.

The combination of the larger effective mass and higher barrier height in GaAs with the higher mobility of InSb is responsible. An estimate of the performance of such a heterocrystal Schottky-barrier diode is given in Table 1. Realizable performance of heterocrystal Schottky-barrier diode is given in Table 1. Realizable performance of heterocrystal diodes will be very dependent on the perfection of the epitaxial material and strain effects introduced from mismatch in lattice constants and thermal expansion coefficients. Clearly, there are many problems to be resolved for heterocrystal mixers.

Much of the current heterocrystal research has been stimulated by a desire to obtain improved efficiency from light emitting diodes and increased reliability from the double heterostructure GaAs-$Al_xGa_{1-x}As$ room temperature laser. Liquid phase epitaxy, vapor phase epitaxy, and molecular beam epitaxy are used to create heterocrystal device structures. Current problems include surface pits, stacking faults, and undesired impurities [7].

CONCLUSION

Our results indicate the potential for extending ultra-low noise Schottky-barrier mixer technology into the submillimeter wavelength region and perhaps to the LWIR. A well developed technology will be required for high quality expitaxial layers (or ion implanted layers), effective surface passivation, and low leakage currents.

A receiver incorporating such diodes offers high sensitivity and wide bandwidth in a wavelength region currently dominated by thermal detectors. The optimum operating temperature for a submillimeter converter appears from equations (2), (5), and Table I to lie between 20°K and 60°K. Temperatures near that of liquid helium will not be required.

REFERENCES

1. F. A. Padovani and R. Stratton, Solid State Electronics 9, 695 (1966).
2. Ragnar Holm, Electric Contacts Handbook, Springer-Verlag, Berlin (1958), p. 17-18.
3. Gerard T. Wrixon, IEEE Trans. on Microwave Theory and Techniques, MTT-24, 702 (1976).
4. Gerard T. Wrixon, IEEE Trans. on Microwave Theory and Techniques, MTT-22, p. 1159, (1974).
5. S. M. Sze, Physics of Semiconductor Devices, Wiley-Interscience, New York (1969).
6. C. Hilsum and A. C. Rose-Innes, Semiconducting III-V Compounds, Pergamon Press, New York (1961).
7. 1974 Proc. 5th Int. Symp. Gallium Arsenide and Related Compounds, The Institute of Physics, London and Bristol (1975).

TABLE I. CALCULATED PARAMETERS FOR SCHOTTKY-BARRIER DIODES*

DIODE MATERIAL	DOPING cm^{-3}	T_{eq} °K	C_j pF	R_ε Ω	f_c Hz	λ_c μm
GaAs	2×10^{17}	23	0.004	6	6.6×10^{12}	45
Si	10^{17}	21	0.003	39	1.4×10^{12}	220
GaP	10^{17}	34	0.002	89	0.9×10^{12}	336
InP	2×10^{17}	56	0.005	5	6.2×10^{12}	48
InSb	3×10^{16}	40	0.004	2	20×10^{12}	15
HgCdTe	10^{16}	28	0.003	2	27×10^{12}	11
GaAs-InSb	2×10^{17}	23	0.004	3	13×10^{12}	23

*Calculations assume a diode diameter of 2 μm. An undepleted epitaxial layer thickness of .005 μm with a transition region thickness of 0.25 μm is assumed except for silicon where the value is taken to be 0.05 μm. Substrate electron concentration is assumed near 10^{19} cm^{-3}.

APPENDIX V

SUBMILLIMETER COMPONENTS

One of the major efforts of this grant involves the determination of submillimeter receiver characteristics. Initial efforts toward using an optically pumped laser as a local oscillator for a low noise receiver resulted in poor results. It was determined that these results were caused by low LO power and poor coupling of both signal and local oscillator to the mixer. Since then, efforts have concentrated on improved mixer configurations, low loss quasi-optical diplexers and improved local oscillator power from optically pumped lasers. Investigations have concentrated on 230 GHz as a working frequency. The mixers are also being assembled so that they can eventually be employed in the sub-harmonic mixing scheme when this technique is mastered at lower frequencies on a NASA Grant.

The following quasi-optical mixer schemes are being investigated:

1. An open structure quasi-optical mixer has been assembled from an existing structure which accepts LO and signal energy from orthogonal directions. In this mount, the incoming energy is focused by a lens onto the whisker contacting the diode. Each direction (LO and signal) has its own movable back-short. The device has been modified to use Schottky barrier diodes. A five-element Tchebyscheff filter has been constructed and inserted in the unit. This filter has the Schottky barrier mixer chip attached to it.

   In this mixer, the signal LO come from different directions so that there is no need for a diplexer. A single diode can be used or a harmonically pumped two diode mixer can be made; in the latter case, the diodes must be positioned to ensure correct phasing. The diodes should be λ_s apart in the direction in which the signal enters the structure, and $2\ \lambda_s$ apart in the direction in which the LO signal (at $\omega_{LO}/2$) enters the mixer; λ_s is the signal wavelength.

2. A biconical antenna mount has been designed and is being assembled. In this mount the incoming energy, both signal and LO come from the same directions in the form of collimated plane wave beams and are incident on the biconical antenna, each of whose cones are 6 λ long (at 230 GHz). The half cone angle θ is $\sim$ 13° which gives an input impedance of $\sim$ 112 Ω. The cones form part of a spherical structure, the upper cone, to which the whisker is soldered is a press-fit and the bottom cone tapers into the first element of the IF filter. The aperture diameter is .5" and a similar size section of the sphere is movable behind the diode to help in RF matching.

   The biconical mixer and its parts are shown in the sketches at the end of this appendix.

3. For use with this mixer a diplexer is required. If the mixer is a sub-harmonically pumped two diode mixer, a simple mesh Fabry-Perot resonator can be used to combine the LO and signal since they are so far apart in frequency.

If, however, the device is to work as a fundamental mixer a more sophisticated polarized interferometric diplexer will be required. This is shown in the sketch at the end of the Appendix and consists of 6 wire grids, two pairs of which form "quarter wave plates" that reflect incident radiation and rotate the plane of polarization 90°. Both grids consist of one set of horizontal and one set of vertical wires spaced $\frac{\lambda}{4}$ from each other. Grid C-C is a wire grid at 45° to the plane of the paper and D-D is a horizontal wire grid. If $\Delta = \frac{2}{\lambda} x$, where x is path length difference between A-A and C-C and B-B and C-C, then for a vertically polarized monochromatic beam incident on grid C-C <u>from point p</u>, the intensity of vertically polarized radiation leaving the interferometer at q is

$$I = \frac{Io}{2} (1 + \cos \Delta)$$

Thus at a fixed value of x, the intensity of vertically and horizontally polarized radiation at q due to a <u>broad band</u> vertically polarized beam at p is as shown.

Now if, as shown in the schematic of the diplexer, the signal inputs vertically, in band, as shown and the LO inputs horizontally out-of-band as shown, both will combine, vertically polarized, with a minimum of loss at the mixer. Wire grids can have reflections and transmission coefficients approaching 100% for the appropriate planes of polarization, from effectively zero frequency up to roughly a wavelength of 2d cms, where d cm is the spacing of the wires. Thus, for operation at 230 GHz, d ≃ .5 mm i.e. .02". These grids should thus be photolithographically etched on mylar backed copper sheets, .002" thick, .02" apart. Note that all six grids are the same type.

This diplexer configuration has been constructed. Currently, work is progressing on the making of grids. Two types of grids are being constructed. Sets of grids of metals on thin plastic substrates are being made while metal wire grids are being wound. A third type using copper sheets on mylar is being developed.

An optically pumped laser has been assembled for use as a local oscillator. Difficulties with a commercial CO_2 laser pump have been experienced in the stability of the source. The laser has been returned to the manufacturer; since receiving the laser back from the manufacturer, the stability appears improved. In the meantime, the optically pumped laser has operated with a CO_2 laser (at Emory University) constructed by Wayne Penn of this laboratory. The submillimeter wave output has been obtained from 2 CH_3OH lines. The CO_2 laser is grating tuned with 20-30 W output on the various lines. A similar laser is currently being constructed in this laboratory to serve as a pump laser in place of the 8 W commercial unit.

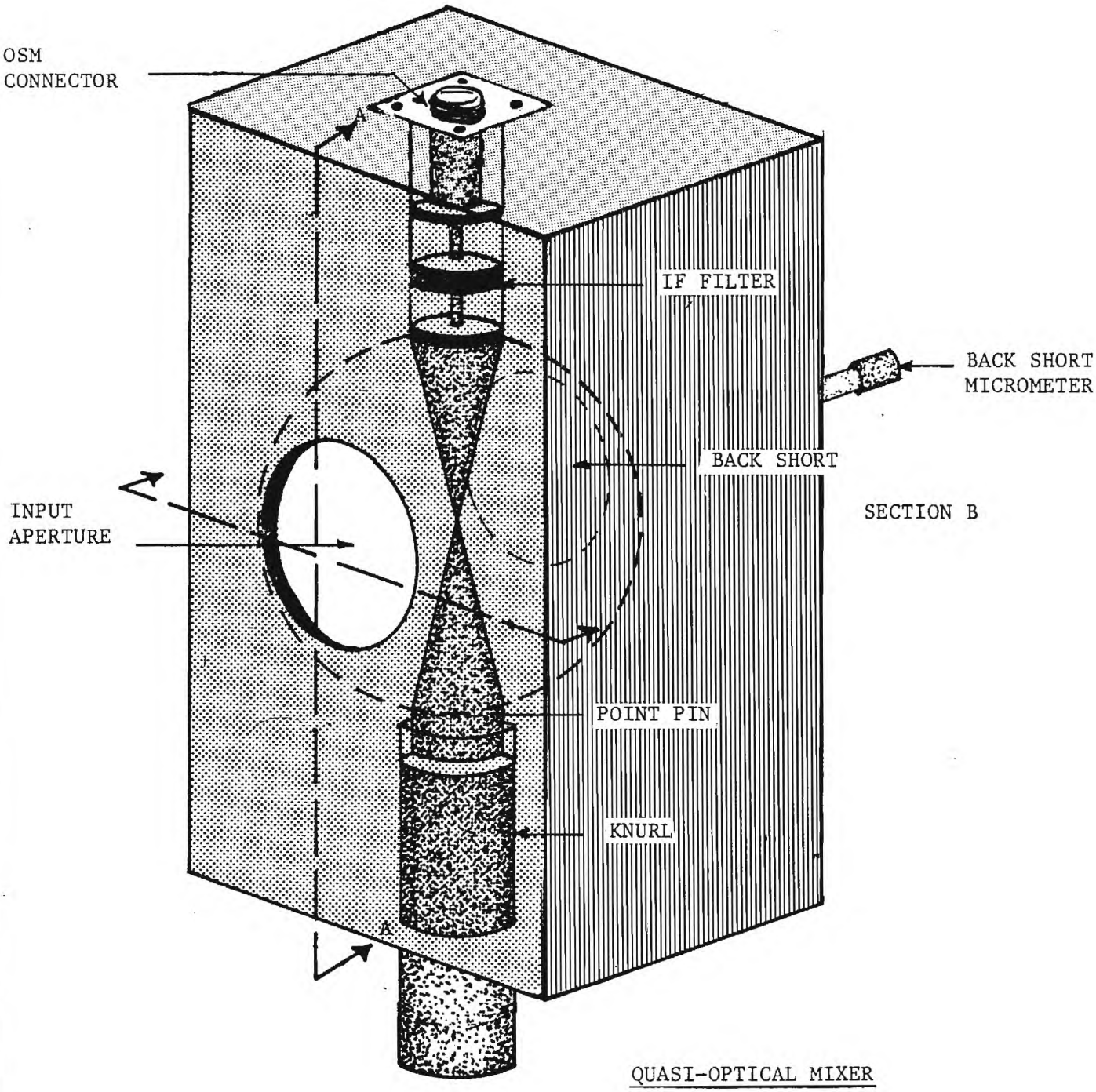

QUASI-OPTICAL MIXER

Overall View

Material Gold-Plated Brass

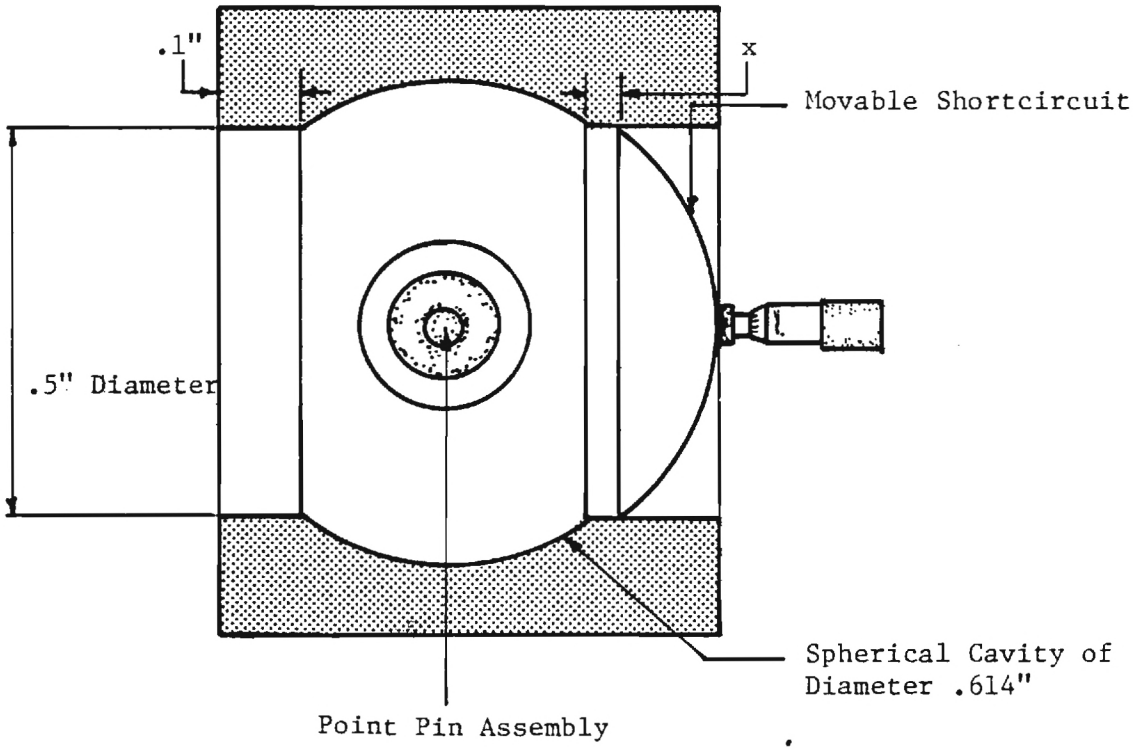
.1"
x
Movable Shortcircuit
.5" Diameter
Spherical Cavity of
Diameter .614"
Point Pin Assembly

SECTION B

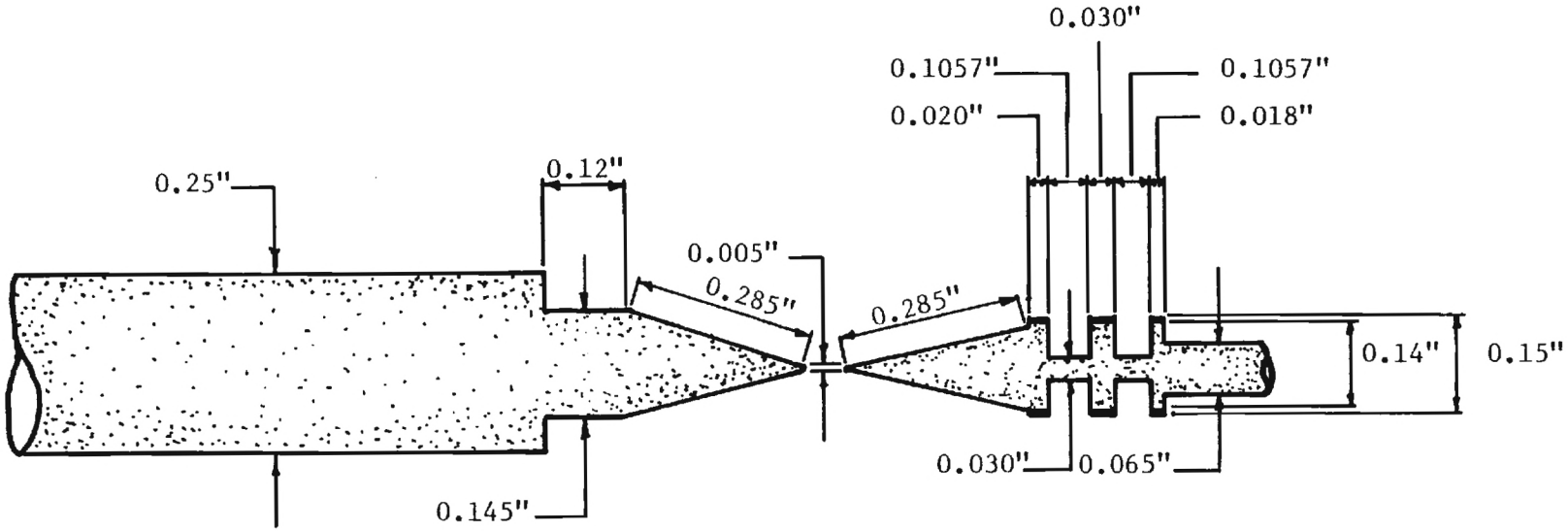

QUASI-OPTICAL MIXER

Point Pins
Not to Scale
Material Coin-Silver or Nickel

4/4

QUASI-OPTICAL MIXER

Diode Mount and IF Filter
Dimensions in inches (± .0005")
Material Coin-Silver or Nickel

For Insulating Section (dark) use
Bondmaster Epoxy E645

2/4

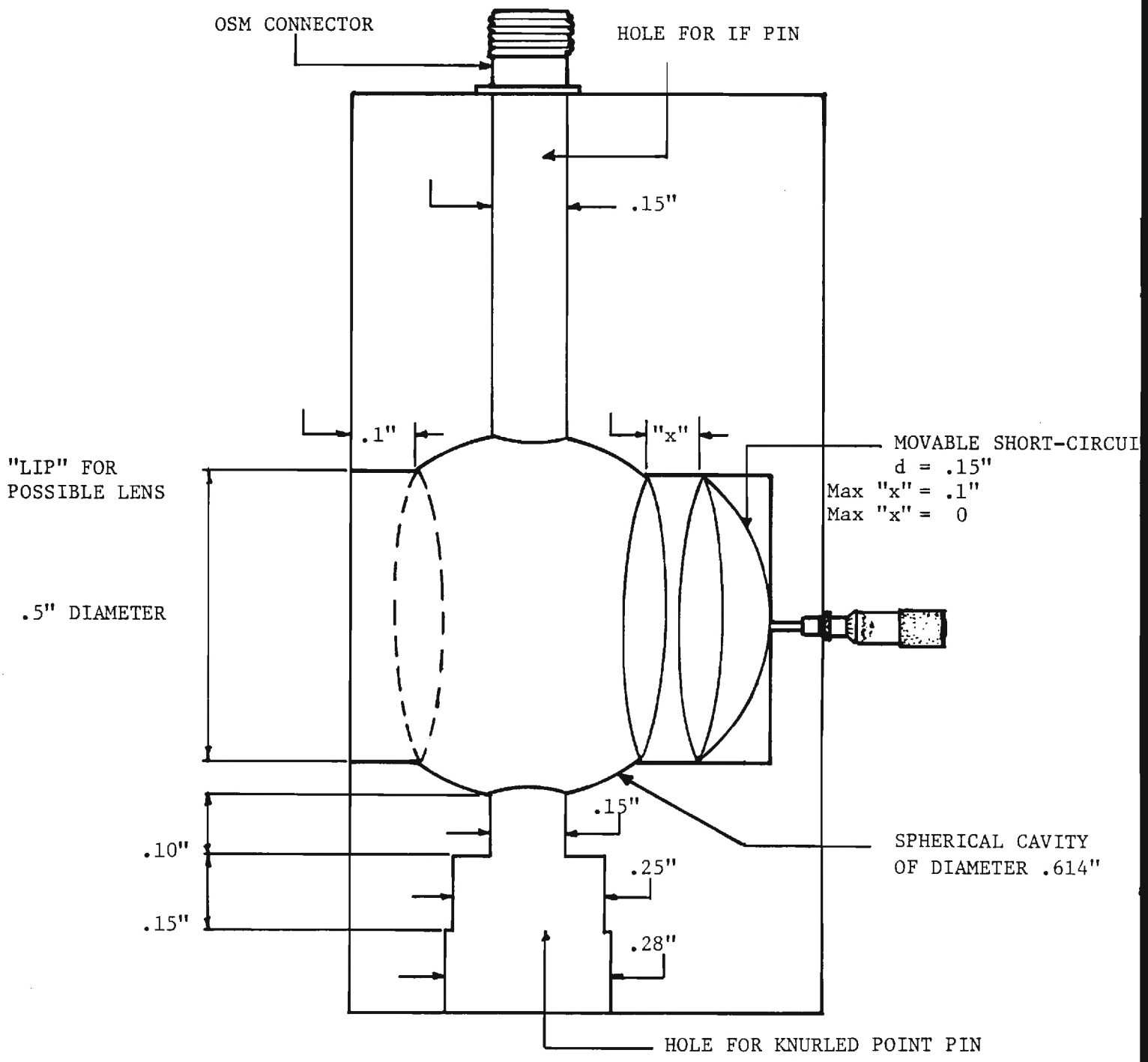

QUASI-OPTICAL MIXER

Section A-A (see 1/4)
Not to Scale
Material Gold-Plated Brass

CONSTRUCTION NOTES:

1. Mixer should be made in two halves, split along Section B (see drawing 1/4).
2. The lengths of the .065" diameter rod beyond the IF filter (joining it to the OSM connector) and of the .025" diameter portion of the point pin (beyond the knurled sections) should be only long enough for machined soundness and rigidity.
3. When fully in, the short circuit should form a continuous part of the spherical cavity (see drawing 3/4).

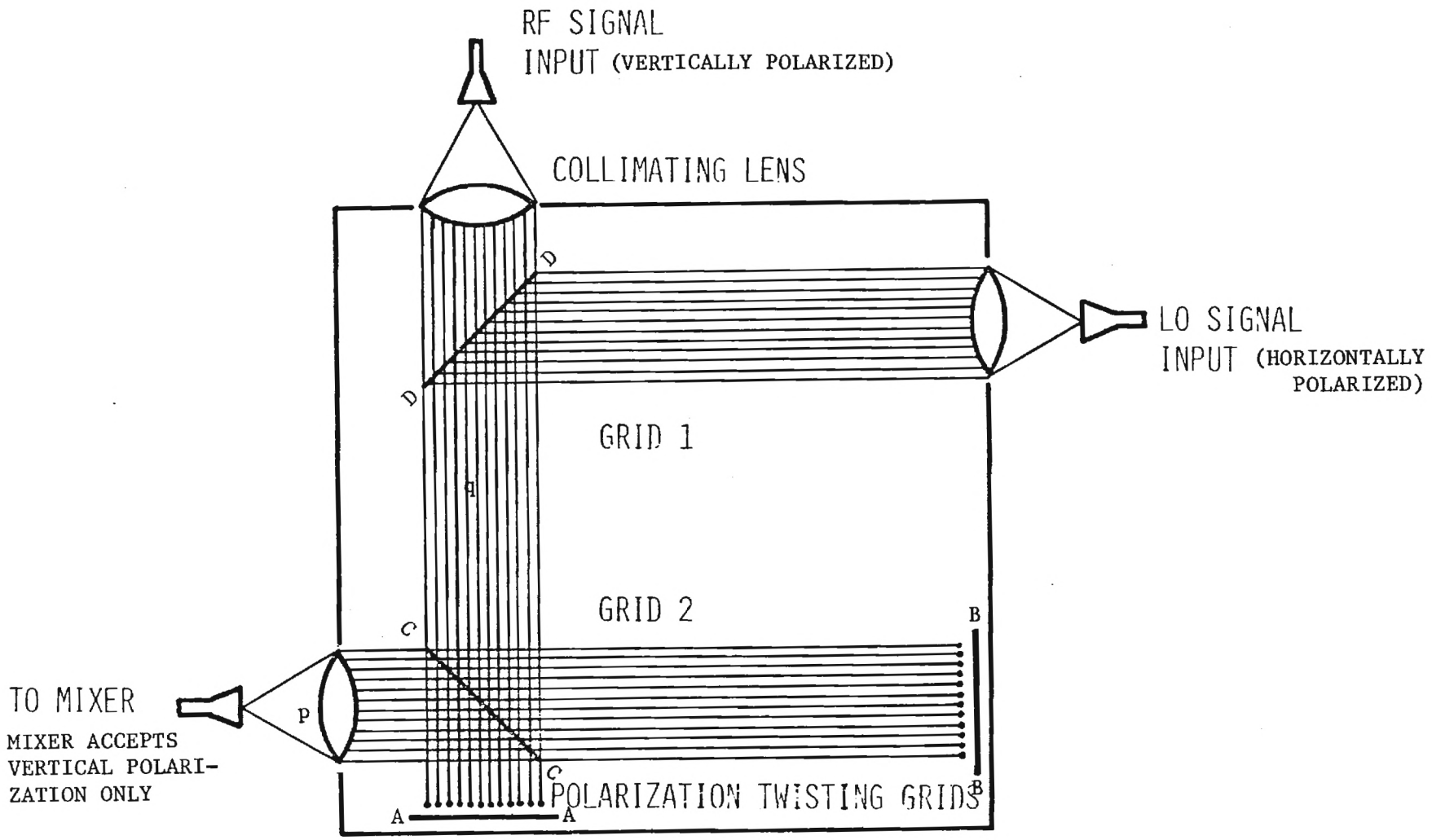

QUASI OPTICAL LO INJECTION DIPLEXER WITH COLLIMATING LENSES

APPENDIX VI

SPECTROSCOPIC OBSERVATIONS

The observation of water vapor absorption in the submillimeter wavelength region is important to the propagation requirements of systems applications in this spectral region. For the absorption measurements, two conventional spectroscopic schemes are being employed. The first method is employing a Fabry-Perot interferometer for observations in the atmospheric window regions, on the wings of the absorption lines and in the region of the absorption line centers. The second method employs an absorption cell of the conventional millimeter wave type to obtain values of line width parameters and line shapes as a function of pressure and temperature.

In addition to these absorption measurements, a parallel plate Stark cell has been assembled for measurements of dipole moments of H_2O from submillimeter wave transitions. Brief discussions of the status of each of these measurement programs are given below.

1. Fabry-Perot Interferometer Measurements

The measurements to be performed with the Fabry-Perot interferometer will cover the spectral region from 125 GHz to approximately 500 GHz, depending upon the availability of power sources to cover the higher frequency region. The apparatus currently being employed is shown in the block diagram of the accompanying figure. The Fabry-Perot interferometer is one which has been used by Frenkel and Wood. It has a Q-value on the order of 300,000. Modifications have been made to provide for temperature control, humidity measurements, and temperature measurements within the chamber.

An insulated water jacket encases the cell for heating and cooling of the walls. The apparatus for measurements of Q and amplitude of the resonator is shown in the block diagram. The third harmonic of a 24 GHz klystron provides markers for measurement of the Q. The klystron is phase-locked to a 5 MHz crystal oscillator to provide stability for the

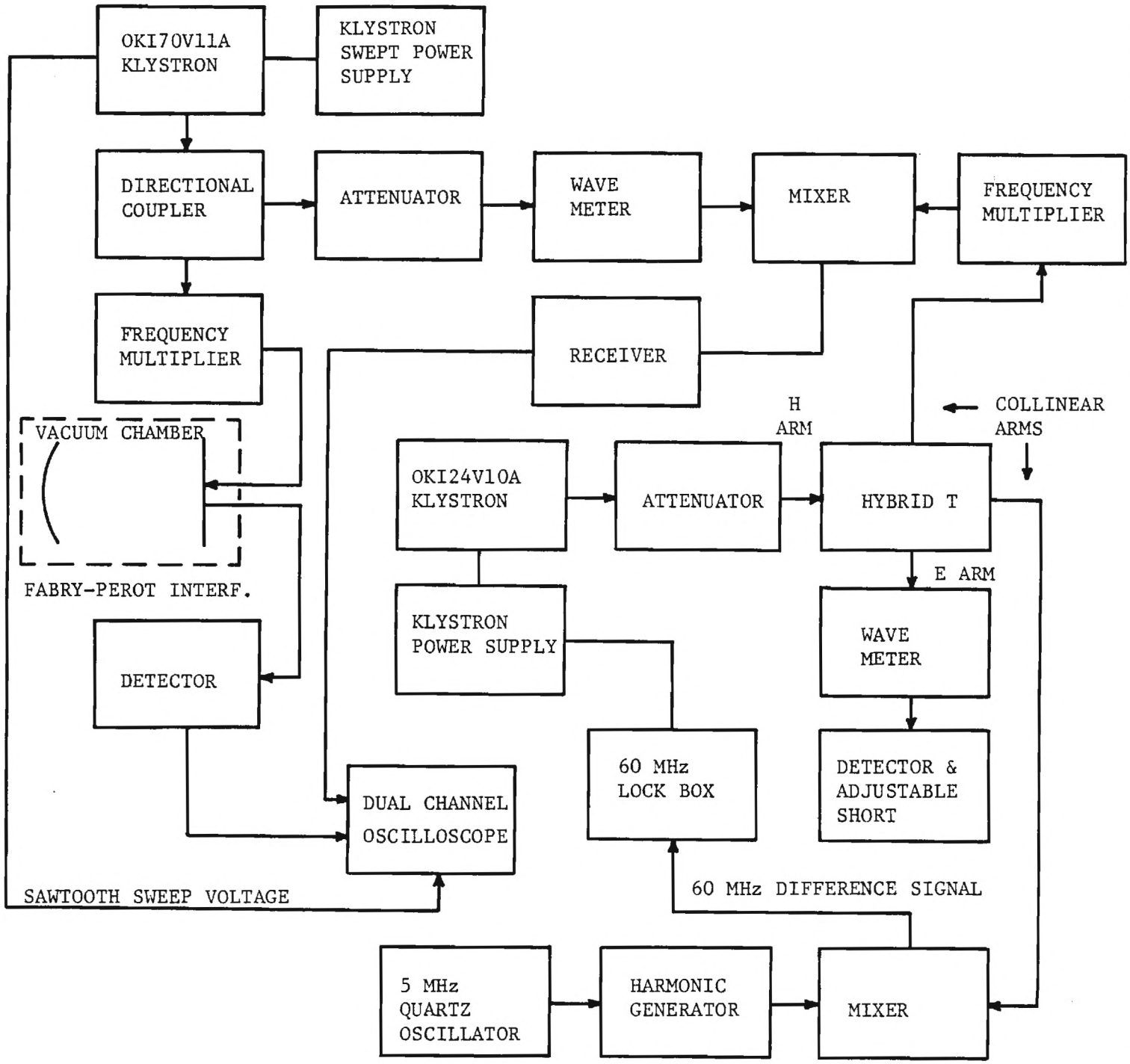

BLOCK DIAGRAM OF MEASUREMENT SYSTEM FOR
FABRY-PEROT INTERFEROMETER A-1861.

frequency markers. Measurements are currently being performed in the region of 140 GHz. The measurements consist of measuring the resonator Q and amplitude with the vapor in and out of the interferometer. The major effort thus far has consisted of achieving accurate frequency, amplitude and pressure values. When satisfactory, reproducible results are obtained, the measurements will be extended to higher frequencies.

The measurements employing the waveguide absorption cell are performed in the pressure-broadening line shape spectrometer shown in the diagram. This work has been delayed by failure of the klystrons which have been employed. Before the failure, however, suitable measurements have been demonstrated on the 183 GHz to insure that pressure-broadening observations can be performed. New klystrons are currently on order.

In order to provide suitable improvements in the measurement accuracy of pressure-broadening effects, a signal-averager is to be purchased. This will allow observation in both the interferometer and waveguide cell to be made with increased accuracy of the attenuation off the line center.

The following measurements are planned for the atmospheric absorption due to water vapor:

1. Absorption measurements every 500 MHz with the Fabry-Perot interferometer from approximately 120 GHz to 500 GHz. The water vapor pressure will range from approximately 10 mtorr to 24 torr. The measurements will be made for H_2O alone and in the presence of combinations of N_2 and O_2.

2. Absorption measurements using the waveguide absorption cell will be performed on H_2O lines in the range up to 500-600 GHz depending upon the availability of sources for harmonic generation. In addition to the measurements on the line, the waveguide cell will be employed for measurements in the wings of the line by taking advantage of the signal sensitivity provided by the signal averager.

3. Monochromatic measurements will be made by using the optically pumped source at individual frequencies throughout the spectrum. A White cell is available for these measurements. In addition, a 230 GHz IMPATT will be available as GFE from AFAL. Absorption

PRESSURE BROADENING-LINE SHAPE SPECTROMETER
FUNCTIONAL DIAGRAM

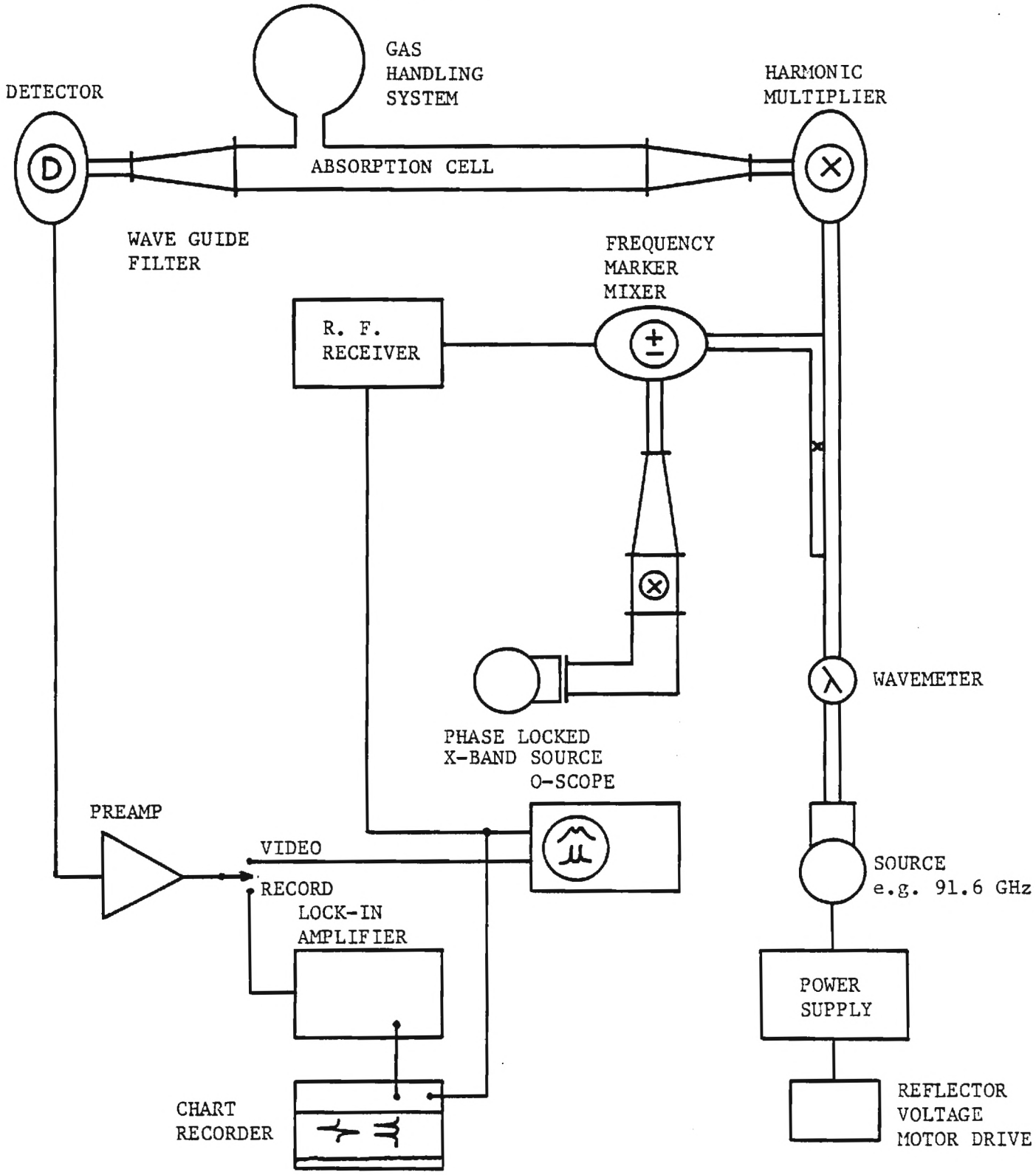

measurements will be compared with propagation measurements being made at EES and elsewhere.

4. A parallel plate Stark cell has been prepared for measurements of the water molecule dipole moment. The cell is fed by horns and lenses. Quartz spacers separate the parallel plates.

APPENDIX VII

MISCELLANEOUS RELATED TOPICS

The receiver research being performed on this grant provides supporting technology for receiver work at 230 GHz and 340 GHz currently being performed by Georgia Tech for MIRADCOM.

A report on long wavelength absorbing smokes and aerosols has been completed during this reporting period and currently a contract is being negotiated on experimental propagation through smokes in the near millimeter wavelength region. J. Gallagher has participated during this period in the HDL Panel Study on near millimeter wave technology. R. G. Shackelford and J. J. Gallagher have completed a study for MIRADCOM on a millimeter wave beamrider system; the results will be presented in a MIRADCOM report. J. J. Gallagher presented an invited paper on the impact of the atmosphere on submillimeter systems at a 1974 SPIE Seminar.

Current activities on an internally funded propagation range will provide data at wavelengths from 35 GHz through the visible region; spectroscopic data being obtained on this grant will support the results of the propagation studies.

A-1861

SECURITY CLASSIFICATION OF THIS PAGE (When Data Entered)

REPORT DOCUMENTATION PAGE		READ INSTRUCTIONS BEFORE COMPLETING FORM
1. REPORT NUMBER Fourth Semi-Annual Technical	2. GOVT ACCESSION NO.	3. RECIPIENT'S CATALOG NUMBER
4. TITLE (and Subtitle) Submillimeter Wave Spectroscopy and Technology		5. TYPE OF REPORT & PERIOD COVERED SEMI-ANNUAL 1 January - June 15, 1978
		6. PERFORMING ORG. REPORT NUMBER
7. AUTHOR(s) J. J. Gallagher & M. D. Blue		8. CONTRACT OR GRANT NUMBER(s) DAAG29-76-G-0280
9. PERFORMING ORGANIZATION NAME AND ADDRESS Engineering Experiment Station Georgia Institute of Technology Atlanta, Georgia 30332		10. PROGRAM ELEMENT, PROJECT, TASK AREA & WORK UNIT NUMBERS
11. CONTROLLING OFFICE NAME AND ADDRESS U. S. Army Research Office Post Office Box 12211 Research Triangle Park, N.C. 27709		12. REPORT DATE August 2, 1978 13. NUMBER OF PAGES
14. MONITORING AGENCY NAME & ADDRESS(if different from Controlling Office)		15. SECURITY CLASS. (of this report) Unclassified 15a. DECLASSIFICATION DOWNGRADING SCHEDULE N/A

16. DISTRIBUTION STATEMENT (of this Report)

Approved for public release; distribution unlimited.

17. DISTRIBUTION STATEMENT (of the abstract entered in Block 20, if different from Report)

N/A

18. SUPPLEMENTARY NOTES

The findings in this report are not to be construed as an official Department of the Army position, unless so designated by other authorized documents.

19. KEY WORDS (Continue on reverse side if necessary and identify by block number)

Submillimeter Waves; Schottky Barrier Diodes; Spectroscopy; Water Molecules; Fabry-Perot Interferometers; Electron Beam Sources; Heterodyne Receivers; Atmospheric Absorption.

20. ABSTRACT (Continue on reverse side if necessary and identify by block number)

Spectroscopic investigations have continued on atmospheric molecules in a large Fabry-Perot interferometer, a waveguide cell and a parallel plate Stark cell. Computer programs have been prepared with the capability for determining low pressure spectroscopic absorption, atmospheric absorption (horizontal) or vertical propagation characteristics. Work continues on receiver and mixer technology for the submillimeter wavelength region. Work on optically pumped lasers as receiver L.O.'s, quasi-optical devices and waveguide filters are continuing efforts.

DD FORM 1 JAN 73 1473 EDITION OF 1 NOV 65 IS OBSOLETE

SECURITY CLASSIFICATION OF THIS PAGE (When Data Entered)

PROGRESS REPORT

(TWENTY COPIES REQUIRED)

1. ARO PROPOSAL NUMBER: P-14104-PX

2. PERIOD COVERED BY REPORT: 1 January, 1978 - 15 June, 1978

3. TITLE OF PROPOSAL: Submillimeter Wave Spectroscopy and Technology

4. CONTRACT OR GRANT NUMBER: DAAG29-76-G-0280

5. NAME OF INSTITUTION: Georgia Institute of Technology
Engineering Experiment Station

6. AUTHOR(S) OF REPORT: J. J. Gallagher, M. D. Blue

7. LIST OF MANUSCRIPTS SUBMITTED OR PUBLISHED UNDER ARO SPONSORSHIP DURING THIS PERIOD, INCLUDING JOURNAL REFERENCES:

Papers presented at Third International Conference on Submillimeter Waves and Their Applications, University of Surrey, Guildford, England, March 29 - April 1, 1978; Paper presented at AGARD Conference, Munich, Germany 4 - 8 September, 1978. See attached abstracts and paper.

8. SCIENTIFIC PERSONNEL SUPPORTED BY THIS PROJECT AND DEGREES AWARDED DURING THIS REPORTING PERIOD:

J. J. Gallagher
O. A. Simpson
W. M. Penn
R. C. Rogers
P. B. Reinhart
J. H. Rainwater
C. H. Branch, Student

14104-PX

Dr. M. D. Blue
Dr. J. J. Gallagher
Georgia Institute of Technology
Engineering Experiment Station
Atlanta, GA 30332

SUBMILLIMETER WAVE SPECTROSCOPY AND TECHNOLOGY
FOURTH SEMI-ANNUAL TECHNICAL REPORT

J. J. Gallagher
M. D. Blue

August 2, 1978

U. S. ARMY RESEARCH OFFICE
Grant No. DAAG29-76-G-0280

GT/Project No. A-1861

Georgia Institute of Technology
Engineering Experiment Station
Electromagnetics Laboratory
Atlanta, Georgia 30332

BRIEF OUTLINE OF RESEARCH FINDINGS

During the past six month period, investigations were performed in the following areas of research:

1. spectroscopic measurements of atmospheric constituents by coherent millimeter wave techniques and laser schemes;
2. construction and testing of an optically pumped laser for use in receiver techniques and spectroscopic applications;
3. continued formulation of computer programs for both spectroscopic analysis and atmospheric propagation analysis;
4. development of a small Fourier spectrometer for both laboratory and field applications;
5. preparation for receiver studies;
6. investigation of liquid phase of water by reflection and transmission of submillimeter wave laser signals.

The research projects which are the tasks of this program are oriented toward topics of importance to the Army's growing interest in Near Millimeter Wave systems. Each of the above tasks can be shown to be related to Army requirements. The following brief discussions outline the work being performed on the above topics:

1.) One of the most important requirements for the application of near millimeter wave systems is a knowledge of the characteristics of the atmosphere. This is emphasized, for example, in the study of millimeter wave beam riders, which demonstrates the requirements placed on transmitter power and receiver sensitivity by atmospheric attenuation [1]. Existing propagation data shows considerable inconsistencies, and the concept of atmospheric absorption anomalies as a transient function of atmospheric conditions is being studied. The correlation of laboratory experiments with propagation experiments is important and difficult. Interaction with chamber walls and condensation effects must be taken into consideration. Measurements which have been made thus far in waveguide cells and Fabry-Perot interferometers have given higher absorption results than predicted by theory.

During the past six months, measurements have been made in the Fabry-Perot interferometer through the 2 mm wavelength transmission window, but high results were still obtained. The cell apparatus is currently undergoing changes to obtain greater stability and improved gas handling capability. The major spectroscopic effort during this period was made in the development of the techniques for employing pulsed submillimeter lasers for spectroscopic investigations of water vapor. The source for these experiments was an optically pumped laser, pumped by a CO_2 TEA laser; this source was constructed on MIRADCOM Contract No. DAAK40-77-C-0047 to be used for fog/smoke propagation studies. Figure 23 of the attached paper to be presented at the AGARD Conference in Munich shows the experimental apparatus. The experiments and the procedures currently being followed for linewidth studies (including non-hydrogen molecules) are briefly discussed in the text of the AGARD paper.

Currently, the CW laser is being set up to use with an absorption cell.

2.) A CW optically pumped laser has been constructed and tested. A small efficient CO_2 laser has been constructed with maximum output power on the P(20) line of 28 watts. The laser is grating tuned. The laser provides greater than 10 watts on 60 individual lines, 15 watts on 50 lines and 20 watts on 30 lines. This laser system is an important tool in the areas of atmospheric spectroscopy and receiver component development.

The laser system is being stabilized to avoid fluctuations, etc. It will use the optically pumped laser output to stabilize the CO_2 laser.

3.) The spectral characteristics of the atmosphere are being calculated in considerable detail. The molecules O_2, H_2O and O_3 are included in a computer program giving absorption to frequencies in excess of 1000 GHz. The program will permit analysis of laboratory data (absorption, linewidth, lineshapes, etc.) and atmospheric propagation data. In the latter case, it serves the purpose of analysis of horizontal propagation and

vertical propagation. This program supports three DoD contracts and can be employed for any near millimeter wave systems analysis. The three DoD programs in which versions of the computer programs developed under this ARO study have been used are --

Contract No. DASG60-78-C-0031 with BMDATC, a study of the feasibility of missile plume detection from a platform within the atmosphere.

Contract No. DAAG39-78-R-9061 with HDL provides for the construction of a near millimeter mobile measurement program and will use the computer programs developed for multi-frequency propagation studies.

A program just starting with NRL (funded by DARPA) will make zenith radiometric measurements at 94 GHz, 140 GHz and 230 GHz and will compare measured atmospheric radiation with the values calculated with the computer codes being developed on this program.

4.) Laboratory and field measurements often require a small portable Fourier Transform Spectrometer (FTS). Many Army field operations can profit from the availability of an apparatus that could provide broad wavelength coverage. A small FTS has been assembled with a microprocessor controller. It will be used in the atmospheric spectroscopy studies and in studies of fog, rain, etc.

5.) In addition to the investigation of the vapor state characteristics of H_2O, investigations of the liquid state characteristics of H_2O in the submillimeter wavelength region are of interest. A study of these characteristics is being performed in conjunction with Dr. Sid Perkowitz and Dr. Brent Bean of Emory University. This work will be part of a doctorate thesis of O. Simpson. When correlated with the vapor state and fog studies being performed, it is expected that the work will provide further information on water clusters, which are of importance to investigations being performed by Hugh Carlon at Edgewood Area, Aberdeen Proving Ground. Reflectivity measurements have been performed on liquid H_2O and absorption measurements are currently underway.

Additional items related to the grant include --

a. A discussion has been held with John Teti of the Navy Surface Weapon Center who sponsors the gyrotron work at NRL. If the gyrotron is to

be a useful field device, spectral characteristics are important. The possibility of our performing heterodyning experiments of the gyrotron against a phase-locked source will be taken under consideration by the Navy.

b. The Third Submillimeter Conference was attended by four Georgia Tech staff members, who presented seven papers. Abstracts of two of the papers, sponsored partially or wholly by ARO, are attached. A brief report of the conference is attached.

c. The techniques of acoustical detection of submillimeter wave signals are being investigated, and an acoustical detection scheme will be constructed to complement the radiation detection methods.

d. Work has begun on a new FIR laser with invar-rod construction, which should have improved stability over the existing laser.

REFERENCE

1. R. G. Shackelford and J. J. Gallagher, "Millimeter Beam Rider System", Technical Report TE-CR-77-7, U. S. Army MIRADCOM, August, 1977.

FOURIER SPECTROMETER ENGINEERING DESIGN

The basic building block of the unit is a single machined block of aluminum. To this block is attached the following: stepper assembly, reflector mount, beam splitter mount, source unit, and Cassegrain collimator output. See Figure I.

Figure II shows the detector assembly. A Cassegrain collector is employed to improve the solid angle to the source. Propagation range with this size aperture is limited to about 40 feet, using a Golay cell for the detector. With larger optics and cryogenic detector, the range can be extended to greater than 500 M.

Figure III shows the overall block diagram of the system. The microprocessor (μP) controls the number of pulses for each step of the motor along with data conversion and data storage. The μP allows for design flexibility in the use of the instrument. The entire system consists of 4 units:

1) Fourier Unit
2) Detector
3) μP and Electronics
4) Lock-in Amp

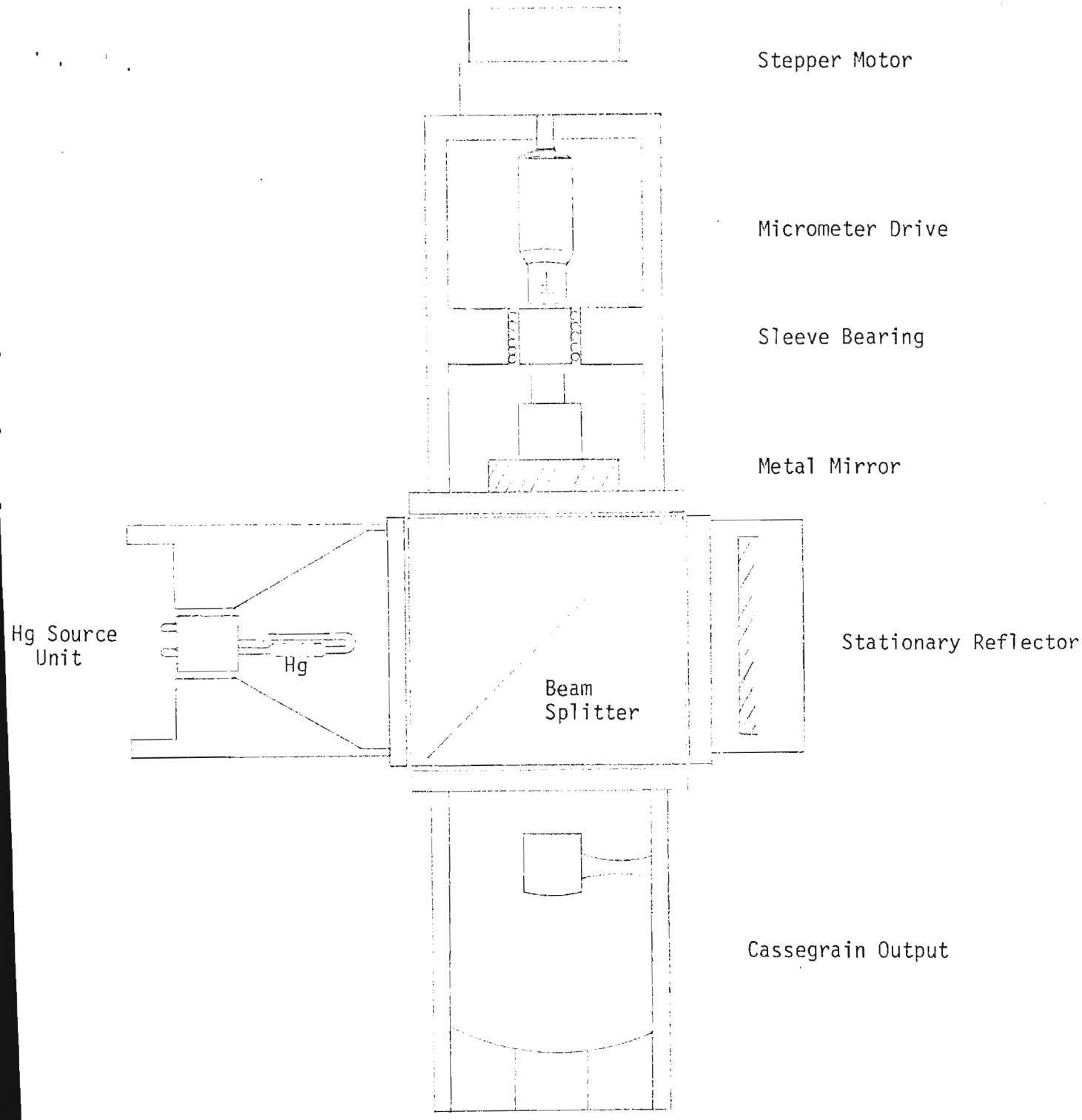

Figure I. Fourier Spectrometer.

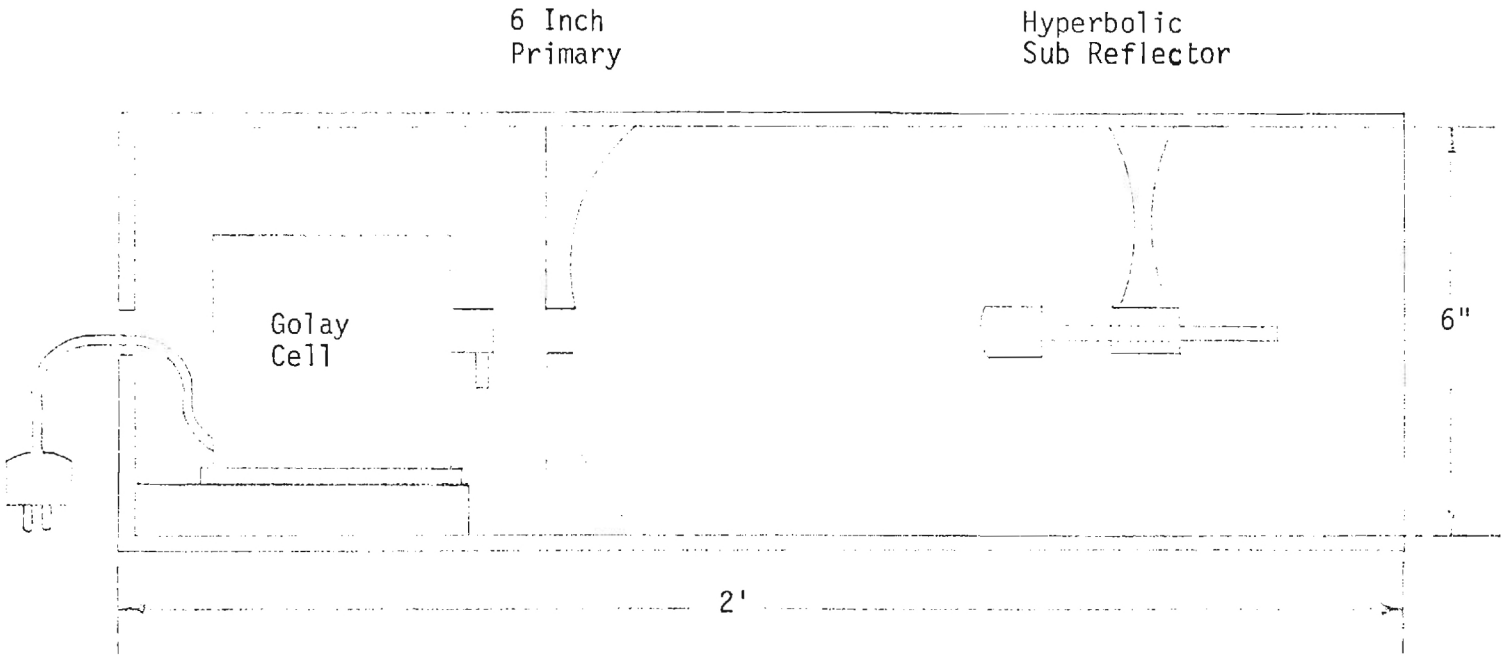

Figure II. Detector.

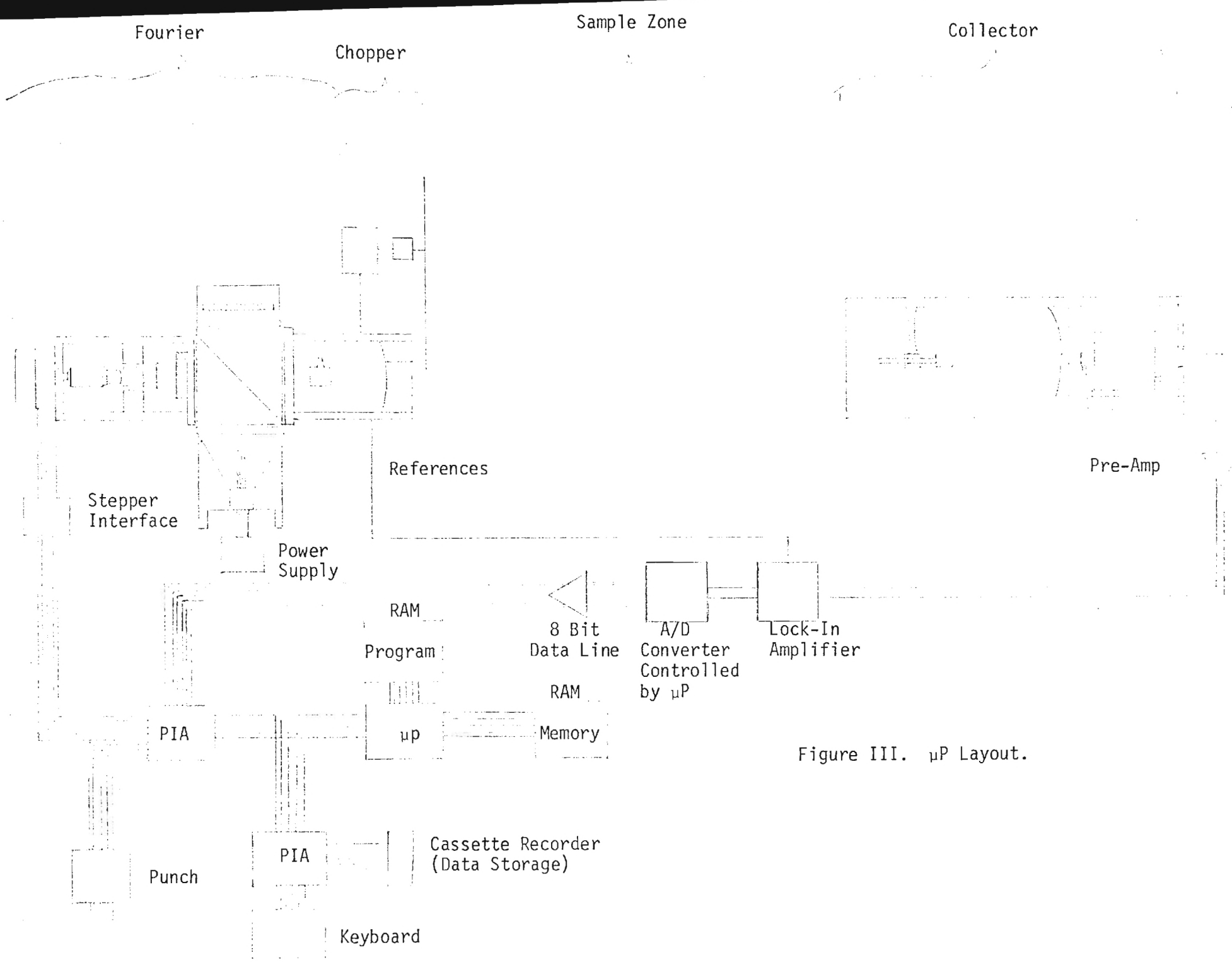

Figure III. µP Layout.

ABSTRACT OF PAPER PRESENTED AT THIRD SUBMILLIMETER CONFERENCE

SUBMILLIMETER SPECTROSCOPY OF ATMOSPHERIC WATER VAPOR

R. Rogers, P. Reinhart, H. Rainwater,
O. Simpson, W. Penn and J. Gallagher

Engineering Experiment Station
Georgia Institute of Technology
Atlanta, Georgia 30332

A study of the attenuation of submillimeter radiation by water vapor is reported. The window regions of 125 - 160 GHz, 210 - 270 GHz and 320 - 370 GHz have been investigated by Fabry-Perot interferometry, line shapes and half widths have been studied by waveguide cell techniques, and monochromatic measurements at single frequencies have been performed by optically pumped lasers, IMPATTS, klystrons and a carcinotron. Absorption due to water vapor alone or mixed with atmospheric vapors has been investigated. These experimental measurements are compared with theoretical calculations based on both Gross and Van Vleck - Weisskopf line-shapes. A discussion of the discrepancy between theoretical calculations and experimental measurements is given.

ABSTRACT OF PAPER PRESENTED AT THIRD SUBMILLIMETER WAVE CONFERENCE

PREDICTION OF THE EXISTENCE OF A SHARP PEAK IN WATER VAPOR EMISSION LINES IN DOWN-LOOKING RADIOMETRY*

J. J. Gallagher and R. W. McMillan
Georgia Institute of Technology, Atlanta, Ga. 30332

The height distribution of atmospheric water vapor has been the subject of dispute for many years. Currently, there is a substantial body of data which suggests that H_2O concentration decreases rapidly with altitude to a density of about 10^{-3} g/m^3 at about 20 km and then starts to increase again with increasing height. Based on this distribution, a technique has been proposed for the remote sensing of stratospheric H_2O which involves measuring the shape of a sharp peak superimposed on the 22.235 GHz emission line when observed looking upward from the ground. In this paper, we present analytical evidence for the existence of a similar peak superimposed on emissions from the stronger H_2O lines which should be observable in down-looking radiometry. The variation in shape of this peak as a function of the stratospheric water vapor distribution is analyzed.

The background temperature T_B measured by a radiometer looking downward from altitude h at an angle θ to the vertical is given by

$$T_B = \int_h^\infty T(Z)\exp[-\tau(h,Z,\theta)]\alpha(Z)\sec\theta dZ \qquad (1)$$

$$+ R\exp[-\tau(0,h,\theta)]\int_h^\infty T(Z)\exp[-\tau(Z,0,\theta)]\alpha(Z)\sec\theta dZ + (1-R)T_E\exp[-\tau(0,h,\theta)] ,$$

where T_E is the earth temperature and T(Z) is the temperature of a stratum of atmosphere of thickness dZ located at altitude Z. The terms of the form $\tau(Z_1,Z_2,\theta)$ are the optical depths between altitudes Z_1 and Z_2 at angle θ, and R is the reflectivity of the earth. The term $\alpha(Z)$ is the atmospheric attenuation coefficient, and is dependent on a number of variables including temperature, pressure, water vapor density, and the form of the emission line shape parameter. The effect of an absorption continuum was not considered in these calculations because there is no analytical basis for its inclusion. In Equation (1), the first term is the direct emission of the atmosphere, the second term is atmospheric emission reflected from the earth, and the third term is the emission of the earth modified by the atmospheric attenuation between the ground and altitude h.

Equation (1) was numerically integrated over the frequency range 100-700 GHz to a height of 50 km using the nine strongest water vapor absorptions below 1000 GHz, and the results of this integration are shown graphically in Figure 1. In making this calculation, a water vapor distribution with a secondary maximum

at an altitude of 50 km is assumed. Note the presence of the characteristic peaks caused by the high altitude water vapor.

The rather strange shape of the predicted emission from high altitude H_2O is caused by a combination of several factors. In regions of low H_2O absorption between lines, the radiometer is able to "see" far into the atmosphere to darker air layers and to the earth itself. At frequencies falling on the wings of the lines, absorption is greater and the radiometer sees only the somewhat upper atmospheric layers. Finally, at the line center frequencies, the absorption is very large and the radiometer sees only a short distance into the atmosphere. However, at these great altitudes, the atmosphere is warm, thus the radiometer at the line center frequency shows a sharp peak in emission due to these warm layers. Because of the relatively high temperature and the low pressure in the stratosphere, it is difficult to conceive of a high-altitude water vapor distribution which does not exhibit these sharp peaks on emission line centers.

Several different upper atmospheric water vapor distributions have been analyzed, and each gives a different emission line shape. It is not known whether a measured line shape could be used to determine a corresponding water vapor distribution, but the observation of a sharp peak in emission will almost certainly indicate the presence of high altitude water vapor.

*This work was supported by the National Aeronautics and Space Administration, Goddard Space Flight Center, Under Grant No. NSG-5012, and by the U. S. Army Research Office under Grant No. DAAG29-76-G-0280.

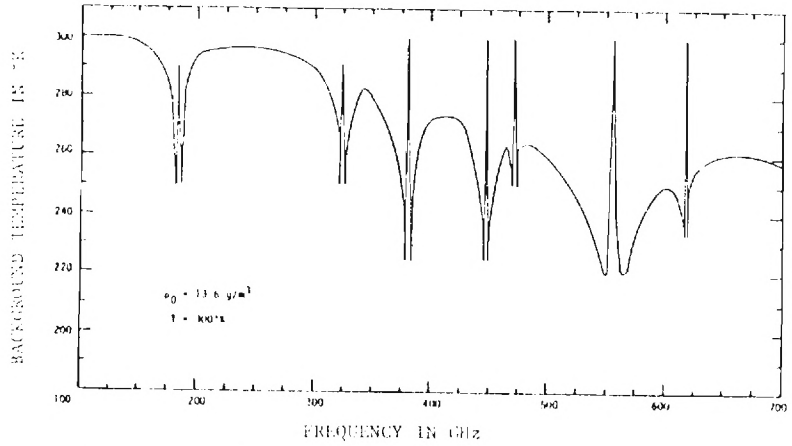

Figure 1. Calculated background temperature due to water vapor observed from an altitude of 50 km.

PAPER TO BE PRESENTED AT
AGARD CONFERENCE IN MUNICH, GERMANY
ON SEPTEMBER 5, 1978

CONCEPTS AND TECHNIQUES IN THE UTILIZATION OF MILLIMETER AND SUBMILLIMETER WAVES

J. H. Rainwater, R. W. McMillan and J. J. Gallagher

Georgia Institute of Technology
Engineering Experiment Station
Atlanta, Georgia 30332

SUMMARY

Extended microwave techniques have resulted in the cross-waveguide and ridged-waveguide harmonic mixers for the higher millimeter wave frequencies in addition to single-ended fundamental mixers, all employing Schottky-barrier diodes. The newly developing technique of subharmonic pumping of an anti-parallel diode pair promises to ease the problem of insufficient local oscillator power. Quasi-optical techniques are being developed to provide more efficient energy coupling, filtering and directing components to replace the poorly performing waveguide devices above 100 GHz. Radiometry as a remote sensing tool is revealing properties of the atmosphere which are not characterized adequately by theory. Propagation measurements in the submillimeter show attenuation to be somewhat greater than previously believed. A millimeter-submillimeter transmitter and receiver system for propagation studies has been constructed at Georgia Tech with an optically pumped laser as a source and a quasi-optical superheterodyne receiver.

1.0 INTRODUCTION

The attractiveness of millimeter and submillimeter waves for remote sensing, weapon guidance and other applications has given impetus to research and development of millimeter and submillimeter devices and systems and has necessitated characterization of atmospheric propagation effects in the atmosphere. The evolution of quasi-optical devices and techniques from a synthesis of microwave and optical practices has proceeded along with the extension of more familiar microwave devices into the millimeter and submillimeter regions.

Georgia Tech is conducting extensive research and development programs aimed at the goal of full utilization of millimeter and submillimeter waves (sometimes collectively referred to as near-millimeter waves, 100-1000 GHz). In the sections to follow, programs and topics are discussed in the areas of extended microwave techniques, quasi-optical devices and methods, radiometry, and measurements of importance to spectroscopy and propagation. Measurements obtained with operational systems will be highlighted and their significance to physical questions and future system applications discussed.

2.0 EXTENSIONS OF MICROWAVE TECHNIQUES

Following the impetus to research and development of centimeter radar that World War II provided, physicists in various laboratories began extending the techniques of microwave radar into the near-millimeter region of the spectrum. While the generation of coherent radiation found realization in extended klystron and traveling wave tube principles, masers, optically and electrically pumped lasers and relativistic electron beam devices, non-thermal detector and mixer technology followed another path. This path paralleled the growth in knowledge of semiconductor physics and technology: the "cat-whisker" diode emerged into a new era of applicability. Current research at Georgia Tech is directed toward developing structures and techniques to utilize the recontactable Schottky-barrier diode, a descendant of the "cat-whisker" diode, as a near-millimeter detector or superheterodyne mixer.

Harmonic superheterodyne mixers, which require local oscillator (LO) pumping at one-half the signal frequency, have been constructed for the near-millimeter in both crossed-waveguide and single-ended configurations. Figure 1 illustrates two mixer structures which are in operation at Georgia Tech. The crossed-waveguide mixer (1a) couples LO energy to the diode through a coupling hole in the LO waveguide, to the signal waveguide. The diode mixes harmonics of the local oscillator with the signal, heterodyning spectral information to a convenient intermediate frequency (IF) for amplification and further processing. IF filtering and matching are accomplished within the barrel part of the mixer using appropriately machined impedance transforming materials. Figure 1b. shows a ridged-waveguide, single-ended mixer designed by G. T. Wrixon of University College, Cork Ireland. This mixer was constructed to operate near 230 GHz and couples both LO and signal frequencies in the same port, in this case a ridged-waveguide which allows simultaneous transmission of the fundamental signal and LO modes to the diode throughout a bandwidth larger than typical rectangular waveguide would provide. IF matching and filtering is achieved within the block by a precision machined stripline, five element, low pass Tchsbyscheff filter. By way of comparison, the best noise figures obtained with a crossed-waveguide mixer at 183 GHz have been 16 dB while the ridged-waveguide mixer is expected to yield noise figures below 15 dB at 230 GHz.

Fundamental mixing in the near-millimeter has been achieved at Georgia Tech with two mixer structures illustrated in Figure 2. Figure 2 shows a conventional single-ended mixer with replacable Sharpless-wafer mounted diodes. This type of mixer is convenient for systems where a field replaceable diode capability is desired. Noise figures of 12 dB have been obtained at 183 GHz with these devices at Georgia Tech. Figure 3 shows another single-ended configuration, designed to ease the difficulty of contacting typical 4 μ diameter diodes with etched, pointed 12 μ diameter whiskers. The mixer block can be partially disassembled for diode contacting in the laboratory and then quickly reassembled for operational use. This mixer, often called a split block mixer, contains

an integral IF matching and filter network in stripline design. Noise figures of 14 dB have been demonstrated at 183 GHz with the split block mixer to date.

Both fundamental and harmonic mixing schemes for the near-millimeter require reliable, stable, LO sources which are always expensive and sometimes unavailable for the higher frequencies. To overcome these disadvantages a new harmonic mixing technique, referred to as subharmonic mixing, is being developed at Georgia Tech. Typically, subharmonic mixing is the process of pumping an anti-parallel diode pair [1] with a LO frequency one-half or one-fourth the signal frequency. The anti-parallel diode configuration, illustrated in Figure 4, has the advantages of reducing conversion loss by suppressing fundamental mixing products and lowering the mixer noise figure through suppression of LO noise sidebands. In addition, a mixer with such an anti-parallel diode pair requires less LO power than its single diode equivalent.

Future mixing schemes at higher near-millimeter wave frequencies will of necessity be of an open structure design because fundamental mode waveguide dimensions approach diode crystal dimensions near 400 GHz. The reader is referred to Gallagher and Blue (reference 2), for examples and discussion of open structure type mixers.

3.0 QUASI-OPTICAL DEVICES AND TECHNIQUES

3.1 Background

The continuing extension of microwave source and detector technology further into the near-millimeter portion of the electromagnetic spectrum has created a need for low-loss components suitable for use at these shorter wavelengths. In particular, the availability of optically pumped lasers [3], extended interaction oscillators, and relativistic electron beam devices [4], as near-millimeter sources, and the development of quasi-optical mixers have contributed to this need.

In the region of frequencies above about 100 GHz, losses in waveguides become significant, and this limitation is further aggravated by poorer performance of couplers, attenuators, wavemeters, and other passive components at higher frequencies. Fortunately, since wavelengths in the submillimeter are small compared to practical optical component dimensions, and excellent transmitting and reflecting materials are available in this frequency region, it is possible to overcome most of these limitations by using quasi-optical techniques.

3.2 Quasi-Optical Antennas

Antennas used in the near-millimeter spectrum are essentially identical in form to those used in the optical portion of the electromagentic spectrum, consisting of lenses and mirrors; but the materials used for fabrication of these elements may be different. Lenses are generally made of plastics such as rexolite, TPX or teflon, and mirrors are made of high-conductivity metals such as are used for optical mirrors. Antenna feeds are usually conical or pyramidal horns, except at the shorter wavelengths where direct focussing of radiation is a practical approach to avoiding waveguide losses.

Diffraction losses in a near-millimeter wave antenna system will be higher than for a corresponding optical system because the full-width Fraunhofer diffraction limited beamwidth is approximately 2.4 λ/d, where d is aperture diameter, at the 90% power points. Although diffraction limited output is easy to achieve in these systems, the above expression shows that near millimeter beamwidths will be several orders of magnitude greater than corresponding beamwidths for optical and near infrared systems. Furthermore, geometrical or ray optics descriptions of quasi-optical devices will require significant corrections for the effects of diffraction [5] since the aperture diameters involved are on the order of one hundred wavelengths instead of several thousands of wavelengths as for the case of visible light.

Microwave lenses are usually machined from a block of rexolite, teflon, polyetheylene, or other suitable low-loss material. Because of the comparatively long wavelengths, and corresponding immunity to slight surface defects, it is possible to machine lenses directly with a hyperbolic shape, thus eliminating spherical aberration. Machine tool cutters can be fashioned from aluminum or other easy-to-work material, and polishing can be done with fine sandpaper.

Fresnel reflection from lens surfaces is a difficult problem to solve in the design of microwave quasi-optics. Lenses are usually made in the plano-convex configuration, and are anti-reflection "coated" by bonding a quarter wavelength thick layer of a dielectric material with a refractive index equal to $n^{1/2}$, where n is the refractive index of the lens, to the surfaces. Unfortunately, such materials are not generally easy to find. Alternatively, quarter wave deep grooves may be machined into the surface with a spacing such that the average index of the grooved volume is equal to $n^{1/2}$. This machining is difficult on the curved surface of the lens, so that this surface is generally left uncorrected. Figure 5 shows the details of the matching of lenses to air by slotting.

Reflecting antennas for near-millimeter systems may take the same variety of configurations as has been devised for optical telescopes including Newtonian, Cassegrain, Gregorian, and variations of these types. The secondary mirror of such a reflecting telescope is usually driven with a feed horn. Because of the comparatively large beamwidth of near-millimeter systems, both primary and secondary mirrors must be made large to minimize spillover power. Reflective optics have the advantage of not requiring the matching layer required in refractive systems, and may be made from commonly used reflecting metals, such as gold and aluminum, which have excellent reflectivity in the near-millimeter spectrum.

Horn antennas may be used as feeds for both lens and mirror antenna systems up to a frequency of about 300 GHz. Corrugated horns have been devised which have minimum side lobes in this range of frequencies. Beyond 300 GHz, sources consist mainly of optically pumped or electric discharge pumped lasers, which use partially reflecting mirrors for output coupling. Figure 6 shows a corrugated horn antenna designed for 30.0 GHz with its associated radiation pattern. Computer programs have been devised to aid in the design of such horns.

3.3 Quasi-Optical Diplexers

The design of diplexers used for coupling both local oscillator and signal power to a single mixer is a difficult problem in the near-millimeter wavelength region that has received some attention during the last few years. This problem is especially important because of the low output power of available local oscillators in the near-millimeter region. Successful diplexer designs must be configured so as not to waste any of this scarce LO power.

A diplexer designed by Martin and Puplett [6] is shown in Figure 7. A signal beam plane polarized at 45° to the normal to the page is incident from the left. This beam is divided into components polarized parallel and perpendicular to the page by wire grid D1. The component perpendicular to the page is reflected from the wire grid and the mirrors A and is recombined at the output of grid D2 with the component polarized parallel to the page. A local oscillator input incident from above, also polarized at 45°, follows essentially the same path, and is combined with the signal in the mixer as shown. The diplexer is tuned by varying the distance of the plane reflectors from the wire grids so as to give constructive interference of signal and local oscillator at the output. Diplexers based on similar interferometric principles have been designed by Wrixon [7], Gustincic [8], and Erickson [9]. Schematic drawings of these devices are shown in Figures 8, 9, and 10.

3.4 Quasi-Optical Filters and Interferometers

Several different types of quasi-optical filters have been devised using Fabry-Perot interferometers in plane, confocal and semiconfocal configurations. Confocal and semiconfocal devices use solid metal mirrors with small coupling holes for input and output radiation. These devices have extremely high Q's, sometimes reaching 10^6, but these higher Q devices generally have higher losses. Plane-mirror Fabry-Perot interferometers may use solid mirrors, wire grids, or perforated metal plates for reflectors. The Q's of these devices depend upon coupling hole size, grid spacing and orientation, and the size of the perforations, respectively.

The four-grid Fabry-Perot interferometer has been analyzed by McMillan and Langley [10] and by McMillan, Branch, and Lamb [11], who have found that this filter is bandpass tunable by either varying the relative grid orientation or by varying the spacing between elements of the two grid pairs. Furthermore, this filter can be made to rotate the plane of polarization of an incident signal on reflection, and there is some indication that this rotation can be carried out on transmission also.

The transmitted power τ for the four-grid array shown in Figure 11a is given by

$$\tau = T^4 \cos^2(\delta-\beta) \left\{ \left[1 + \frac{\sin^2\gamma(1-R^2\cos^2\gamma - RT\sin^2\gamma)}{\cos^2\gamma(1-2R\cos 2\phi_1 + R^2)} \right]^2 + 4RT\sin^4\gamma \left[\frac{\sin\delta + R\cos^2\gamma\sin(2\phi_1-\delta)}{\cos^2\gamma(1-2R\cos 2\phi_1 + R^2)} \right]^2 \right\}^{-1} \quad (1)$$

where R and T are reflectivity and transmissivity of a single grid for radiation polarized parallel and perpendicular to the wires, respectively, β is the angle of input polarization, γ is the angle between the grids, ϕ_1 is the phase shift between elements of a grid pair, and δ is the total phase shift through the grid. The grid angles θ and α are defined as shown in Figure 11b. Using this equation, tunable grid filters have been constructed which have performances which agree well with theory. Figure 12 shows measured and calculated results for a filter of this type.

A very useful three-grid quasi-optical filter has been designed by Saleh [12, 13], who has achieved excellent agreement of measured transmission with theory based on measurements made at 50 GHz. The bandpass characteristics of this filter are similar to those of the four-grid filter discussed above, and it is also tunable by varying the angle of the interior grid of the three-grid array.

One of the most effective quasi-optical devices which is used in the near-millimeter wave region is the interferometer. The device has taken many forms in the applications which have been addressed so far, and their use can be seen in many future system applications. Both Fabry-Perot and Michelson interferometers have been employed, and for the Fabry-Perot interferometer, high-Q and low Q devices exist depending upon the application for the apparatus. The devices can be parallel plate, semi-confocal or confocal interferometers and can be employed as either waveguide coupled or horn/lens coupled resonators. Figure 13 shows an example of the use of one of these interferometers in a molecular beam spectrometer [14].

3.5 Miscellaneous Components

Submillimeter analogs for many optical devices have been devised, including polarizers, beam splitters, quarter wave plates, attenuators, and the Fresnel rhomb. Each of these component types will be discussed briefly in this section.

Wire grids are extensively used as polarizers and beam splitters in the submillimeter, and recent advances in fabrication techniques have extended the usefulness of these devices into the near infrared. When used as a polarizer, the component polarized parallel to the wires is reflected and the component perpendicular to the wires is transmitted. Beam splitter applications use these same properties, with the result that the wire grid is a polarizing beam splitter.

A beam splitter based on frustrated total internal reflection (FTIR) has been described by Baker and Valenzuela [16], which uses two identical low-loss dielectric prisms which form a cube when joined together. The prisms are separated on a face diagonal of the cube, and the attenuation and resultant off-axis coupling can be varied by changing the spacing along this diagonal. These devices are described analytically by Fellers [17]. This beam splitter consists of two 90° prisms with a small gap between them. If no gap exists, an incident beam would be transmitted without change of direction, whereas in the absence of one prism, the

incident beam would be totally internally reflected, emerging at an angle of 90° to the incident beam. With a gap between the prisms, the beam is partially transmitted and partially reflected. Figure 14 shows the configuration of the double-prism while the transmittance as a function of wavelength is shown in Figure 15. The reflected signal is R = 1-T.

The double-prism can be employed for several applications. Figure 16 shows it employed as an attenuator [18]. The attenuation as a function of the prism separation is given in Figure 17 for both parallel and perpendicular polarization, relative to the plane of incidence. The curves were obtained by using $\varepsilon = 2.54$ for the dielectric constant of rexolite. Figure 18 shows the double-prism as a directional coupler, the coupling of which can be varied as a function of the prism separation. Figure 19 shows the prisms fed by a 300 GHz carcinotron with a horn/lens system. The detector is shown at the left of this figure. A micrometer adjusts the separation of the prisms for use as an attenuator and/or a directional coupler.

Wave plates may be fabricated from birefringent materials in a manner similar to that used for optical retarders. Because of its good transparency throughout much of the submillimeter region [19], crystalline quartz is a good choice for this application, but practical quartz wave plates may be prohibitively thick at the longer wavelengths because of its low birefringency. For generating circular polarization, a Fresnel rhomb has been devised by Strauch et al [20]. This device was used to analyze Zeeman components in submillimeter spectroscopy, and is shown in Figure 20.

3.6 Uses and Limitations of Quasi-Optics

It appears likely that optical techniques will provide many of the methods required to extend the usefulness of the wavelength region between 10 and 1000 microns for remote sensing, spectroscopic and military applications. Submillimeter analogs of many optical and microwave components are available, and concentrated effort by many workers is resulting in the discovery of new techniques at a rapid pace.

The availability of sources such as optically pumped lasers, relativistic electron beam devices, and extended interaction oscillators, will surely stimulate the development of quasi-optical techniques in the near millimeter spectral region. This development may not be as fast as that associated with the evolution of the laser in the visible and near infrared, because lasers are readily available and have reached a high level of development; and because most of the optical techniques used with lasers were well known before the laser was invented.

Of the areas that should be pushed to speed up development, the availability of a reliable duplexer for the near millimeter spectrum would appear to be important. The development of suitable matching techniques, such as antireflection coatings; and the design of quasi-optical microwave devices, such as isolators and circulators would also be helpful.

4.0 RADIOMETRY

4.1 Theoretical Aspects

The properties of the atmosphere, as they affect the propagation of near-millimeter radiation, can be characterized by the remote sensing technique of radiometry. In radiometric terminology the effective brightness temperature of the sensed medium, called the antenna temperature, is determined by a radiometer. The effective background sky brightness temperature T_b, measured by a radiometer at altitude h with an infinitesimally narrow beamwidth looking upward at zenith angle θ, is

$$T_b = \int_h^\infty \alpha(Z)T(Z) \cdot \exp\left(-\int_h^Z \alpha(Z')\sec\theta \, dZ'\right)\sec\theta \, dZ, \qquad (2)$$

in which T(Z) is the temperature of a stratum of atmosphere of thickness dZ located at altitude Z. The parameter $\alpha(Z)$ is the atmospheric absorption coefficient which depends on several factors in addition to the line shape factor. There is also a strong dependence on altitude because the density of water vapor molecules decreases rapidly with increasing altitude. These dependences are discussed in detail by McMillan, et al [21].

Equation (2) must in general be solved numerically because of the complex nature of the absorption coefficient $\alpha(Z)$. A computer was programmed to solve this equation using the Gross analytical line shape [22], an empirical modification to the Gross line shape proposed by Gaut and Reifenstein [23], and the Schulze-Tolbert empirical line shape [24]. The water vapor density and temperature variables used in the calculations were obtained from ground level measurements made at the time radiometric measurements were made.

4.2 Experimental Aspects

A Dicke superheterodyne radiometer has been developed to measure the emission spectrum of atmospheric water vapor from 160 to 210 GHz. The radiometer, as shown in Figure 21, employs a crossed wave guide harmonic mixer containing a recontactable Schottky-barrier diode. The diode junction is made by a 12.7μ diameter gold plated phosphor-bronze whisker etched into a 1μ tip. Water cooled millimeter wave reflex klystrons, operating at one-half the signal frequency, are used as local oscillators to provide the radiometer a tuning range spanning the 183.3 GHz emission line. The IF output of the harmonic mixer is amplified by two Avantek AM2020-M FET amplifiers centered at 1.6 GHz in a bandwidth of 1.4 GHz. An Aertech 4-diode Schottky-barrier square law second detector provides a DC signal for synchronous detection.

A Fabry-Perot wire grid interferometer has been constructed to function as a tunable bandpass filter in order to effectively eliminate detecting signals at the third harmonic of the local oscillator. The output of the interferometer is focused into a conical, corrugated horn through a 77 mm focal length rexolite lens. The horn feeds the harmonic mixer through WR-5 waveguide.

The chart-recorded output of the radiometer is calibrated at each measurement frequency by observing the DC output change as an ambient load (300°K) is replaced by a calibration load (98°K). The temperature difference between the ambient reference load and a calibration load determines a scale factor from which the antenna temperature of the sky can be determined. The Georgia Tech radiometer has demonstrated total system noise figures as low as 14 dB which corresponds to 0.22°K minimum detectable temperature.

4.3 Comparison of Experimental with Theoretical Data

The calculations discussed in Section 4.1 were made under the conditions measured at the ground based radiometer site at the time the radiometer measurements were made. Figure 22 shows typical results obtained in this way. The three curves are the calculated results using the Gross, modified Gross, and Schulze-Tolbert line shapes; and the points represent measured values of antenna temperature obtained during the late mornings and early afternoons of 7 July and 25 August 1977, respectively. Since the skirts of the water vapor absorption lines extend to frequencies far removed from their center frequencies, a total of six of the stronger lines extending in frequency up to 556.7 GHz were considered in the calculations.

Figure 22 shows that none of the line shapes considered give good agreement with experiment, although the Schulze-Tolbert expression comes closest. The measurements of antenna temperature away from the absorption line peak, which show disagreement with theory, are given more credibility by the fact that the radiometer consistently measures ambient temperature at frequencies near the line peak, in agreement with theory. Measurements near the line peak therefore provide another method of calibrating the radiometer and serve to confirm data in the wings. This type disagreement has also been observed in propagation experiments in this frequency region, especially under conditions of high humidity. For a time, this excess attenuation was thought to be due to water vapor dimers, but it has been shown that dimers will not account for the magnitude of the observed attenuation. H. A. Gebbie [25] has characterized this disagreement as "anomalous absorption". The continued generation of experimental data is needed to improve the analytical models of atmospheric absorption so that attenuation can be calculated with some degree of certainty in the near-millimeter region.

5.0 NEAR-MILLIMETER WAVE PROPAGATION STUDIES

The measurement of atmospheric parameters can be performed by a combination of techniques, which include laboratory spectroscopic measurements, propagation of monochromatic signals and broadband incoherent source propagation. Each of these processes contribute significant information toward the understanding of the atmosphere. In performing laboratory experiments, care must be taken in both the experimental techniques and the interpretation of the data.

5.1 Laboratory Measurements

Spectroscopy of the millimeter-submillimeter wavelength region is closely related to the molecular constituents of the atmosphere. Currently, at Georgia Tech, an extensive program on water vapor absorption is being performed. The water molecule, despite the long history of its spectroscopic observation, is still a difficult molecule to understand with respect to its contribution to atmospheric attenuation. Clustering, difficulties of accurately determining densities, adequacy of line shape theory and interaction of the molecule with the measurement apparatus can seriously affect the analysis of the data. As a result, several laboratory techniques are being employed at Georgia Tech to provide a broad spectral coverage, permit observations in the transmission windows and on the spectral lines, and provide redundancy of results by a variety of techniques. Both coherent and incoherent spectroscopic methods are being employed. Spectrometric apparatus includes large Fabry-Perot spectrometers (for non-resonant absorption measurements), waveguide cells for line width and line shape measurements at reduced pressures, parallel plate Stark cells for dipole moments and Fourier spectrometers for broad band measurements.

Propagation through long cells with optically pumped lasers and a carcinotron complement the absorption measurements being made with the above apparatus. The optically pumped lasers provide a large number of emission lines across the submillimeter wavelength region. The technique shown schematically in Figure 23 has been employed to utilize a TEA laser-pumped submillimeter laser for observations at discrete wavelengths throughout the spectral region of interest. Because of the amplitude instability of the TEA laser, it is necessary to provide a monitor of the emission before transmission through the absorption cell. The reference channel and signal channel outputs are averaged over several pulses and compared with the gas in and out of the cell. Detection is achieved by either pyroelectric detectors or Schottky barrier diodes.

The many techniques which are available for providing data on atmospheric absorption should contribute significantly to an understanding of the absorption mechanism. However, the results continue to produce values which are higher than the theoretical values based upon a monomer water molecule. The suggestion has been made by Derek Martin [26] to perform measurements in the spectral region between absorption lines of molecules that do not contain hydrogen. This would allow the checking of line width/shape theory for molecules without hydrogen bonding. It would give an indication if the theory is correct and the hydrogen bonding in water is causing the difficulties or if further theoretical work is required. Currently, Georgia Tech is initiating a program of measurements on non-hydrogen molecules, OCS, CO, ICN, SO_2, N_2O, NO and PF_3. These measurements will be extended to hydrogen - containing molecules, $CH_3C\ell$, NH_3, CH_3CN, CH_3NC, HCN, CH_3F, CHF_3 and H_2S, before continuing the H_2O measurements.

5.2 A Near-Millimeter Wave System For Propagation Studies

5.2.1 Optically Pumped Source

The optically pumped laser used for propagation studies is a pulsed device pumped by a Lumonics CO_2 TEA laser. The pump laser has an output of 2-10 joules depending on the transition, and outputs ranging from 35W to 25kW have been obtained with the far infrared laser, also depending on the transition being excited.

Figure 24 is a sketch of the far infrared laser. The end boxes are machined from a single piece of aluminum to minimize leaks. The waveguide is a section of 38 mm glass pipe which may be chosen to be any convenient length up to 2 m by using standard glass pipe lengths. A zinc selenide window couples in the CO_2 radiation, and the laser mirrors are made from tightly stretched square nickel meshes. For most applications, the input mesh has a period of .0625 mm and the output mesh is 0.125 mm. The mirrors have x--y adjustments and the output mirror has a translation adjustment in addition. Invar rods are used between the end boxes for good stability.

In testing this laser, a total of 27 lines were seen in 4 gases. No attempt was made to observe a large number of lines, since the primary interest in propagation measurements lies in the atmospheric window regions. However, previously unreported lines were observed in $C_2H_2F_2$ and CH_3I. For most gases. a pressure of 1 to 5 torr produced good output.

5.2.2 Superheterodyne Receiver

The receiver used in conjunction with the transmitter described in the previous section is shown in block form in Figure 25. The receiver is of quasi-optical design, a Fabry-Perot interferometer being used to diplex signal and local oscillator radiation into a single-ended ridged waveguide mixer. The Fabry-Perot grid spacing is adjusted to reflect the local oscillator frequency (110-115 GHz) while transmitting the signal (220-230 GHz). The IF frequency, 6.75-7.25 GHz, is amplified with 60 dB of gain and then detected with a square law detector for video presentation of the transmitter pulse.

5.2.3 Propagation Facility

A meteorologically instrumented propagation range is being assembled at Georgia Tech to provide comparative measurements for wavelengths from the visible through the millimeter wavelength region. The following sources are being made available with appropriate receivers:

An argon laser at 0.5 μm;

A YAG:Nd laser at 1.06 μm;

A 10.6 μm CO_2 laser;

An optically pumped laser (outputs at several wavelengths across the submillimeter region);

A 1 mm carcinotron

A 2.1 mm klystron

A 3 mm klystron

An 8 mm klystron

Simultaneous operation of all systems is planned.

6.0 CONCLUSIONS

The instrumentation and measurements described in this paper are designed to contribute to an understanding of the atmospheric characteristics relevant to applications in the near-millimeter wavelength region. Among these applications, for which further discussion can be given, are radiometric work for airborne applications for Project Storm Fury and ground mapping, theoretical studies of satellite radiometric observations of millimeter/submillimeter water lineshapes as a means of determining water vapor distribution, a transportable propagation facility and trends in military applications of near millimeter wave technology.

ACKNOWLEDGEMENTS

The research activities described within this paper are sponsored by the following U. S. Government grants and contracts:

NASA/Goddard Space Flight Center - Grant. No. NSG-5012

U. S. Army Research Office (ARO) - Grant No. DAAG29-76-G-0280

U. S. Army, Contract No. DAAK40-77-C-0047

REFERENCES

1. M. Cohn, et al, "Harmonic Mixing With An Antiparallel Diode Pair", IEEE Trans. MTT, Vol. 23, No. 8, (Aug. 1975).

2. J. J. Gallagher and M. D. Blue, "Submillimeter Wave Spectroscopy and Technology Second Semi-Annual Technical Report", U. S. Army Research Office, Grant No. DAAG29-76-G-0280, Engineering Experiment Station, Georgia Institute of Technology, (Sept. 1977).

3. J. J. Gallagher, M. D. Blue, B. Bean and S. Perkowitz, "Tabulation of Optically Pumped Far Infrared Laser Lines and Applications to Atmospheric Transmission", Infrared Phys., Vol. 17, pp. 43-55, (1977).

4. J. J. Gallagher, H. A. Ecker, M. D. Blue and R. G. Shackelford, "Applications at Submillimeter Wave Gigawatt Sources", ARPA Order Number 2840, Contract N00014-75-C-1011, (Sept. 1975).

5. R. H. Garnham, "Quasi-Optical Components", in Millimeter and Submillimeter Waves, F. H. Benson, Ed., London, Fliffe Bucks, Ltd., 1969, Chapter 21.

6. D. H. Martin and E. Puplett, "Polarized Interferometric Spectrometry For the Millimetre and Submillimetre Spectrum", Infrared Physics 10. 105 (1969).

7. G. T. Wrixon, University College, Cork, Ireland, private communication, (1977).

8. J. J. Gustincic, "A Quasi-Optical Radiometer", Second International Conference on Submillimeter Waves and Their Applications, San Juan, Puerto Rico, (1976).

9. N. R. Erickson, "A Directional Filter Diplexer Using Optical Techniques for Millimeter to Submillimeter Wave Lengths", IEEE Trans. Microwave Theory Tech., to be published.

10. R. W. McMillan and J. B. Langley, "Analysis of Submillimeter Wave Fabry-Perot Interferometers Made of Four Wire Grids", Second International Conference on Submillimeter Waves and Their Applications, San Juan, Puerto Rico, (1976).

11. R. W. McMillan, C. H. Branch, and G. M. Lamb, "Polarization Twisting, Bandpass Tunable Fabry-Perot Filters for Submillimeter Applications", Third International Conference on Submillimeter Waves and Their Applications, Guildford, England, (March, 1978).

12. A. A. M. Saleh, "An Adjustable Quasi-Optical Bandpass Filter - Part I: Theory and Design Formulas", IEEE Trans. Microwave Theory Tech., Vol. MTT-22, No. 7, pp. 728-734, (July, 1974).

13. _____, "An Adjustable Quasi-Optical Bandpass Filter - Part II: Practical Considerations", IEEE Trans. Microwave Theory Tech., Vol. MTT-22, No. 7, pp. 734-739, (July, 1974).

14. R. E. Cupp, R. A. Kempf, and J. J. Gallagher, "Hyperfine Structure in the Millimeter Spectrum of Hydrogen Sulfide: Electric Resonance Spectroscopy on Asymmetric-Top Molecules", Phys. Rev. 171, 60, (1968).

15. A. E. Costley, K. H. Hursey, G. F. Neill and J. M. Ward, "Free-standing fine-wire grids: Their manufacture, performance, and use at millimeter and submillimeter wavelengths", J. Opt. Soc. Amer. 67, No. 7, pp. 979, (July, 1977).

16. H. D. Baker and G. R. Valenzuela, "A Double Prism Ateenuator for Millimeter Waves", IRE Trans. Microwave Theory Tech., Vol. MTT-10, pp. 392-393, (Sept. 1962).

17. R. G. Fellers, "Measurements in the Millimeter to Micron Range", Proceedings IEEE, Vol. 55, No. 6, pp. 1003-18, (June, 1967).

18. B. H. Garnham, "Optical and Quasi-Optical Transmission Techniques and Components Systems for Millimeter Waves", RRE Report 3020.

19. A. M. Frank, "A Birefringent Polarization-Independent Beam Splitter for the Submillimeter", Third International Conference on Submillimeter Waves and Their Applications", Guildford, England, (March, 1978).

20. R. G. Strauch, R. E. Cupp, M. Lichtenstein and J. J. Gallagher, "Quasi-Optical Techniques in Millimeter Spectroscopy", Symposium on Quasi-Optics, Polytechnic Institute of Brooklyn, (June 8-10, 1964).

21. R. W. McMillan, J. J. Gallagher, and A. M. Cook, "Calculations of Antenna Temperature, Horizontal Path Attenuation, and Zenith Attenuation Due to Water Vapor in the Frequency Band 150-700 GHz", IEEE Trans. Microwave Theory Tech., Vol. MTT-25, No. 6, pp. 484-488, (June, 1977).

22. E. P. Gross, "Shape of Collision-broadened Spectral Lines", Phys. Rev., Vol. 97, pp. 394-403, (Jan. 1955).

23. N. E. Gaut and E. C. Reifenstein, III, Environmental Research and Technology Report No. 13, NASA Contract NAS8-26275, Waltham, Mass., (Feb., 1971).

24. A. E. Schulze and C. W. Tolbert, "Shape, Intensity, and Pressure Broadening of the 2.53 - Millimeter Wave-Length Oxygen Absorption Line", Nature, Vol. 200, No. 4908, pp. 474-740, (Nov. 23, 1963).

25. H. A. Gebbie, "New Molecular Absorbers in the Earth's Atmosphere and Their Submillimeter Spectra", Second International Conference on Submillimeter Waves and Their Applications, San Juan, Puerto Rico, (Dec. 1976).

26. D. H. Martin, Private Communication, (1978).

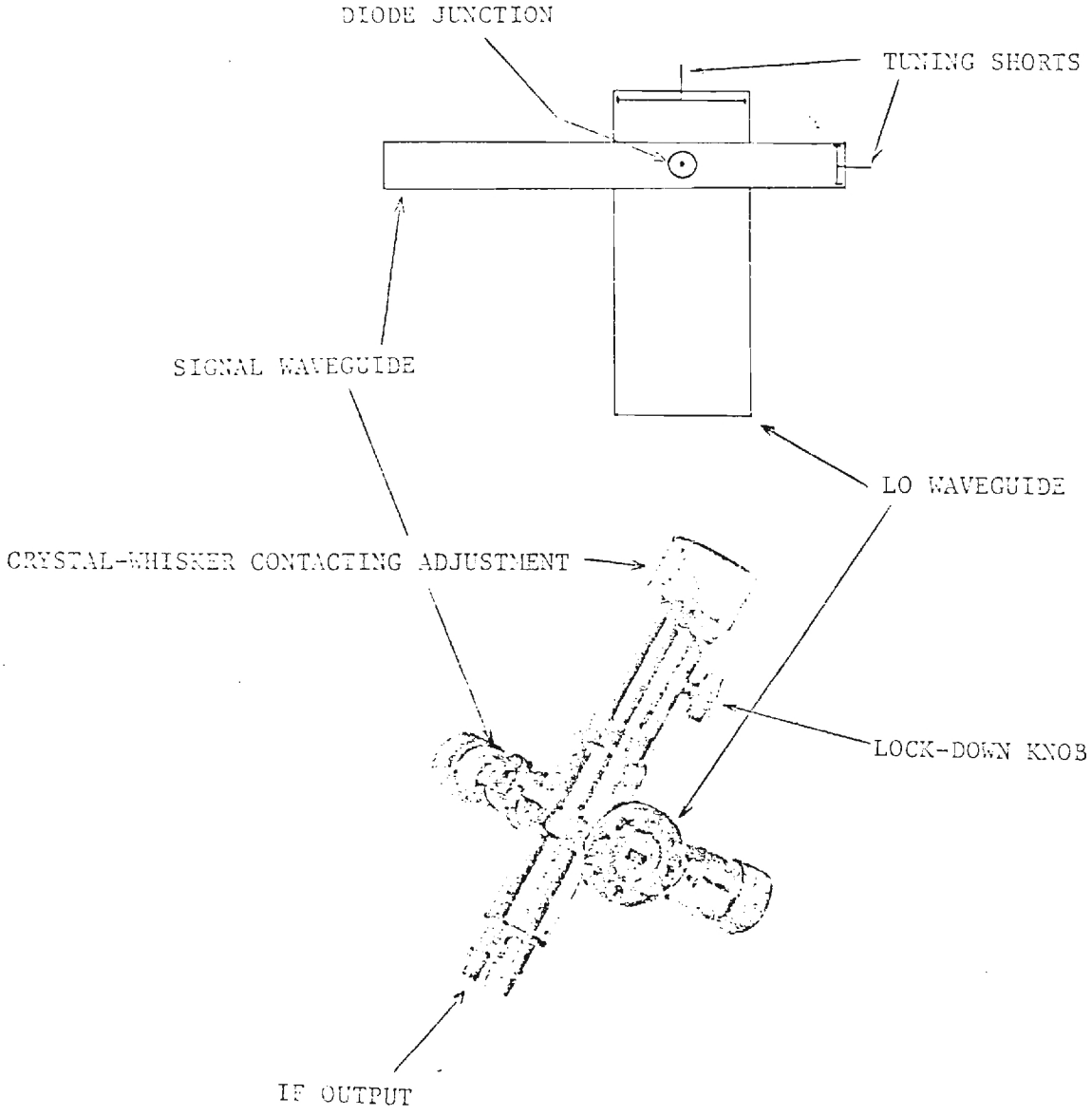

Figure 1(a). Crossed-waveguide Mixer.

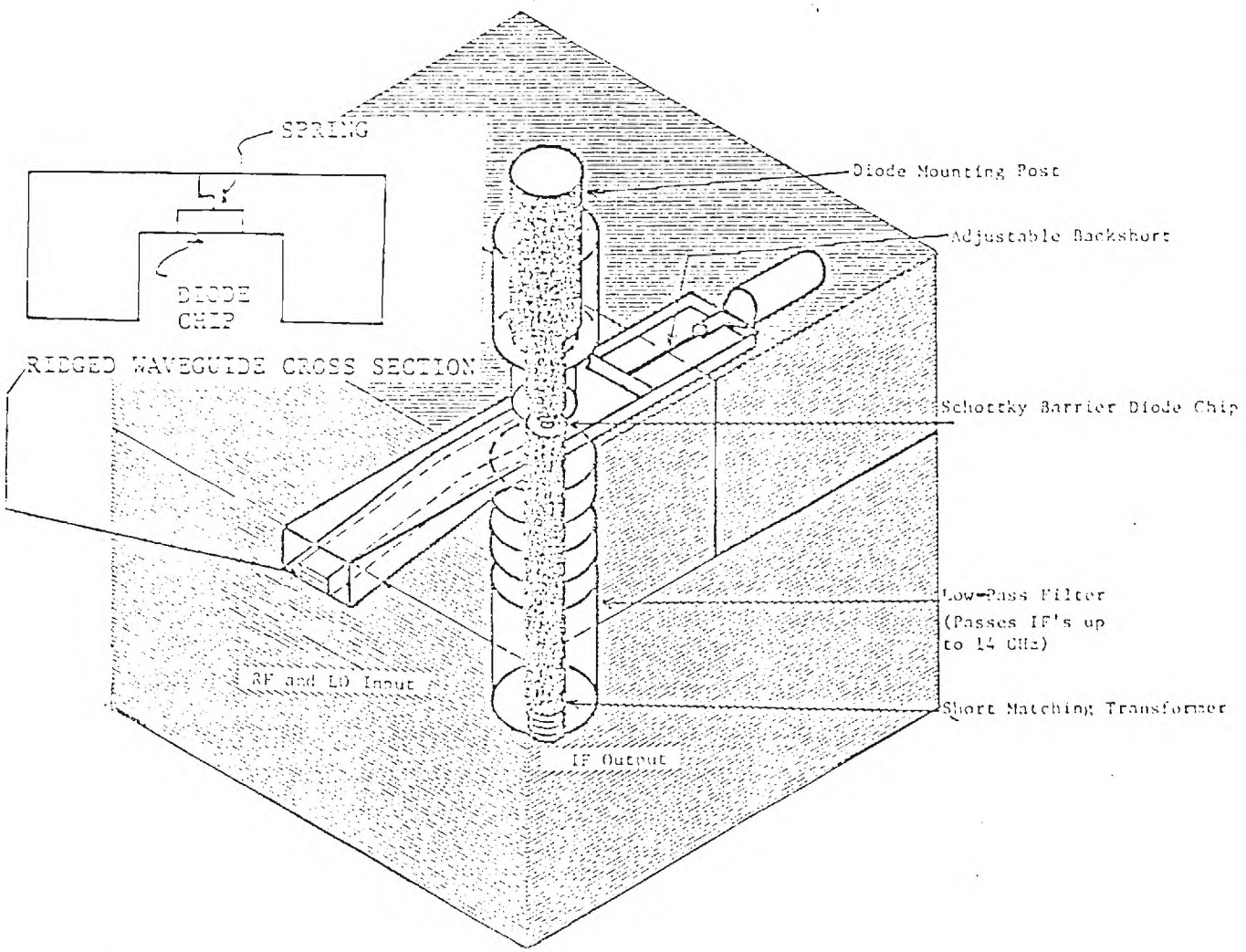

Figure 1(b). Ridged-waveguide Mixer.

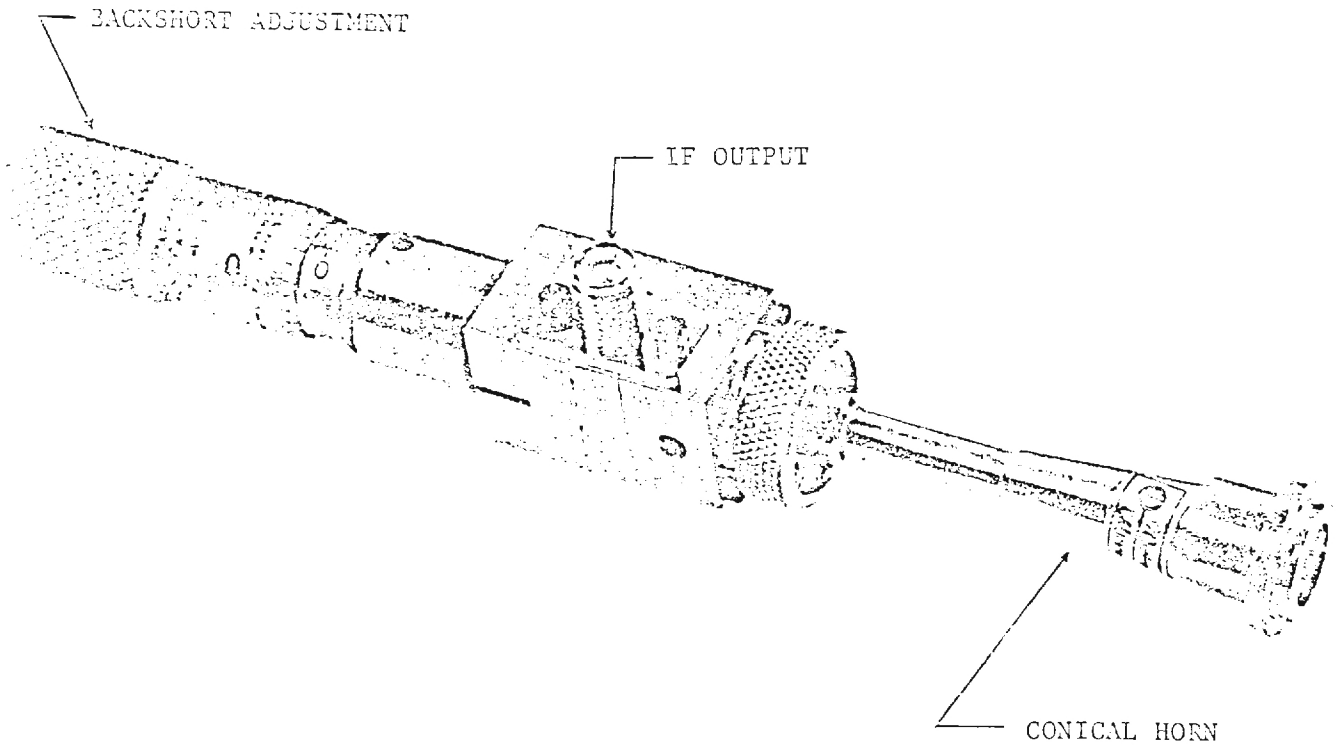

Figure 2. Sharpless-wafer mixer, shown without diode wafer.

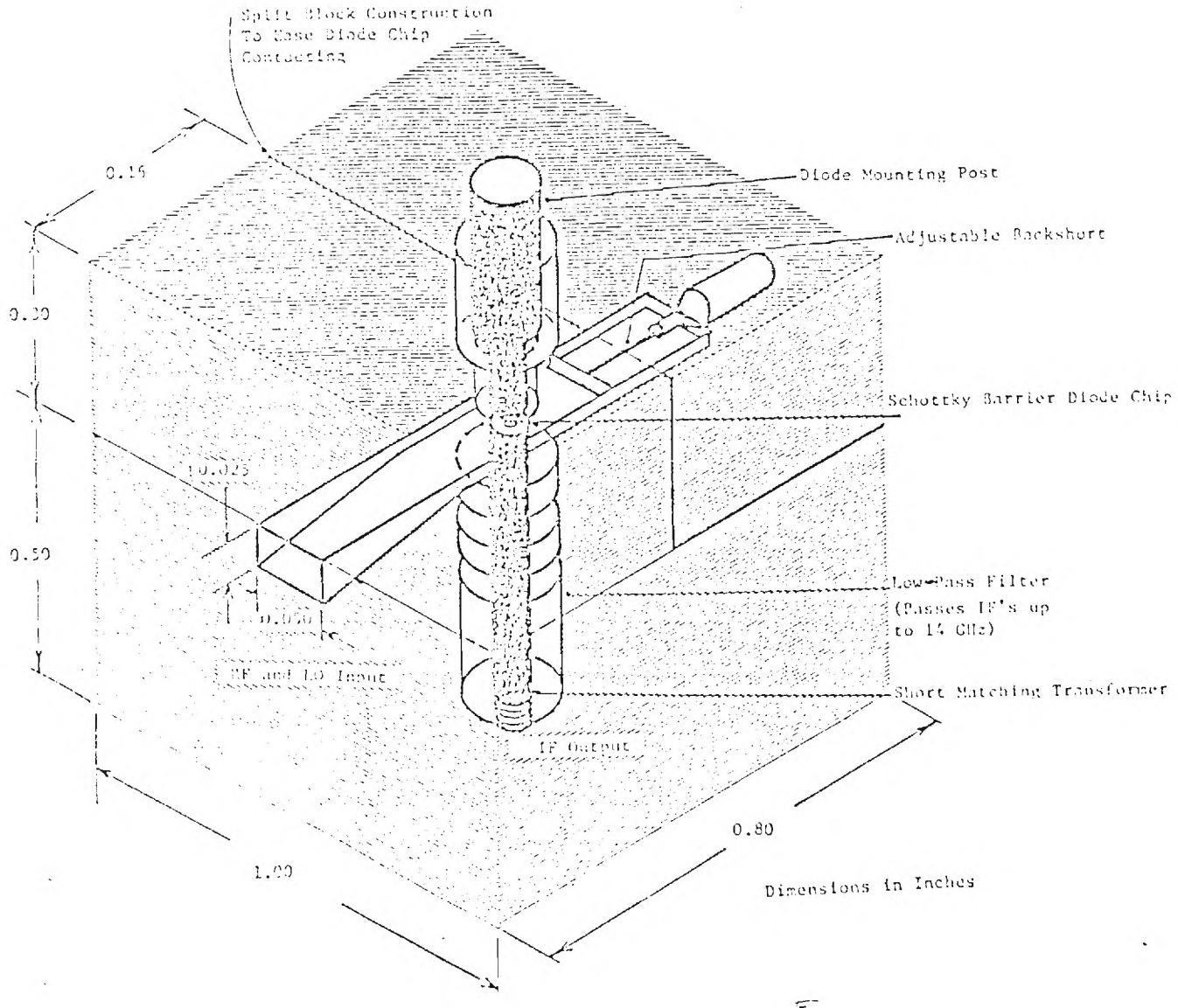

Figure 3. Split Block Mixer (Dimensions shown are for WR-5 Waveguide Band, 140 - 220 GHz.)

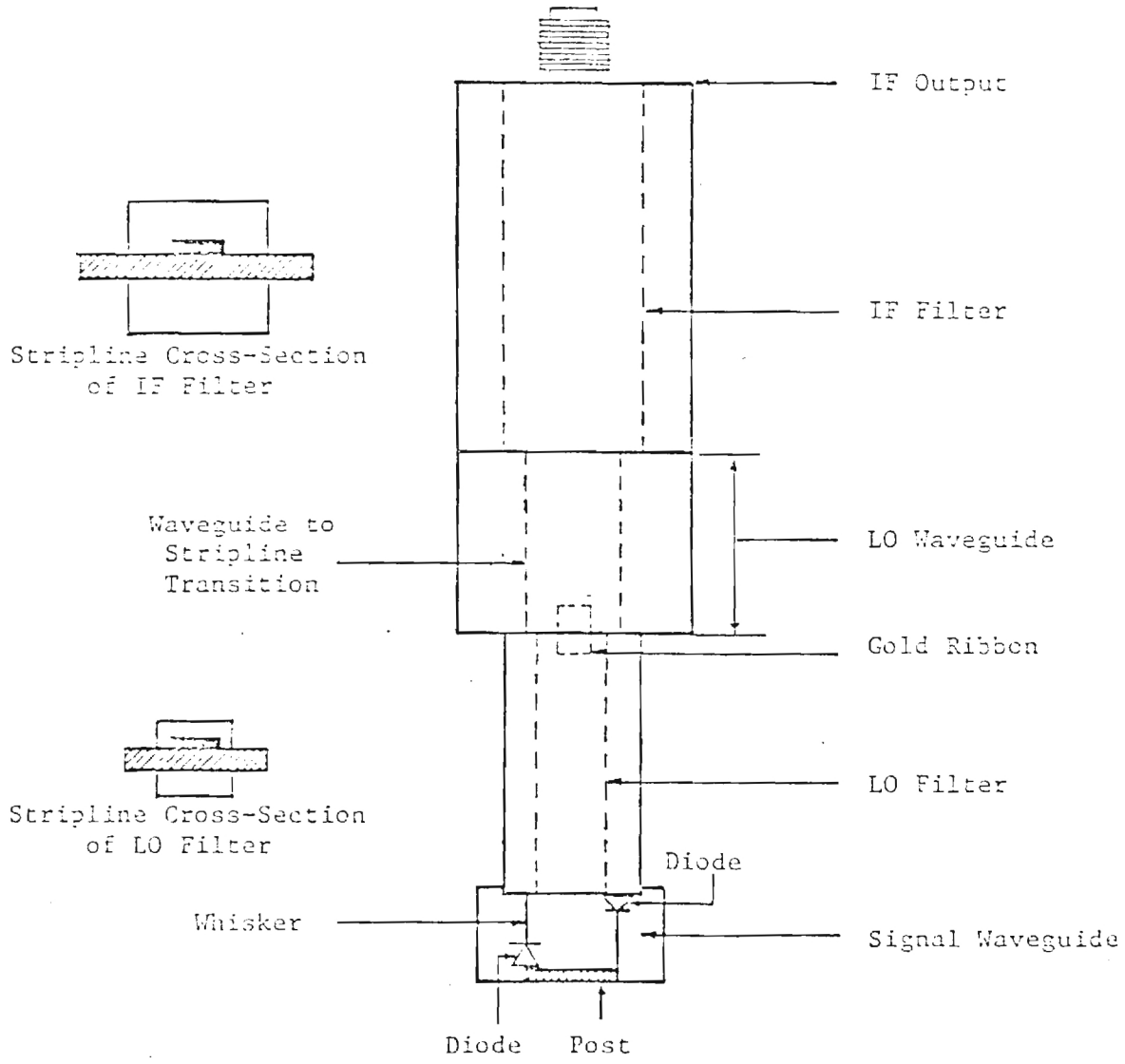

Figure 4. Subharmonic Mixer Showing Anti-parallel Diodes.

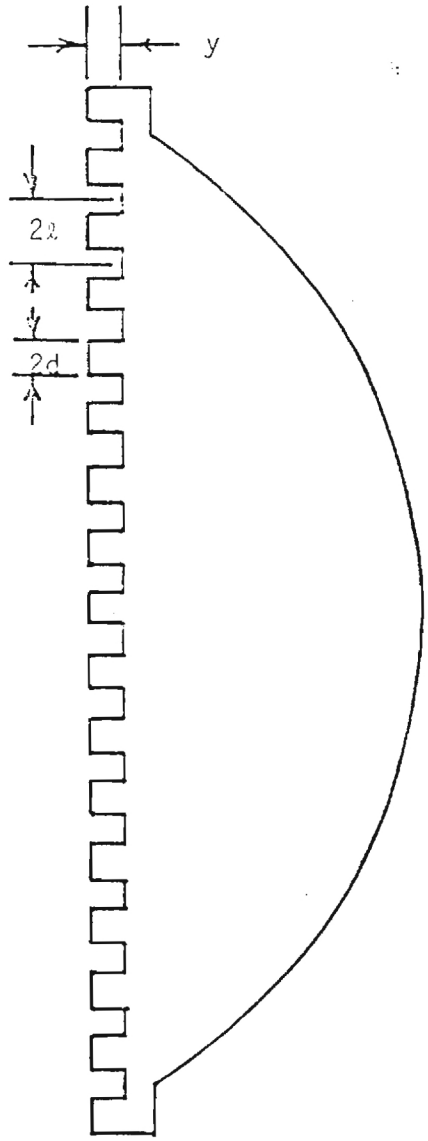

TYPICAL
PARAMETERS
FOR
REXOLITE
AT 168 GHz

λ = 0.36 mm
d = 0.13 mm
y = 0.28 mm

Figure 5. Detail of Matching Lens to Air by Slotting.

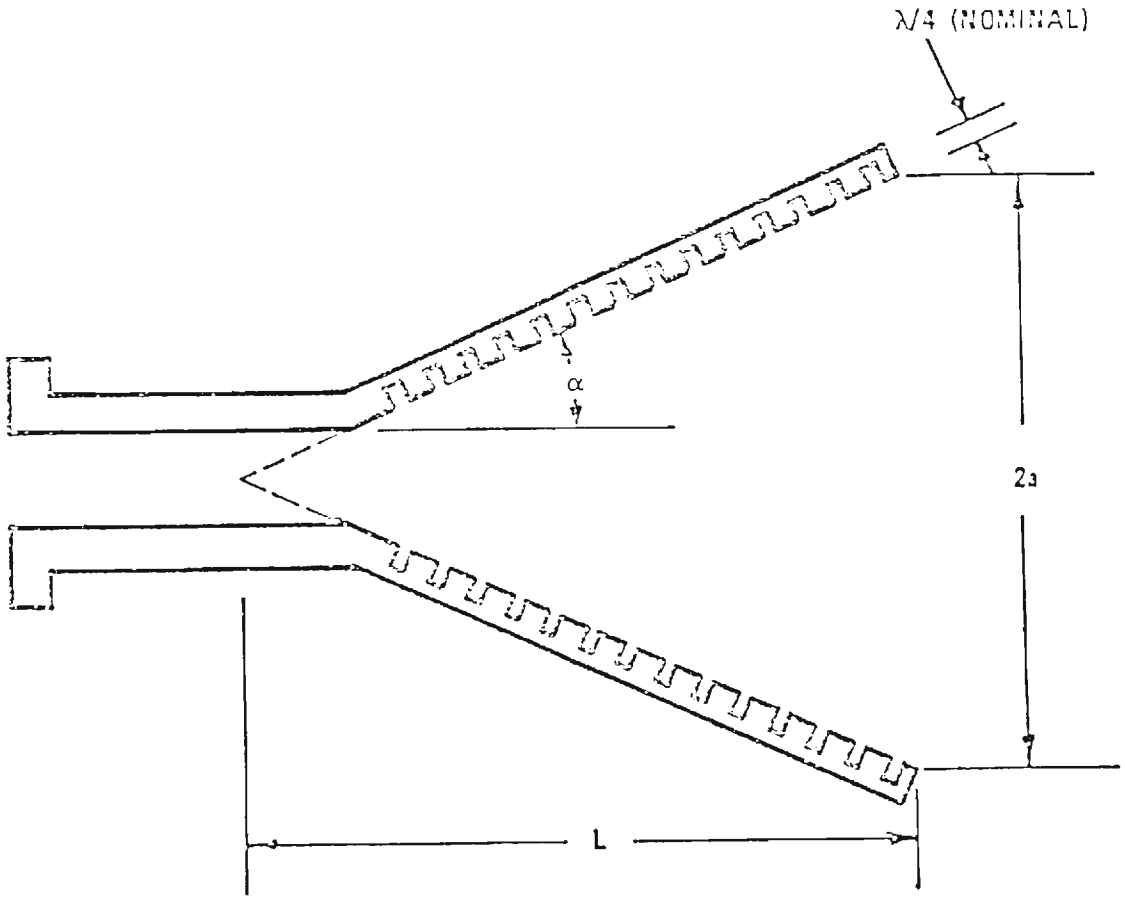

Figure 6(a). Conical Corrugated Horn Geometry used in Calculations.

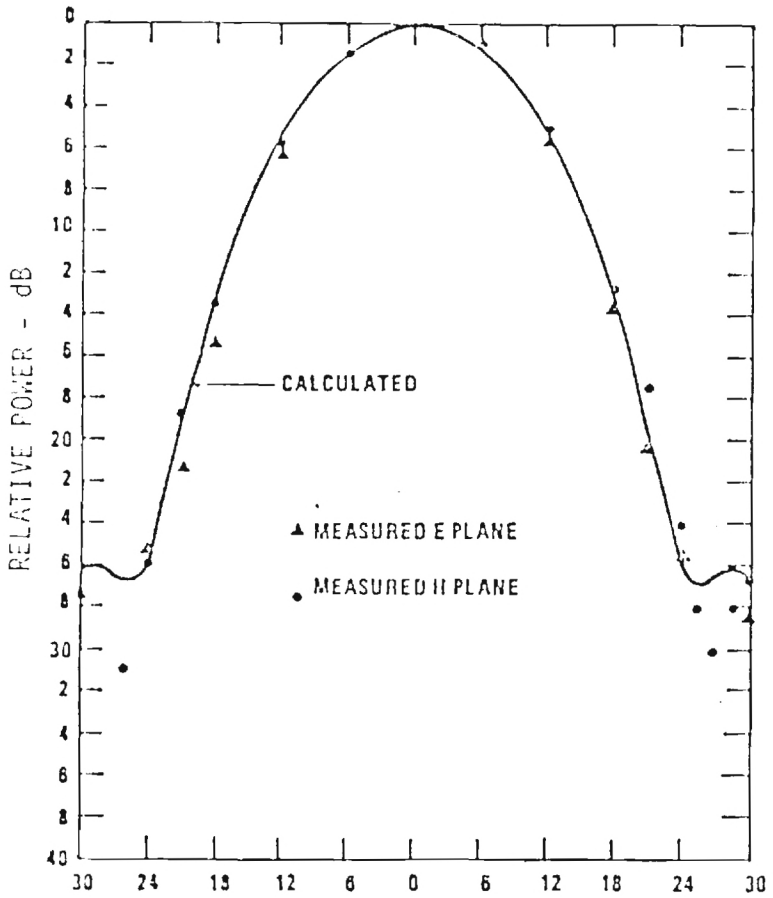

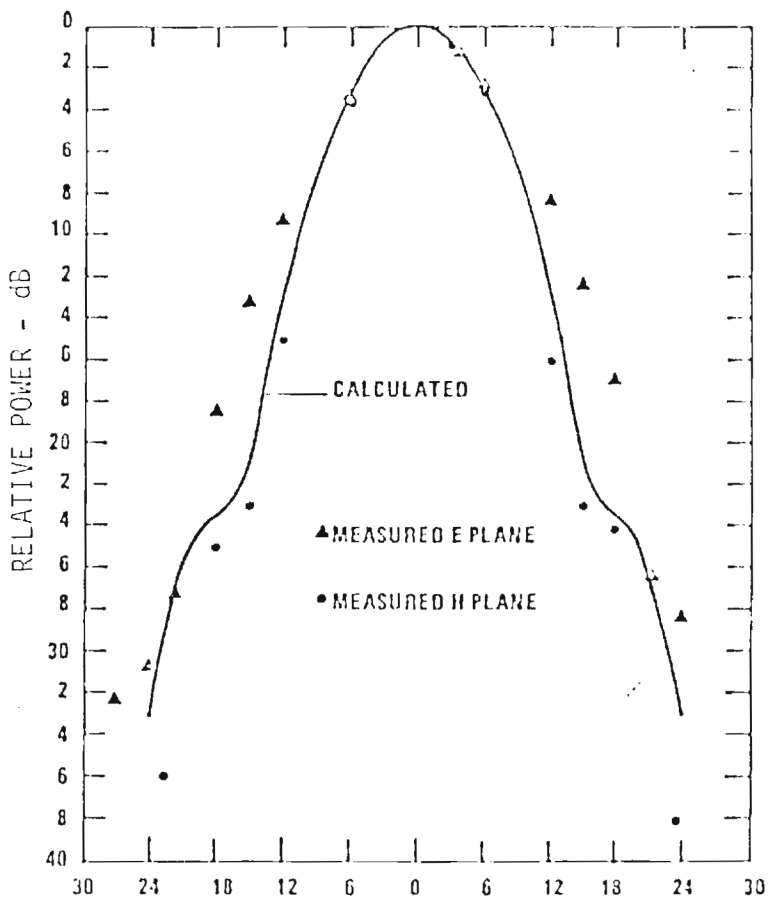

Figure 6(b). Comparison of Calculated and Measured Antenna Patterns.

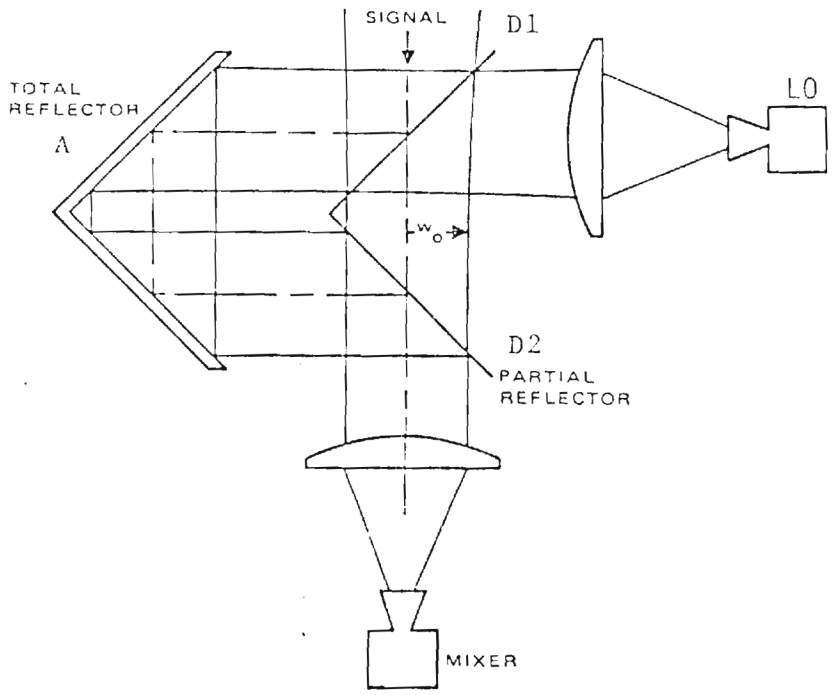

Figure 7. Schematic diagram of the Diplexer designed by Martin and Puplett [6].

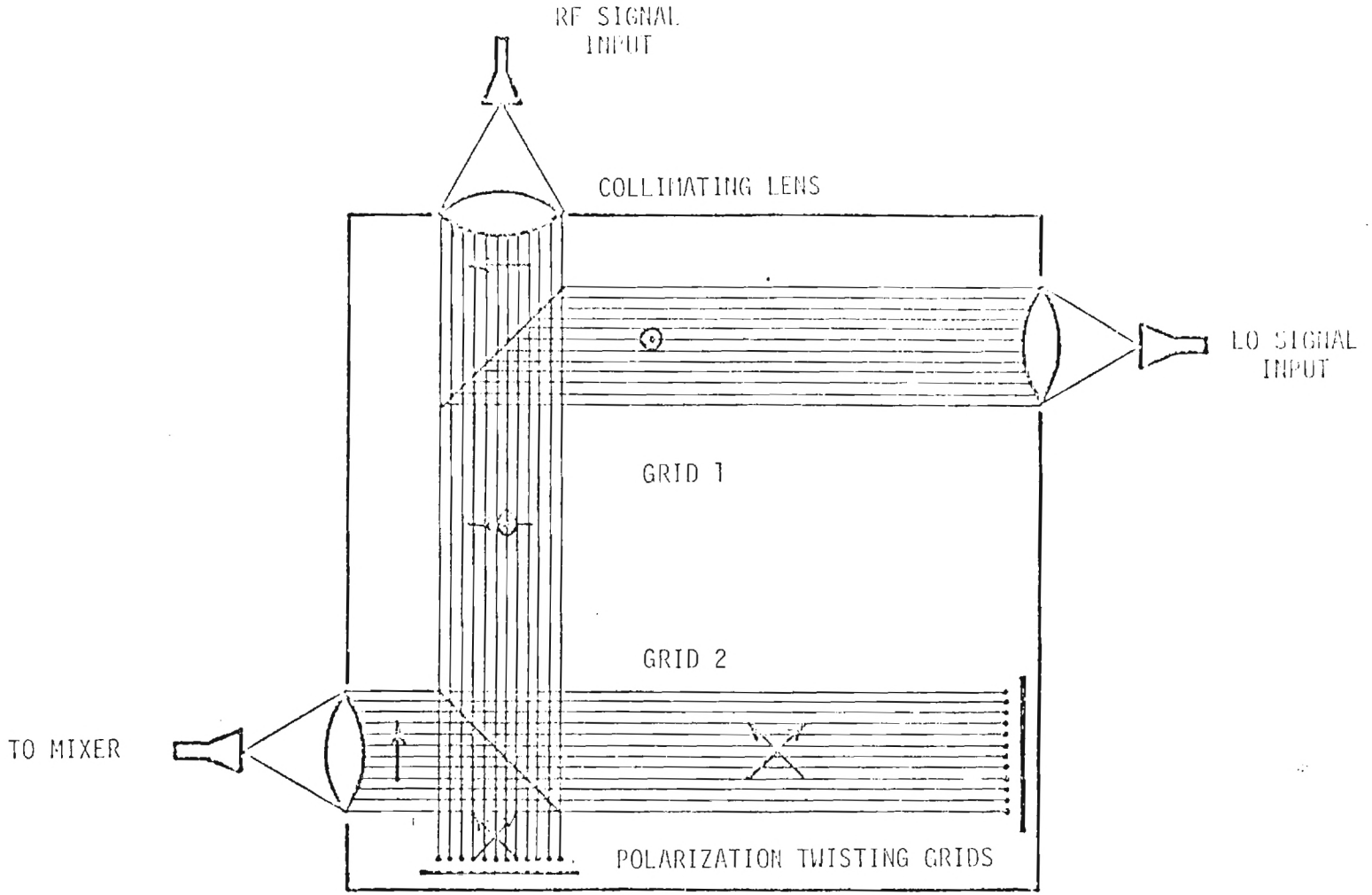

Figure 8. Quasi-Optical LO Injection Diplexer with Collimating Lenses.

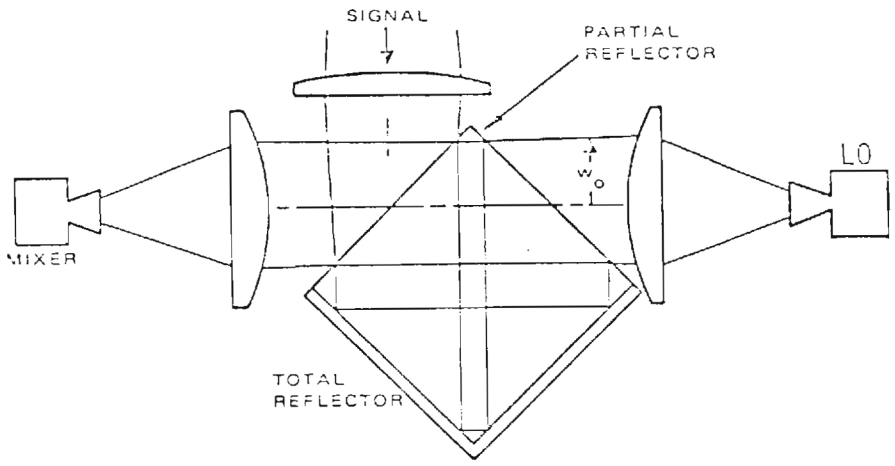

Figure 9. Quasi-Optical Diplexer using a square resonator. After Gustincic.

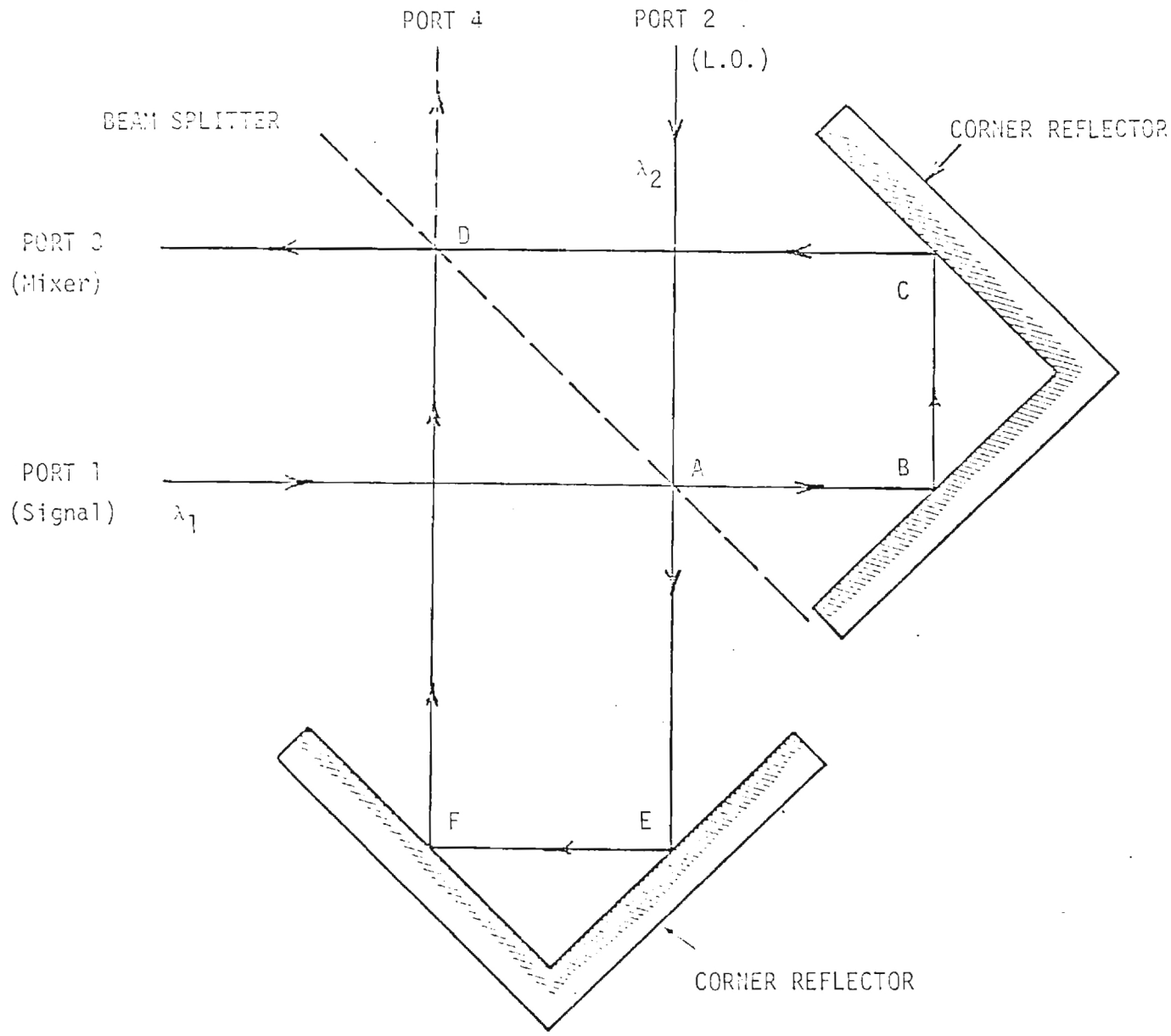

Figure 10. A directional filter quasi-optical diplexer. After Erickson.

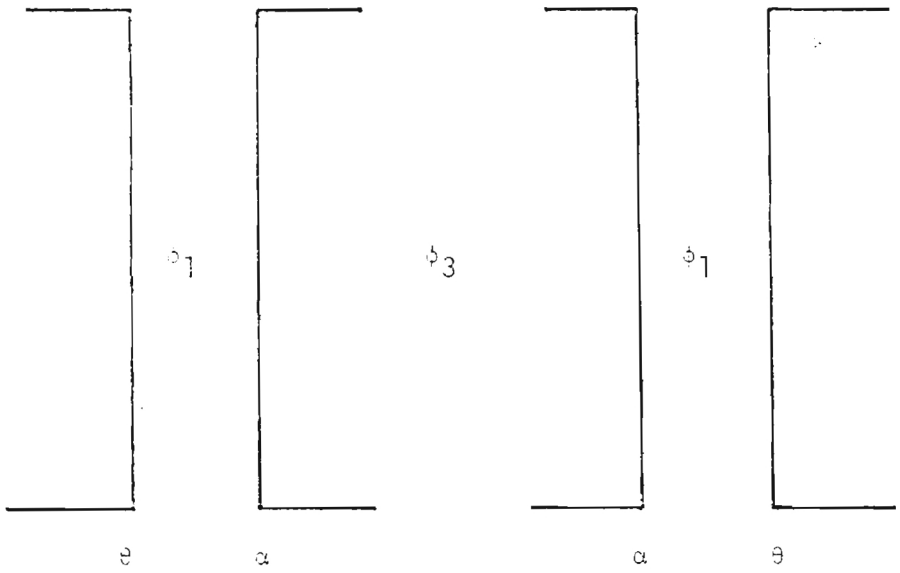

Figure 11(a). Two Pairs of Grids Forming an Interferometer.

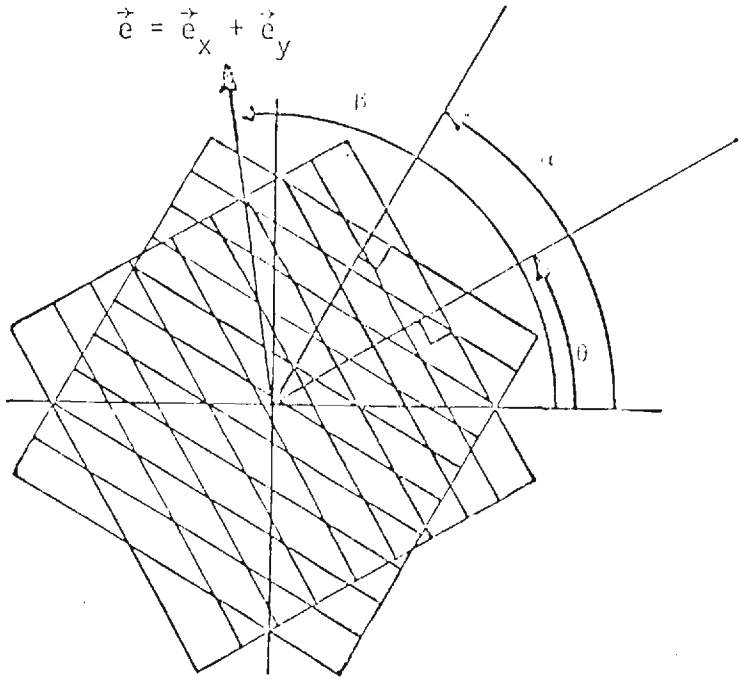

Figure 11(b). Definition of Wire Grid Parameters.

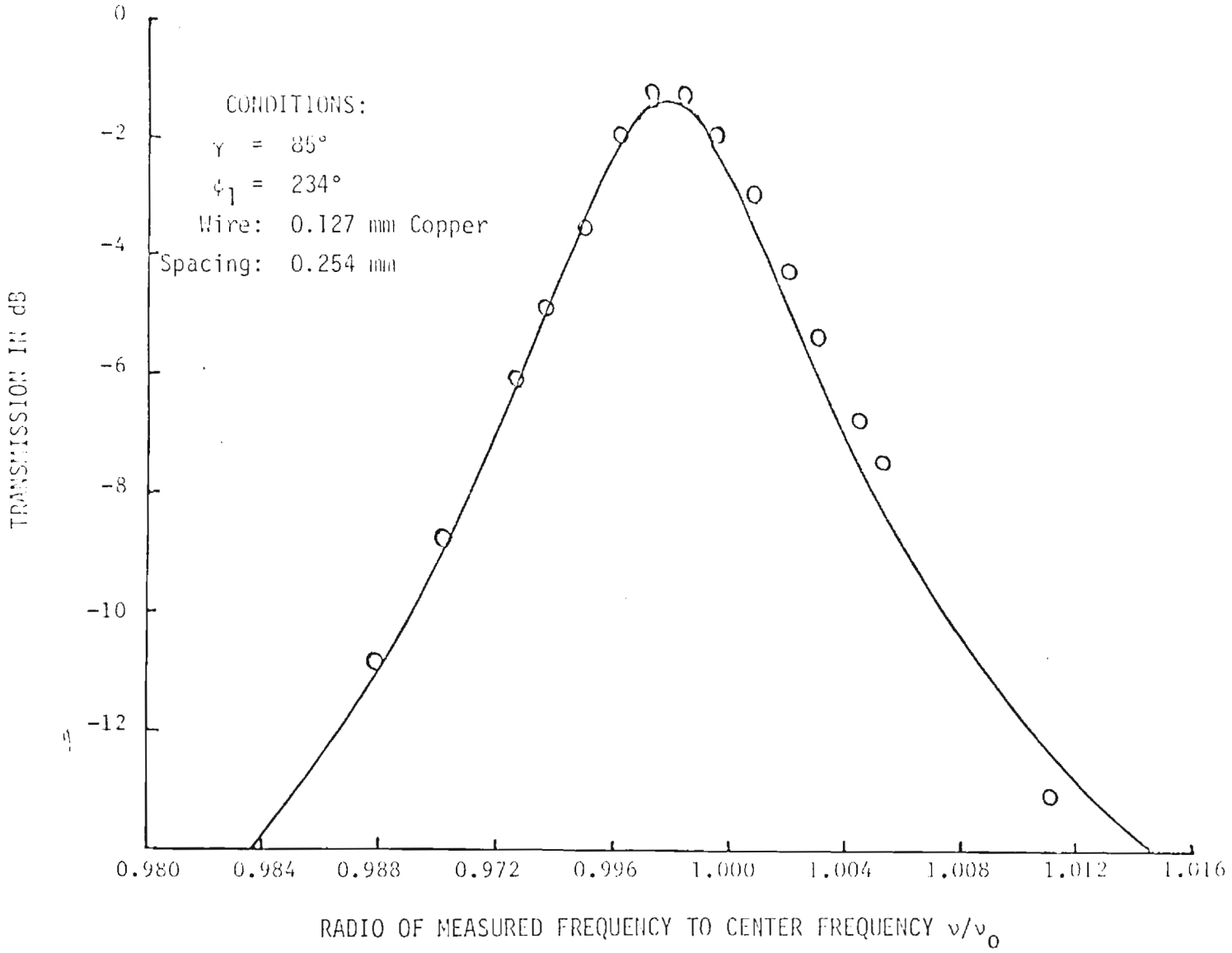

Figure 12. Grid Interferometer transmission as a function of frequency. The center frequency appears to be offset because of the presence of a frequency dependent factor in the transmission loss term.

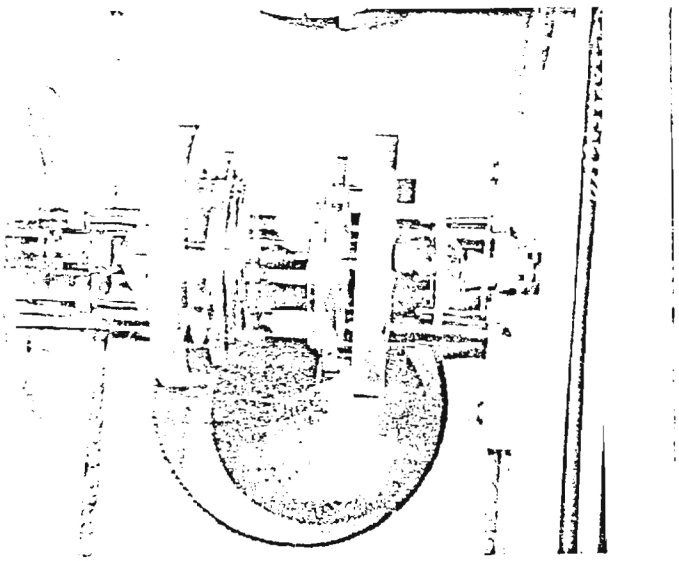

Figure 13. Parallel Plate Fabry-Perot Interferometer used in Molecular Beam Studies [14].

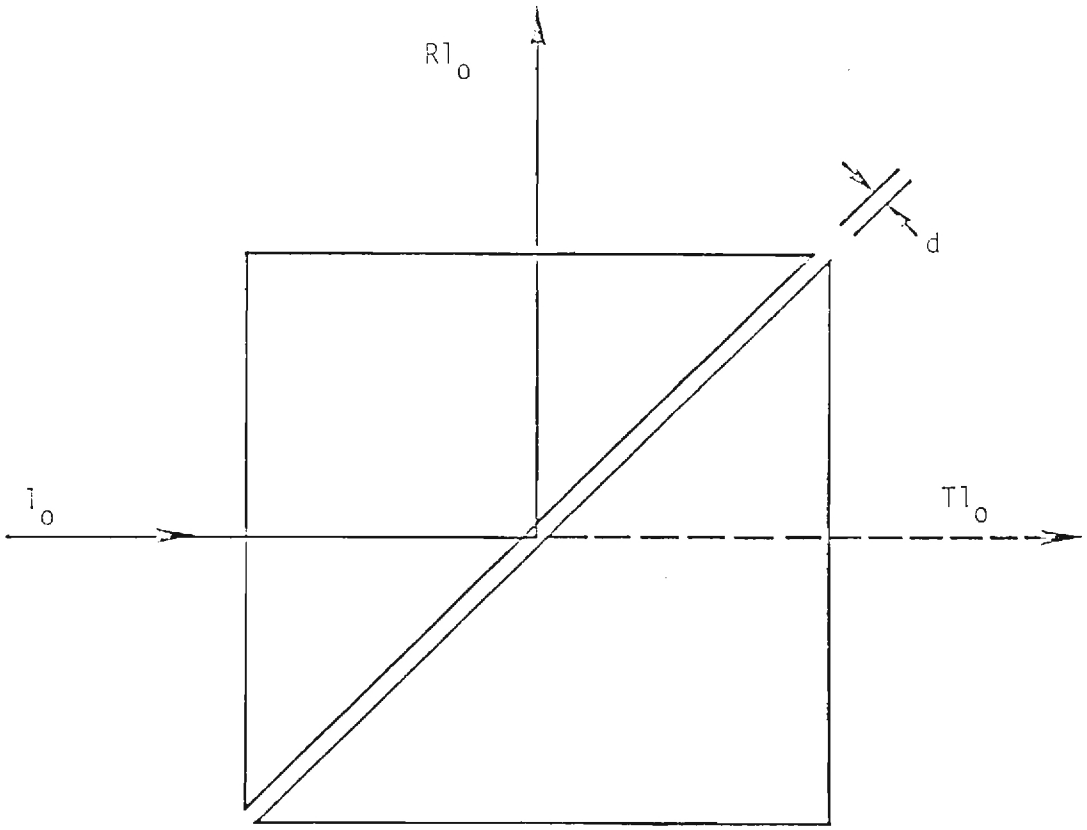

Figure 14. Double prism configuration.

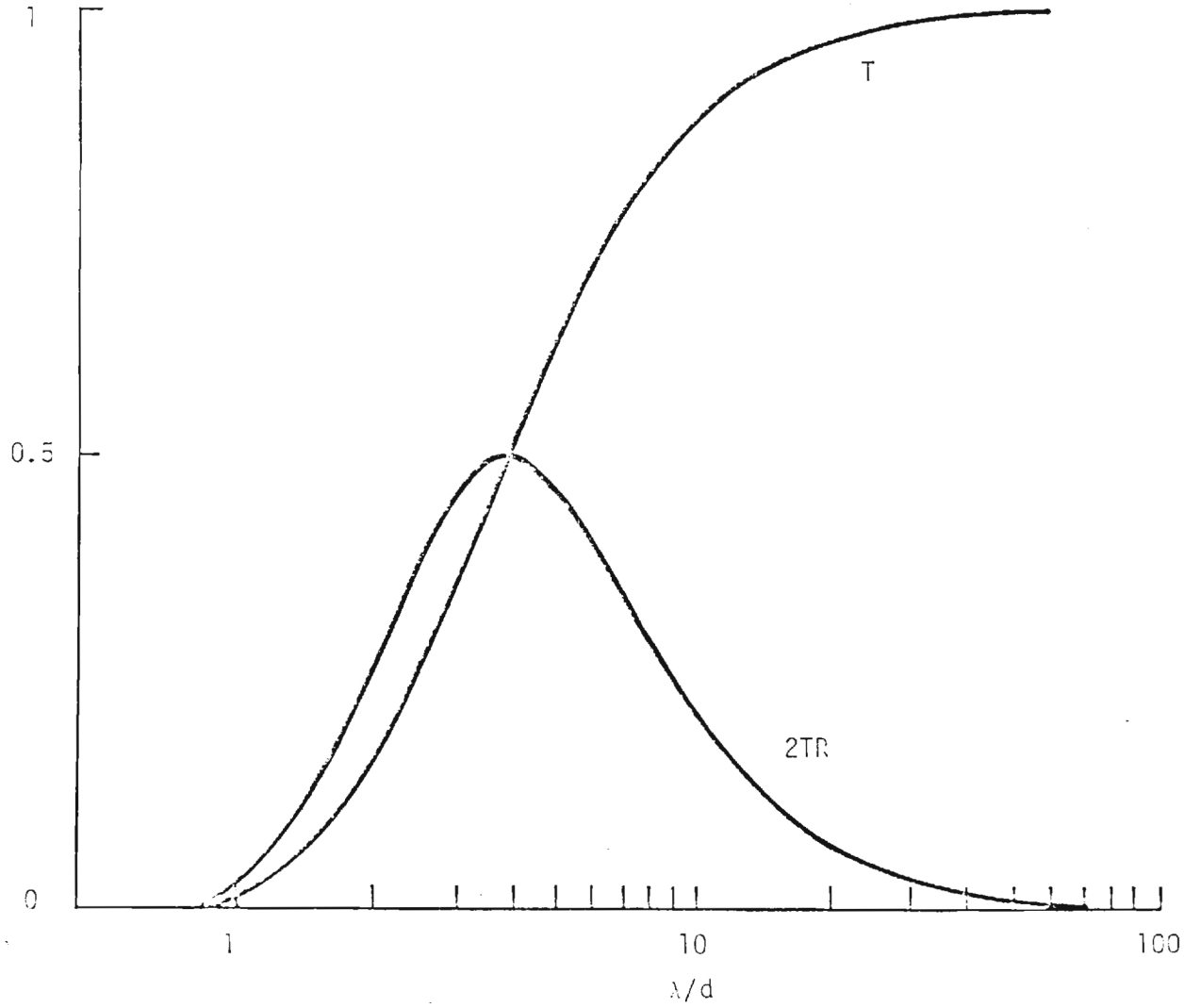

Figure 15. Transmittance of double prism as function of λ/d.

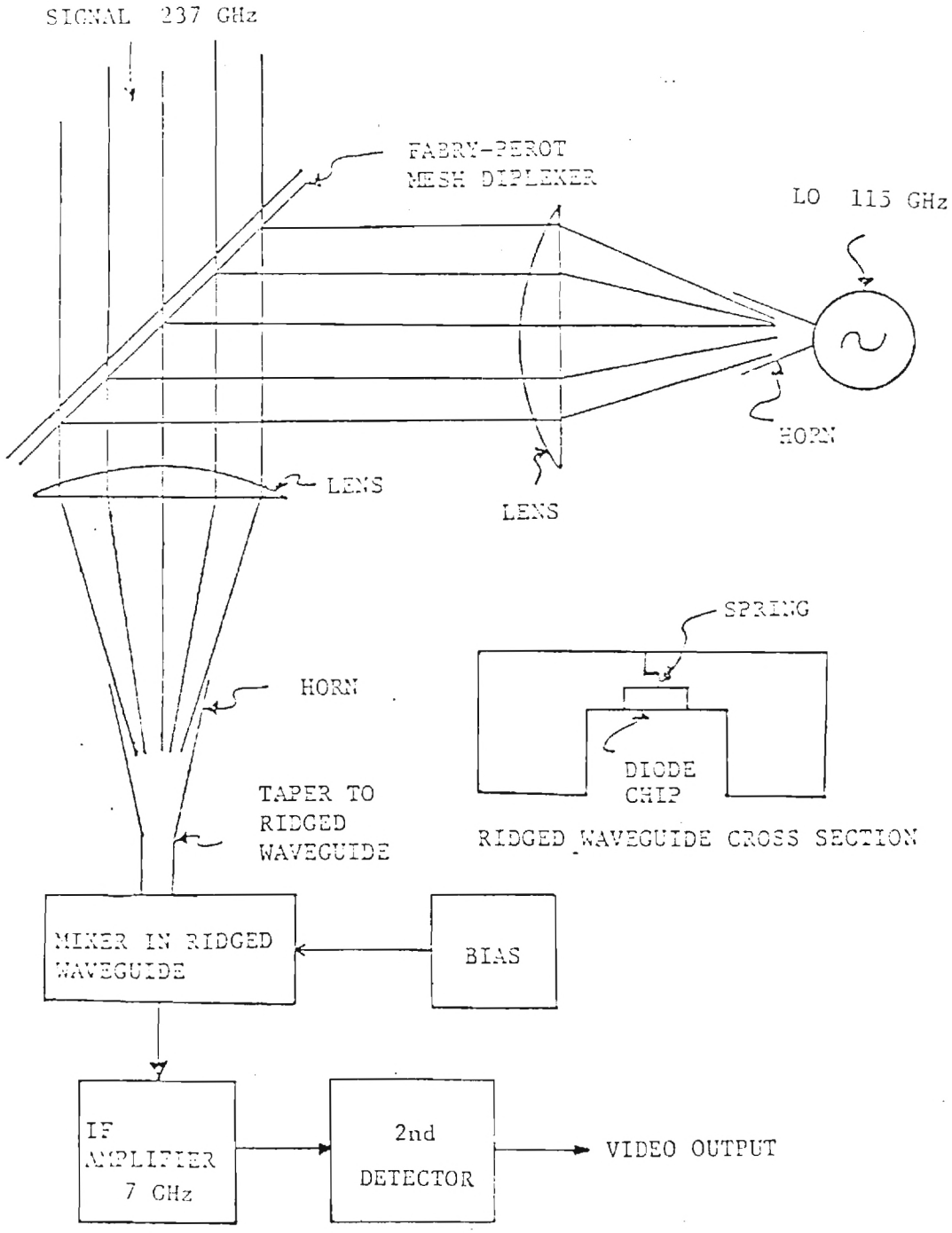

Figure 25. Superheterodyne Receiver.

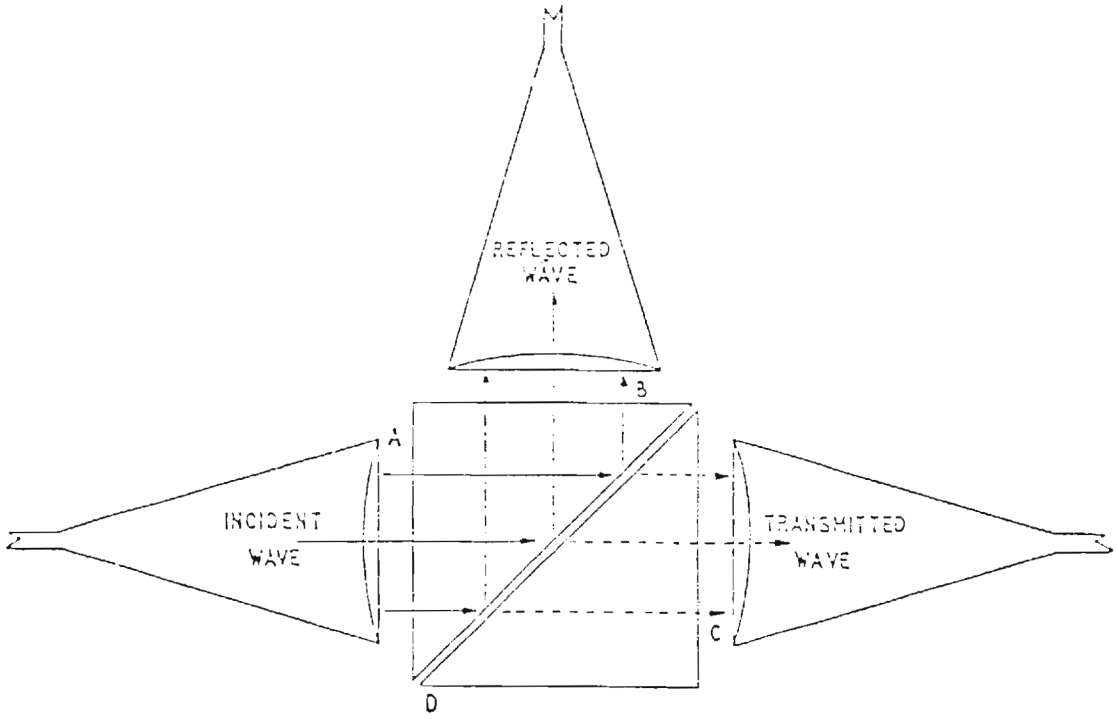

Figure 16. The Double-Prism Attenuator as used at millimeter wavelengths.

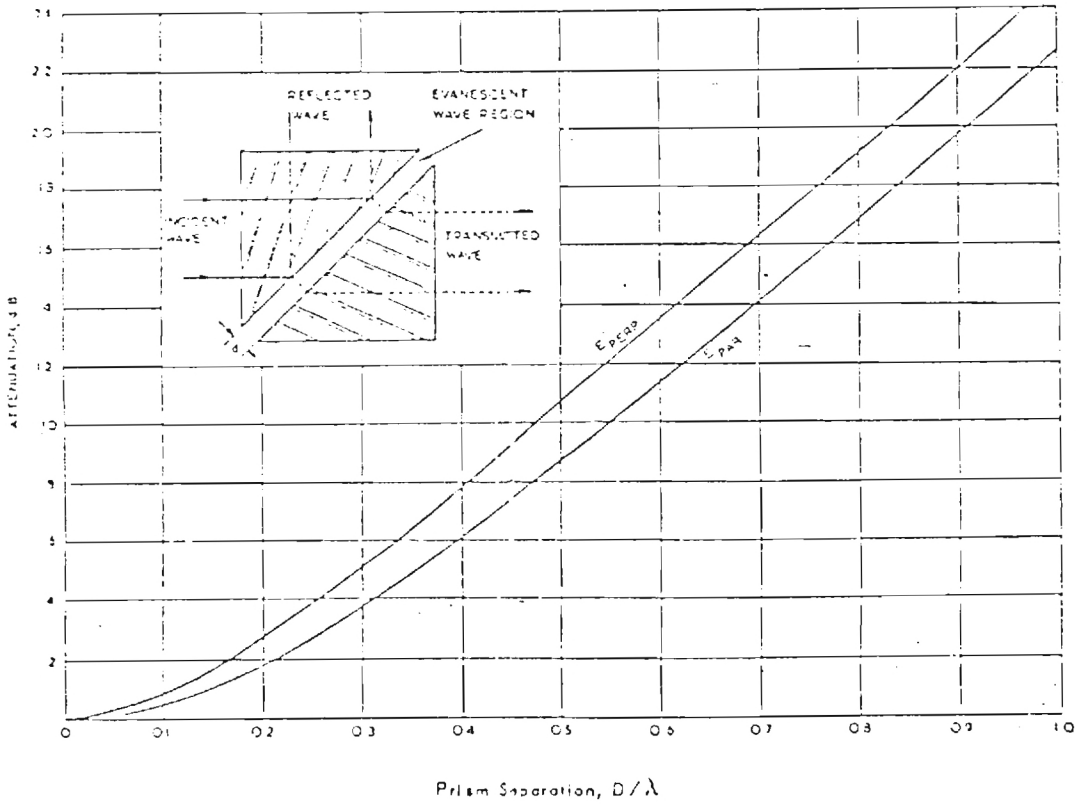

Figure 17. Graph of Attenuation -vs- Air Gap.

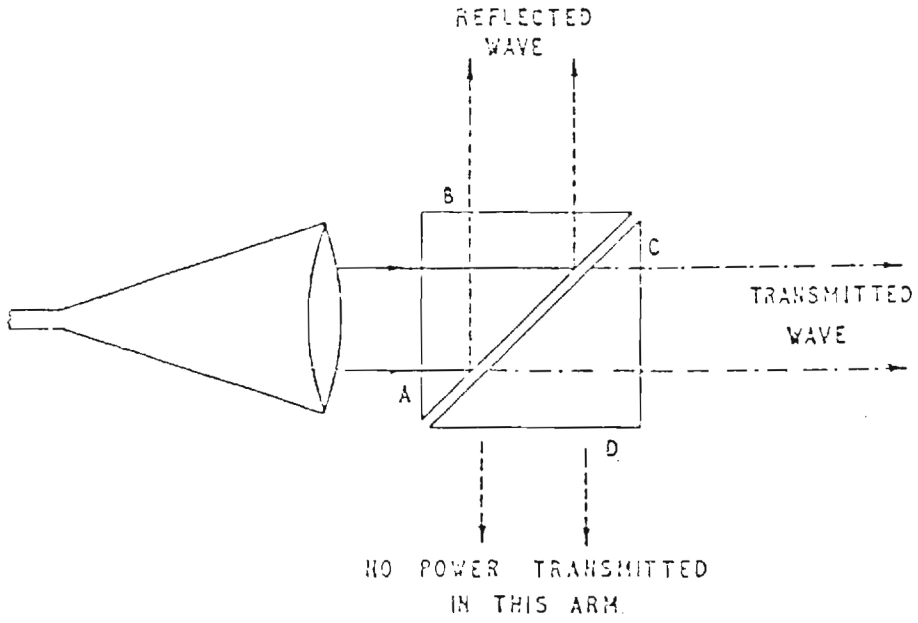

Figure 18. Optical Directional Coupler using the Double-Prism System.

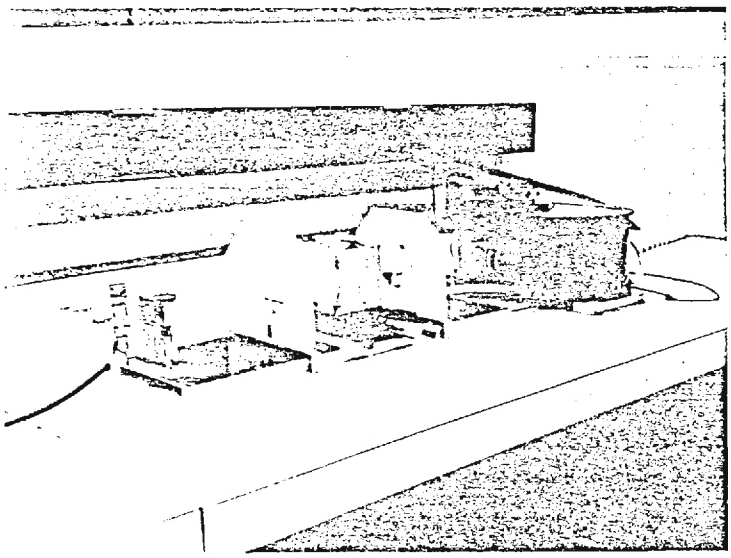

Figure 19. Double-Prism used with 300 GHz Carcinotron.

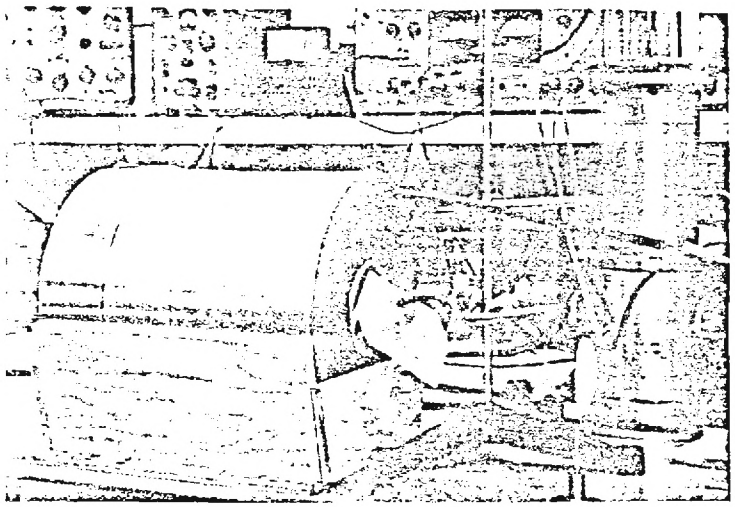

Figure 20. Side View of Fresnel Rhomb used as circular polarizer in Zeeman effect experiment.

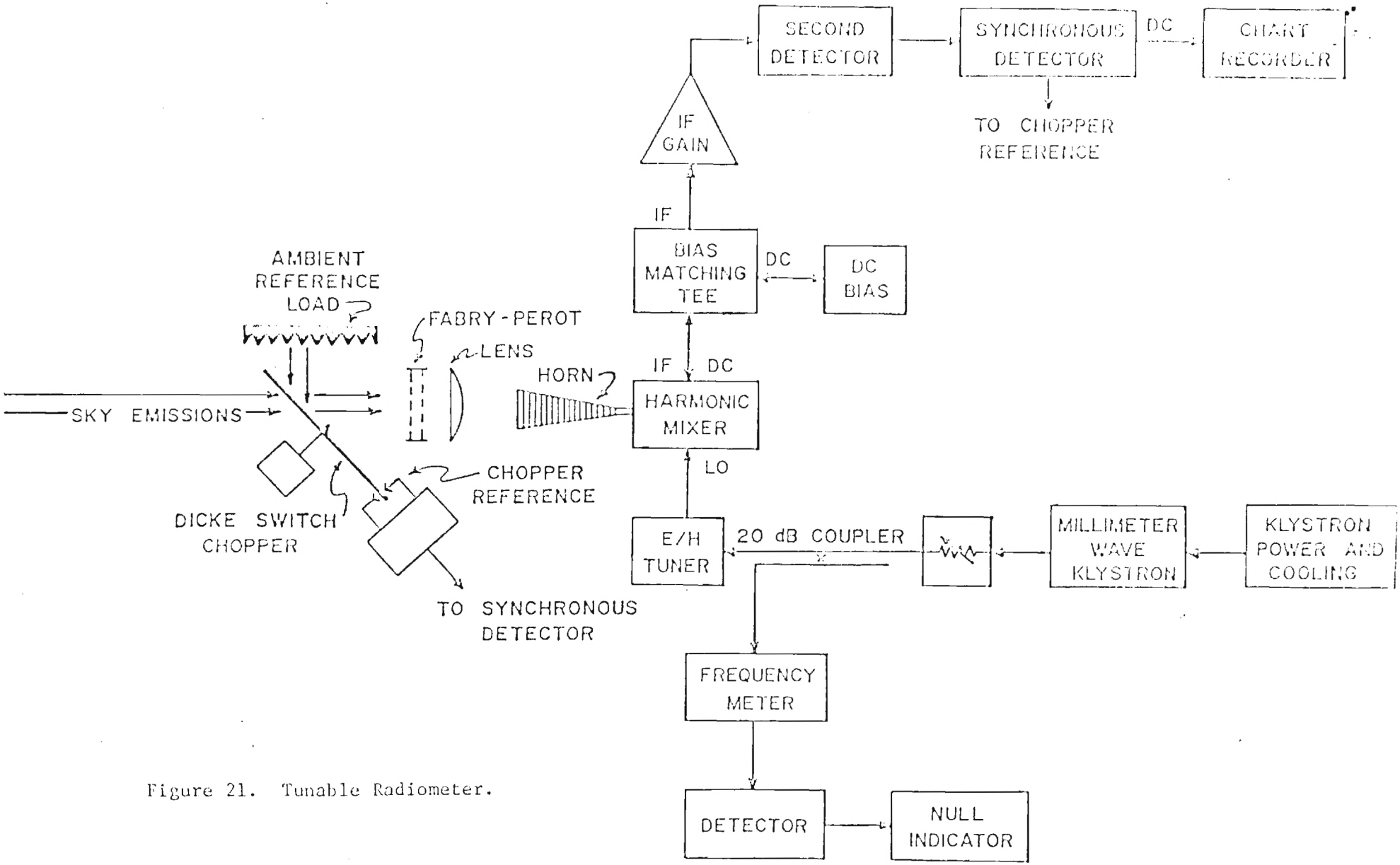

Figure 21. Tunable Radiometer.

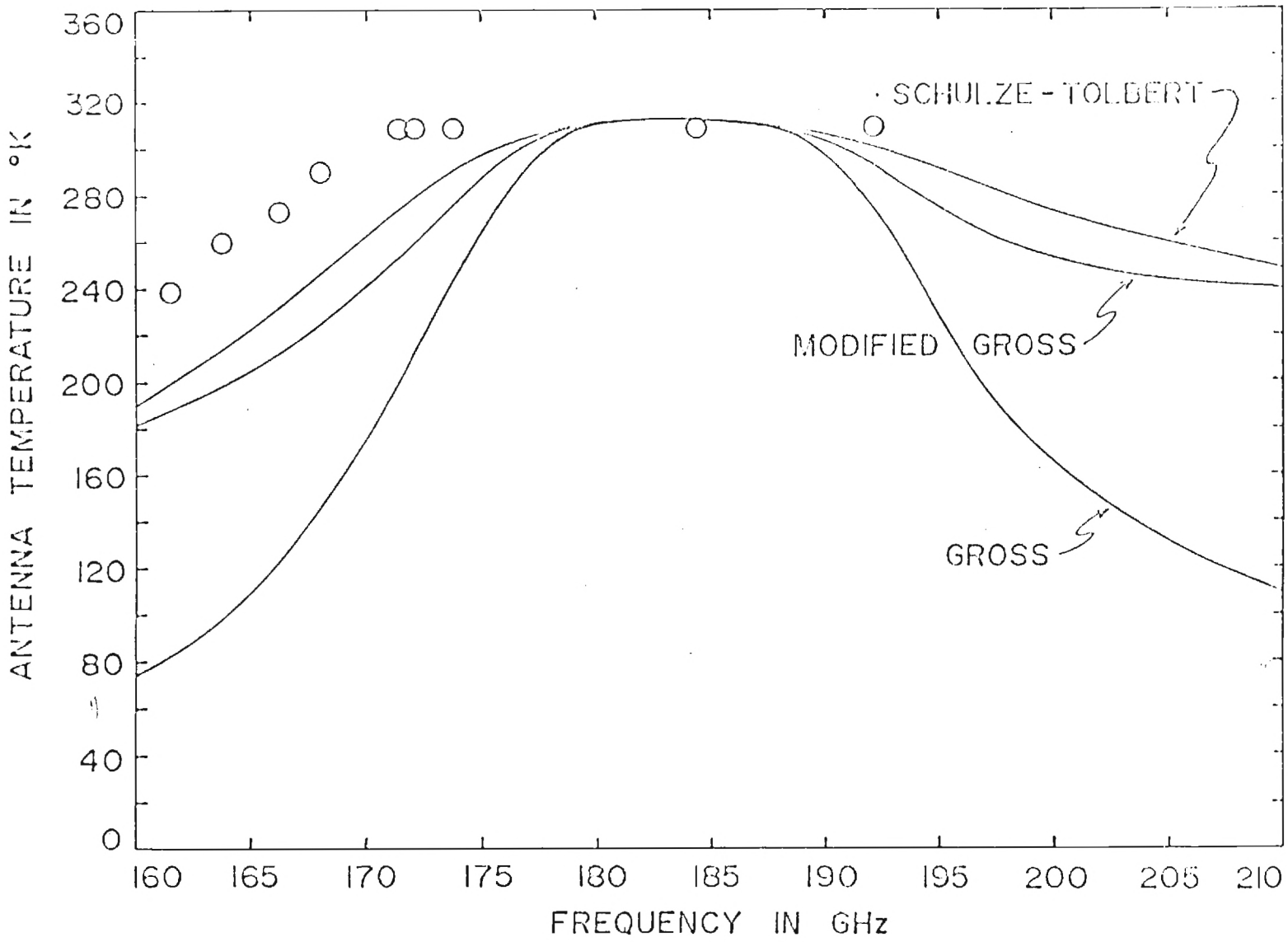

Figure 22(a). Radiometric Data. Antenna Temperatures measured on 7 July 1977. The solid lines are calculated curves using the various line shape factors, and the circles are experimental points. The surface water vapor density was 20.2 g/m^3 and the temperature was 111.0°F for these measurements.

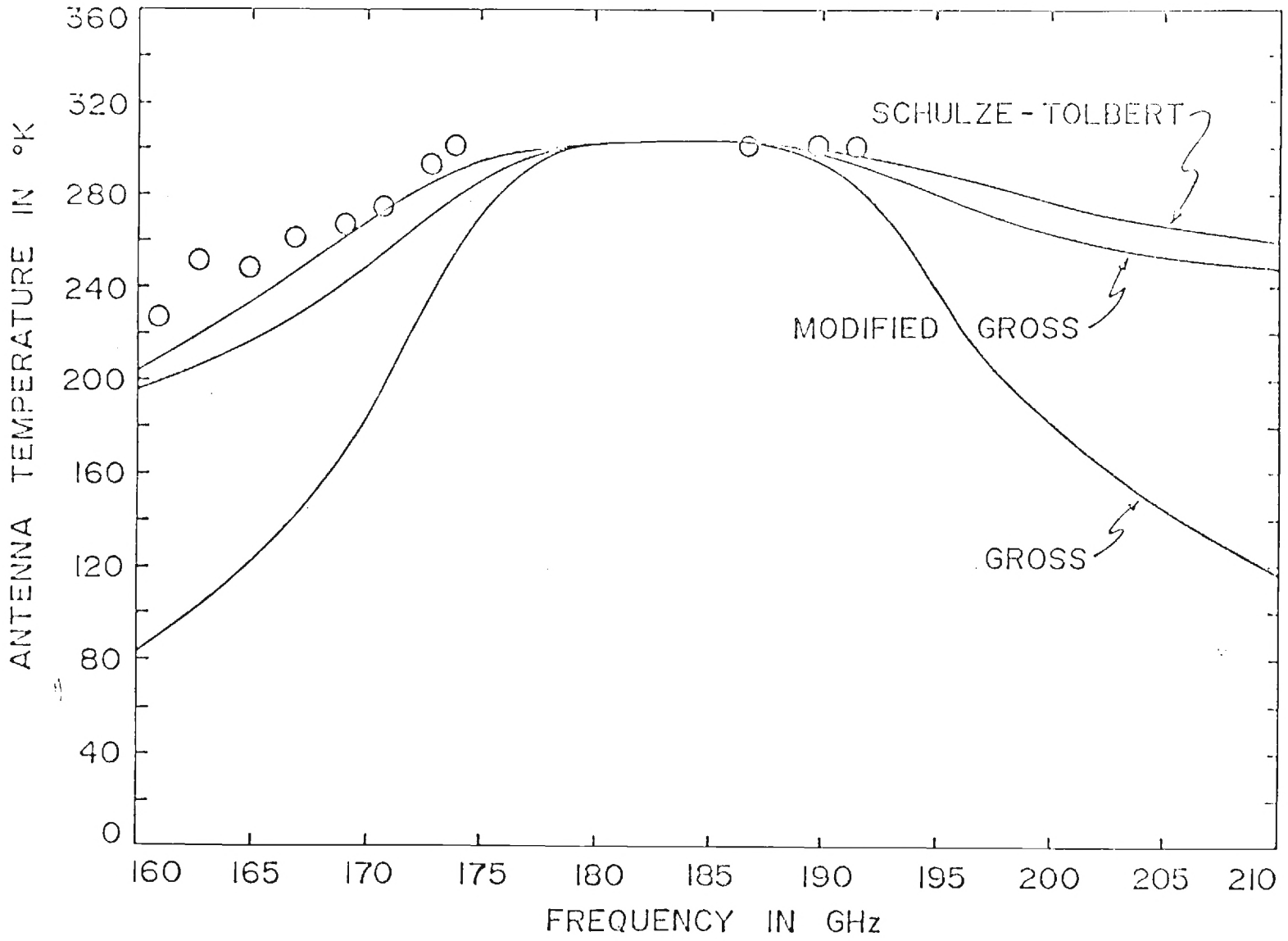

Figure 22(b). Radiometric Data. Antenna temperatures measured on 25 August 1977. The surface water vapor density was 22.9 g/m^3 and the temperature was 301.3°K for these measurements.

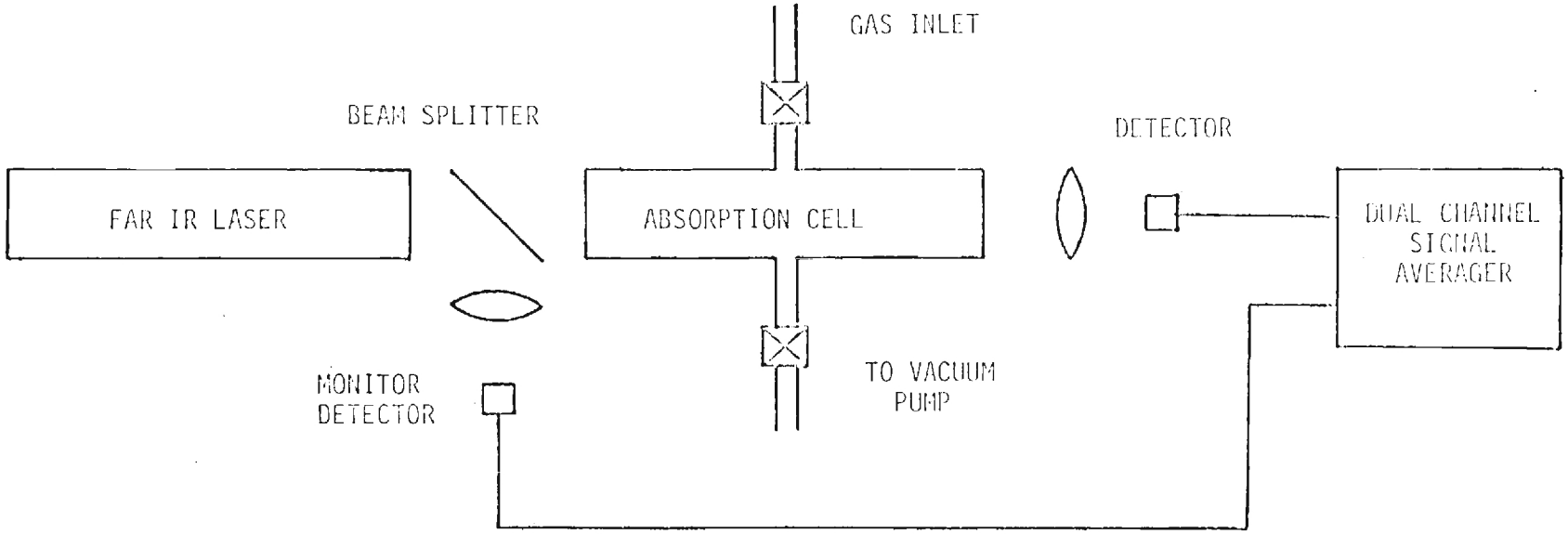

Figure 23. Apparatus used for Far Infrared Absorption Measurements using a Pulsed Far Infrared Laser.

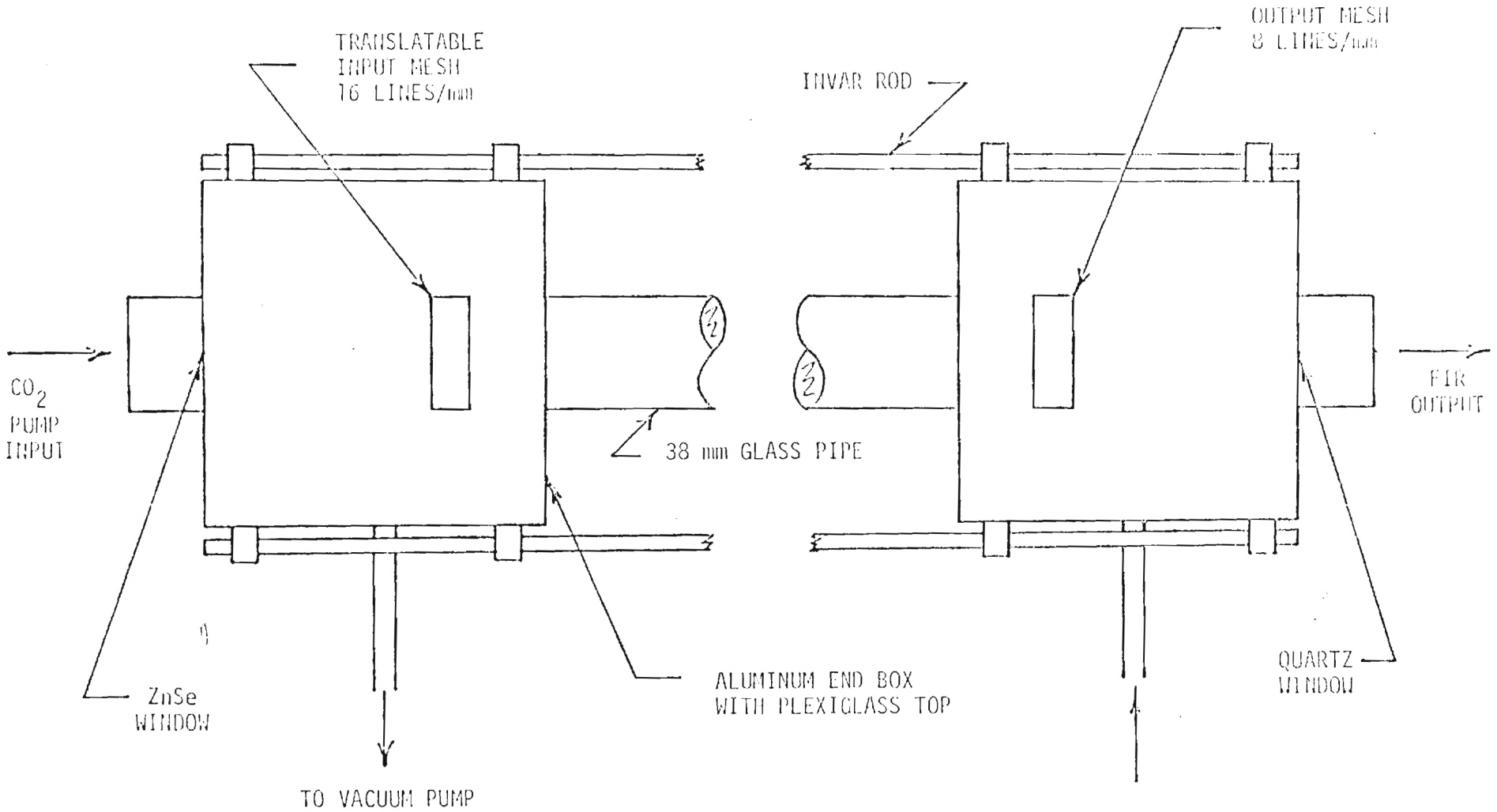

Figure 24. Schematic of Far Infrared Pulsed Laser.

SYNOPSIS OF
THE THIRD INTERNATIONAL CONFERENCE
ON SUBMILLIMETER WAVES
AND THEIR APPLICATIONS

Guildford, England

March 29 - April 1, 1978

1.0 INTRODUCTION

The third in the series of submillimeter conferences was attended by about 300 people from sixteen (16) different countries. Previous meetings in this series were held in Atlanta, Georgia in 1974 and in San Juan, Puerto Rico in 1976. The conference was held at the University of Surrey in Guildford, England, which is about thirty miles south of London. Meetings were conducted in three parallel sessions, but each day began with a general session covering a topic of wide interest. In this way, twenty-six different sessions were held during the three and one half day conference, which covered fourteen different subjects.

Attendees from Georgia Tech were M. D. Blue, J. J. Gallagher, R. W. McMillan, and J. H. Rainwater. A total of seven papers were presented by Georgia Tech personnel, including two which were based on work wholly or partially supported by ARO Grant DAAG29-76-G-0280. These Papers are listed at the end of this report. Travel Expenses of $925.00 were paid from grant funds for the travel of J. J. Gallagher. The other Georgia Tech conferees were supported by other funding.

2.0 SESSIONS ATTENDED

Sessions on the subjects of gas lasers; the atmosphere; electron beam sources; detectors, mixers, receivers; and measurement techniques and components were attended. A brief review of each of these sessions is given below.

2.1 Gas Lasers

The area of gas lasers has seen notable improvement since the last submillimeter conference. Approximately 1000 lines between 100 GHz and 3000 GHz have been observed, and pulsed output powers of 1 MW have been attained. CW powers of up to 0.5 W on selected wavelengths have also been observed. These advances were outlined in an invited paper by D. T. Hodges of Aerospace Corporation.

Many of the papers in the laser sessions were devoted to techniques for designing laser cavities and improving gas discharge and beam quality. A recurring problem in this area of submillimeter research is the accurate measurement of laser output power. Wide variations of measured power from a given laser were noted when different measuring devices were used. The attainment of megawatt power levels from far infrared (FIR) lasers was reported in two different papers.

Tunable FIR radiation has been generated by Stark tuning of the laser gas and by Raman scattering. In addition, second harmonic generation and frequency mixing has been carried out at submillimeter wavelengths.

2.2 The Atmosphere

Great interest in atmospheric effects was evidenced by the fact that there were three separate sessions on this subject. Anomalous absorption, defined as residual absorption observed after allowance has been made for all known phenomena, was the subject of an invited paper by H. A. Gebbie of Appleton Laboratories. Apparently, little progress has been made in explaining this absorption.

FIR lasers are being increasingly used to measure atmospheric absorption, and two papers gave results of measurements of this type. Several papers also dealt with absorption measurements using a Michelson interferometer and with such measurements made with a superheterodyne receiver using the sun as a radiation source. Atmospheric

radiometry and the effects of the atmosphere on astronomical observations in the FIR were subjects of other papers.

2.3 Electron Beam Sources

Both relativistic electron beam (REB) and backward wave oscillator sources were treated in this session. A review of principal results obtained in generating submillimeter radiation by coherent scattering from an intense REB was given in an invited paper by S. P. Schlesinger of Columbia University. A review of progress in the development of cyclotron masers (gyrotrons) was given by V. L. Granatstein of NRL. Pulsed power outputs and wavelengths obtained with these devices range from 200 - 300 kW at 1 cm to 10 kW at 800 μm. The submillimeter backward wave oscillator or carcinotron was also discussed, and it was noted that a wavelength coverage of 10 mm to 0.2 mm has been demonstrated.

Solid state sources were also discussed during this session. J. J. Purcell et al, of Plessey claim that the IMPATT can be used as a fundamental oscillator to 300 GHz, and usable harmonic components enable this range to be extended to 1000 GHz at milliwatt power levels. K. Mizuno et al, of Tohoku University have obtained output from IMPATTs up to 420 GHz, including 10 mW at 200 GHz and 10 μW at 400 GHz. This group also reported on frequency stabilization of these devices at 98 GHz.

2.4 Detectors, Mixers, and Receivers

Reports of research on photon drag, photoconductive, pyroelectric, Sckottky barrier, bolometer, and Josephson detectors were given in four separate conference sessions dealing with detectors, mixers, and receivers. In an invited paper, G. T. Wrixon of University College reviewed the status of Schottky barrier mixers and provided an enlightening overview of submillimeter wave diplexers. He also discussed quasi-optical diode mounting schemes including biconical re-

sonators and long wire (whisker) antennas. It is interesting to note that a paper given by W. M. Kelly of University College showed that InSb Schottky barrier diodes do not perform as well as GaAs diodes since the advantages expected because of higher carrier mobility are offset by plasma resonance effects.

Several papers dealt with open structure coupling schemes using long wire antennas. H. R. Fetterman et al, of MIT reported on a Schottky barrier diode receiver which used a corner reflector and a whisker which served as a long wire antenna. By using an FIR laser at 671 GHz for a local oscillator, they obtained a double sideband conversion loss of 11.9 dB. Open structure mixers were also discussed by H. Kräutle et al, of Max-Planck-Institut who measured antenna patterns at 890 GHz. Dielectric plate antennas for Schottky barrier detectors were treated in a paper by Daiku et. al., of Tohoku Institute of Technology who built miniature Yagi antennas on dielectric substrates.

2.5 Measurement Techniques and Components

Interference filters, dielectric waveguides, Fabry-Perot filters, mesh gratings, and polarizers were the subjects of papers in this session. Metallic mesh interference filters useful to low temperatures were discussed by G. D. Holah et al of Heriot-Watt University. These filters typically have transmissions of 40 - 90% and bandwidths of 5 cm^{-1} (150 GHz) at frequencies of 40 - 150 cm^{-1}. Computer analysis of metallic mesh gratings was discussed by C. H. Ma of the University of Mississippi who obtained analytical results on transmission and reflection of these devices which agree well with experiment. A submillimeter polarization independent beam splitter made of quartz was the subject of a paper by A. M. Frank of Lawrence Livermore.

The paper on polarization-twisting, bandpass tunable Fabry-Perot filters by R. W. McMillan, C. H. Branch, and G. M. Lamb was also presented in this session. The paper was very well received, as evidenced

A-1861

SUBMILLIMETER WAVE SPECTROSCOPY AND TECHNOLOGY

THIRD SEMI-ANNUAL TECHNICAL REPORT

J. J. Gallagher

M. D. Blue

February 8, 1978

U. S. ARMY RESEARCH OFFICE

Grant No. DAAG29-76-G-0280

Georgia Institute of Technology
Engineering Experiment Station
Electromagnetics Laboratory
Atlanta, Georgia 30332

SECURITY CLASSIFICATION OF THIS PAGE *(When Data Entered)*

REPORT DOCUMENTATION PAGE		READ INSTRUCTIONS BEFORE COMPLETING FORM
1. REPORT NUMBER Third Semi-Annual Technical	2. GOVT ACCESSION NO.	3. RECIPIENT'S CATALOG NUMBER
4. TITLE *(and Subtitle)* Submillimeter Wave Spectroscopy and Technology		5. TYPE OF REPORT & PERIOD COVERED SEMI-ANNUAL 1 July - 31 December, 1977
		6. PERFORMING ORG. REPORT NUMBER
7. AUTHOR(s) J. J. Gallagher & M. D. Blue		8. CONTRACT OR GRANT NUMBER(s) DAAG29-76-G-0280
9. PERFORMING ORGANIZATION NAME AND ADDRESS Engineering Experiment Station Georgia Institute of Technology Atlanta, Georgia 30332		10. PROGRAM ELEMENT, PROJECT, TASK AREA & WORK UNIT NUMBERS
11. CONTROLLING OFFICE NAME AND ADDRESS U. S. Army Research Office Post Office Box 12211 Research Triangle Park, N.C. 27709		12. REPORT DATE February 8, 1978 13. NUMBER OF PAGES
14. MONITORING AGENCY NAME & ADDRESS*(if different from Controlling Office)*		15. SECURITY CLASS. *(of this report)* Unclassified 15a. DECLASSIFICATION/DOWNGRADING SCHEDULE N/A

16. DISTRIBUTION STATEMENT *(of this Report)*

Approved for public release; distribution unlimited.

17. DISTRIBUTION STATEMENT *(of the abstract entered in Block 20, if different from Report)*

N/A

18. SUPPLEMENTARY NOTES

The findings in this report are not to be construed as an official Department of the Army position, unless so designated by other authorized documents.

19. KEY WORDS *(Continue on reverse side if necessary and identify by block number)*

Submillimeter Waves; Schottky Barrier Diodes; Spectroscopy; Water Molecules; Fabry-Perot Interferometers; Electron Beam Sources; Heterodyne Receivers; Atmospheric Absorption.

20 ABSTRACT *(Continue on reverse side if necessary and identify by block number)*

Spectroscopic investigations have continued on atmospheric molecules. Work continues on receiver and mixer technology for the submillimeter wavelength region. Work on optically pumped lasers as receiver L.O.'s, quasi-optical devices and waveguide filters are continuing efforts. A CO_2 laser for optical pumping has been constructed. A Fourier spectrometer for atmospheric and spectroscopic measurements has been designed and constructed.

DD FORM 1 JAN 73 1473 EDITION OF 1 NOV 65 IS OBSOLETE

SECURITY CLASSIFICATION OF THIS PAGE *(When Data Entered)*

PROGRESS REPORT

(TWENTY COPIES REQUIRED)

1. ARO PROPOSAL NUMBER: P-14104-PX

2. PERIOD COVERED BY REPORT: 1 July, 1977 - 31 December, 1977

3. TITLE OF PROPOSAL: Submillimeter Wave Spectroscopy and Technology

4. CONTRACT OR GRANT NUMBER: DAAG29-76-G-0280

5. NAME OF INSTITUTION: Georgia Institute of Technology, Engineering Experiment Station

6. AUTHOR(S) OF REPORT: J. J. Gallagher and M. D. Blue

7. LIST OF MANUSCRIPTS SUBMITTED OR PUBLISHED UNDER ARO SPONSORSHIP DURING THIS PERIOD, INCLUDING JOURNAL REFERENCES:

   See attached abstracts.

8. SCIENTIFIC PERSONNEL SUPPORTED BY THIS PROJECT AND DEGREES AWARDED DURING THIS REPORTING PERIOD:

   J. J. Gallagher
   J. H. Rainwater
   P. B. Reinhart
   R. Rogers
   W. M. Penn
   A. M. Cook, Student
   C. H. Branch, Student
   O. Simpson, Student

Dr. M. D. Blue
Dr. J. J. Gallagher
Georgia Institute of Technology
Engineering Experiment Station
Atlanta, GA 30332

BRIEF OUTLINE OF RESEARCH FINDINGS

During the past six months, work has been proceeding on the spectroscopy of atmospheric constituents. Several techniques have been employed; these techniques and the results to date will be discussed in a paper which has been accepted for presentation at the Third International Conference On Submillimeter Waves and Their Applications to be held at Guildford, England on March 29, 1978. The abstract for this work is attached. A technical report will be prepared in April on this subject detailing the results to date.

Investigations are underway on an acoustic detector which will be employed for spectroscopic work using optically pumped lasers.

Difficulties experienced with a commercial CO_2 laser used as a source for an optically pumped submillimeter laser has resulted in the construction of a grating tuned 20-30 W CO_2 laser. This source is being used for both spectroscopy and receiver development. A quasi-optic mixer has been designed and delivery from Custom Microwaves is expected during March. This mixer will be integrated with the quasi-optic diplexer and optically pumped laser to form the submillimeter receiver.

A small Fourier spectrometer has been built for use on propagation, spectroscopy and field trips. The instrument when completely checked out will provide the Army with a technique for broad band observations with compact, inexpensive apparatus. A technical report on this apparatus will be issued during the next reporting period.

A paper has been submitted for presentation at the AGARD Symposium on "Millimeter and Submillimeter Wave Propagation and Circuits". A copy of the abstract is attached.

A paper reviewing submillimeter techniques and applications is in preparation for submission to the Proceedings of IEEE. This will be completed during the month of February.

A paper on the "Prediction of the Existence of a Sharp Peak in Water Vapor Emission Lines in Down-Looking Radiometry" has also been accepted for presentation at Guildford. The abstract for this paper is attached.

SUBMITTED FOR PRESENTATION AT THE AGARD SYMPOSIUM ON
"MILLIMETER AND SUBMILLIMETER WAVE PROPAGATION AND CIRCUITS"

CONCEPTS AND TECHNIQUES IN THE UTILIZATION OF MILLIMETER AND SUBMILLIMETER WAVES

J. H. Rainwater, R. W. McMillan and J. J. Gallagher

Engineering Experiment Station
Georgia Institute of Technology
Atlanta, Georgia 30332

The attractiveness of millimeter and submillimeter waves for remote sensing, weapon guidance and other applications has given impetus to research and development of millimeter and submillimeter devices and systems and has necessitated characterization of atmospheric propagation effects in the atmosphere. The evolution of quasi-optical devices and techniques from a synthesis of microwave and optical practices has proceeded along with the extension of more familiar microwave devices into the millimeter and submillimeter regions.

Georgia Tech is conducting extensive research and development programs aimed at the goal of millimeter and submillimeter wave utilization. The programs described briefly below, involve atmospheric propagation and component development.

SUBMILLIMETER RADIOMETRY

A Dicke superheterodyne radiometer has been developed to measure the emission spectrum of atmospheric water vapor from 160 to 210 GHz. The radiometer employs a quasi-optical Fabry-Perot bandpass filter and a Schottky barrier crossed wave guide harmonic mixer. Theoretical calculations of the emission line shape have been performed using various models and compared with experimental data. The emission data can be used to calculate atmospheric absorption in the submillimeter region due to water vapor.

QUASI-OPTICAL DEVICES AND TECHNIQUES

Theoretical calculations and experimental data on Fabry-Perot type wire grid and metal mesh devices have been performed. These devices can be configured as tunable bandpass filters, power dividers, diplexers and couplers in the millimeter and submillimeter region. Quasi-optical apparatus currently being employed include Fabry-Perot spectrometers and wavemeters, diplexers and attenuators.

EXTENSIONS OF MICROWAVE TECHNIQUES

The incorporation of Schottky barrier diodes in structures suitable as detectors and mixers in the millimeter and submillimeter regions has been designed, built and tested at Georgia Tech. An airborne radiometer using fundamental mixing at 183 GHz with system noise figures below 10 dB has been operated. The development of submillimeter, subharmonic mixing techniques from a study of microwave models is being performed. A submillimeter optically pumped laser is employed as the local oscillator, and a 225 GHz IMPATT is available as an alternate source.

SPECTROSCOPIC MEASUREMENTS

Spectroscopy of the millimeter-submillimeter wavelength region is closely related to the molecular constituents of the atmosphere. An extensive program on water vapor absorption is being performed. Both coherent and incoherent spectroscopy are being investigated. Spectrometers include large Fabry-Perot spectrometers (for non-resonant absorption measurements), waveguide cells for line width and line shape measurements at reduced pressures, parallel plate Stark cells for dipole moments and Fourier spectrometers. Straight absorption measurements with an optically pumped laser and a carcinotron complement the other measurements.

PROPAGATION MEASUREMENTS

A meteorologically instrumented propagation range is being assembled at Georgia Tech to provide comparative measurements for wavelengths from the visible through the millimeter wavelength region. The following sources will be employed with appropriate receivers:

An argon laser at 0.5 μm

A YAG:Nd laser at 1.06 μm

A 10.6 μm CO_2 laser

An optically pumped laser operating at 880 μm

A 1 mm Carcinotron

A 1.3 mm IMPATT

A 2.1 mm klystron

A 3 mm klystron

A 8 mm klystron

Simultaneous operation of all systems are planned. Descriptions will be given of the systems and preliminary results of measurements.

In addition to the discussion of the above subjects, description will be given of Georgia Tech work on a CO_2 TEA-laser optically pumped source with outputs for propagation at 230 GHz and 340 GHz, and its associated superheterodyne receiver, construction of a portable propagation facility, radiometric work for airborne applications for Project Storm Fury and ground mapping, theoretical studies of satellite radiometric observations of millimeter/submillimeter water lineshapes as a means of determining water vapor distributions, and the trends suggested by recent studies of military applications.

TO BE PRESENTED AT THE THIRD INTERNATIONAL CONFERENCE
ON SUBMILLIMETER WAVES AND THEIR APPLICATIONS

PREDICTION OF THE EXISTENCE OF A SHARP PEAK IN WATER VAPOR EMISSION LINES IN DOWN-LOOKING RADIOMETRY*

J. J. Gallagher and R. W. McMillan
Georgia Institute of Technology, Atlanta, Ga. 30332

The height distribution of atmospheric water vapor has been the subject of dispute for many years. Currently, there is a substantial body of data which suggests that H_2O concentration decreases rapidly with altitude to a density of about 10^{-3} g/m^3 at about 20 km and then starts to increase again with increasing height. Based on this distribution, a technique has been proposed for the remote sensing of stratospheric H_2O which involves measuring the shape of a sharp peak superimposed on the 22.235 GHz emission line when observed looking upward from the ground. In this paper, we present analytical evidence for the existence of a similar peak superimposed on emissions from the stronger H_2O lines which should be observable in down-looking radiometry. The variation in shape of this peak as a function of the stratospheric water vapor distribution is analyzed.

The background temperature T_B measured by a radiometer looking downward from altitude h at an angle θ to the vertical is given by

$$T_B = \int_h^o T(Z)\exp[-\tau(h,Z,\theta)]\alpha(Z)\sec\theta dZ \qquad (1)$$
$$+ R\exp[-\tau(0,h,\theta)] \int_h^o T(Z)\exp[-\tau(Z,0,\theta)]\alpha(Z)\sec\theta dZ + (1-R)T_E\exp[-\tau(0,h,\theta)] ,$$

where T_E is the earth temperature and T(Z) is the temperature of a stratum of atmosphere of thickness dZ located at altitude Z. The terms of the form $\tau(Z_1,Z_2,\theta)$ are the optical depths between altitudes Z_1 and Z_2 at angle θ, and R is the reflectivity of the earth. The term $\alpha(Z)$ is the atmospheric attenuation coefficient, and is dependent on a number of variables including temperature, pressure, water vapor density, and the form of the emission line shape parameter. The effect of an absorption continuum was not considered in these calculations because there is no analytical basis for its inclusion. In Equation (1), the first term is the direct emission of the atmosphere, the second term is atmospheric emission reflected from the earth, and the third term is the emission of the earth modified by the atmospheric attenuation between the ground and altitude h.

Equation (1) was numerically integrated over the frequency range 100-700 GHz to a height of 50 km using the nine strongest water vapor absorptions below 1000 GHz, and the results of this integration are shown graphically in Figure 1. In making this calculation, a water vapor distribution with a secondary maximum

at an altitude of 27 km was assumed. Note the presence of the characteristic peaks caused by this high altitude water vapor.

The rather strange shape of the predicted emission from high altitude H_2O is caused by a combination of several factors. In regions of low attenuation between lines, the radiometer is able to "see" far into the atmosphere to warmer air layers and to the earth itself. At frequencies falling on the skirts of the lines, absorption is greater and the radiometer sees only the colder upper atmospheric layers. Finally, at the line center frequencies, the absorption is very large and the radiometer sees only a short distance into the atmosphere. However, at these great altitudes, the atmosphere is warm, thus the region near the line center frequency shows a sharp peak in emission due to these warm layers. Because of the relatively high temperature and the low pressure in the stratosphere, it is difficult to conceive of a high-altitude water vapor distribution which does not exhibit these sharp peaks on emission line centers.

Several different upper atmospheric water vapor distributions have been analyzed, and each gives a different emission line shape. It is not known whether a measured line shape could be used to determine a corresponding water vapor distribution, but the observation of a sharp peak in emission will almost certainly indicate the presence of high altitude water vapor.

*This work was supported by the National Aeronautics and Space Administration, Goddard Space Flight Center, Under Grant No. NSG-5012, and by the U. S. Army Research Office under Grant No. DAAG29-76-G-0280.

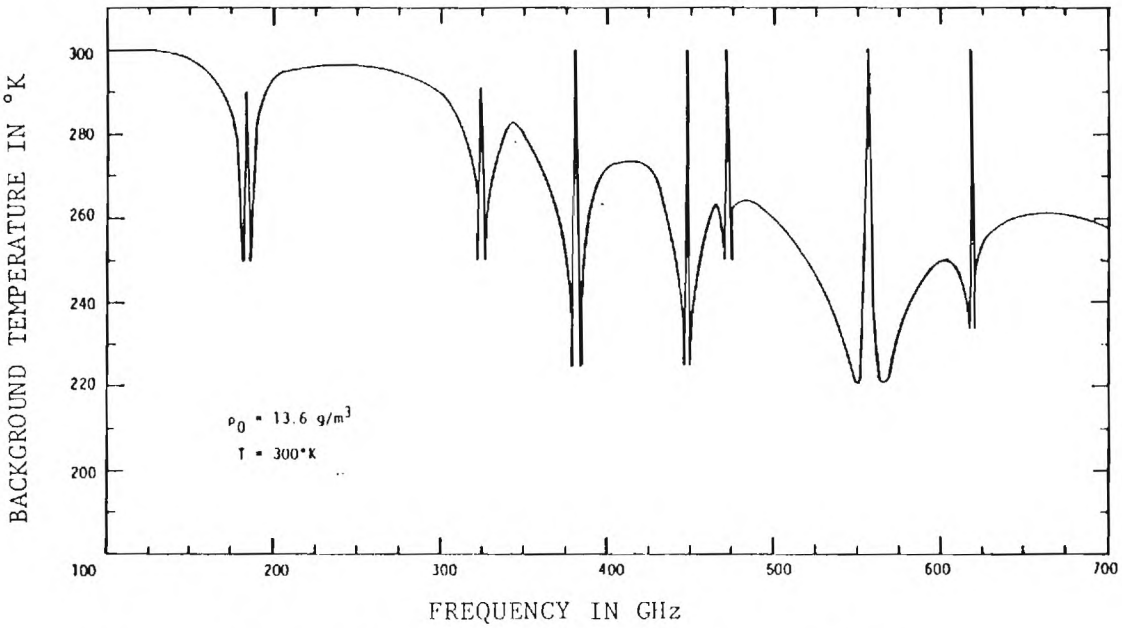

Figure 1. Calculated background temperature due to water vapor observed from an altitude of 50 km.

TO BE PRESENTED AT THE THIRD INTERNATIONAL CONFERENCE
ON SUBMILLIMETER WAVES AND THEIR APPLICATIONS

SUBMILLIMETER SPECTROSCOPY OF ATMOSPHERIC WATER VAPOR

R. Rogers, P. Reinhart, H. Rainwater,
O. Simpson, W. Penn and J. Gallagher

Engineering Experiment Station
Georgia Institute of Technology
Atlanta, Georgia 30332

A study of the attenuation of submillimeter radiation by water vapor is reported. The window regions of 125 - 160 GHz, 210 - 270 GHz and 320 - 370 GHz have been investigated by Fabry-Perot interferometry, line shapes and half widths have been studied by waveguide cell techniques, and monochromatic measurements at single frequencies have been performed by optically pumped lasers, IMPATTS, klystrons and a carcinotron. Absorption due to water vapor alone or mixed with atmospheric vapors has been investigated. These experimental measurements are compared with theoretical calculations based on both Gross and Van Vleck - Weisskopf line-shapes. A discussion of the discrepancy between theoretical calculations and experimental measurements is given.

A-1861

PROGRESS REPORT

(TWENTY COPIES REQUIRED)

1. ARO PROPOSAL NUMBER: P-14104-PX

2. PERIOD COVERED BY REPORT: 1 July, 1978 - 31 January, 1979

3. TITLE OF PROPOSAL: SUBMILLIMETER WAVE SPECTROSCOPY AND TECHNOLOGY

4. CONTRACT OR GRANT NUMBER: DAAG29-76-G-0280

5. NAME OF INSTITUTION: Engineering Experiment Station
Georgia Institute of Technology

6. AUTHOR(S) OF REPORT: J. J. Gallagher, M. D. Blue

7. LIST OF MANUSCRIPTS SUBMITTED OR PUBLISHED UNDER ARO SPONSORSHIP DURING THIS PERIOD, INCLUDING JOURNAL REFERENCES:

8. SCIENTIFIC PERSONNEL SUPPORTED BY THIS PROJECT AND DEGREES AWARDED DURING THIS REPORTING PERIOD:

J. J. Gallagher
V. T. Brady
W. D. Fife
P. B. Reinhart
O. A. Simpson, Student
J. R. Hodges, Student
R. H. Platt, Student
D. R. Davis, Student
A. V. Pallone, Student

14104-P

Dr. M. D. Blue
Dr. J. J. Gallagher
Georgia Institute of Technology
Engineering Experiment Station
Atlanta, GA 30332

BRIEF OUTLINE OF RESEARCH FINDINGS

During the reporting period from 1 July, 1978 - 31 January, 1979, investigations continued on spectroscopic investigations of H_2O employing both optically pumped laser techniques and conventional millimeter wave techniques. Improvement of the optically pumped laser techniques for superheterodyne receiver/radiometry systems has continued, but this work has been delayed by construction of a quasi-optical mixer. The following work has been performed during this period:

1.) A paper on work jointly sponsored by ARO and NASA was presented by R. W. McMillan at the AGARD Symposium in Munich, Germany on September 5, 1978. The abstract of the paper, published in the AGARD Conference Preprint No. 245, "Millimeter and Submillimeter Wave Propagation and Circuits", is attached. A trip report and review of the conference, prepared by McMillan, is attached.

2.) A paper on a "Submillimeter Wave Transmitter/Receiver System", was presented at the Laser '78 conference. The abstract is attached. Whereas the work was sponsored by MIRADCOM, the TEA Laser - optically pumped FIR Laser has been used for spectroscopic investigations on this program and will continue to be employed for the remainder of the task. The configuration in which it is employed is shown in the figure below the abstract.

3.) An investigation of the optical constants of liquid water with an optically pumped laser was performed by O. A. Simpson of this laboratory during the past period in conjunction with the Emory Physics Department. An abstract is attached of the work performed. A paper is in preparation and the work will be presented at the March APS meeting in Chicago, Illinois.

4.) A talk was presented at the Optical Society of America (Washington D. C. Chapter) on "Optical Techniques in the Near-millimeter Wave Region", describing techniques which include those currently being employed on this program.

5.) Measurements were performed, at the request of Dr. Ed Stuebing of the Chemical Laboratory, Aberdeen Proving Ground, on film material which he supplied. The film was checked for transmission and reflection by a Fourier Transform Spectrometer over the spectral range from 20 cm^{-1} to 240 cm^{-1} and compared with the values obtained for a clear sheet of material.

6.) A group of papers has been accepted for presentation at the MIRADCOM Workshop on Atmospheric Effects on Missile Guidance to be held in March, 1979. They do not cover work performed under this program but are of interest to the general subject of Millimeter/Submillimeter Technology. For this reason, abstracts of the papers are attached.

CONCEPTS AND TECHNIQUES IN THE UTILIZATION OF MILLIMETER AND SUBMILLIMETER WAVES

J. H. Rainwater, R. W. McMillan and J. J. Gallagher

Georgia Institute of Technology
Engineering Experiment Station
Atlanta, Georgia 30332

SUMMARY

Extended microwave techniques have resulted in the cross-waveguide and ridged-waveguide harmonic mixers for the higher millimeter wave frequencies in addition to single-ended fundamental mixers, all employing Schottky-barrier diodes. The newly developing technique of subharmonic pumping of an antiparallel diode pair promises to ease the problem of insufficient local oscillator power. Quasi-optical techniques are being developed to provide more efficient energy coupling, filtering and directing components to replace the poorly performing waveguide devices above 100 GHz. Radiometry as a remote sensing tool is revealing properties of the atmosphere which are not characterized adequately by theory. Propagation measurements in the submillimeter show attenuation to be somewhat greater than previously believed. A millimeter-submillimeter transmitter and receiver system for propagation studies has been constructed at Georgia Tech with an optically pumped laser as a source and a quasi-optical superheterodyne receiver.

TRIP REPORT

AGARD SYMPOSIUM AND SEVERAL EUROPEAN LABORATORIES

2-17 September, 1978

Robert W. McMillan

This trip was made for two reasons: (1) to attend the Symposium on Millimeter and Submillimeter Wave Propagation and Circuits sponsored by the Advisory Group for Aerospace Research and Development (AGARD) of the North Atlantic Treaty Organization, and (2) to visit several European laboratories doing infrared, submillimeter and millimeter wave research. A paper entitled "Concepts and Techniques in the Utilization of Millimeter and Submillimeter Waves" was presented at the Symposium. The visits to other laboratories in Europe were accomplished at little additional cost because of the savings in air fare effected by staying in Europe for two weeks instead of one week.

James J. Gallagher of the Engineering Experiment Station at Georgia Tech was originally scheduled to make this trip, but was forced to withdraw on the day before leaving because of an illness in his family. Robert W. McMillan, who co-authored the paper presented at the meeting, went in his place.

In the balance of this report, discussions of the pertinent papers presented at the conference, together with descriptions of the visits to the various laboratories, are presented in some detail.

The AGARD symposium was attended by about 140 people. The meeting opened with a session on Military Systems and Applications in which several papers of interest were presented. N. Currie and F. Dyer of Georgia Tech presented a paper on the effects of the environment on millimeter wave performance in which they discussed radar clutter and propagation through adverse weather and snow. L. Cram of EMI in England presented two very interesting papers on the development of model radar systems between 30 and 900 GHz and on microwave holography. This latter technique has some promise in microwave imaging if large detector arrays can be built.

A session on solid state sources included papers on both IMPATT and Gunn oscillators. J. Ondria of TRG reported on results obtained with a wideband mechanically tunable 75-110 GHz CW Gunn Oscillator. T. T. Fong of Hughes Aircraft gave a paper on Hughes IMPATT devices above 100 GHz.

Submillimeter receivers were treated in the next session and very interesting papers were given by N. Keen of Max-Planck-Institut and K. Kuenzi of the University of Bern. Keen discussed recent advances in millimeter wave Schottky barrier mixers and described some new techniques which give improved performance, resulting in the "Mottky" diode, which is apparently a combination of a metal oxide - metal and a Schottky barrier diode. Kuenzi described a 230 GHz subharmonic mixer built by himself, H. Berger, and Martin Schneider at the University of Bern. Schneider was formerly at Bell Laboratories and did the pioneering work on the subharmonic mixer. The mixer described in their paper is very similar to the device being developed at Georgia Tech and has achieved a conversion loss of 9 dB DSB.

The paper by Rainwater, McMillan and Gallagher of Georgia Tech was presented in a session on New Technologies and Integration Techniques. Component development, propagation, radiometry, and quasi-optics were discussed in this paper which appeared to be very well received. Most of the balance of this session was devoted to integrated circuits and microstrip techniques.

Short sessions on Components and Circuits, Tubes, and Special Devices were next in the program. Millimeter backward wave oscillators or carcinotrons were treated by B. Epsztein of Thomson - CSF, and gyrotron oscillators were discussed by V. Granatstein et al of the Naval Research Laboratory. Papers on the subject of millimeter wave optically pumped lasers were given by R. Devinne and J. Mahieu of France and earlier by Dean Hodges of the Aerospace Corporation.

The conference concluded with a session on propagation which included a paper by W. Keiser et al of the Netherlands comparing theoretical and experimental results on propagation through rain at 94 GHz.

Measurements of sea reflectivity and rain attenuation at 81 GHz were discussed by R. Sherwell of England, and an interesting paper on rain attenuation at 74 GHz was given by M. Kharadly et al of the University of British Columbia.

The symposium ended at noon on Friday, and a visit was made on Friday afternoon to the Siemens Company division in Munich which makes carcinotron (backward wave) oscillators. The progress of Siemens in this area was discussed with Erich Glas and Peter Burger, who stated that they are in the process of developing a tube which will cover the range 110-170 GHz. Tubes are currently marketed which extend in frequency to 110 GHz. Several years ago, they began development of a 400 GHz tube, but were forced to abandon the effort because of a lack of funds. Although Thomson-CSF has built tubes which operate at much higher frequencies, the Siemens tubes have the advantage of requiring lower acceleration voltages and less complicated power supplies.

On Monday 11 September, Professor Dr. Fritz Kneubühl of the Swiss Federal Technical Institute in Zürich was visited. His group has been very active in the infrared and submillimeter technology areas, and has lately performed some interesting work on shock waves in liquids. Professor Kneubühl has built a transversely excited HCN laser and a balloon-borne solar radiance measuring experiment. A novel method of stabilizing a CO_2 pump laser for a far infrared laser using a gain cell filled with the FIR laser gas was also in use at this laboratory.

The Max-Planck-Institut (MPI) in Stuttgart was visited on 12 September, and the work at this laboratory was discussed with Drs. Fritz Keilmann, David Mead, and Mark Johnson. Dr. Keilmann has been active in CO_2 laser work, but has recently been studying biological effects of millimeter wave radiation. He has found that the growth rates of some bacteria are enhanced and those of others are retarded by irradiation with millimeter waves. Dr. Mead has constructed a dual beam far infrared spectrometer and has used it to measure transmission of many materials in the FIR. Dr. Ludwig Genzel of MPI is building a microwave dual beam spectrometer which uses several of the Siemens BWO tubes as sources.

The European Space Agency at Noordwijk, Holland was visited on 13 September and Drs. Thijs De Graauw, Frans Van Vliet, and Swer Lindholm were contacted. Frequency locking of the Thomson-CSF carcinotron oscillators was discussed with Dr. DeGraauw. Apparently, no one else has been able to accomplish this type of locking. This group is in the process of building a 230 GHz receiver. Their mixers are very similar to the Georgia Tech split block mixers, and they have achieved conversion losses of about 9 dB derived from a double sideband noise figure. Dr. Van Vliet has built InSb bolometer detectors for 230 GHz with lower conversion loss, but the bandwidth of these devices is limited to about 1 MHz.

On Thursday 14 September, a visit was made to Appleton Laboratory in England. The work at this laboratory was discussed with Drs. Ron Bohlander, Alistair Gebbie, and Roger Emery. This laboratory has traditionally done extensive work in millimeter wave and infrared propagation, and has several propagation experiments running simultaneously. They are also building Schottky-barrier mixers using diodes furnished by G. T. Wrixon, but have no performance results at the present time.

The European Millimeter Diode Laboratory at University College in Cork, Ireland was visited on 15 September. Drs. G. T. Wrixon and William Kelley discussed the fabrication of gallium arsenide Schottky-barrier mixer diodes. It appears that this laboratory is hampered by the lack of millimeter wave test equipment to measure diode performance. At present, diodes are sent to Max-Planck-Institut in Bonn, Germany for RF characterization.

The trip was concluded in Atlanta on 17 September. The total cost of the trip was $1,969.16 of which $700 was paid by NASA grant NSG-5012 (internal project no. A-1642) and the balance was divided equally between internal accounts H-240-300 and H-240-100.

A SUBMILLIMETER WAVE TRANSMITTER/RECEIVER SYSTEM*

R. W. McMillan, M. J. Sinclair, J. H. Rainwater,
E. A. Pickens, G. R. Loefer, J. J. Gallagher, R. G. Shackelford

Georgia Institute of Technology
Engineering Experiment Station
Atlanta, Georgia 30332

G. T. Wrixon

Department of Electrical Engineering
University College, Cork, Ireland

ABSTRACT

The availability of stable, relatively high power optically pumped far infrared lasers has provided a valuable tool for spectroscopic and propagation measurements in the wavelength range between 100μ and 1 mm. Likewise, the refinement of the gallium arsenide Schottky barrier mixer diode, along with several techniques for coupling power into these devices, has given a means of receiving power from these lasers with good sensitivity. This paper describes a transmitter/receiver system which uses a pulsed, optically pumped laser as the transmitter and a GaAs Schottky barrier diode mixer as the receiver. The laser is pumped by a transversely excited atmospheric pressure (TEA) CO_2 laser which has an output of 8 joules on the strongest lines. The receiver uses a 115 GHz klystron local oscillator which is harmonically mixed with the signal at either 239 GHz or 337 GHz to give an IF output of 7 GHz. A quasi-optical Fabry-Perot diplexer is used to couple signal and local oscillator into the mixer. During the course of this work, three far infrared transitions were observed which had not been previously reported in the literature.

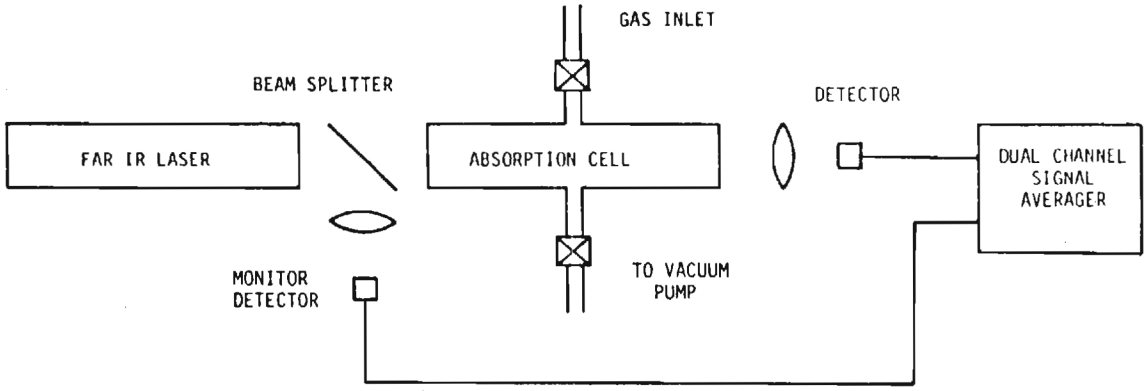

Fig.23 Apparatus used for Far infrared absorption measurements using a pulsed Far infrared laser

FAR INFRARED MEASUREMENTS OF THE OPTICAL CONSTANTS OF LIQUID WATER WITH AN OPTICALLY PUMPED LASER*

O. A. Simpson, B. L. Bean†, and S. Perkowitz
Physics Department
Emory University
Atlanta, Georgia 30322

A tunable far infrared optically pumped laser has been used to measure the reflection R and transmission of liquid water at 25°C. The laser covered the range 8.22 to 175.7 cm^{-1} with an average spacing between lines of 8 cm^{-1}. The optical data were used to find the complex index of refraction n-ik with typical errors of 2%. A small peak in n was observed near 55 cm^{-1}. This feature is correlated with other published infrared and Raman data and is strongly temperature dependent. The values of R, n, k and the absorption coefficient α are given in graphical and tabular form.

*Work partially supported by the Army Research Office.

†Present Address: Science Applications Inc.
Drawer E
White Sands Missile Range, New Mexico 88002

THE EFFECTS OF ATMOSPHERIC TURBULENCE AND ADVERSE WEATHER ON NEAR-GROUND 94 AND 140 GHz SYSTEMS*

Donald E. Snider
U. S. Army Atmospheric Sciences Laboratory
White Sands Missile Range, New Mexico

James C. Wiltse and Robert W. McMillan
Georgia Institute of Technology
Engineering Experiment Station
Atlanta, Georgia 30332

During measurements of millimeter wave propagation through battlefield dust made during the recent DIRT I tests at White Sands Missile Range, clear air signal fluctuations of up to $\pm$ 2 dB were observed. These fluctuations are thought to be due to atmospheric turbulence, and may be explained by using the theory developed by Armand [1] and other authors. This theory is compared to the DIRT I experimental results, using appropriate choices for the atmospheric parameters. Based on this theory, an estimate of the variance of angle of arrival fluctuations is also given.

Using standard methods for relating attenuation to rain and fog, climatological information for the Fulda region of West Germany has been used to estimate performance degradation for 95 and 140 GHz systems. Between five and ten percent of the time, depending on the month, a light rain (up to 3 dB/km) will be falling. A thick fog with visibility less than 100 m occurs on the average less than four percent of the time. Due to the nature of the data base, these fog occurrences must be treated as upper limits.

1. N. A. Armand, A. O. Izyumov, and A. V. Sokolov, "Fluctuations of Submillimeter Waves in a Turbulent Atmosphere", Radio Engineering and Electronic Physics, Vol. 16, No. 8, pp 1259-66, (August 1971).

*This work was supported by the U. S. Army Atmospheric Sciences Laboratory and by Battelle Columbus Laboratories under Contract No. DAAG29-76-D-0100.

MEASUREMENTS OF ATTENUATION DUE TO SIMULATED BATTLEFIELD DUST AT 94 AND 140 GHz*

J. J. Gallagher, R. W. McMillan, and R. C. Rogers
Georgia Institute of Technology
Engineering Experiment Station
Atlanta, Georgia 30332

Donald E. Snider
U. S. Army Atmospheric Sciences Laboratory
White Sands Missile Range, New Mexico

During the fall of 1978, a series of measurements, called DIRT I, of electromagnetic wave propagation through simulated battlefield dust were conducted at White Sands Missile Range. This paper gives an overview of the entire DIRT I tests as well as detailed results of those tests for millimeter wave (94 and 140 GHz) frequencies.

Attenuation measurements were made over an instrumented 2 km range. In the center of the range, explosive charges of different sizes were detonated, and the resulting signal level was compared to that existing before the explosive event. Measurements were also made of attenuation caused by artillery shells fired into the center of the range, and of that caused by burning diesel oil and rubber.

Both magnitude and duration of attenuation were found to vary with the amount of the explosive, sometimes reaching 30 dB and 20 seconds respectively. Copies of chart recorder tracings showing attenuation of both explosion products and oil smoke are presented. Oil smoke propagation measurements show scintillations of 3 to 5 dB.

*This work was supported by the U. S. Army Atmospheric Sciences Laboratory through Army Research Office Contract N. DAAG29-77-C-0026

TIME: 20 Minutes Visual Aid: Overhead Projector

TWO PROBLEMS IN UNDERSTANDING THE ROLE OF WATER DIMERS IN ATMOSPHERIC ABSORPTION*

R. A. Bohlander
Georgia Institute of Technology
Engineering Experiment Station
Atlanta, Georgia 30332

ABSTRACT

A model of the water dimer having a single linear hydrogen bond has been used to predict the pure rotation and rotation-vibration band absorption by this species. Using Fourier spectroscopy, we have looked for this in the difference between measured and predicted absorption by water molecules in the wavenumber ranges 8 to 50 cm^{-1} (240 to 1,500 GHz) and 300 to 600 cm^{-1}. However, the present model of dimmer absorption does not satisfactorily account for the excess observed absorption by water vapor in the laboratory or by the atmosphere containing water vapor. The nature of the disagreement is different in laboratory and field studies. When equilibrium samples of water vapor are studied in the laboratory, the temperature dependence and over all magnitude of excess observed absorption are in reasonable agreement with prediction for dimers, but the shape of the spectrum is very different. This suggests that the average molecular pair structure is different at normal temperatures from the ground state structure of dimers found by Dyke and others in 1977 in molecular beams. It is well-known that excess absorption will be found in the atmosphere when comparison is made with predictions for known constituents. Even if laboratory spectra of water vapor are used to improve the predictions, there is a residual observed. It is characterized by more variability and a steeper temperature dependence than can be attributed to equilibrium concentrations of water dimers. Nevertheless, there are indications the residual may be due to water substance in some form.

TIME: 20 Minutes VISUAL AID: Slide Projector (2 x 2) or Overhead Projector

*Work performed at Appleton Laboratory, Slough, England.

NEAR MILLIMETER WAVE MOBILE MEASUREMENT FACILITY (NMMW/MMF)*

J. J. Gallagher, W. M. Penn and L. C. Bomar
Georgia Institute of Technology
Engineering Experiment Station
Atlanta, Georgia 30332

ABSTRACT

The Near Millimeter Wave Mobile Measurement Facility (NMMW/MMF) will provide the means for performing measurements in the near millimeter wavelength region at various locations where there are weather conditions of interest or where smoke tests may be conducted. The MMF will consist of two vans and will contain transmitters, backscatter receivers and one-way video link receivers at 3.2 mm, 2.1 mm, and 1.3 mm wavelengths. In addition, broadband coverage ($\sim$ 3 mm - 0.7 mm) will be simultaneously performed with a Fourier Transform Spectrometer (FTS). The MMF will be accompanied by the ASL meteorological van and its data collection and processing system will interface with that of the ASL van.

The design of the entire MMF has been established, the performance of the NMMW systems analyzed, and the measurement capability of the facility determined. The capabilities of the MMF include attenuation measurements (one-way transmission and temporal fluctuations - short term at $\sim$ 200 Hz or greater rate), backscatter from rain/other hydrometeorites, multipath effects, clutter, target scintillation, doppler spectral characteristics and bistatic operation. The data processing system will permit on-site calculation of effects on the near millimeter wave signals. This paper will present a discussion of the project status, provisions made for additions to the MMF and the schedule for

completion and availability of the facility for measurements.

*This work is sponsored by the Harry Diamond Laboratories under Contract No. DAAG39-78-C-0044.

TIME: 15 Minutes

VISUAL AID: Overhead Projector

SEASONAL ATMOSPHERIC EMISSION AT 94 GHz*

J. Hank Rainwater, J. J. Gallagher, P. B. Reinhart
Georgia Institute of Technology
Engineering Experiment Station
Atlanta, Georgia 30332

A novel beam-waveguide millimeter radiometer feeding a 10 foot parabolic dish has been used to measure seasonal atmospheric emissions at 94 GHz. The radiometer incorporates a beam waveguide in the RF section which allows Dicke switching and calibration to be accomplished at the focal points between the beam waveguide lenses. A unique directional waveguide filter, designed and built at Georgia Tech, using a single circularly polarized cavity is used to inject the LO into a Schottky barrier mixer. The radiometric antenna half-power beamwidth is under 0.1°, thus these measurements represent atmospheric variations occurring within small spatial elements. Measurements to date have been made during high humidity, summertime conditions and show large emission variations due to clouds and other atmospheric conditions. Ground based measurements at the zenith and celestial equator with varying data integration times have been made. Antenna temperatures of the solar radiosphere have also been measured at a variety of azimuthal angles and atmospheric conditions. Theoretical calculations incorporating state-of-the-art H_2O, O_2, and O_3 absorption line shape expressions, water vapor distribution, temperature and pressure profiles, have been performed and exhibit a disparity with experimental measurements.

During February (1979) measurements will again be performed emphasizing temporal atmospheric fluctuations with high spatial resolution. The empirical measurements will be reduced into a variety of formats including a power spectral density plot to aid understanding of atmospheric "clutter". Theoretical calculations will be compared with the measurements and differences analyzed.

*This measurement program is funded by the Naval Research Laboratory under Contract No. N00173-78-C-0165 to the Georgia Institute of Technology.

TIME: 20 Minutes

VISUAL AID: Overhead Projector

A-1861

FINAL TECHNICAL REPORT
PROJECT NO. A–1861

SUBMILLIMETER WAVE SPECTROSCOPY AND TECHNOLOGY

by
J. J. Gallagher

Prepared for
U.S. ARMY RESEARCH OFFICE

Under
Grant No. DAAG29–76–G–0280

October 8, 1979

GEORGIA INSTITUTE OF TECHNOLOGY
Engineering Experiment Station
Atlanta, Georgia 30332

GT EES

1979

REPORT DOCUMENTATION PAGE

READ INSTRUCTIONS BEFORE COMPLETING FORM

1. REPORT NUMBER: FINAL TECHNICAL
2. GOVT ACCESSION NO.
3. RECIPIENT'S CATALOG NUMBER

4. TITLE (and Subtitle): SUBMILLIMETER WAVE SPECTROSCOPY AND TECHNOLOGY
5. TYPE OF REPORT & PERIOD COVERED: FINAL TECHNICAL, 1 January - 30 June, 1979
6. PERFORMING ORG. REPORT NUMBER

7. AUTHOR(s): J. J. Gallagher
8. CONTRACT OR GRANT NUMBER(s): DAAG29-76-G-0280

9. PERFORMING ORGANIZATION NAME AND ADDRESS:
Engineering Experiment Station
Georgia Institute of Technology
Atlanta, Georgia 30332

10. PROGRAM ELEMENT, PROJECT, TASK AREA & WORK UNIT NUMBERS

11. CONTROLLING OFFICE NAME AND ADDRESS:
U. S. Army Research Office
P. O. Box 12211
Research Triangle Park, NC 27709

12. REPORT DATE: October 8, 1979
13. NUMBER OF PAGES

14. MONITORING AGENCY NAME & ADDRESS (if different from Controlling Office)

15. SECURITY CLASS. (of this report): Unclassified
15a. DECLASSIFICATION/DOWNGRADING SCHEDULE: N/A

16. DISTRIBUTION STATEMENT (of this Report)

Approved for public release; distribution unlimited.

17. DISTRIBUTION STATEMENT (of the abstract entered in Block 20, if different from Report)

N/A

18. SUPPLEMENTARY NOTES

The view, opinions, and/or findings contained in this report are those of the author(s) and should not be construed as an official Department of the Army position, policy, or decision, unless so designated by other documentation.

19. KEY WORDS (Continue on reverse side if necessary and identify by block number)

Submillimeter Waves; Schottky Barrier Diodes; Spectroscopy; Heterodyne Receivers; Atmospheric Absorption.

20. ABSTRACT (Continue on reverse side if necessary and identify by block number)

The investigations performed during the final 6-months of the program are described. These included optically-pumped laser spectroscopy of liquid water and water vapor and submillimeter receiver investigations. Papers on work performed during this period are attached.

PROGRESS REPORT

(TWENTY COPIES REQUIRED)

1. ARO PROPOSAL NUMBER: P-14104-PX

2. PERIOD COVERED BY REPORT: 31 January, 1979 - 30 June, 1979

3. TITLE OF PROPOSAL: SUBMILLIMETER WAVE SPECTROSCOPY AND TECHNOLOGY

4. CONTRACT OR GRANT NUMBER: DAAG29-76-G-0280

5. NAME OF INSTITUTION: Engineering Experiment Station
Georgia Institute of Technology

6. AUTHOR(S) OF REPORT: J. J. Gallagher

7. LIST OF MANUSCRIPTS SUBMITTED OR PUBLISHED UNDER ARO SPONSORSHIP DURING THIS PERIOD, INCLUDING JOURNAL REFERENCES:

See attached sheet.

8. SCIENTIFIC PERSONNEL SUPPORTED BY THIS PROJECT AND DEGREES AWARDED DURING THIS REPORTING PERIOD:

O. A. Simpson, Graduate Student
J. J. Gallagher
W. Fife

14104-P

Dr. M. D. Blue
Dr. J. J. Gallagher
Georgia Institute of Technology
Engineering Experiment Station
Atlanta, GA 30332

BRIEF OUTLINE OF RESEARCH FINDINGS

During the last six month period of the Grant, work was performed on the spectroscopy of water in both liquid and vapor state. These investigations were performed with an optically pumped laser as the submillimeter radiation source. The details of this work have been presented in the following Conference papers and journal submissions:

1. O. A. Simpson, B. L. Bean and S. Perkowitz, "Far Infrared Optical Constants of Liquid Water Measured With An Optically Pumped Laser," accepted for publication in the Journal of the Optical Society of America - December, 1979 issue.

2. O. A. Simpson, R. A. Bohlander, J. J. Gallagher and S. Perkowitz, "Measurements of Far Infrared Water Vapor Between Lines With An Optically Pumped Laser," presented at The Conference on Microwave Spectroscopy and Coherent Radiation, Duke University, June, 1979 and submitted to the Journal of Physical Chemistry.

3. R. A. Bohlander et al, "Excess Absorption by Water Vapor and Comparison With Theoretical Dimer Absorption," Proceedings of the Workshop on Water Vapor, Vail, Colorado, September 11-13, 1979.

4. O. A. Simpson, R. A. Bohlander, J. J. Gallagher and S. Perkowitz, "Submillimeter Spectroscopy of Water Vapor," Conference on Microwave Spectroscopy and Coherent Radiation, Duke University, June, 1979.

5. O. A. Simpson, B. L. Bean and S. Perkowitz, "Submillimeter Laser Spectroscopy of Liquid Water," The Conference on Microwave Spectroscopy and Coherent Radiation, Duke University, June, 1979.

6. J. J. Gallagher, "Applications of Millimeter and Submillimeter Spectroscopy to Atmospheric Propagation," Conference on Microwave Spectroscopy and Coherent Radiation, Duke University, June, 1979 (Invited Paper).

7. O. A. Simpson, S. Perkowitz, R. A. Bohlander and J. J. Gallagher, "Far-Infrared Laser Spectroscopy of Water Vapor and Liquid Water," Digest of the Fourth International Conference on Infrared and Millimeter Waves, Miami, Florida, December 10-15, 1979.

These measurements with the optically pumped laser are the initial measurements of this nature and will be extended to obtain detailed data on atmospheric absorption. The work is part of the requirements for the doctorate degree of O. A. Simpson.

A quasi-optical diplexer and bi-conical Schottky barrier mixer have been constructed and are undergoing tests with an optically pumped laser as local oscillator. This work will be reported when final results are obtained.

Two manuscripts currently in preparation have been partially supported by ARO. Copies of these will be forwarded to the ARO Physics Division upon completion. They are a paper on Submillimeter Wave Techniques, for the Proceedings of the IEEE, and one on Quasi-Optics, which will be a chapter in the Academic Press series on Millimeter through IR Physics.

During the course of this program, many topics on submillimeter spectroscopy and techniques have been investigated and reported in previous semi-annual reports. Many of these topics have potential applications in the area of NMMW military systems. A paper, presented at the 1979 IRIS Conference and at the 1979 SPIE Conference as invited papers, shows the importance of spectroscopy related to atmospheric effects and research on technology in this spectral region. This paper is a result of partial support by HDL under ARO Contract No. DAAG29-77-C-0026. A technical report presenting an overview of the research performed under this grant is in preparation and will be submitted to the ARO Physics Division.

ACCEPTED FOR PUBLICATION IN THE JOURNAL
OF THE OPTICAL SOCIETY OF AMERICA
FINAL VERSION

FAR INFRARED OPTICAL CONSTANTS OF LIQUID WATER MEASURED WITH AN OPTICALLY PUMPED LASER*

O. A. Simpson, B. L. Bean,† and S. Perkowitz
Physics Department
Emory University
Atlanta, Georgia 30322

A tunable far infrared optically pumped laser has been used to measure the reflection R and transmission of liquid water at 25°C. The laser covered the range 8.22 to 175.7 cm^{-1} with an average spacing between lines of 8 cm^{-1}. The optical data were used to find the complex index of refraction n-ik with typical errors of 2%. A small peak in n was observed near 55 cm^{-1}. This feature correlates with published Raman data. The values of R, n, k and the absorption coefficient α are given in graphical and tabular form.

*Work partially supported by the Army Research Office under Grant No. DAAG29-76-G-0280.
†Present address: Science Applications Inc., Drawer E, White Sands Missile Range, New Mexico 88002.

I. INTRODUCTION

Liquid water absorbs so heavily in the far infrared (FIR) range that it is difficult to accurately measure its transmission. Many workers have determined the complex index of refraction n-ik with varying degrees of precision.[1] Afsar and Hasted (AH) have avoided the absorption problem by using reflection dispersive Fourier transform spectroscopy. They first measured n-ik at a water temperature of 19°C[2] and later accurately found n-ik at 4, 30, and 57°C.[3] An alternate method is to directly measure the transmission through a sizable water pathlength with a high power optically pumped FIR laser. Since free surface reflection measurements are also feasible with a laser, FIR laser spectroscopy gives n-ik in an elegantly simple manner. In this paper we present laser results between 8.22 and 175.7 cm^{-1} at a water temperature of 25°C. Our data are superior to the previously reported results at this temperature,[4] provide better low frequency coverage than was available to AH, and give evidence for a temperature dependent low frequency feature near 55 cm^{-1}. The general agreement between the results of AH and our data is so good as to confirm the validity of both experimental techniques.

II. EXPERIMENTAL METHODS AND RESULTS

A block diagram of the experimental apparatus is shown in Fig. 1. A 25 W CO_2 laser drives a FIR laser of the waveguide type. Details of this laser spectrometer (and early water measurements) have been previously reported,[5,6] but some improvements have been made. A new CO_2 laser was constructed with a PZT mounted ZnSe mirror to allow tuning of the line

center frequency to match the absorption transition frequency. Sampling of the FIR beam (signal I_s) by the pyroelectric detector D_1 allowed the CO_2 laser to be frequency stabilized so as to keep the FIR power constant. This helped to eliminate amplitude fluctuations in the FIR laser output caused by instabilities in the CO_2 laser. An opto-acoustic detector[7] on the FIR cavity aided in tuning difficult absorption transitions.

The main signal entered the Fabry-Perot interferometer (FP) which was used both to measure the wavelength and as a filter to eliminate unwanted wavelengths that may have lased simultaneously with the desired signal. The FIR beam was then divided by BS_2. The reference signal I_B, after detection and amplification by a Golay cell and lock-in amplifier, entered the denominator channel of the ratiometer RA. The signal I_A was, as will be described, reflected from or transmitted through the water sample and then detected by another Golay cell. This signal, after lock-in amplification, became the numerator signal in the ratiometer. This ratioing process was important in eliminating additional source fluctuations in the FIR power level. Values of I_A/I_B from the ratiometer were the basic experimental signal.

Although there are hundreds of optically pumped FIR lines arising from dozens of pumped media, it is simplest to work with only a few media when possible. We obtained 23 FIR lines between 8.22 and 175.7 cm^{-1} using only four pumped gases as has been fully described elsewhere.[8] This frequency range and coverage is comparable to that available to AH in their dispersive Fourier work.

Free surface measurements of the reflection coefficient R were made

on distilled water at 25±1°C. A mirror deflected the FIR beam to near-normal incidence with the horizontal water surface and a second mirror directed the reflected beam into the detector. The 7.5° incident angle was small enough that the assumption of normal incidence introduced a negligible error. In addition, the FIR radiation was unpolarized which further decreased this error. The water was placed in a container several mm deep, so that the back surface reflection was totally negligible. The water container could be replaced when desired with a standard reflector, a gold coated mirror of 99 ± 1% reflectivity. The coincidence of the water and mirror surfaces on interchange was constantly monitored by the reflection of a fixed HeNe laser beam.

For each FIR frequency several values of I_A/I_B were determined for reflection from the water surface and reflection from the standard mirror. The ratio of the two values of I_A/I_B then yielded R with typical random errors under 1%. The measured values are given in Table I.

An adjustable pathlength cell with crystalline quartz windows was used in the transmission measurements. The cell was mounted on a translation stage-fixed stage arrangement with a high accuracy (0.002 mm/division) micrometer head screw drive. A dial gauge, attached directly to the cell housing, gave a second determination of pathlength changes for comparison with the micrometer drive. Values of I_A/I_B were measured at increments of 5μm to an accuracy of 1μm over an average change in pathlength of 60μm. These data made it possible to determine the Lambert absorption coefficient α from the relation[9]

$$\alpha = - \frac{\Delta[\ell n(I_A/I_B)]}{\Delta x} \qquad (1)$$

where x is the pathlength. An error weighted least squares fit was applied to the data at each laser frequency f to determine $\alpha(f)$ and the associated error, typically 2%. The resulting values of α are shown in Fig. 2.

Values of $k = \alpha/4\pi f$ were calculated from the measured absorptions and together with the appropriate R, were used to determine n from the normal incidence expression:

$$n = \frac{1 + R}{1 - R} + \left[\left(\frac{1+R}{1-R}\right)^2 - (k^2+1)\right]^{1/2} \qquad (2)$$

The results are plotted in Fig. 3. Numerical values of all the measured and derived optical quantities are given in Table I.

III. DISCUSSION

Our data at 25°C are in excellent agreement with those of AH[3] at 30°C. Other published data near 25°C disagree strongly with these combined results. The 19°C values AH[2] found for n are well below the present data between 50 and 150 cm^{-1} and even lie below their own later 4°C data between 70 and 150 cm^{-1}. The Downing and Williams[1] values for n at 27°C, on the other hand, are significantly greater than the present results above 100 cm^{-1}. These conflicting observations could be reconciled only if the FIR properties of water show radical and non-monotonic temperature dependences between 4 and 30°C. This possibility remains to be explored, but the good agreement between the present data at 25°C and the AH data at 30°C suggests that the results at 19 and 27°C are experimental anomalies.

An interesting feature of the laser results is the small maximum in n near 55 cm^{-1}. Raman measurements[10,11,12] have shown the presence of a small peak near 60 cm^{-1} at 25°C but earlier FIR data[4] do not exhibit this feature because of the relatively poor signal-to-noise ratio. The peak magnitude is

clearly greater than the random error in our measurements, however.

IV. CONCLUSIONS

Our laser measurements of n and k at 25°C are in excellent agreement with the 30°C reflection dispersion Fourier data of Afsar and Hasted. The random errors in the measurements are comparable. Assuming that there is no strong temperature dependence in the general optical properties of water in this temperature range, the agreement attests to the validity of both experimental techniques.

Our data exhibit a low frequency peak near 55 cm^{-1} which appears to correlate with similar structure seen in Raman data. The Raman peak is believed to arise from hydrogen bond stretching and bending motions.[10] We have begun to examine the peak behavior by making multi-oscillator, relaxation model, and Kramers-Kronig analyses of our highly accurate reflectivity data. Preliminary results suggest that relaxation rather than resonant effects dominate in this frequency region. This analysis is continuing and we plan also to study the position and amplitude of the peak vs temperature. The laser spectrometer will be used for further accurate measurements as a function of temperature, with potential for shedding light on basic molecular processes in water.

V. ACKNOWLEDGEMENTS

The authors are grateful to Professor Dudley Williams for suggesting the laser surface reflection measurements and for his encouragement of the work. We also thank M. N. Afsar for providing a preprint of the recent work at 4, 30 and 57°C and for his helpful discussions.

REFERENCES

1. Thorough reviews of FIR work in water are given by P. S. Ray, "Broadband Complex Refractive Indices of Ice and Water," Appl. Opt. 11, 1836 (1972); and H. O. Downing and D. Williams, "Optical Constants of Water in the Infrared," J. Geophys. Res. 80, 1656 (1975).

2. M. N. Afsar and J. B. Hasted, "Measurements of the Optical Constants of Liquid H_2O and D_2O between 6 and 450 cm^{-1}," J. Opt. Soc. Am. 67, 902 (1977).

3. M. N. Afsar and J. B. Hasted, "Submillimeter Wave Measurements of Optical Constants of Water at Various Temperatures," Infrared Physics 18, 835 (1978).

4. M. S. Zafar, J. B. Hasted, and J. Chamberlain, "Water-Submillimeter Dielectric Dispersion," Nature 243, 106 (1973).

5. B. L. Bean and S. Perkowitz, "Far-infrared Transmission Measurements with an Optically Pumped FIR Laser," Appl. Opt. 11, 2617 (1976).

6. B. L. Bean and S. Perkowitz, "Submillimeter - Far Infrared Spectroscopy in the Liquid and Solid States with a Tunable Optically Pumped Laser," J. Opt. Soc. Am. 7, 911 (1977).

7. G. Busse, E. Basel, and A. Pfaller, "Application of the Opto-Acoustic Effect to the Operation of Optically Pumped Far-Infrared Gas Lasers," Appl. Phys. 12, 387 (1977).

8. B. L. Bean and S. Perkowitz, "Complete Frequency Coverage for Submillimeter Laser Spectroscopy with Optically Pumped CH_3OH, CH_3OD, CD_3OD, and CH_2CF_2," Optics Letters 1, 202 (1977).

9. D. A. Draegert, N. W. B. Stone, B. Curnutte, and D. Williams," Far Infrared Spectrum of Liquid Water," J. Opt. Soc. Am. 56, 64 (1966).

10. G. E. Walrafen, "Liquid Water: Dielectric Properties," in Water: A Comprehensive Treatise, F. Franks, Ed., (Plenum, New York, 1972), pp. 151-165.

11. G. E. Walrafen in Structure of Water and Aqueous Solutions, W. A. P. Luck, Ed., (Verlag Chemie-Physik Verlag, Weinheim, 1974), pp. 319-320.

12. O. F. Nielsen, "The Structure of Liquid Water; a Low Frequency (10 - 400 cm^{-1}) Raman Study," Chem. Phys. Letters 60, 515 (1979).

$f(cm^{-1})$	$\lambda(\mu m)$	R	$\alpha(cm^{-1})$	n	k
8.2	1217	0.297	121	2.857	1.174
11.2	890	0.249	150	2.462	1.062
13.1	764.1	0.228	148	2.437	0.902
14.3	699.5	0.228	171	2.383	0.950
17.5	570.5	0.201	173	2.306	0.784
21.2	471	0.191	199	2.252	0.746
24.0	417	0.185	215	2.231	0.714
24.6	406.4	0.184	206	2.267	0.665
26.8	372.7	0.179	235	2.197	0.696
30.3	330	0.164	228	2.155	0.598
34.2	292.6	0.161	259	2.126	0.604
35.5	281.5	0.155	250	2.112	0.560
39.4	254	0.147	221	2.125	0.447
43.6	229.1	0.144	289	2.050	0.527
52.1	191.7	0.140	285	2.079	0.435
54.5	183.6	0.147	355	2.082	0.519
61.3	163	0.140	339	2.076	0.440
69.1	144.8	0.136	405	2.025	0.466
84.2	118.8	0.134	457	2.034	0.432
98.4	101.6	0.131	605	1.976	0.489
103.6	96.5	0.136	696	1.985	0.534
141.6	70.6	0.122	986	1.845	0.554
175.7	56.9	0.095	1147	1.652	0.519

Table I. Measured values of reflection R and absorption coefficient α, and derived values of the index of refraction n-ik for liquid water at 25°C.

FIGURE CAPTIONS

Figure 1. Block diagram of the FIR laser spectrometer: m, mirrors; G, grating; L, lens; SA, spectrum analyzer; PZT, piezoelectric transducer; C, chopper; D, detectors; BS, beamsplitters; FP, Fabry-Perot interferometer; S, water sample; LI, lock-in amplifier; RA, digital ratiometer; FS, frequency stabilizer; SC, stripchart recorder; OAD, opto-acoustic detector.

Figure 2. Laser results for the absorption coefficient of liquid water at 25°C. The symbols for the laser experimental points are slightly larger than the typical random errors.

Figure 3. Laser results for the real part of the index of refraction of liquid water at 25°C. The symbols for the laser experimental points are slightly larger than the typical random errors.

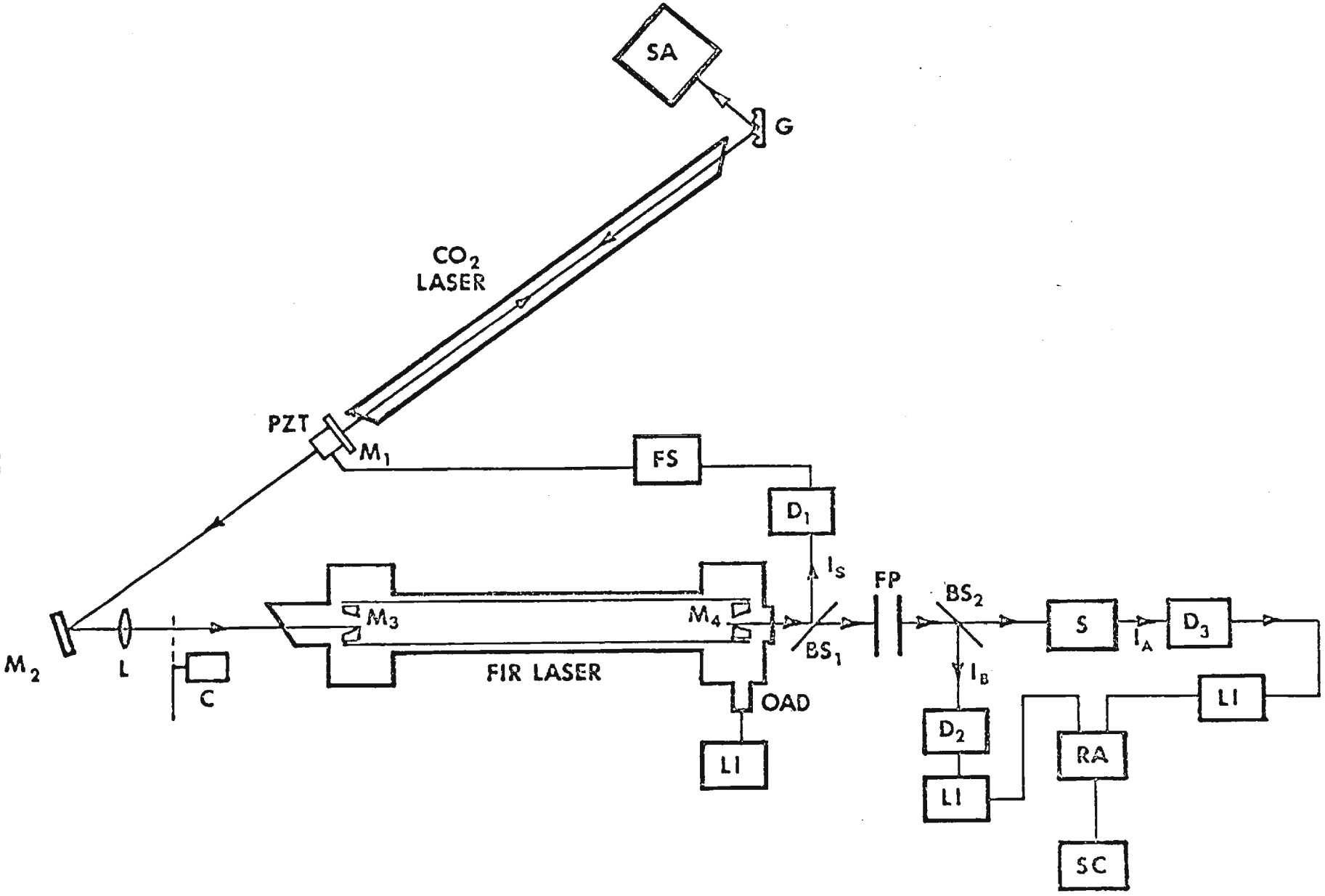
SA
G
CO_2 LASER
PZT
M_1
FS
D_1
I_S
FP
BS_2
S
I_A
D_3
M_2
L
C
M_3
M_4
BS_1
FIR LASER
OAD
LI
I_B
D_2
LI
RA
LI
SC

Fig. 1

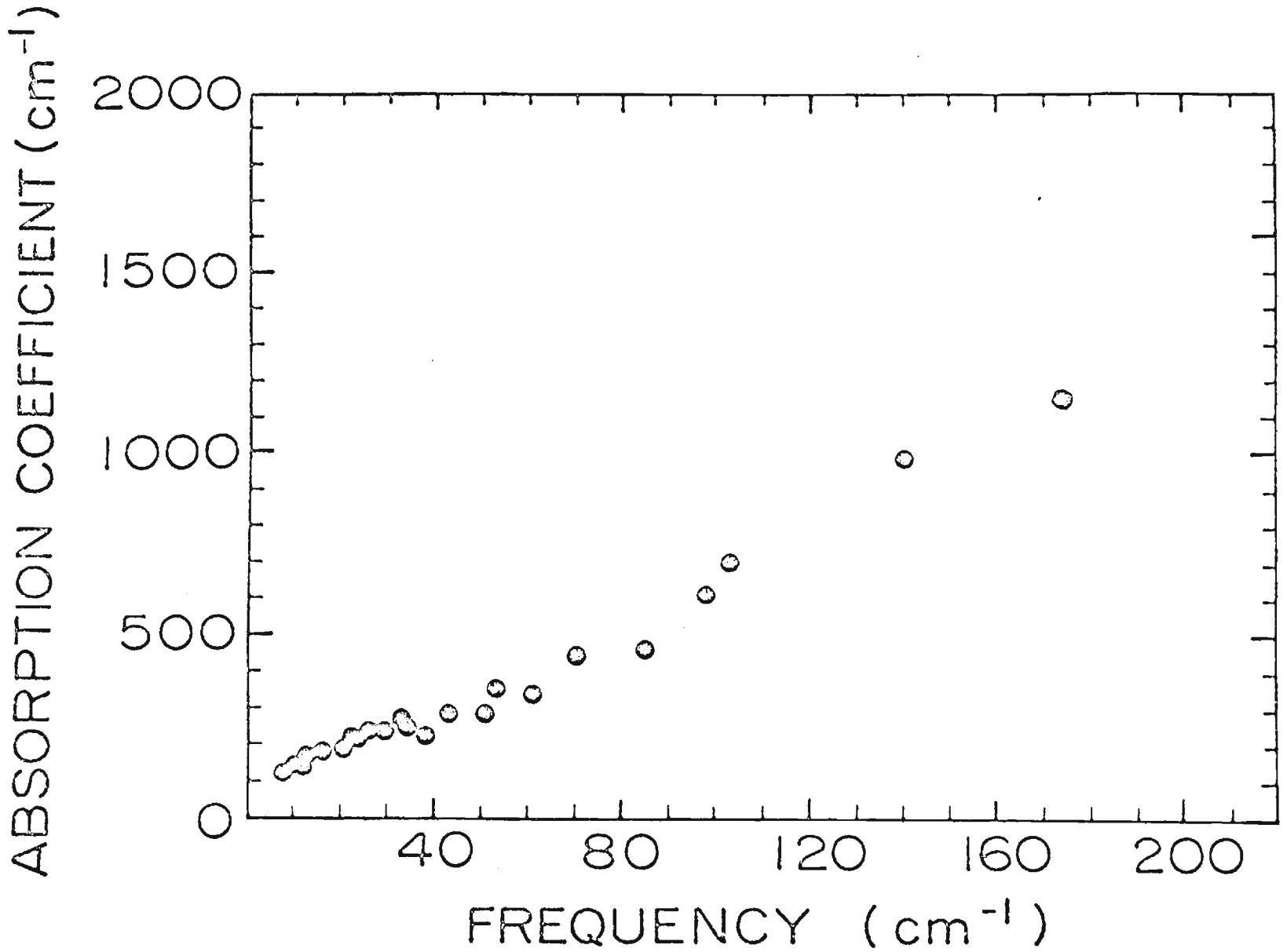
ABSORPTION COEFFICIENT (cm⁻¹)
2000
1500
1000
500
0
40
80
120
160
200
FREQUENCY (cm⁻¹)

Fig. 2

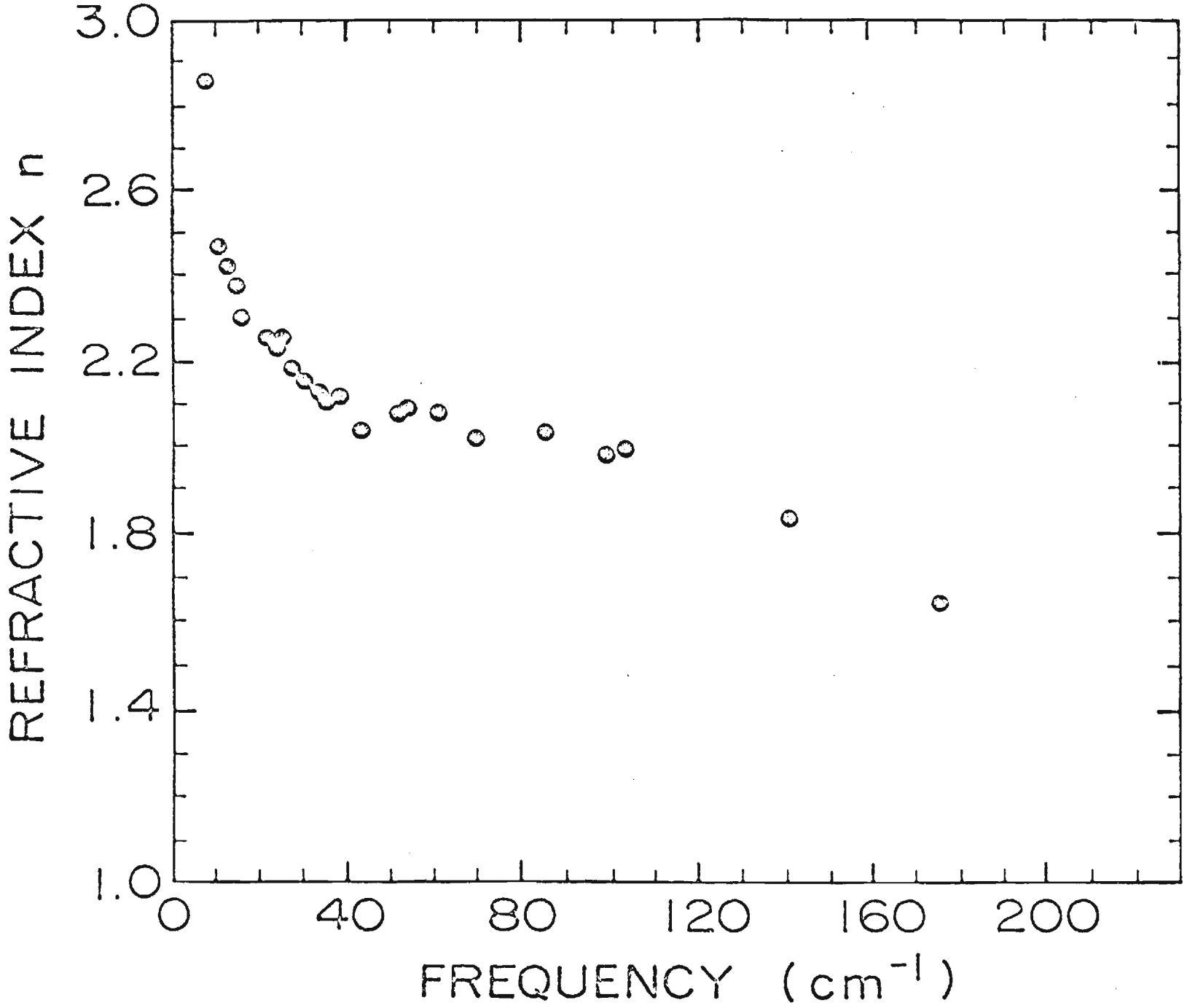
REFRACTIVE INDEX n
3.0
2.6
2.2
1.8
1.4
1.0
0
40
80
120
160
200
FREQUENCY (cm⁻¹)

Fig. 3

MEASUREMENTS OF FAR INFRARED WATER VAPOR ABSORPTION BETWEEN LINES WITH AN OPTICALLY PUMPED LASER*

O. A. Simpson, R. A. Bohlander, J. J. Gallagher
Engineering Experiment Station
Georgia Institute of Technology
Atlanta, Georgia 30332

S. Perkowitz
Department of Physics
Emory University
Atlanta, Georgia 30322

A tunable far-infrared optically pumped laser has been used to measure the absorption by equilibrium samples of water vapor at 25°C in the line gaps between 8.17 and 103.6 cm^{-1}. The experimental results are compared with calculations of predicted absorption based on the line shape formula given by Gross. Excess absorption has been found which is in reasonable agreement with other published data. New data are presented for the region 60 to 105 cm^{-1}.

*Work supported by the Army Research Office under Grant No. DAAG29-76-G-0280

I. INTRODUCTION

In the far infrared (FIR) or submillimeter spectral region water vapor is the dominant absorber in the atmosphere. Previous studies of water vapor, both in the laboratory and atmosphere have shown absorption between lines which is in excess of that predicted by existing line shape formulae.[1, 2, 3] This excess absorption has been attributed to errors in theoretical line shapes,[1] to water dimers,[2-7] and/or molecular aggregates or clusters.[8] Considering the recent growth of atmospheric applications in the FIR-submillimeter region, the lack of a firm understanding of how radiation and water molecules interact only underscores the need for more hard data from controlled experiments.

The present study is an initial effort to measure the absorption by equilibrium samples of water vapor of radiation from a tunable FIR optically pumped laser.[9] The use of a pumped FIR laser is a unique feature of our measurements. The high power of this device gives a signal-to-noise ratio which is superior to any other available broadband FIR source.

Data are presented for various water vapor pressures at 25°C for seven laser frequencies between 8.17 and 103.6 cm^{-1}. The frequencies chosen lie in the gaps between strong monomer lines as shown in Fig. 1 and were taken from the National Physical Laboratory table.[10] Only those frequencies well removed from line shoulders were chosen in order to minimize the error in predicted absorption due to uncertainty in the laser frequency. Although the family of discrete FIR laser lines does not provide continuous spectral coverage, there was no difficulty in finding lines which met this criteria.

Our measured absorptions are in excess of the theoretical values at each of the laser frequencies and at all pressures. The derived excess absorption agrees reasonably well with other published data obtained with Fourier spectrometers and HCN lasers and provides new information in the spectral region between 60 and 105 cm^{-1}.

II. THEORETICAL AND EXPERIMENTAL METHODS

The predicted absorption at each laser frequency was calculated using the line shape formula given by Gross[11, 12]:

$$\alpha(\nu) = \frac{nS}{\pi}\left[\frac{4\nu^2\delta}{(\nu^2 - \nu_o^2)^2 + 4\nu^2\delta^2}\right]$$

for the contribution of a line centered at wavenumber ν_o to the absorption coefficient α at wavenumber ν. Here δ is the half-width at half maximum, S is the line intensity, and n is the absorbing medium number density. There is very little difference in choosing the Gross formula over other commonly used line shape formulae (Van Vleck-Weisskopf, Lorentz, etc.). These are all based on instantaneous impact theory and give essentially idential results in the spectral region studied. The formula given by Van Vleck and Weisskopf[13] does predict less absorption below 15 cm^{-1}, but in this region excess absorption is large enough that the difference is not significant.

The water line frequencies, intensities, and initial state energies for

the 346 lines used were taken from the AFGL[14] table with self-broadening line width coefficients taken from calculations by Benedict and Kaplan[15]. The modification of line parameters for temperature and pressure was done as described by McClatchey with the exception of the temperature dependent exponent of the line widths, which were determined separately for each line from values of widths tabulated at two temperatures by Benedict and Kaplan.

The measurements were made with an optically pumped waveguide type FIR laser spectrometer, which is shown in block diagram form in Fig. 2. This apparatus has been extensively described elsewhere[16,17,18] and only relevant details will be given here. The laser provides a large selection of individual FIR lines with a typical power of milliwatts CW in each line. The frequencies have been determined with great accuracy by various workers, but as a precaution against possible error in the published laser frequencies, a Fabry-Perot interferometer was used to measure and confirm each of the seven wavelengths.

The water vapor was contained in a straight glass pipe absorption cell of length 3.44 m and diameter 10 cm. The ends of the cell had crystalline quartz windows offset 15° to the laser beam path. Initial measurements with the cell had resulted in much larger absorption than expected, which was determined to be due to interference effects. The offset of the windows was helpful in eliminating these interference effects, as were several co-axial absorbing bellows placed at several points along the cell. Distilled water

was evaporated and introduced into the cell through a perforated tube running the cell length. When sufficient vapor had entered the cell, the system was closed and allowed to reach equilibrium at room temperature, 25 $\pm$ 1°C. The static vapor pressure was measured with a Baratron MKS capacitance manometer, which had an accuracy of $\pm$2%.

To measure transmission the output from a Golay detector preceding the absorption cell was electronically divided into the output of another Golay detector following the cell. For each FIR laser frequency, several values of this ratio were determined for transmission through the cell evacuated and for various water vapor pressures. The resulting ratio of the two separately determined values then yielded the measured water vapor power transmission coefficient. This method has the important advantage of eliminating any fluctuations in the FIR power arising from laser instabilities. Measured values of the water vapor absorption at 43.649 cm^{-1} are shown in Fig. 3 as an example, together with the predicted absorption based on the Gross line shape.

The excess absorption coefficient was calculated according to the equation

$$\alpha_{excess} = -\ell n(T_M/T_G) \; / \; L$$

where L is the pathlength, T_M and T_G are the measured and theoretical transmission respectively. As shown in Fig. 4 for the frequency 43.649 cm^{-1}, a straight line showing excess absorption depending on density squared fits the data within experimental undertainty. Such a relationship, determined by an error weighted least squares fit was found for each of the other laser

frequencies. This result was expected, since in both speed of sound[19] and calorimetric data[20] the third and higher order virial terms have been reported to be negligible. The observed excess absorption, normalized to density squared, is shown in Fig. 5 for each of the laser frequencies.

III. DISCUSSION

In a study of molecular absorption one has to keep in mind the limitations of present line shape formulae that are based on the assumption of instantaneous collisions. Excluded from these, of course, are a wide range of possible molecular interactions. This particular weakness in theory introduces difficulties in interpreting new information; however, such formulae are widely used. Hence, calculations in the present study can be readily reproduced by other researchers.

Our measurements of the excess absorption in the FIR spectral region by water vapor are in general agreement with other reported work, but we have observed a somewhat larger excess absorption at 50 cm^{-1}. It should be noted that similar studies on water vapor with a HCN maser[2] also resulted in slightly greater excess absorption that that from broadband FIR source measurements. In addition, there is new evidence of an unexpected decrease in the excess absorption at higher frequencies. These results are preliminary and more laser lines will be used to increase resolution in this frequency region.

REFERENCES

1. D. E. Burch, J. Opt. Soc. Am. 58, 1383-1394 (1968).

2. W. J. Burrough, R. G. Jones, and H. A. Gebbie, J. Quant. Spectrosc. Radiat. Transfer 9, 809-824 (1969).

3. R. A. Bohlander, Ph.D. Thesis, Imperial College of Science and Technology, University of London (1979).

4. A. A. Viktorova, S. A. Zhevakin, Sov. Phys. - Dokl. 11, 1059-1062, 1065-1068. (1967).

5. A. A. Viktorova, S. A. Zhevakin, Sov. Phys. - Dokl. 15, 836-839, 852-855 (1971).

6. A. A. Viktorova, S. A. Zhevakin, IZV VUZ. Radiophys. 18, 211-221 (1975).

7. D. T. Llewellyn-Jones, R. J. Knight, and H. A. Gebbie, Nature 274, 876-878 (1978).

8. H. R. Carlon, "Introduction to Polymolecular Water Clusters and Their Infrared Activity," Draft Report, Defense Developm. Eng. Lab., U. S. Army, Edgewood Aresenal, Md., (1977).

9. T. Y. Chang and T. J. Bridges, Opt. Commun., 1, 423-425 (1970).

10. D. J. E. Knight, "Ordered List of Optically Pumped Laser Lines With Frequencies," National Physical Lab. Report No. Qu 45 (1979).

11. E. P. Gross, Phys. Rev. 97, 395-403 (1955).

12. R. J. Emery, Appl. Opt. 7, 1247 (1968).

13. J. H. Van Vleck and V. F. Weisskopf, Rev. Mod. Phys. 17, 227-236 (1945).

14. R. A. McClatchey, W. S. Benedict, S. A. Clough, D. E. Burch, R. F. Calfee, K. Fox, L. S. Rothmann, and J. S. Garing. AFCRL Atmospheric Absorption Line Parameters Compilation, Air Force Cambridge Research Laboratories Report AFCRL-TR-73-0096. (1973).

15. W. S. Benedict, L. D. Kaplan, J. Quant. Spectrosc. Radiat. Transfer 4, 453-469 (1964).

16. B. L. Bean and S. Perkowitz, Appl. Opt. 11, 2617 (1976).

17. B. L. Bean and S. Perkowitz, J.O.S.A. 67, 911-913 (1977).

18. O. A. Simpson, B. L. Bean, and S. Perkowitz, J.O.S.A., to be published.

19. R. A. Bohlander and H. A. Gebbie, Nature 253, 523-525 (1975).

20. J. A. Goff and S. Gratch, Trans. Am. Soc. Heat. Vent. Engrs. 52, 95-122 (1946).

FIGURE CAPTIONS

Figure 1a, b. Theoretical water vapor absorption based on the Gross line shape formula with laser frequencies in the gaps shown by arrows.

Figure 2. Block diagram of the FIR laser spectrometer: m, mirrors; G, grating; L, lens; SA, spectrum analyzer; PZT piezoelectric transducer; C, chopper; D, detectors; BS, beamsplitters; FP, Fabry-Perot interferometer; S, water vapor sample; LI, lock-in amplifier; RA, digital ratiometer; FS, frequency stabilizer, SC, stripchart recorder; OAD, opto-acoustic detector.

Figure 3. The measured water vapor absorption at 43.649 cm^{-1}. Theoretical absorption shown by X's for comparison.

Figure 4. Density dependence of excess absorption at 43.649 cm^{-1}. Straight lines fitted by weighted least squares.

Figure 5. Observed excess absorption coefficients divided by density squared for each laser frequency.

Fig. 1a

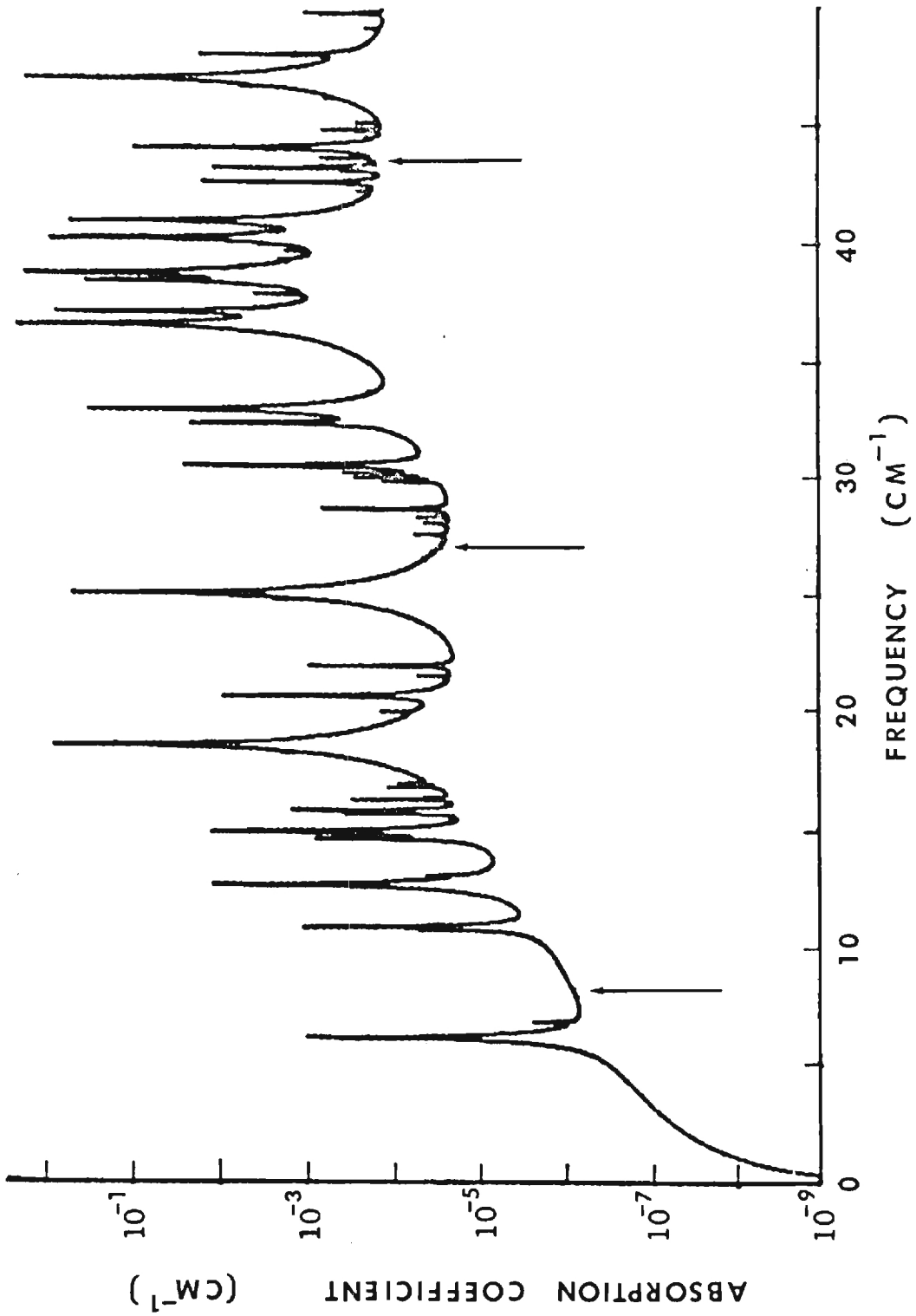
ABSORPTION COEFFICIENT (CM^{-1})
10^{-1}
10^{-3}
10^{-5}
10^{-7}
10^{-9}
0
10
20
30
40
FREQUENCY (CM^{-1})

Fig. 1b

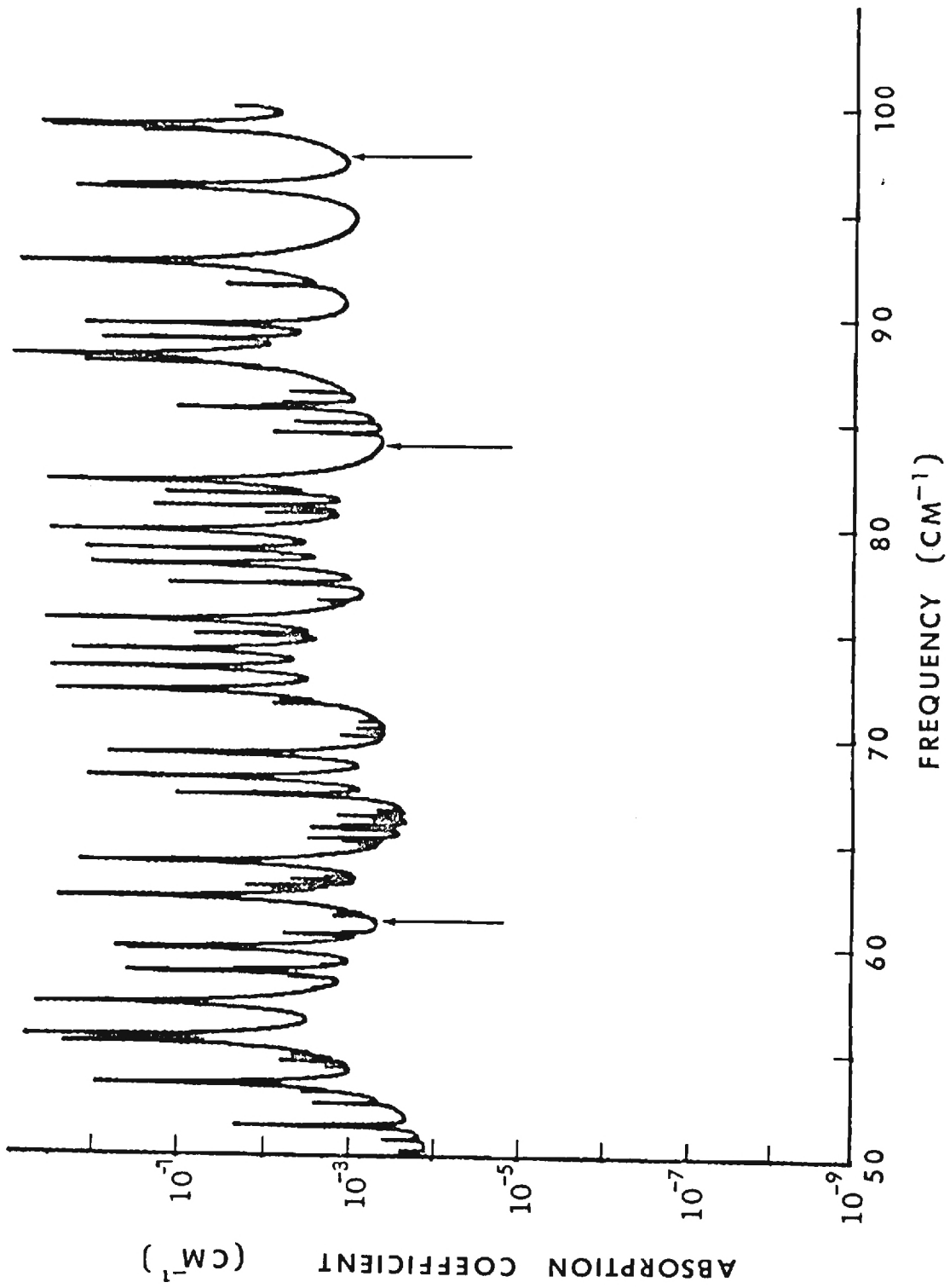
ABSORPTION COEFFICIENT (CM⁻¹)
10⁻¹
10⁻³
10⁻⁵
10⁻⁷
10⁻⁹
50
60
70
80
90
100
FREQUENCY (CM⁻¹)

Fig. 2

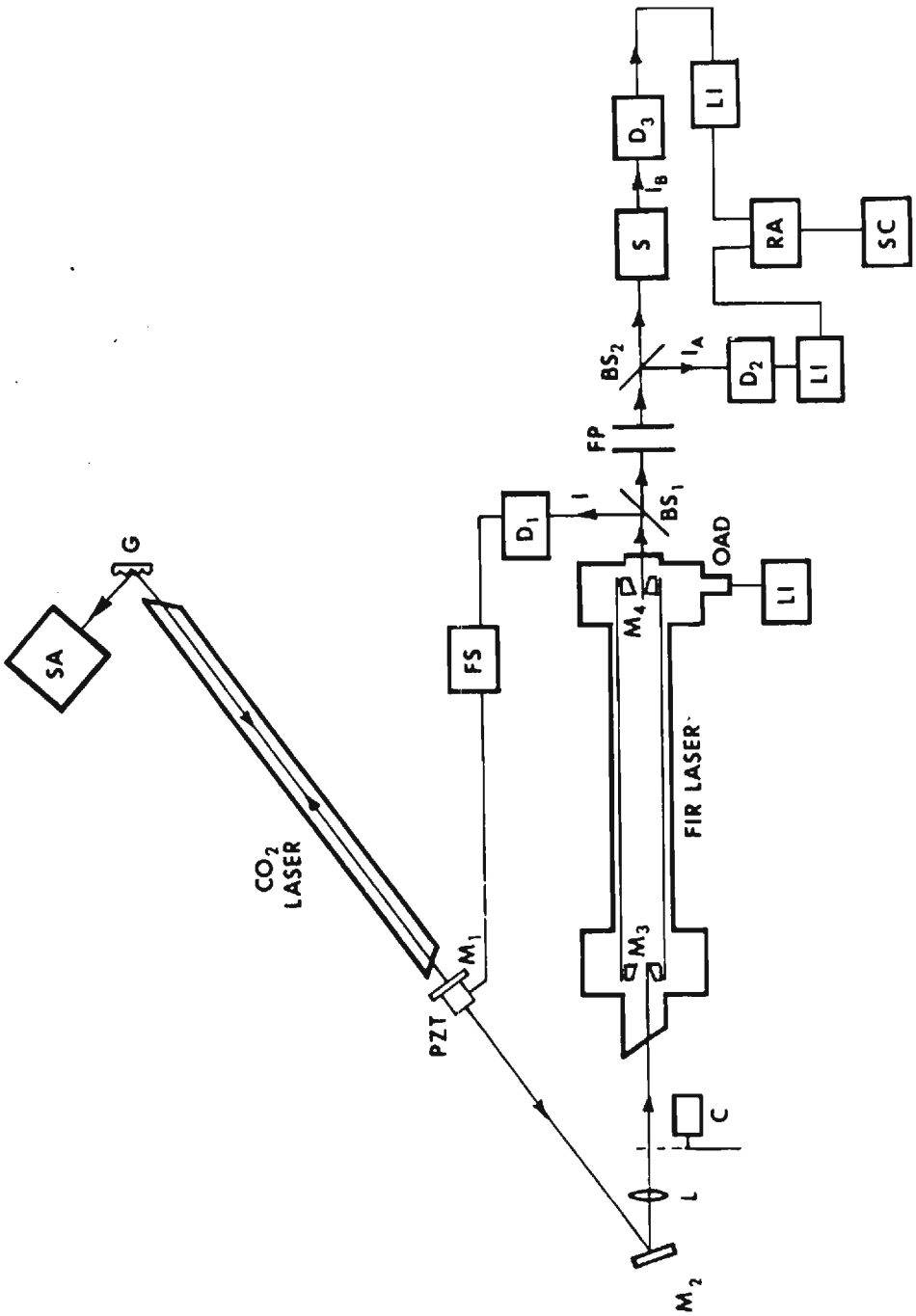
SA
G
CO_2 LASER
M_1
PZT
FS
D_1
I
BS_1
FP
BS_2
I_A
D_2
LI
I_B
D_3
LI
S
RA
SC
OAD
LI
M_4
FIR LASER
M_3
C
L
M_2

Fig. 3

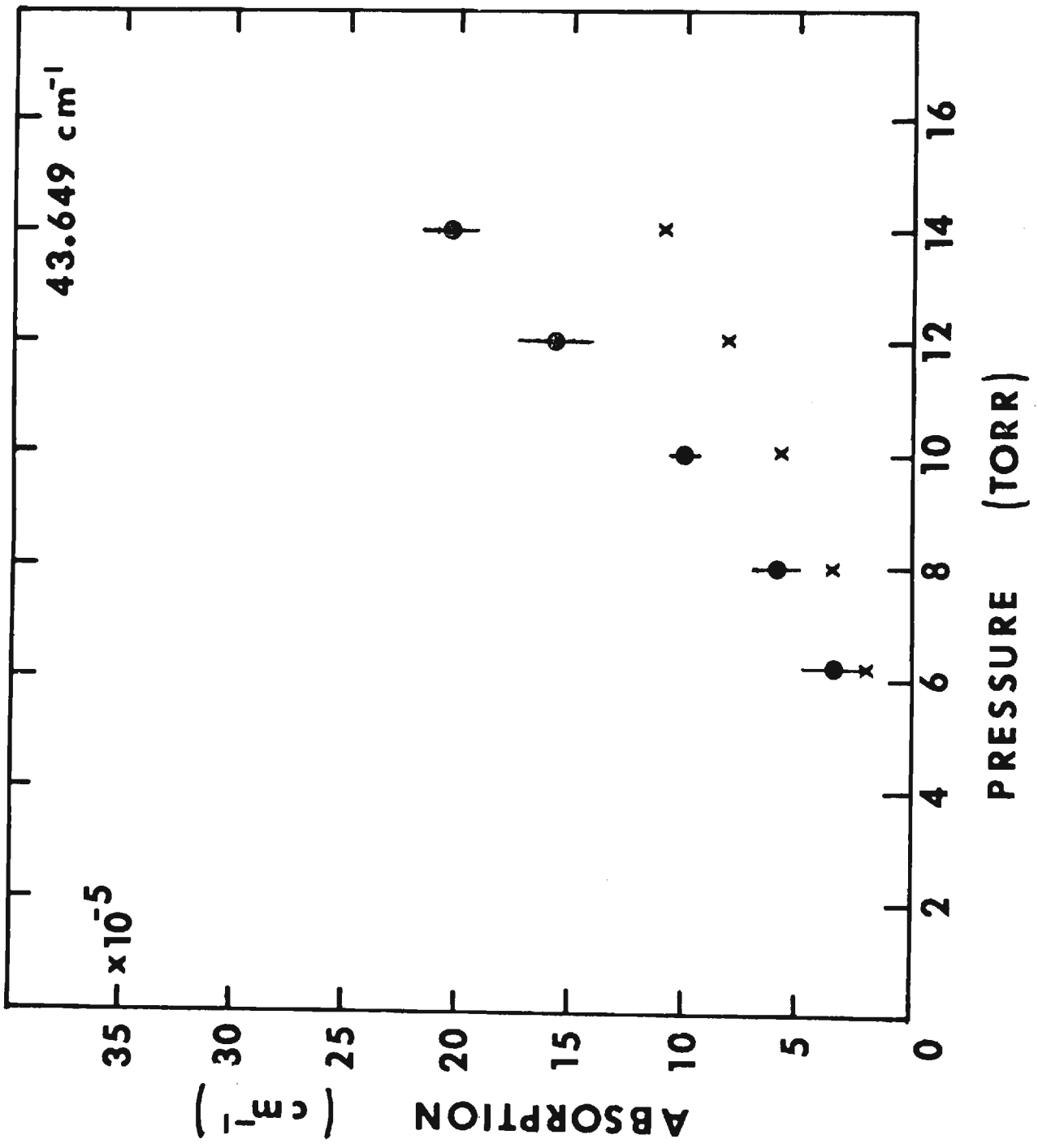
43.649 cm⁻¹
ABSORPTION (cm⁻¹)
×10⁻⁵
0
5
10
15
20
25
30
35
2
4
6
8
10
12
14
16
PRESSURE (TORR)

Fig. 4

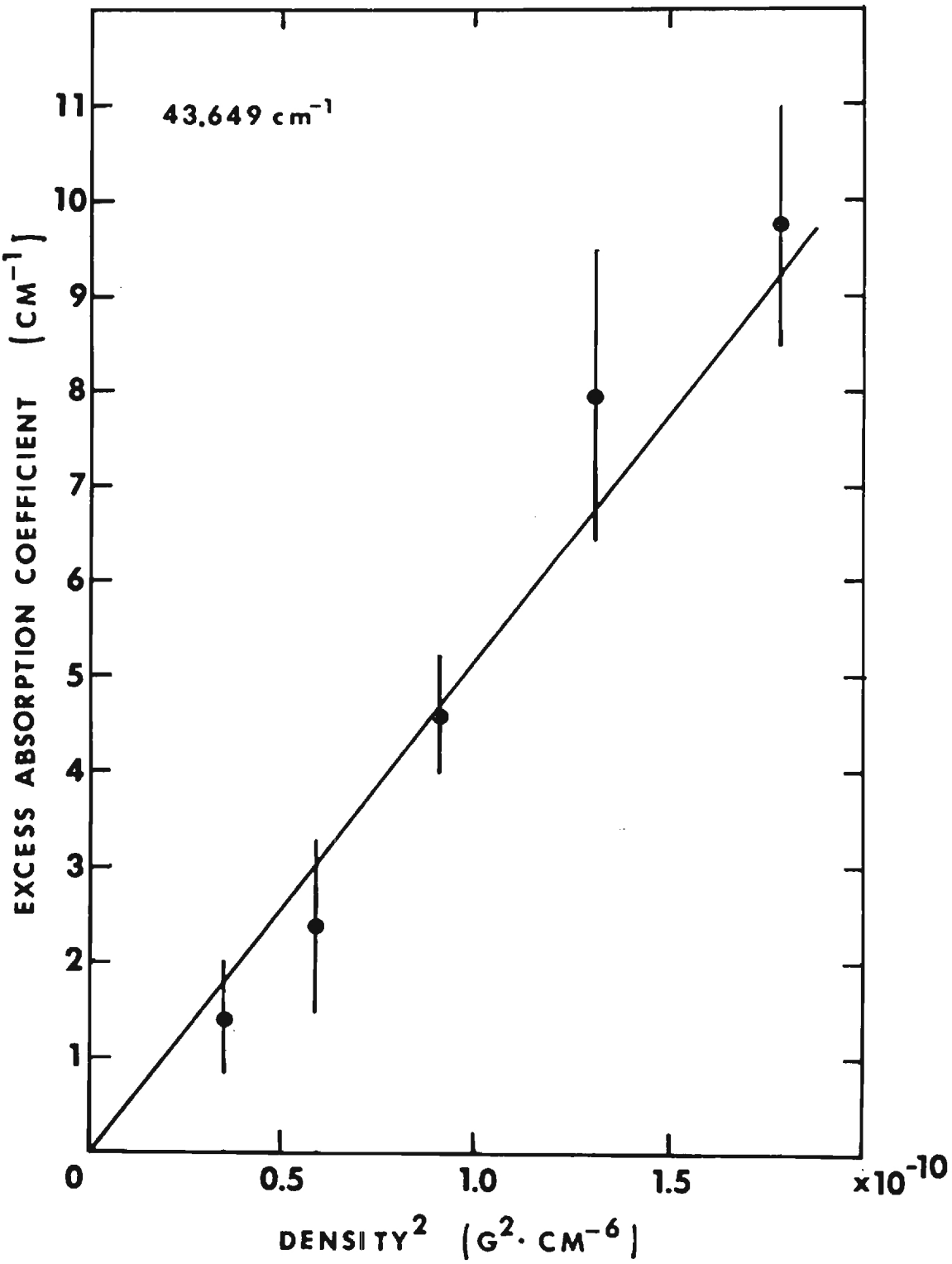
43.649 cm⁻¹
EXCESS ABSORPTION COEFFICIENT (CM⁻¹)
DENSITY² (G²·CM⁻⁶)
0
0.5
1.0
1.5
x10⁻¹⁰
1
2
3
4
5
6
7
8
9
10
11

Fig. 5

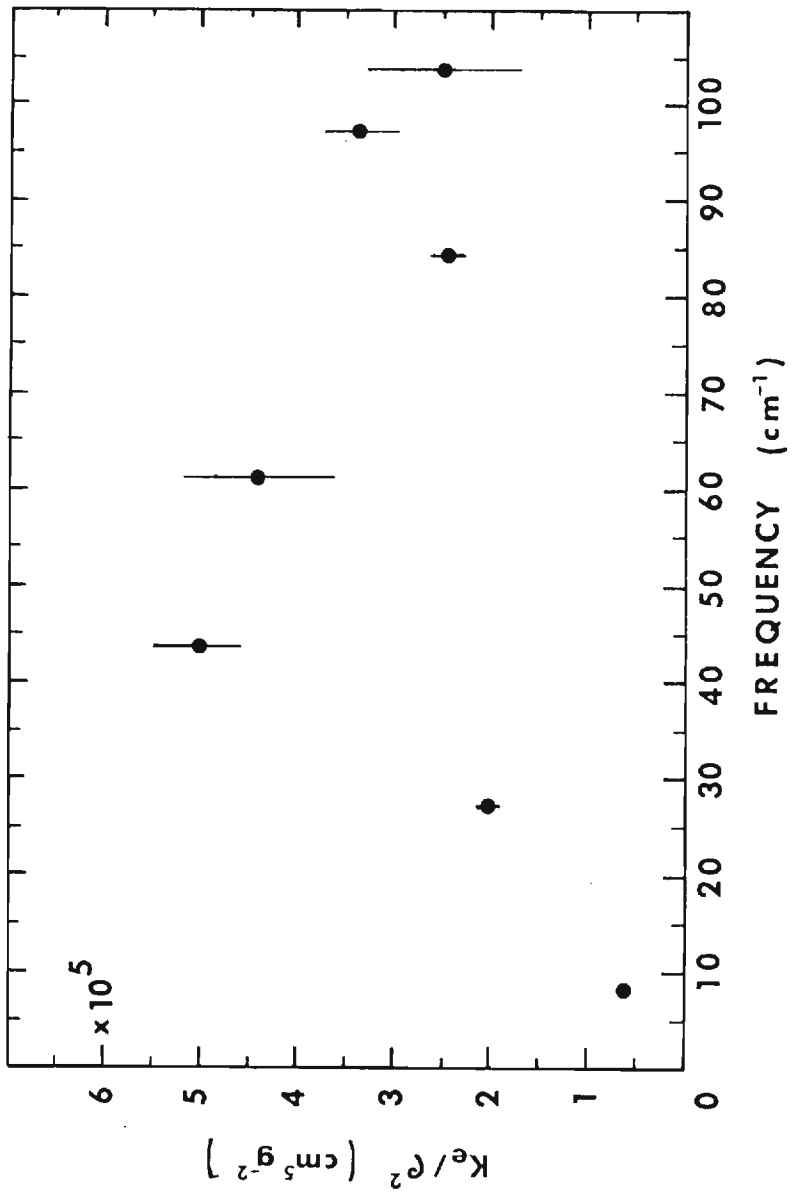
K_e/ρ^2 ($cm^5 g^{-2}$)
$\times 10^5$
0
1
2
3
4
5
6
10
20
30
40
50
60
70
80
90
100
FREQUENCY (cm^{-1})

DIGEST OF THE FOURTH INTERNATIONAL CONFERENCE ON INFRARED AND MILLIMETER WAVES, MIAMI BEACH, FLORIDA, 10-15 DECEMBER, 1979

FAR-INFRARED LASER SPECTROSCOPY OF WATER VAPOR AND LIQUID WATER*

O. A. Simpson and S. Perkowitz
Physics Department
Emory University
Atlanta, Georgia 30322 U.S.A.

R. A. Bohlander and J. J. Gallagher
Engineering Experiment Station
Georgia Institute of Technology
Atlanta, Georgia 30332 U.S.A.

Introduction

We have used a far infrared (FIR) optically pumped laser to measure both the reflection and transmission of liquid water and the absorption by water vapor of radiation in the spectral region betwen 8.22 and 175.7 cm^{-1}. The pumped laser is a unique feature of our measurements. The high power of this device gives a signal-to-noise ratio which is superior to that available from broadband FIR sources.

The optical data for liquid water were used to determine the complex refractive index n-ik [1]. Data for measured absorption by water vapor were compared with calculations of predicted absorption based on the line shape formula given by Gross. Our measured absorptions are in excess of the theoretical values at each of the laser frequencies and at all pressures.

Experimental Methods and Results

The FIR laser was of the waveguide type and has been described elsewhere [1-3]. A ratioing process using two detectors was helpful in eliminating any fluctuations in the FIR power arising from laser instabilities.

Free surface measurements of the reflection coefficient R were made on distilled water at 25 $\pm$ 1°C for near normal incidence with typical random errors under 1%. An adjustable pathlength cell was used to determine values of the liquid water transmission at increments of 5 μm to an accuracy of 1 μm over an average change in pathlength of 60 μm. The Lambert absorption coefficient α was determined at each laser frequency f by least squares fittings and used to calculate values of $k = \alpha/4\pi f$. Each k with the appropriate R was used to determine n from the normal incidence relation. The results for n are shown in Fig. 1.

Measurements of the absorption by water vapor were performed using a straight glass pipe absorption cell of length 3.44 m and diameter 10 cm. Distilled water was evaporated and introduced into the cell through a perforated tube running the cell length. To measure transmission the output from a Golay detector preceeding the absorption cell was electronically divided into the output of another Golay detector following the cell. The quotient of the two ratios for transmission through the evacuated cell and for various water vapor pressures yielded the measured water vapor power transmission coefficient.

The predicted absorption was calculated at each laser frequency using the line shape formula given by Gross [4,5]:

$$K(\nu) = \frac{ns}{\pi}\left[\frac{4\nu^2\delta}{(\nu^2-\nu_o^2)^2 + 4\nu^2\delta^2}\right]$$

for the contribution of a line centered at frequency ν_o to the absorption coefficient K at frequency ν. Here δ is the half-width at half maximum, s is the line intensity, and n is the absorbing medium number density. The water line frequencies, intensities, and initial state energies were taken from the AFGL [6] table with self-broadening line width coefficients taken from calculations by Benedict and Kaplan [7]. The modification of line parameters for temperature and pressure was done as described in the AFGL table with the exception of the temperature dependent exponent of the line widths, which were determined separately for each line from values of width tabulated at two temperatures by Benedict and Kaplan.

The excess absorption coefficient was calculated according to the equation

$$K_{excess} = -\ell n(T_M/T_G)/L$$

where L is the pathlength and T_M and T_G are the measured and theoretical transmission respectively. Measured values of the water vapor absorption at 43.649 cm^{-1} are shown in Fig. 2 as an example, together with the predicted absorption based on the Gross line shape. The observed excess absorption, normalized by the density squared is shown in Fig. 3 for each of the laser frequencies.

Conclusions

The FIR laser has made it possible to obtain highly precise data in liquid water. The liquid data cover a broader range than the results of Afsar [8], but agree well where they overlap. These two sets of laser data are the definitive FIR results on liquid water to date.

The derived excess absorptions of water vapor extend the frequency range of other published data obtained with Fourier spectrometers [9,10] and HCN lasers [10,11] and provide new information in the spectral region between 60 and 105 cm^{-1}.

*This work was partially supported by the Army Research Office.

References

[1] O. A. Simpson, B. L. Bean, and S. Perkowitz, J. Opt. Soc. Am., in press.

[2] B. L. Bean and S. Perkowitz, Appl. Opt. 11, 2617 (1976).

[3] B. L. Bean and S. Perkowitz, J. Opt. Soc. Am. 67, 911-913 (1977).

[4] E. P. Gross, Phys. Rev. 97, 395-403 (1955).

[5] R. J. Emery, Appl. Opt. 7, 1247 (1968).

[6] R. A. McClatchey, W. S. Benedict, S. A. Clough, D. E. Burch, R. F. Calfee, K. Fox, L. S. Rothmann, and J. S. Garing, AFCRL Atmospheric Absorption Line Parameters Compilation, AFCRL Report AFCRL-TR-73-0096(1963).

[7] W. S. Benedict and L. O. Kaplan, J. Quant. Spectros. Radiat. Transfer 4, 453-469 (1964).

[8] M. N. Afsar and J. B. Hasted, Infrared Physics 18, 835 (1978).

[9] D. E. Burch, J. Opt. Soc. Am. 58, 1383-1394 (1968).

[10] R. A. Bohlander, Ph.D. Thesis, Imperial College of Science and Technology, University of London (1979).

[11] W. J. Burroughs, R. G. Jones, and H. A. Gebbie, J. Quant. Spectrosc. Radiat. Transfer 9, 809-824 (1969).

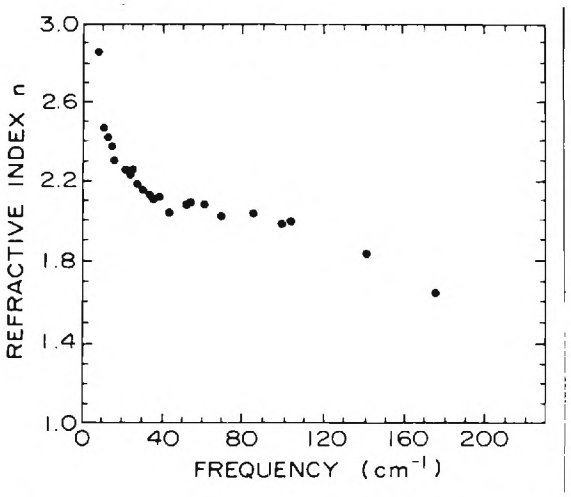

Fig. 1. Laser results for the real part of the index of refraction of liquid water at 25°C. The symbols for the laser experimental points are slightly larger than the typical random errors.

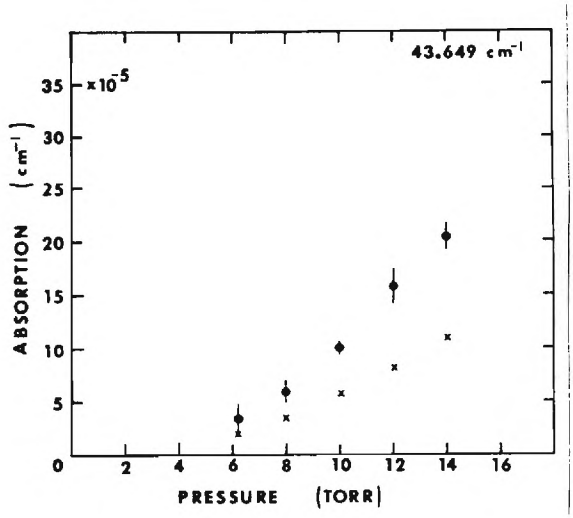

Fig. 2. The measured water vapor absorption at 43.649 cm^{-1}. Theoretical absorption shown by X's for comparison.

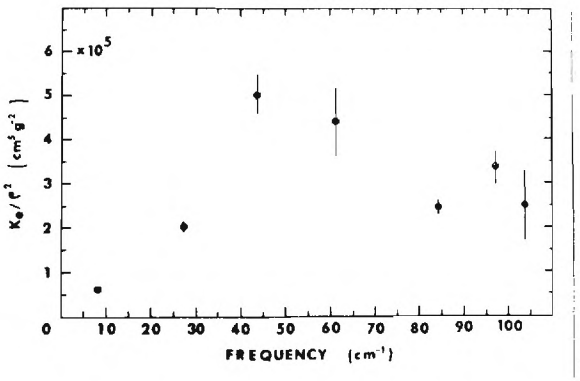

Fig. 3. Observed excess absorption coefficients divided by density squared for each laser frequency.

COLUMN 8 1/2" x 4 3/16"

Excess Absorption by Water Vapor and Comparison with Theoretical Dimer Absorption

R. A. Bohlander
Appleton Laboratory, Slough, England
Present address: Georgia Institute of Technology
Engineering Experiment Station
Atlanta, Georgia 30332

R. J. Emery and D. T. Llewellyn-Jones
Appleton Laboratory, Slough, England

G. G. Gimmestad
University of Colorado, Boulder, Colorado
Present address: Michigan Technological University
Keweenaw Research Center, Houghton, Michigan 49931

H. A. Gebbie
Imperial College of Science and Technology
University of London, London, England

O. A. Simpson and J. J. Gallagher
Georgia Institute of Technology
Engineering Experiment Station
Atlanta, Georgia 30332

S. Perkowitz
Department of Physics
Emory University
Atlanta, Georgia 30332

ABSTRACT

Absorption by water vapor has been measured in wavenumber ranges from 8 to 105 cm^{-1} and 300 to 600 cm^{-1}. The excess over prediction with the Gross line shape has been compared with theoretical dimer absorption. The temperature dependence and over-all magnitude of excess absorption are in reasonable agreement with prediction for dimers, but the shape is different. The limitations of the present theory of dimer absorption are discussed.

1. Introduction

It is well-known that established line shape formulas based on an impact approximation are unable to predict molecular absorption in the wings of absorption lines. In the case of water, observed absorption has been found to exceed prediction in the gaps between lines from the microwave to the infrared regions of the spectrum. The desire for a better theoretical model has been spurred by interest in the propagation of radiation through water vapor in the atmosphere.

To get an improved theory of the shape of water vapor absorption lines, more detailed information about molecular interactions during collisions will be needed than is available at the present time. Since two water molecules can form a weak hydrogen bond, dimers have also been suggested (Viktorova and Zhevakin 1967, 1971, 1975) as another possible source of excess absorption. This paper reports studies of excess absorption in the laboratory in the wavenumber ranges 8 to 105 cm^{-1} and 300 to 600 cm^{-1}, and comparisons are made with a calculated theoretical spectrum of water dimers. This is in the nature of a progress report and is not a definitive test of whether dimers are important since there are significant limitations in our understanding of dimer structure at normal temperatures. Many of the details of this study have been given in the thesis of Bohlander (1979) and further publications will follow.

2. Excess Absorption--Definition

One cannot measure excess absorption *per se*: it is the difference between observed absorption and prediction based on a line shape formula. Thus it is important to define carefully how the prediction is made. We have used the parameters for the frequency, intensity, and widths of lines given by McClatchey et al. (1973), Benedict and Kaplan (1963), Flaud, Camy-Peyret and co-workers (1976, 1977), and Toth and Margolis (1975). Commonly used line shape formulas are the Gross or kinetic line shape formula (Gross 1955), the Van Vleck-Weisskopf formula, and the modified Lorentz

formula (Van Vleck and Weisskopf 1945), and from these there is little to choose theoretically. They all invoke the key assumption that collisions are instantaneous. We have chosen the Gross formula. Numerical results with the formulas mentioned are negligibly different in the wavenumber range studied except with the Van Vleck-Weisskopf formula below 15 cm^{-1}. It predicts somewhat less absorption, but the conclusions of this paper would not be changed if this formula had been used.

Preliminary predictions of the absorption spectrum were made including all the pure rotation band lines in the calculation. We then made shortened tables of lines from which predictions in 50 cm^{-1} intervals differed negligibly* from a full calculation. In this way typically 400 and no more than 700 lines were needed at any given frequency for subsequent calculations, compared with 2600 pure rotation lines below 700 cm^{-1} in the complete tabulation we used.

Some workers have used much more abbreviated lists of lines in their calculation of the pure rotation line absorption (see eg. Burch 1968; Burch et al. 1974; Frenkel and Wood 1964; Gaut and Reifenstein 1971): they have selected only lines near the frequency of interest. Excess absorption in this case varies slowly with frequency and can be incorporated in an easy-to-use empirical formula to predict absorption. However, in physical terms, these selections of lines are rather arbitrary and cause confusion when values of excess absorption are compared, since allowance must be made for the various omissions of absorption lines. Moreover, observations have shown that some of the empirical formulations have oversimplified the dependence of absorption on the water vapor density and temperature. We have determined these dependences from observations and will consider them in relation to the dimer model.

*The tolerance was 0.2 dB/km for a water vapor density of 26 g m^{-3}.

3. Theoretical Dimer Absorption

We have made theoretical calculations of the absorption spectrum of dimers from existing information about their structure. A number of theoretical chemists have made molecular orbital calculations in order to find the hydrogen bond energy and the most stable structure, shown in Figure 1. Dill et al. (1975) give a useful review, and more recent work is described by Matsuoka et al. (1976). These predictions were found to be consistent with high resolution measurements (Dyke et al., 1977) of microwave transitions between rotation levels in the ground vibrational state of dimers in molecular beams. Therefore, the ground vibrational state appears to be well-understood in terms of the predicted lowest energy structure.

Since the hydrogen bond is weak, the water dimer has low-lying vibration levels, and only four percent of the population is estimated to be in the ground vibrational state at normal temperatures. Thus it is an important question whether dimers retain approximately the lowest energy configuration at these temperatures. Using an empirical model* of the potential energy between two water molecules, Owicki, Shipman and Scheraga (1975) have concluded that barriers to internal rotation are low. In this situation the orientations of the two water molecules in a dimer would not be well-confined to configurations near the lowest energy one. We felt it was probably premature, and was in any case a difficult problem, to try to calculate a theoretical dimer spectrum that would take account of internal rotation. Rather we have calculated a theoretical spectrum for the more tractable case in which the dimer is assumed to undergo rigid rotation and small-amplitude harmonic vibration. Comparison with the spectrum of excess absorption in water vapor has been used as a test of this theory and as an indication whether there may be the need to consider internal rotation.

The dimer's expected pure rotation band in the rigid rotor approximation comes at a low frequency because the dipole moment (2.6 D) measured by Dyke et al. (1977) was found to be nearly parallel to the line between the heavy oxygen atoms. The peak of the predicted band is at 16 cm^{-1} (480 GHz) as shown in Figure 2. One might expect the spectrum to be almost that of a symmetric top with a rotation inertial constant of 0.2 cm^{-1} and with only small perturbations due to the light hydrogen atoms. Early calculations of the dimer spectrum were made on that basis (Viktorova and Zhevakin 1967, 1971, 1975;

*Electrons and nuclei were placed in fixed positions to reproduce the dipole moment of water and the structure of ice.

Braun and Leidecker 1974). However, molecular beam studies (Dyke et al. 1977) have shown a much more complicated spectrum below 1.6 cm^{-1}(48 GHz). This is attributed to inversion tunnelling, but few assignments of the observed lines have been made. Therefore, we have not attempted to calculate rotational structure in detail and have used smoothed band contours.

The remainder of the predicted absorption is assigned to six intermolecular vibration modes involving the hydrogen bond. We have calculated the normal intermolecular vibrational frequencies for the dimer from a recent molecular orbital study of intermolecular potential energy (Matsuoka et al., 1976).* ** Most of the modes involve partial rotation of the monomers within the dimer, and, since this causes large dipole moment oscillations, the predicted absorption intensity is large. Intensities were calculated with the assumption that the charge distribution remains fixed on the monomer units during vibrations.**

In addition, we need to know the number density of dimers to be able to calculate their absorption in dB/km. Although dimers have been observed in molecular beams, we know nothing from this about equilibrium concentrations. These we have estimated in the usual way (see e.g. Bolander et al. 1969) from experimental values of the second virial coefficient (Goff and Gratch, 1946). Typical calculated dimer concentrations are of the order of a part in 1000 of the monomer concentration. Uncertainties in the theory on which these calculations are based will be discussed later. Dimer concentrations are proportional to the square of the water vapor density, and their dependence on temperature is determined by the hydrogen bond energy. The best theoretical values of the latter are around .15 to .16 eV; the value estimated from the temperature dependence of the second virial coefficient is 0.12 eV (Bohlander, 1979).

*There is fairly good agreement between the vibration force constants from this study and those from other recent molecular orbital studies (Curtiss and Pople 1975; Kistenmacher et al. 1974).

**Values of the frequencies and intensities are also in reasonable agreement with those found by Owicki et al. (1975) using an empirical potential energy model.

4. Observations in the Laboratory

The spectral ranges that are most accessible to experimental study are in the wings of the monomer pure rotation band and include the predicted dimer pure rotation band and the predicted bands for hydrogen bond bending. We have studied water vapor without a foreign broadening gas since this would give the widest possible spectral ranges in which to search for dimer absorption. Uncertainties in the theory of collision broadening by a foreign gas are also avoided.

We began the study using Fourier transform spectroscopy and wide-band radiation taken from Mercury lamp or glow bar sources. Helium-cooled bolometers and Golay cell detectors were used. For the spectral ranges 12 to 50 cm^{-1} and 300 to 600 cm^{-1}, White-type absorption cells provided path lengths between 20 and 200 meters. A selection of observed spectra is given in Figure 3. They represent one minus the ratio of spectra obtained with a sample and with a vacuum in the absorption cell. The dashed curves show expected monomer absorption. One can see that in the gaps between lines in these wavenumber ranges, excess absorption is a considerable fraction of the total. Whether the excess absorption was due to collisions between two molecules or due to dimers, it was expected that it would be proportional to the density squared, and this was found to be true within experimental certainty.

Due to the presence of numerous strong monomer lines, one can get only a fragmentary picture of the excess absorption's spectral shape, as shown for the near millimeter region in Figure 4. Some results of Burch (1968) and Burroughs et al. (1969) are shown to be in good agreement. Measurements were also made by one of us (DLJ) with an HCN maser and are shown in the figure at 29.7 cm^{-1}. Some of these measurements were made with a large untuned cavity which Llewellyn-Jones will discuss elsewhere in these proceedings. He will also present further data in the range 2 to 15 cm^{-1} obtained with this facility.

At Georgia Tech and Emory University, two of us (O. A. S. and S. P.) have embarked on new measurements with an optically pumped laser described elsewhere (Bean and Perkowitz 1976, 1977). Preliminary results are shown

with solid circles. There is the potential for more precise measurements because of the power and stability of the laser, and, as shown, this is being used to extend the frequency range covered. The absorption cell is a straight pipe 3.4 m long designed to be used with a single pass through it. However, there has been difficulty in eliminating multiple passes arising from stray reflections. This has been largely corrected with baffles, but there is possibly a residual effect which may explain why these data show somewhat larger excess absorption at lower wavenumbers than previous data.

The integral of the observed excess absorption shown in Figure 4 is about the same as that predicted by the dimer model, but the shape of the spectrum is different. This is also true for the higher wavenumber range studied (Figure 5). Here observed excess absorption is represented by a smooth curve that fits our data and that of Burch et al. (1974) within the experimental uncertainty. As previously noted by Roberts et al. (1976), this seems to have the form of an exponential decrease with frequency in the range 300 to 600 cm^{-1}. Further discussion of the shape of excess absorption will be given, following consideration of the observed temperature dependence.

Typical results in the low and high frequency regions are given in Figure 6. The excess absorption data are plotted in this way to find the value of the energy E that characterizes the temperature dependence; this in turn can be compared with the estimated dimer energy of formation. The dotted lines show the temperature dependence of the predicted monomer component of the absorption. This is governed mainly by the Boltzmann distribution of the energy levels from which nearby absorption transitions arise; the slope therefore switches sign from one side of the monomer pure rotation band to the other. The temperature dependence of the excess absorption is more nearly uniform. Values of E given in Figure 7 are near the dimer energy of formation estimated from the temperature dependence of the second virial coefficient (Bolander et al. 1969; Bohlander, 1979).

5. Discussion

There are in general terms two possible ways of interpreting the discrepancy between the shape of observed excess absorption and that of predicted dimer absorption:

(1) Dimers at normal temperatures may have significantly different mean structures than they have at low temperatures, or

(2) The contributions by dimers to the excess absorption may be less important than possible contributions by unbound molecular pairs, i.e., there may be additional collision broadening of monomer lines.

Although hydrogen-bonded complexes are floppy species, it was not entirely unreasonable to try the assumption that water dimers vibrate harmonically with small amplitudes. Thomas (1975) has found vibration bands of the complex H_2O—HF which were easily recognizable despite some anharmonicity. Of course, H_2O—HF has a much higher binding energy than the water dimer (an energy of formation of ~ 0.3 eV instead of 0.12 eV), and this may mean that barriers to internal rotation are also higher. If water dimers have low barriers to internal rotation, this type of internal motion could be more important than vibration, and the mean dimer structure could be significantly different than it is at low temperatures. In studies of the more weakly bound van der Waals' complexes, examples have been found of vibrating species, of internally rotating species, and of intermediate cases (Ewing 1976). According to the theoretical study made of barriers of internal rotation by Owicki et al. (1975), mentioned earlier, there are five barriers and three of them have heights less than 100 cm^{-1}. Since 1/2 kT is of this order, it is likely that internal rotation is important at normal temperatures. Further exploration of the barriers with molecular orbital methods would be of interest.

The other principal assumption we have made in calculating theoretical dimer absorption is that the second virial coefficient of water vapor is entirely due to the presence of dimers, and on this assumption we have estimated the concentration of dimers. It is interesting that the excess absorption derived from observations is similar in magnitude to the predicted dimer absorption. However, the principle of spectroscopic stability can be applied here according to rules given by Gordon (1963), and one finds that any pair of water molecules, whether they are bound or unbound, will have about the same integrated absorption cross-section at frequencies in the far infrared (below the frequencies of the vibration bands of the monomer). It follows that we are not able to say from our measurements whether the second virial coefficient and the excess absorption are due to bound or unbound species.

Present theories discount the importance of unbound pairs at normal temperatures, but there are some simplifications made. For molecules with a spherically symmetric form of potential energy, Stogryn and Hirschfelder (1959) have shown that dimers are responsible for nearly all of the second virial coefficient when the dimer binding energy exceeds kT. In the case of water, the energy of dimer formation is more than 4kT, but it is not known whether the generalization of Stogryn and Hirschfelder can be extended to the case of molecules of low symmetry, such as water. Calculations of dimer concentrations may also be done from a knowledge of the intermolecular potential energy (Viktorova and Zhevakin 1971; Braun and Leidecker 1974; Lane 1975; Lie and Clementi 1976: Bohlander 1979). While reasonable agreement with experimental values of the second virial coefficient have been obtained in recent calculations, much uncertainty remains about the reliability of the approximations made. Therefore, the possibility of a significant contribution by unbound pairs to excess absorption cannot be ruled out.

6. Conclusions

(1) We have found that excess absorption by water vapor is similar in magnitude to predicted dimer absorption and has a similar temperature dependence.

(2) There are large discrepancies between the shape of excess absorption and that predicted for dimers.

(3) Further theoretical work is needed on internal rotation in dimers and on the theoretical concentrations of dimers at normal temperatures.

7. Acknowledgements

This work was supported in part by the Appleton Laboratory (U.K. Science Research Council), by the U.S. Army Research Office, and by NATO.

8. References

Bean, B. L. and Perkowitz, S. 1976, Appl. Opt. 15, 2617-2618.

Bean, B. L. and Perkowitz, S. 1977, J. O. S. A. 67, 911-913.

Benedict, W. S. and Kaplan, L. D. 1964 J. Quant. Spectrosc. Radiat. Transfer 4, 453-469.

Bohlander, R. A. 1979 Ph.D. Thesis, Imperial College of Science and Technology, University of London.

Bolander, R. W., Kassner, J. L. and Zung, J. T. 1969 J. Chem. Phys. 50, 4402-4407.

Braun, W. C. and Leidecker, H. 1974 J. Chem. Phys. 61, 3104-3113.

Burch, D. E. 1968 J. Opt. Soc. Am. 58, 1383-1394.

Burch, D. E., Gryvnak, D. A. and Gates, F. J. 1974 Continuum absorption by H_2O between 330 and 825 cm^{-1}, Air Force Cambridge Research Laboratories Report, AFCRL-TR-74-0377.

Burroughs, W. H., Jones, R. G. and Gebbie, H. A. 1969 J. Quant. Spectrosc. Radiat. Transfer 9, 809-824.

Camy-Peyret, C., Flaud, J. M., Maillard, J. P. and Guelachvili, G. 1977 Mol. Physics 33, 1641-1650.

Curtiss, L. A. and Pople, J. A. 1975, J. Mol. Spectrosc. 55, 1-14.

Dill, J. D., Allen, L. C., Topp, W. C. and Pople, J. A. 1975 J. Am. Chem. Soc. 97, 7220.

Dyke, T. R. 1977 J. Chem Phys. 66, 492-497.

Dyke, T. R., Mack, K. M. and Muenter, J. S. 1977 J. Chem. Phys. 66, 498-510.

Ewing, G. E. 1976, Can. J. Phys. 54, 487-504.

Flaud, J.-M., Camy-Peyret, C. and Maillard, J. P. 1976 Mol. Physics 32, 499-521.

Frenkel, L. and Woods, D., 1966, Proc. IEEE 54, 498-505.

Gaut, N. E. and Reifenstein, E. C. 1971, Environmental Research and Technology, Report No. 13, Concord, Mass.

Goff, J. A. and Gratch. S. 1946 Trans. Am. Soc. Heat. Vent. Engrs. 52, 95-122.

Gordon, R. G. 1963 J. Chem. Phys. 38, 1724-1729.

Gross, E. P. 1955, Phys. Rev. 97, 395-403.

Gryvnak, D. A., Burch, D. E., Alt, R. L. and Zgonc, D. K. 1976 Infrared Absorption by CH_4, H_2O, and CO_2, Air Force Geophysics Laboratory Report AFGL-TR-76-0246.

Kistenmacher, H., Lie, G. C., Popkie, H. and Clementi, E. 1974, J. Chem Phys. 61, 546-561.

Lane, J. G. 1965 J. Chem. Phys. 62, 1605-1606.

Lie, G. C. and Clementi, E. 1976 J. Chem. Phys. 64, 5308-5309.

McClatchey, R. A., Benedict, W. S., Clough, S. A., Burch, D. E., Calfee, R. F. Fox, K., Rothmann, L. S. and Garing, J. S. 1963 AFCRL Atmospheric Absorption Line Parameters Compilation, Air Force Cambridge Research Laboratories Report AFCRL-TR-73-0096.

Matsuoka, O., Clementi, E. and Yoshimine, M. 1976 J. Chem. Phys. 64, 1351-1361.

Roberts, R. E., Selby, J. E. A. and Biberman, L. M. 1976 Appl. Opt. 15, 2085-2090.

Stogryn, D. E. and Hirschfelder, J. O. 1959 J. Chem. Phys. 31, 1531-1545. Errata. (1960) J. Chem. Phys. 33, 942-943.

Thomas, R. K. 1975 Proc. R. Soc. Lond. A 344, 579-592.

Toth, R. A. and Margolis, J. S. 1975 J. Mol. Spectrosc. 57, 236-245.

Van Vleck, J. H. and Weisskopf, V. F. 1945 Rev. Mod. Phys. 17, 227-236.

Viktorova, A. A. and Zhevakin, S. A. 1967 Sov. Phys. - Dokl. 11, 1059-1062, 1065-1068.

Viktorova, A. A. and Zhevakin, S. A. 1971 Sov. Phys. - Dokl. 15, 836-839, 852-855.

Viktorova, A. A. and Zhevakin, S. A. 1975 Izv. VUZ. Radiophys. 18, 211-221.

KNOWN LOWEST ENERGY DIMER STRUCTURE

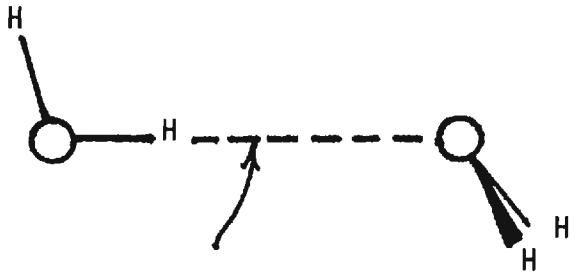

LINEAR HYDROGEN BOND

DIMER DIPOLE 2.6 D

=

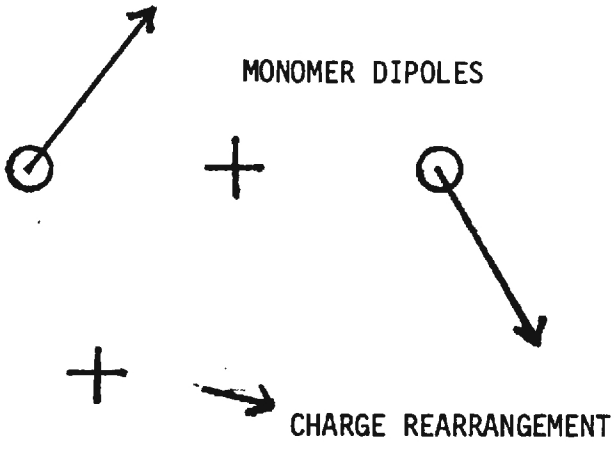

Figure 1

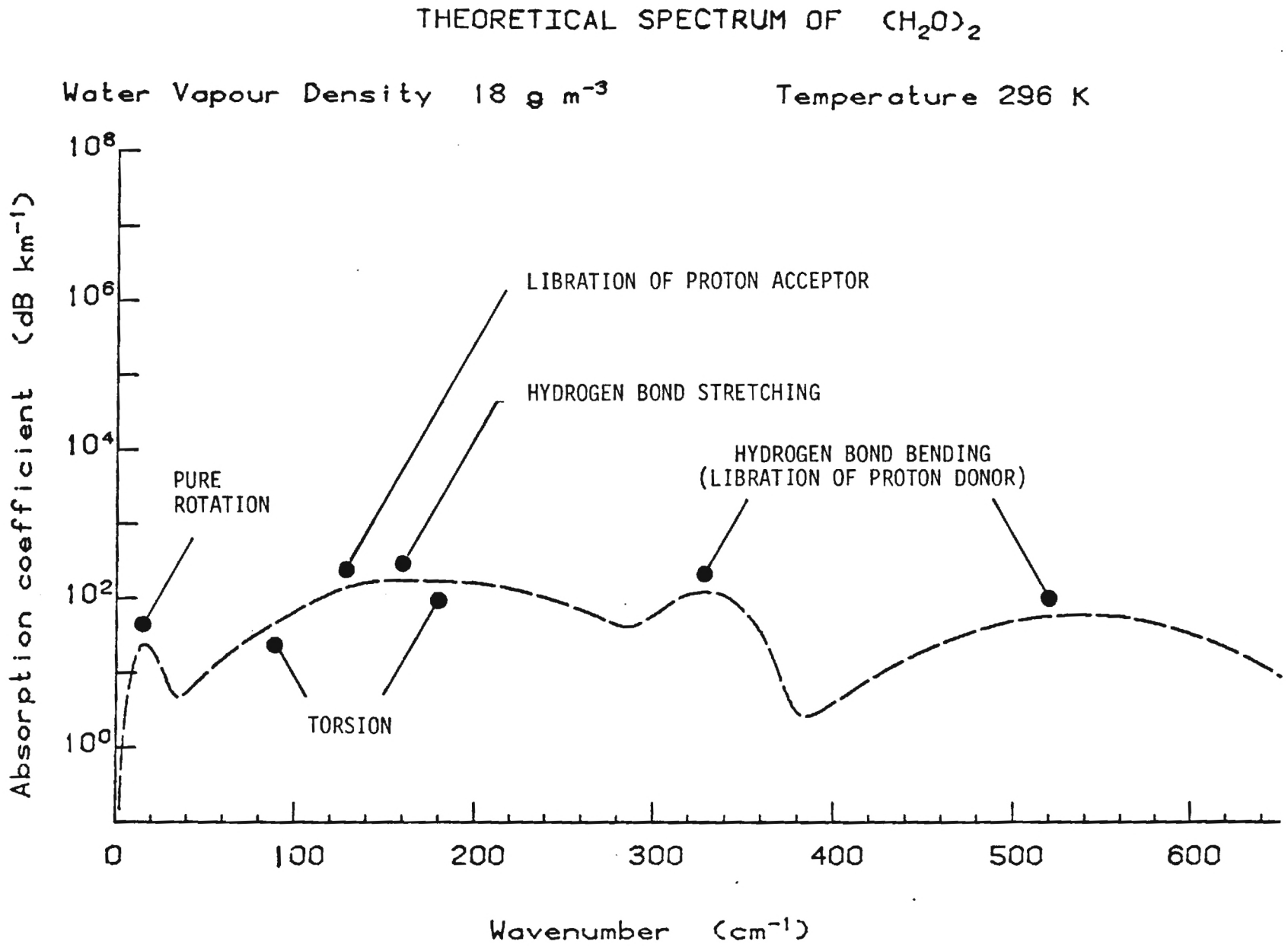
THEORETICAL SPECTRUM OF $(H_2O)_2$
Water Vapour Density 18 g m^{-3}
Temperature 296 K
Absorption coefficient (dB km^{-1})
10^8
10^6
10^4
10^2
10^0
LIBRATION OF PROTON ACCEPTOR
HYDROGEN BOND STRETCHING
HYDROGEN BOND BENDING
(LIBRATION OF PROTON DONOR)
PURE
ROTATION
TORSION
0
100
200
300
400
500
600
Wavenumber (cm^{-1})

Figure 2

ABSORPTION SPECTRUM OF WATER VAPOR

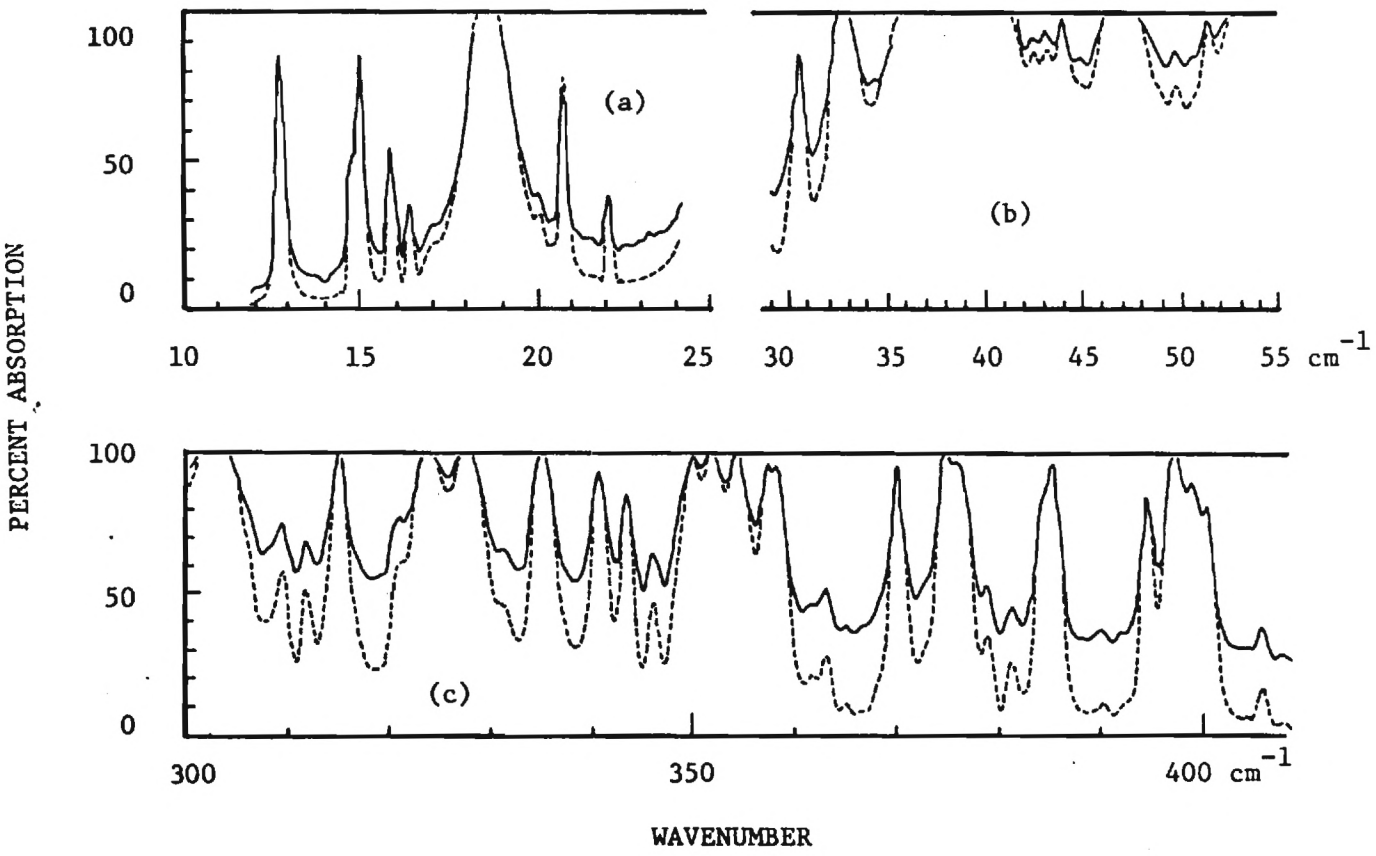

	WATER DENSITY	TEMPERATURE	PATH LENGTH	RESOLUTION	UNCERTAINTIES IN PERCENTAGE ABSORPTION
	g m^{-3}	K	m	cm^{-1}	
(a)	17	294	45	0.23	$\pm$1.25
(b)	15	294	103	0.5	$\pm$ 7 <40 cm^{-1} $\pm$ 1.6 >40 cm^{-1}
(c)	8.6	283	133	1.25	$\pm$2

Figure 3

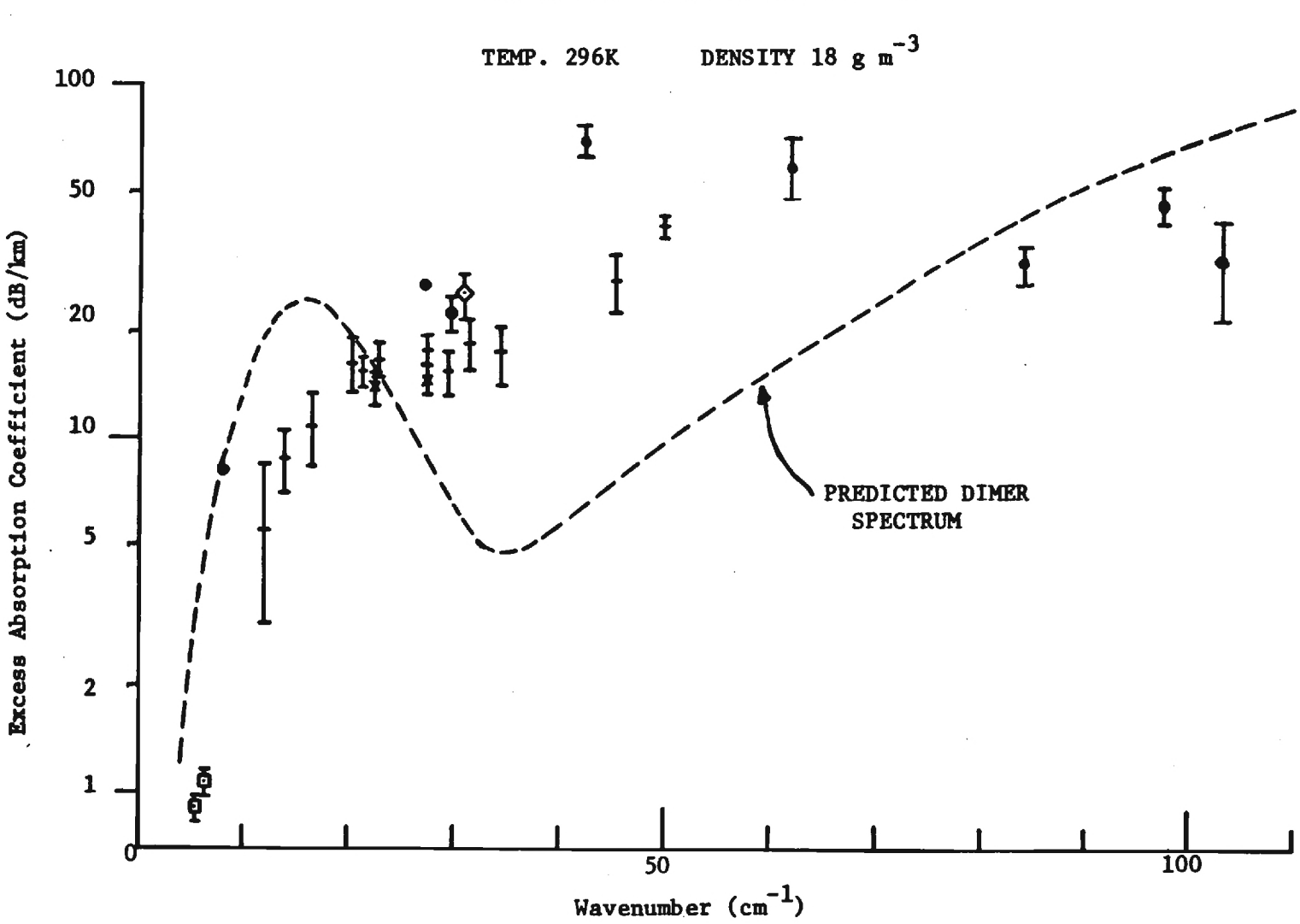
EXCESS ABSORPTION BY WATER VAPOR
TEMP. 296K DENSITY 18 g m^{-3}
Excess Absorption Coefficient (dB/km)
100
50
20
10
5
2
1
0
50
100
Wavenumber (cm^{-1})
PREDICTED DIMER SPECTRUM
PRESENT OBSERVATIONS: + FOURIER SPECTROSCOPY
o HCN MASER
● OPTICALLY PUMPED LASER
X BURCH (1968)
◇ BURROUGHS ET AL. (1969)
□ FRENKEL AND WOODS (1966)

Figure 4

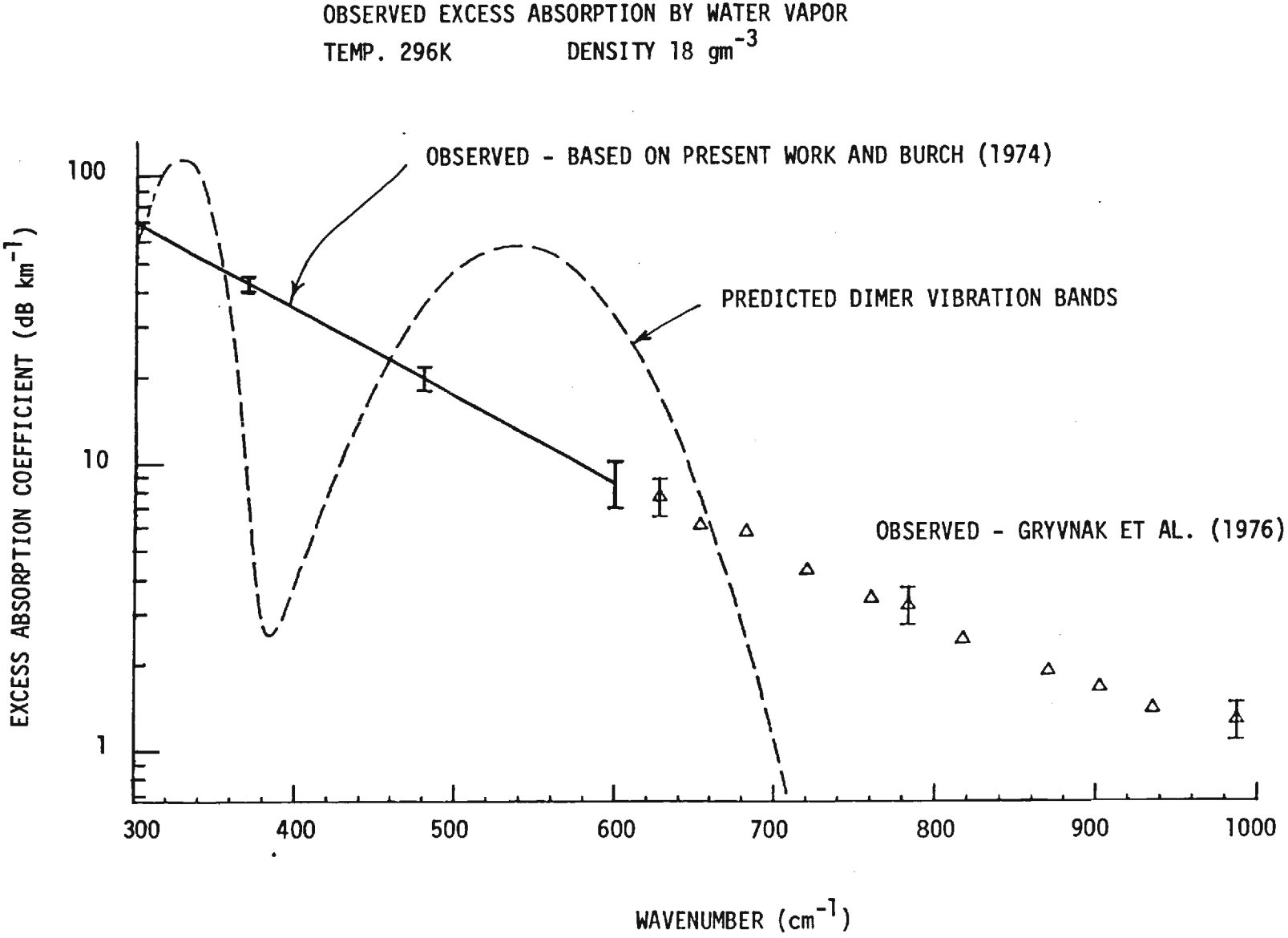
OBSERVED EXCESS ABSORPTION BY WATER VAPOR
TEMP. 296K DENSITY 18 gm^{-3}
OBSERVED - BASED ON PRESENT WORK AND BURCH (1974)
PREDICTED DIMER VIBRATION BANDS
OBSERVED - GRYVNAK ET AL. (1976)
EXCESS ABSORPTION COEFFICIENT (dB km^{-1})
100
10
1
300
400
500
600
700
800
900
1000
WAVENUMBER (cm^{-1})

Figure 5

OBSERVED TEMPERATURE DEPENDENCE OF THE
EXCESS ABSORPTION COEFFICIENT K_e

K_e/ρ^2 assumed $\propto$ exp[-E/(kT)], ρ = water vapor density

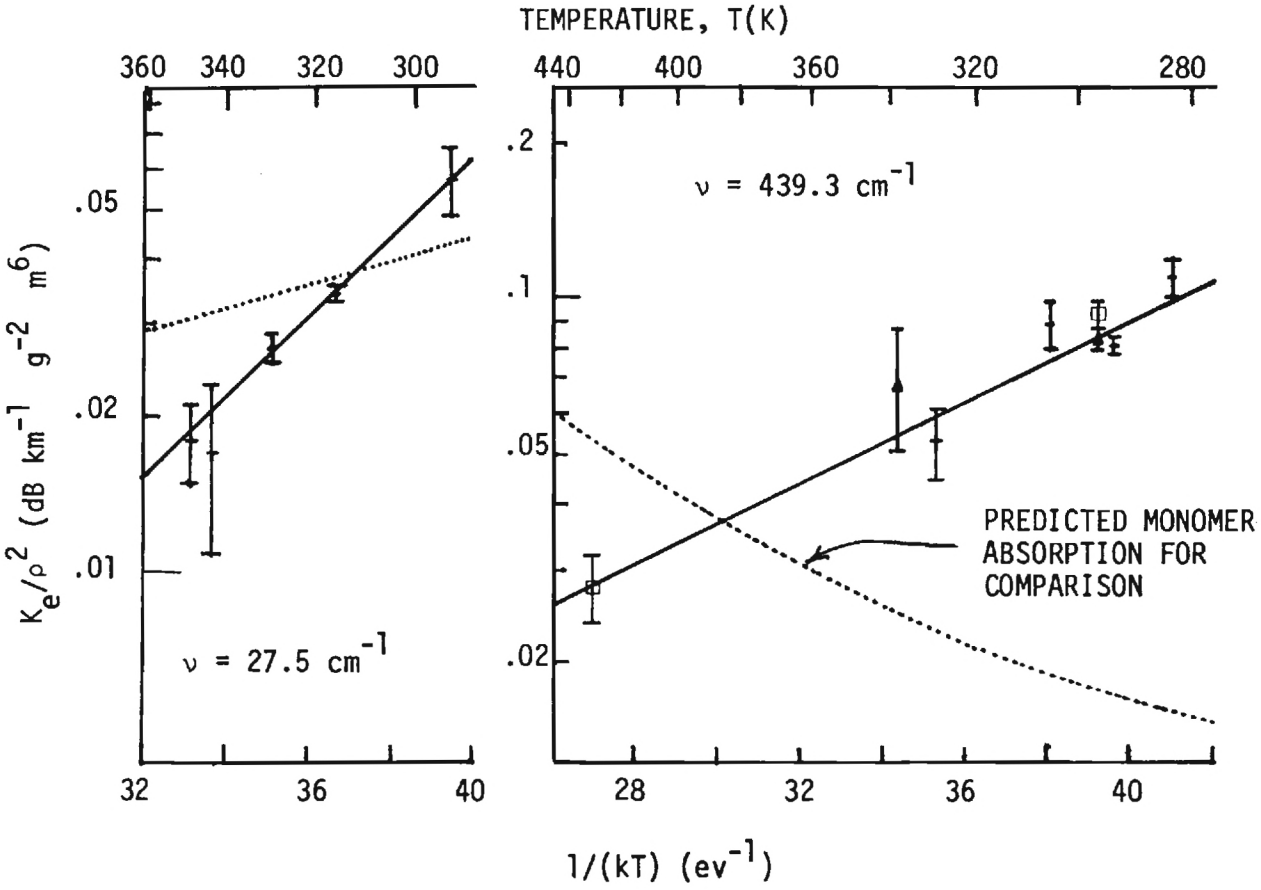

Figure 6

ENERGY CHARACTERIZING OBSERVED TEMPERATURE DEPENDENCE
OF EXCESS ABSORPTION

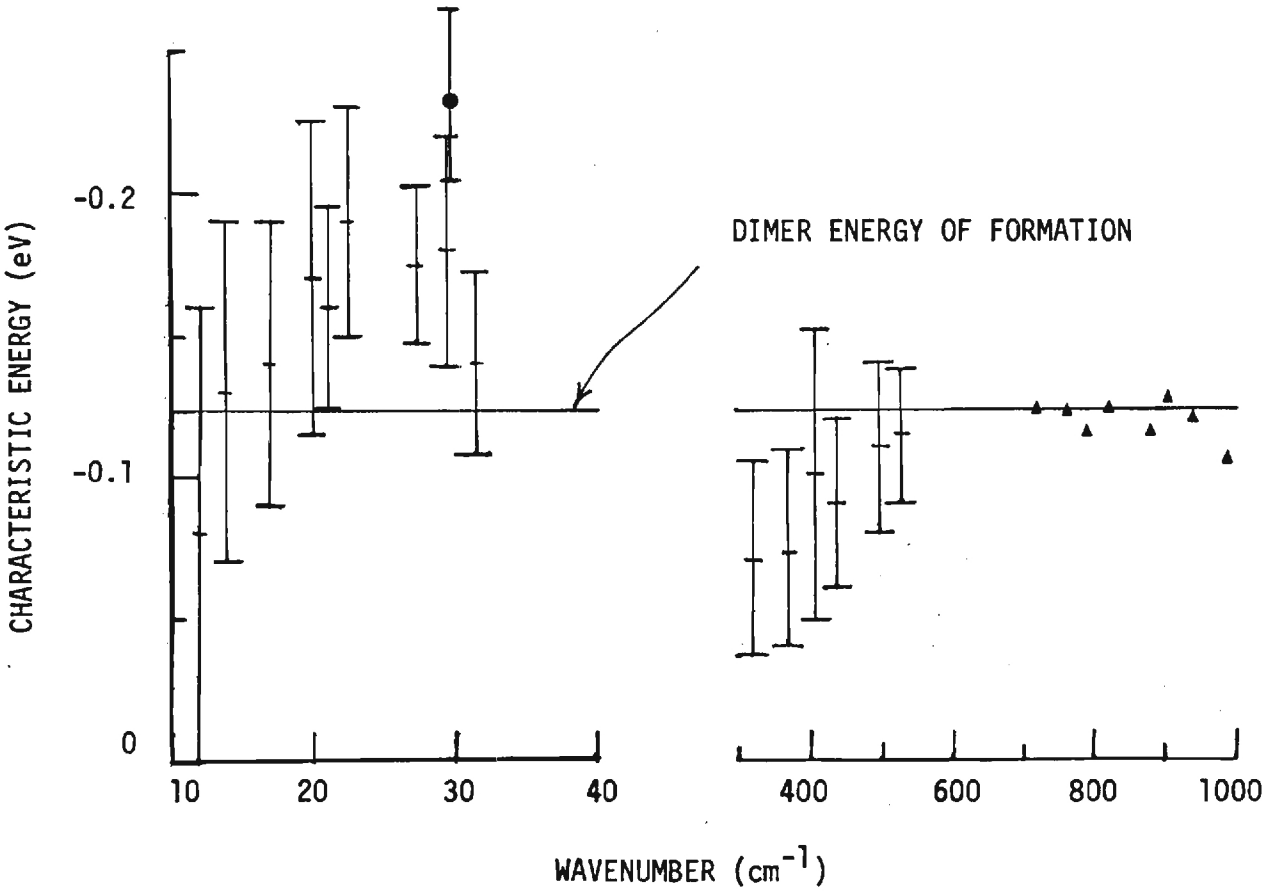

PRESENT WORK + FOURIER TRANSFORM SPECTROSCOPY

● MASER

GRYVNAK ET AL. (1976) ▲

Figure 7

PRESENTED AT 1979 IRIS CONFERENCE AND THE 23rd ANNUAL SPIE CONFERENCE, SAN DIEGO, CA., 27-31 AUGUST, 1979.

Military systems applications at near-millimeter wavelengths

J. J. Gallagher, R. W. McMillan and R. G. Shackelford

Engineering Experiment Station, Georgia Institute of Technology
Atlanta, Georgia 30332

Abstract

The near-millimeter wavelength region (3.2mm - 0.3mm) is being investigated for military systems applications during adverse weather and in the presence of smokes, dust and other particulate clouds. The use of near-millimeter wavelengths (NMMW) has advantages and disadvantages relative to the use of the infrared and microwave regions. The atmosphere is a dominant factor in determining the operation of military systems in the NMMW region. Systems currently under consideration for NMMW applications include beam rider and command guidance, missile plume detectors, low-angle tracking radars, terminal homing systems, target acquisition radars, fuze systems, quasi-imaging radars and hybrid (IR/NMMW) systems. Recent NMMW technological developments (e. g., sources, receivers, components, phenomenology and measurements) have been advancing at a rapid pace to meet system needs.

Introduction

Weapon guidance systems operating in the visible/infrared spectral regions have been successfully developed for tactical use over a broad spectrum of engagement scenarios. These include direct systems employing beam riders, command guidance, semi-active and active guidance modes which have demonstrated effective operation in clear weather, but are inoperable in certain severe atmospheric conditions and in the presence of smokes, dust and other particulate clouds. Since molecular absorption in the atmosphere is low over broad spectral windows throughout the visible/infrared, the primary attenuation mode is Mie scattering by water droplets in haze and fog, and by particulates in smokes and other aerosols.

On the other hand, the near-millimeter wavelength region is affected less by adverse weather, smokes, and aerosols than the visible/IR wavelength regions. Rain attenuation of NMM wavelength radiation is comparable to rain attenuation in the IR region. Because of its improved transmission under adverse environmental conditions, near-millimeter wavelengths are being considered for military applications. The NMMW spectral region will not prove to be an ideal operational region for all systems applications, but will, in several cases, provide a compromise adverse weather capability for limited range applications with resolution better than that of the microwave region.

In recent years, millimeter and near-millimeter wave systems applications have been the subjects of workshops[1], reports[2] and study panels[3]. This paper will draw upon material presented in these references, with the majority of information originating from the Harry Diamond Laboratories study[3]. A primary purpose of many of these investigations has been the identification of NMMW systems technology requirements, some of which will be briefly discussed following a summary of potential applications.

Advantages and disadvantages of NMMW region

The near-millimeter wavelength region has usually been dismissed in the past as a region of high attenuation, relative to the microwave region, and as a region of poor angular resolution relative to the visible/IR wavelength regions. However, several factors enter into the evaluation of the wavelength region which is chosen for operation of a particular system during adverse weather. It will be seen in the next section that transmission in adverse weather improves considerably in going from visible/IR wavelengths to NMM/MM wavelengths, and further improves at centimeter wavelengths. On the basis of this comparison, it would appear that centimeter or longer wavelengths would be the most appropriate for systems operation in adverse weather. Moreover, it has been shown that transmission through smokes and aerosols also follows a pattern of decreasing with increasing wavelength. Aimpoint accuracy requirements, however, tend to eliminate the centimeter wavelength region on the basis of a number of practical considerations. For example, the required accuracy for target tracking or target designation usually falls within the range of 0.1 to 0.5 mrad resulting in antenna dimensions of about 0.5 to 1 m for millimeter wavelengths and 5 to 10 meters for centimeter wavelengths. This consideration alone rules out a centimeter wavelength system for applications where the weapon system platform would be vehicle- or helicopter-mounted. Analysis of NMMW systems requires then that several factors be weighed in determining their potential in currently conceived tactical applications. Tables 1 - 4 list advantages and disadvantages of the NMMW spectral region relative to microwave and

infrared wavelengths. Some of the listed advantages might be questioned; thus, whereas the best of RF and optical techniques can be combined at NMM wavelengths, this can also be considered a necessity because of the nature of the spectral region. On the other hand, disadvantages such as component deficiencies and lack of data will be reduced or removed as work progresses at NMM wavelengths.

Whereas several of the NMMW disadvantages can be expected to diminish, the limiting factor for systems applications is the atmospheric effect, which cannot be avoided. The factor $e^{-\alpha R}$, where α is the atmospheric attenuation and R is the weapon-target range, is present in all propagation expressions. In the analysis and discussions of NMMW systems, their performance is dominated by their capability to operate under various atmospheric conditions. Since the major role for NMMW tactical systems will be during inclement weather or in the presence of smoke, the characteristics of a NMMW system, when such conditions prevail, are extremely important.

Table 1. Advantages for NMMW Region Relative to Microwave Region

1. Greater Resolution
2. Smaller Beam Angle θ_B for Given Antenna Diameter, D, and Conversely Smaller D for Given θ_B
3. Reduced Multipath Potentially Improved Low-Angle Tracking
4. Low Off-axis Detectability Providing High Security
5. Covertness Due to Exponential Fall-off With Range in High Attenuation Regions
6. Tracking Through Plumes Improved Over Microwave Systems
7. Smaller Components Allowing More Compact On-board Missile Systems
8. Clutter More Diffuse, Doppler Shift is Greater, Glint Should be Less
9. Integration of Hybrid IR/NMMW Systems Possible
10. Countermeasures More Difficult

Table 2. Advantages for NMMW Region Relative to Optical Region

1. Improved Transmission in Smoke and Fog, Providing Better Low Visibility Operation
2. Harder to Jam; More Covert
3. Improved Eye Safety
4. Better Coherent Receiver Techniques
5. Source Stabilization More Easily Performed
6. Potentially Lower Cost
7. Reduced Background
8. Both RF and Optical Technology Applicable

Table 3. Disadvantages for NMMW Region Relative to Microwave Region

1. Poor Heavy Rain Transmission
2. Atmospheric (clear) Absorption is Higher
3. Larger Rain Backscatter
4. Current Receiver Noise Figures are Poorer
5. Higher Precision Manufacturing Required
6. Solid State Source Efficiencies Fall as Frequency Squared
7. Poorer Source Stability
8. Inferior Waveguide Power Handling Capability
9. Higher Cost for NMMW Systems

Table 4. Disadvantages for NMMW Region Relative to Optical Region

1. Lower Resolution
2. Higher Glint
3. Lack of Relevant Data
4. Video Detection Less Sensitive
5. Component Technology Currently Worse
6. NMMW Laser Sources Less Efficient
7. Solid State and Tube Sources Chirped, Less Monochromatic Than Optical Lasers
8. Components Currently Larger and Heavier

Atmospheric effects

Whereas the NMMW region offers an advantage over optical systems during adverse weather, clear weather NMMW propagation suffers greater attenuation than experienced in the IR/visible region, and is, in addition, for most systems restricted to spectral windows. The NMMW region has strong O_2 and H_2O absorption lines with water the major absorber. Between these broad lines lie the transmission windows. Figure 1 shows the horizontal attenuation across the NMMW region from 100 GHz to 1000 GHz at sea level and 4 km altitude[4]. Also shown is the weak O_2 absorption at sea level. Because of the strong absorption at the

short wavelength end of this spectral region, tactical ground-to-ground or ground-to-air applications are confined to the longer wavelength windows which are centered about the following wavelengths:

Wavelength (mm)	Horizontal Attenuation (dB/km)	Zenith Attenuation (dB)
3	0.3	1.25
2.1	0.5	0.91
1.3	1.75	2.1
0.88	9.0	9.9
0.72	17	22

Included in this listing are approximate horizontal attenuation (dB/km) for 5.91 g/m^3 of H_2O at sea level and the zenith attenuation (dB) for 7.5 g/m^3 of H_2O at sea level. A more comprehensive indication of the horizontal attenuation across the electromagnetic spectrum (3 cm - 0.3 μm) is given[5] in Figure 2. A clear air curve for H_2O density of

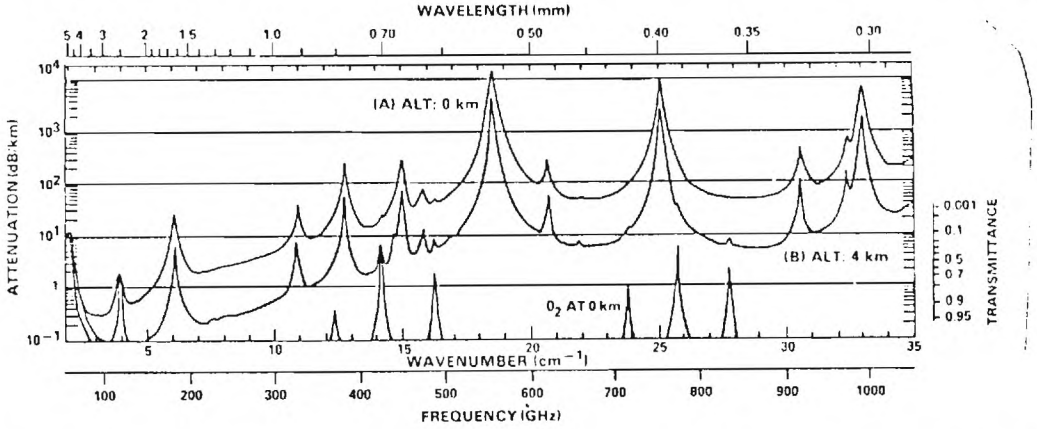

Figure 1. Spectral plots of the attenuation by the (1962) U.S. Standard Atmosphere at sea level and 4 km altitude. The water vapor density is 5.91 g/m^3 at sea level and 1.10 g/m^3 at 4 km altitude. The lower curve represents O_2 only at sea level. For comparison, the attenuation for this same model atmosphere is approximately 0.2 dB/km in the 10 micrometer window and less than 0.1 dB/km near 3.8 micrometers[4].

7.5 g/m^3 at 20°C shows the high attenuation in the submillimeter region surrounded by the low microwave and IR/visible attenuation. From the fog and rain curves of Figure 2, the

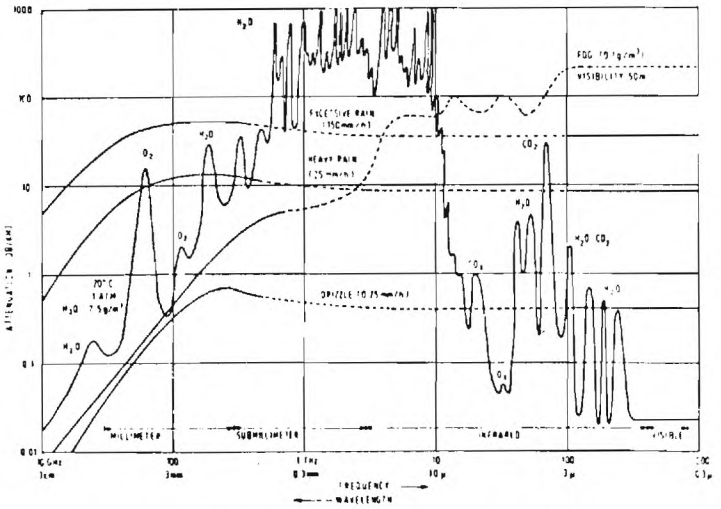

Figure 2. Attenuation by atmospheric gases, rain and fog[5].

advantage of NMMW systems during heavy fog and the comparable NMMW and IR attenuation during rain are demonstrated. A similar figure[6], Figure 3, shown increasing attenuation for clouds with decreasing wavelength, indicating an advantage for satellite or aircraft-to-ground sys-

tems applications. Near millimeter wave attenuation by aerosols is highly dependent on the

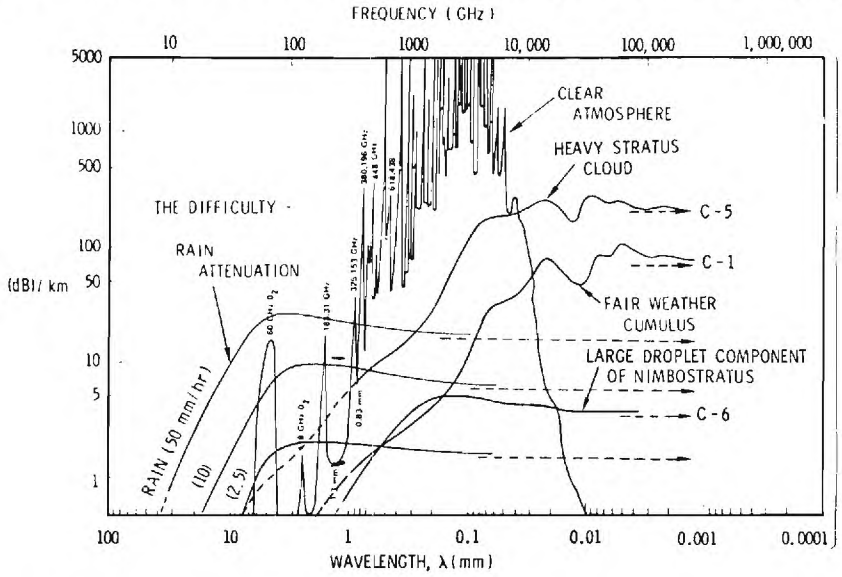

Figure 3. Summary of sea-level atmospheric attenuation[6].

type of aerosol and its particle size distribution and concentration. Table 5 shows the size range and concentration of water droplets in rain, fog and clouds. It can be seen from this table that the larger size range of rain droplets (7-700 μm) would cause significant scattering losses at near millimeter wavelengths were its concentration not extremely low compared to the concentration of water droplets in fogs and clouds. For both rain and fog, the attenuation is an almost linear function of bulk water density with the frequency dependence for attenuation in rain being negligible over the NMM spectral region from 94 to 340 GHz.

Table 5. Comparative Water Droplet Size and Density For Rain, Fog, and Clouds [8, 9, 10]

Rain				
	Light (r = 1 mm/hr)	Moderate (r = 4 mm/hr)	Heavy (r = 25 mm/hr)	Cloudburst (r = 100 mm/hr)
Size Range (μm)	7 - 100	10 - 300	10 - 500	50 - 700
Droplet Density (m^{-3})	350	500	700	1,250
Water Density (g/m^3)	0.04	0.17	1.0	4.2

Fog		
	Thin (vis. ~ 300 m)	Thick (vis. ~ 50 m)
Size Range (μm)	< 0.1	0.02 - 0.2
Droplet Density (m^{-3})	2×10^{10}	1.3×10^{11}
Water Density (g/m^3)	0.023	0.35

Clouds				
	Cumulonimbus	Cumulus Congestus	Fair Weather Cumulus	Strato Cumulus
Size Range (μm)	-	8 - 12	3 - 5	2 - 4
Droplet Density (m^{-3})	-	-	1.6×10^8	3×10^8
Water Density (g/m^3)	6.0	2.5	0.5	0.2

For aerosols resulting from smokes, dust or other battlefield-generated debris, the attenuation is primarily due to scattering, and secondarily to absorption. Preliminary indications[7] are that propagation through existing screening smokes is very high, and that the development of effective smokes for the NMMW region is questionable because of the difficulties involved with generating and dispensing smokes with the appropriate particle size distribution and settling rate. Attenuation of millimeter radiation by ground ex-

plosions of munitions has been shown to be relatively high for short periods of time[7]. Although the attenuation cleared much faster for NMM waves than for the IR/optical bands, nevertheless, loss of NMMW track or acquisition of a target could occur during a barrage or critically placed explosion so that these effects must be considered in greater detail in the future.

It is important at this point to demonstrate millimeter wave propagation under conditions of high absolute humidity and high bulk water content, since these are the conditions under which all military systems are expected to operate. Examples are given for the three cases: clear weather (high absolute humidity), rain and fog.

Clear weather

In high visibility conditions with a lack of precipitation and fog, the attenuation of near millimeter radiation in dB/km is directly proportional to absolute humidity. This linear relationship is shown in Figure 4 on a plot of temperature-humidity data which was abstracted from a psychrometric chart. Table 6 shows the two-way path loss for a range of 3 km at frequencies of 94, 140 and 220 GHz for various atmospheric conditions. Note that the attenuation of 220 GHz radiation is very high for warm, humid conditions although the total path loss is only 18 dB (3 dB/km) for the standard atmosphere (T = 300°K, ρ = 7.5 g/m^3).

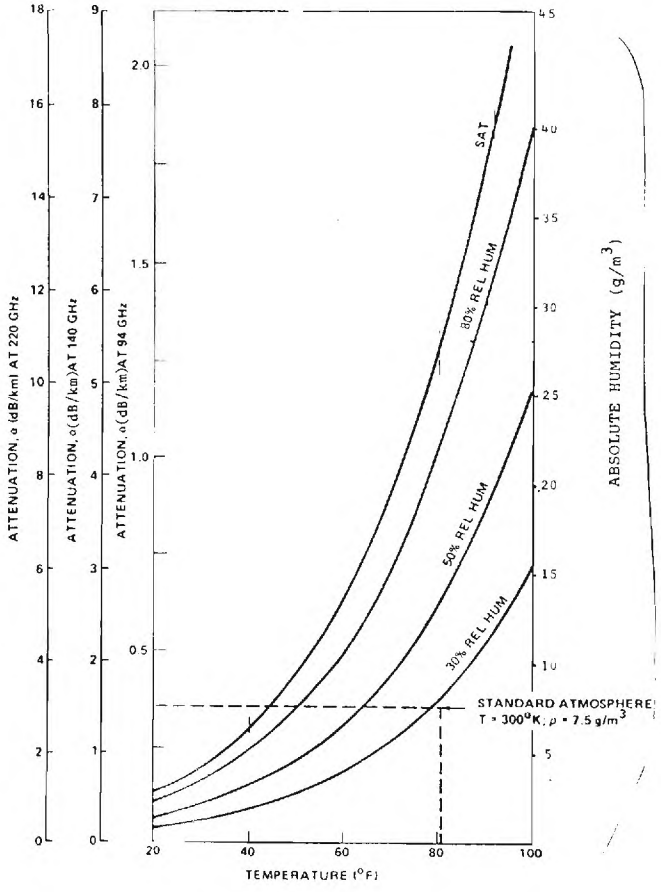

Figure 4. Atmospheric absorption by water vapor.

Table 6. Two-Way Path Loss In dB For Atmospheric Attenuation Over A Range of 3 km

Frequency (GHz)	Relative Humidity	T = 90°F			T = 65°F			T = 40°F		
		30%	50%	80%	30%	50%	80%	30%	50%	80%
94		3.1	5.2	8.4	1.4	1.9	3.0	0.6	0.9	1.4
140		13.2	21.9	35.4	5.7	9.3	15.0	2.7	3.3	6.2
220		26.4	43.8	70.8	11.4	18.6	30.0	4.5	6.5	12.3

The impact of these attenuation figures on system design can be shown by solving the radar equation for a typical set of system parameters; the radar range equation is of the form

$$S/N = \frac{P_p \tau G^2 \lambda^2 \sigma_T}{(4\pi)^3 R^4 K T N_f L_T} \qquad (1)$$

where P_p = peak power of the transmitter; τ = pulse width of the transmitter (it has been assumed that the receiver bandwidth = $1/\tau$); G = gain of the transmitting/receiving antenna; λ = free space wavelength; σ_T = radar cross section of the target; R = range to target; K = Boltzmann's constant; N_f = noise figure of the receiver, and L_T = total radar system loss (atmospheric & signal processing + waveguide and components).

Assuming the following parameters:

τ = 200 nsec.; λ = 1.3 mm (230 GHz); G = 47.6 dB (6" aperture with η = 0.5); σ_T = 50 m^2; KT = 4.14 x 10^{-21} (T = 300°K); L_s = signal processing loss = 3 dB; L_w = waveguide and component loss = 8 dB; N_f = 12 dB.

we may write

$$S/N(dB) = P_T(dBW) - 40 \log R(km) - 2\alpha(dB/km)R(km) + 15.2$$

Figures 5 and 6 show S/N vs R for different values of P_T for atmospheric conditions of T = 27°C and ρ = 7.5 g/m^3 (standard atmosphere) and T = 30°C and ρ = 28 g/m^3 (relative humidity ≈ 80%). For these two cases, Table 7 shows the peak power versus range required for S/N = 14 dB (P_d = 0.9, P_{fa} = 10^{-7}). Note that for large α, the S/N vs R curves are very steep, and only small changes in range occur for large changes in P_T at a given S/N. With a maximum peak power of 10 kW, for example, the high visibility range will be limited to about 1.5 km on a warm humid day, and to about 3 km on a warm dry day. These calculations are for single pulse transmission only.

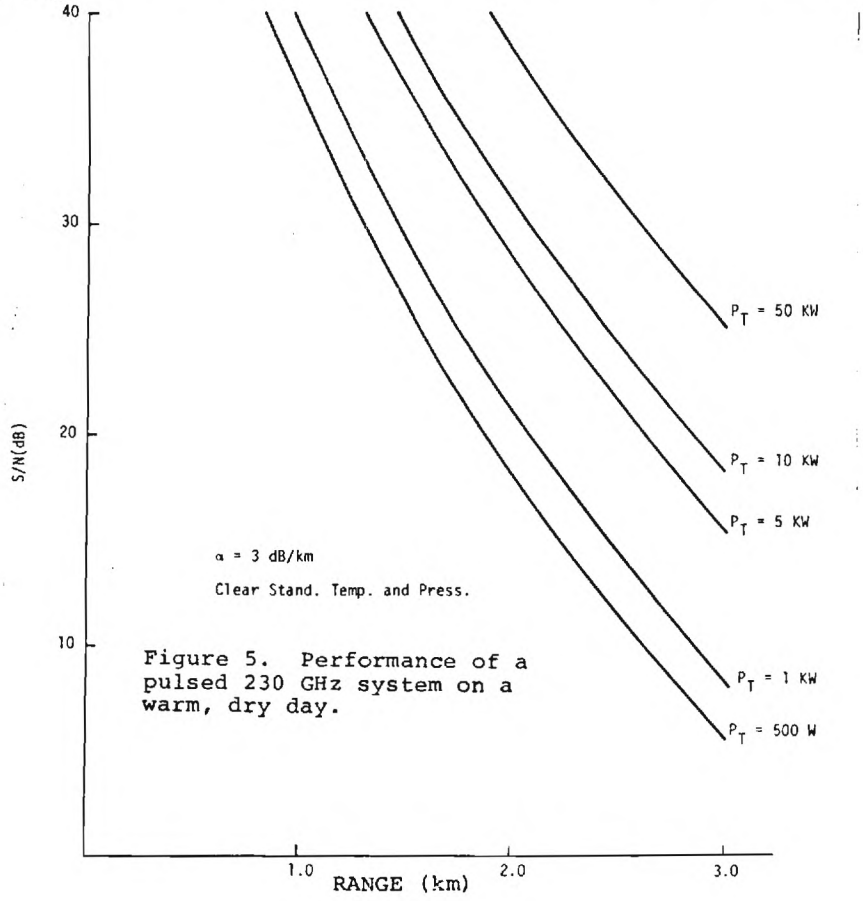

Figure 5. Performance of a pulsed 230 GHz system on a warm, dry day.

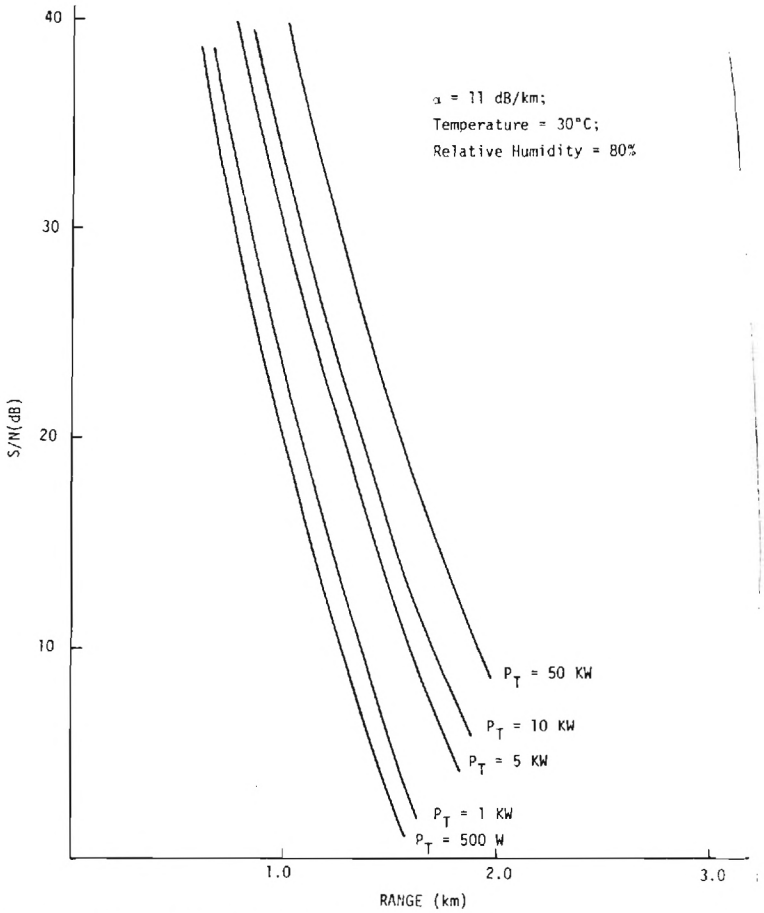

Figure 6. Performance of a 230 GHz pulsed system on a warm, humid day.

Table 7. Required Power To Achieve S/N = 14 dB

Range (km)	Warm, Dry T = 27°C, ρ = 7.5 g/m^3 P_T(KW)	Warm, Humid T = 30°C, ρ = 28.0 g/m^3 P_T(KW)
1.0		0.1
1.25		1.0
1.5		7.2
1.75		47.0
2.0	0.2	284.5
2.25	0.4	
2.5	0.9	
2.75	1.8	
3.0	3.6	

Although the performance of a system operating in the 230 GHz window degrades rapidly in warm humid weather, in many parts of the world these conditions are present for only a small percentage of the time. An example is the climatological conditions of Western Europe. Figure 7 shows the attenuation for three near-millimeter frequencies based on the mean maximum daily temperature and relative humidity for Bayreuth, West Germany. These data predict that the mean attenuation during the summer months will be less than 7 dB/km, and for this figure, a range of 2.0 km would be possible with a 10 kW pulse source.

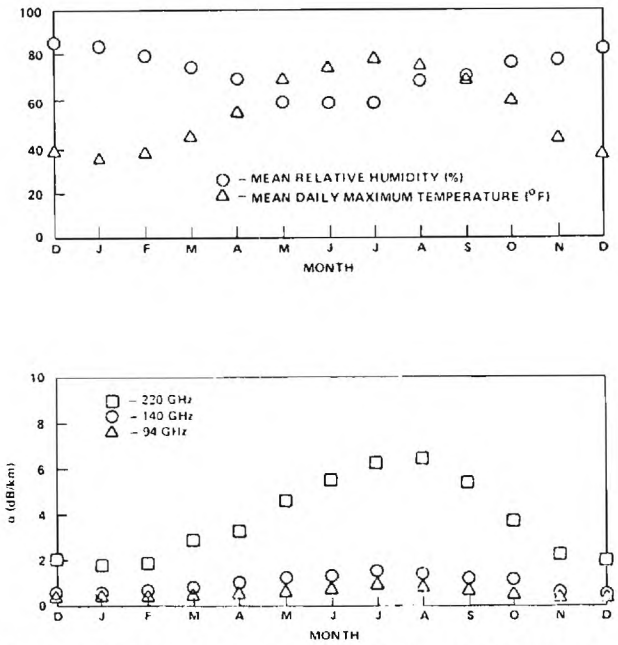

Figure 7. Millimeter wave atmospheric absorption by water vapor - Bayreuth, West Germany.

Rain. Although differences exist in predicted rain attenuation for the NMMW region[11], most models predict the following relationships:

$$\alpha(\text{dB/km}) = Ar^B, \tag{2}$$

where A and B are constants for the frequency region 94 - 340 GHz, and r is the rain rate in millimeters per hour. Based on the available data, the relation

$$\alpha(\text{dB/km}) = r^{0.85} \tag{3}$$

provides a reasonably close fit throughout the NMMW spectrum. As might be expected, a warm rainy day will be a problem for a system at 220 GHz because of strong absorption by both water vapor and bulk water. For example at T = 26.7°C (80°F), and r = 4 mm/hr. (a moderate rain rate), the attenuation is 11 dB/km (water vapor) plus 3 dB/km (rain) or 14 dB/km total. Figure 8 shows the S/N versus range at three power levels, and again it is evident that for a given value of S/N, large increases in power result in small increases in range. For this atmospheric condition, a peak power level of about 50 kW would be required for a range of 1.5 km at S/N = 14 dB whereas a range of about 1.2 km would be possible at the same value of S/N with only 5 kW peak power. An order of magnitude increase in power only results in about 0.3 km increase in range for this condition.

Fog. Attenuation of NMMW radiation by fog is also dominated by bulk water absorption, although a slight frequency dependence is also present. A good fit to available fog attenuation data is provided by the expression

$$\alpha(\text{dB/km}) = 0.035\ \rho(\text{g/m}^3)\ f^{1.03}(\text{GHz}) \tag{4}$$

This relationship along with the optical visibility is shown in Figure 9. For a 30 meter visibility radiation fog, with liquid water content of 0.75 g/m^3, the attenuation by water absorption at 230 GHz is approximately 9 dB/km. As shown in Figure 7, the mean maximum daily temperature of Bayreuth, West Germany during the winter months (the season of greatest incidence of fog) is about 0-4°C; therefore a reasonable fog scenario is 30-100 m visibility with temperature 0-4°C, for which the attenuation at 230 GHz would be approximately 4 dB/km to 11.5 dB/km. These conditions have been bracketed by the calculations presented in Figures 5 and 8. It is significant to point out that a 100 m visibility fog at T = 4°C (40°F) results in an attenuation of only 4.5 dB/km at 230 GHz compared with about 50 dB/km in the 8-12 μm band and about 150 dB/km at a wavelength of 0.6 μm.

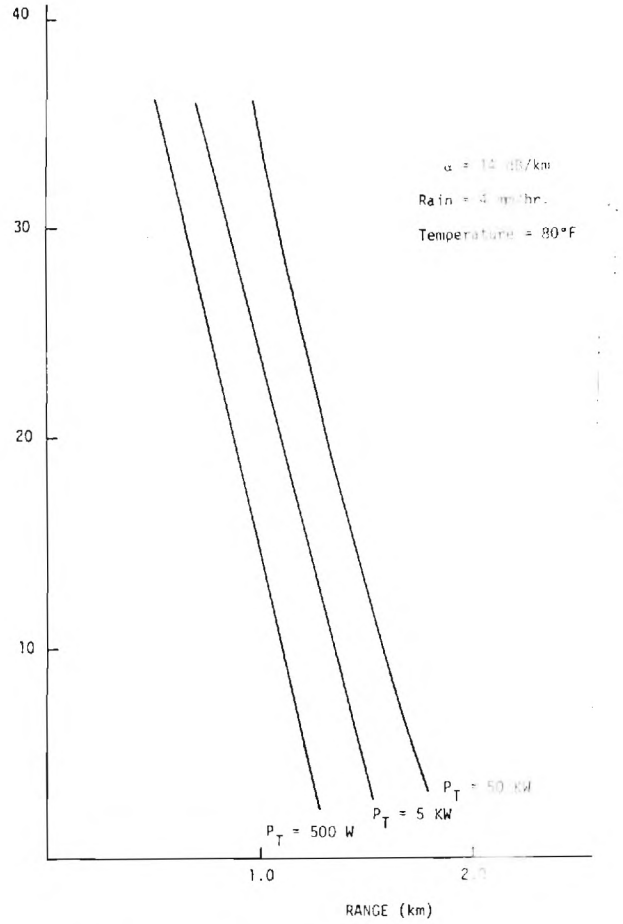

Figure 8. Performance of 230 GHz pulsed system in rain.

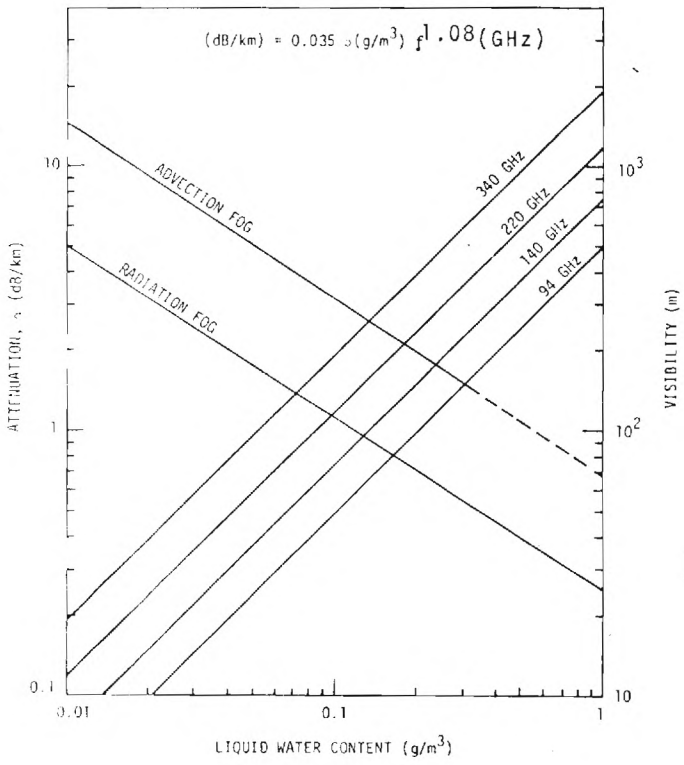

Figure 9. Millimeter wave attenuation by fog.

A summary of atmospheric propagation data, convenient for system calculations, is given in Table 8. The majority of information presented thus far has dealt with atmospheric effects appropriate to radar or communication applications. An equally important consideration is the influence of the atmosphere and environment on radiometric signals. When observing a target in its surroundings, it is important to know the brightness temperature contrast between target and other objects. This contrast is a function of frequency, the atmosphere, and target and background characteristics (reflectivity, emissivity, etc.). The antenna temperature of a radiometer looking downward from altitude h at an angle θ to the vertical is given by

$$T_B = \int_h^0 T(z)\exp[-\tau(h,z,\theta)]\alpha(z)\sec\theta dz + R\exp[-\tau(o,h,\theta)]\int_h^0 T(z)\exp[-\tau(z,o,\theta)]\alpha(z)\sec\theta dz + (1-R)T_E\exp[-\tau(o,h,\theta)]$$

where T_E is the temperature of the earth- or ground-based target and $T(z)$ is the temperature of a stratum of atmosphere of thickness dz located at altitude Z. The terms of the form $\tau(Z_1, Z_2, \theta)$ are the optical depths between altitudes Z_1 and Z_2 at angle θ, and R is the reflectivity of the earth or target. The optical depths τ are given by

Table 8. Summary Of Propagation Data

Attenuation, α (dB/km)
Water Density, ρ (g/m^3)

λ (μm)	α Clear Rel. Humidity = 100% T = 32°F ρ = 4.8	68°F 17.4	α Fog Radiative Fog R_V = 400m ρ = 0.014	200 0.038	100 0.11	30 0.71	α Fog Advection Fog 400 0.063	200 0.18	100 0.4	α Rain mm/hr 1	4	10	α Cloud Fair Weather Cum.	Nimbo-Strat.
1				80		500							95	570
4													120	640
10.6	0.3	1.2	7	20	58	373	17	63	140	1	2.6	6	50	500
337	50	185	0.6	1.5	4.3	28	2.5	7.1	15.8	1	3	7	3	20
724	10	37	0.3	0.9	2.6	17	1.0	4.3	9.6	1	3	7	2	7
880	7	24	0.3	0.7	2.0	14	1.2	3.5	7.9	1	3	7	1.5	6
1300	2	6	0.2	0.5	1.4	9	0.8	2.3	5.1	1	3	7	0.8	4
2300	1	3	0.1	0.2	0.6	4	0.4	1.0	2.2	1	3	8		2
3200	0.2	0.9	0.1	0.2	0.5	3.2	0.3	0.8	2	1	3	8		1.5

Notes: (1) for α_{CLEAR} at other Rel. Hum., scale down from 100% given

(2) for a fog situation, $\alpha_{TOTAL} = \alpha_{CLEAR}$ (RH = 100%) + α_F (likewise for clouds)

(3) for a rain situation, $\alpha_{TOTAL} = \alpha_{CLEAR}$ (RH = 100%) + α_R

$$\tau(Z_1, Z_2, \theta) = \int_{Z_1}^{Z_2} \alpha(Z) \sec \theta dZ \qquad (6)$$

so that the first term of Equation (5) is the contribution of the intervening atmosphere between the radiometer and target, the second term represents atmospheric emission reflected from the target to the radiometer, and the third term is the target's emission attenuated by the atmosphere between the radiometer and target. The target or earth background reflectivity is given by R, the target (earth) temperature is T_E and the atmospheric attenuation is $\alpha(Z,\nu)$. It is seen from these relations that not only atmospheric absorption by O_2 and H_2O is important, but hydrometeorite absorption and scattering and atmospheric thermal emission are also determining factors for the radiometric antenna temperature, which is reduced further in value when the target fill factor for the antenna is less than one.

Preissner[12] has shown the brightness temperature contrast for different weather conditions and different materials for the microwave through NMMW spectral region. Figure 10 demonstrates the brightness temperature contrast between vegetation and concrete for three different altitudes for a clear standard atmosphere (ρ_{H_2O} = 7.5 g/m^3, T = 20° C and P = 760 mmHg at sea level). At all altitudes given, a detectable brightness temperature contrast exists, except possibly at 230 GHz for 3 km and 8 km, where the temperature contrast is on the order of 3-5° K and the minimum detectable temperature is approximately 0.5-3° K for a 1 GHz bandwidth and a 10 msec time constant. Figure 11 shows the brightness temperature contrast (concrete and vegetation) for a radiometer at 3 km altitude for several atmospheric conditions. Rain severely degrades NMMW radiometric response and fog of visibility of 100 m or less results in considerable loss of contrast. A more significant indication of radiometric capability to detect a military target is the brightness temperature contrast for metal relative to vegetation. Figures 12a and 12b show contrasts for metal, water and concrete relative to vegetation. For metal, detectable contrasts are observed for all conditions except the 25 mm/hr rain. It must be emphasized, however, that, for metal, reflectivity of 1 has been used and no fill factor reduction has been employed. Both conditions are unlikely. Systems applications require further consider-

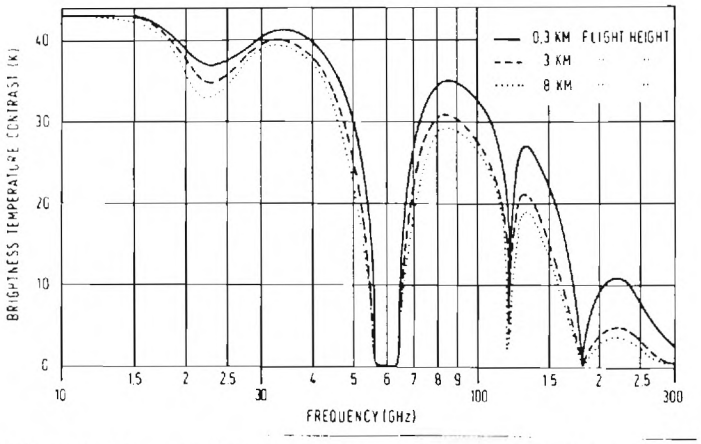

Figure 10. Brightness temperature contrast between vegetation and concrete for three different heights[12].

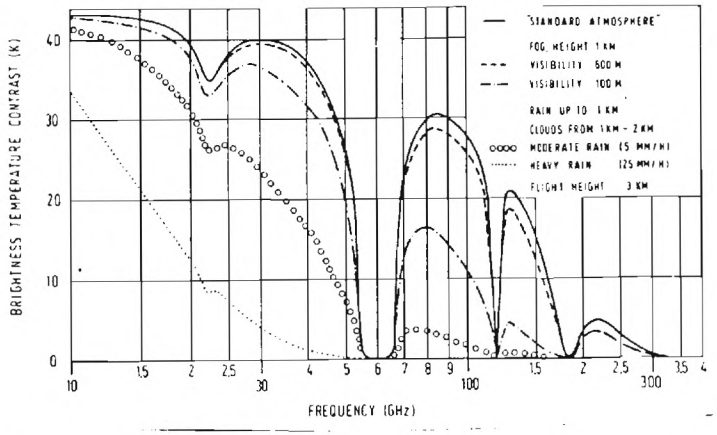

Figure 11. Brightness temperature contrast between vegetation and concrete for different weather conditions[12].

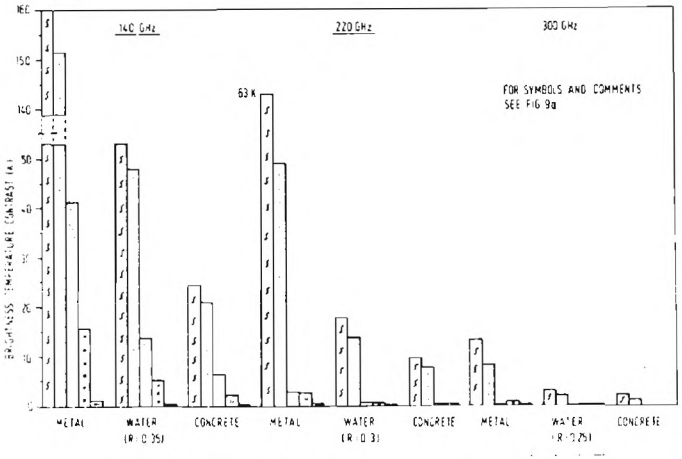

Figure 12a. Brightness temperature contrast for different objects, weather conditions and frequencies (11 GHz, 140 GHz, 90 GHz)[12].

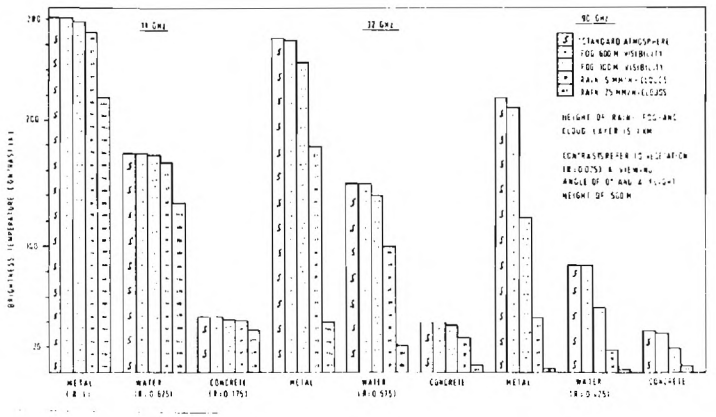

Figure 12b. Brightness temperature contrast for different objects, weather conditions and frequencies (140 GHz, 220 GHz, 300 GHz)[12].

ation of these effects with inclusion of antenna pattern and fill factor effects.

Very little data exist for atmospheric turbulence in the NMMW region; fluctuation of intensity and signal angle of arrival for NMMW systems have been studied by Armand et al.[13] and by Snider, Wiltse and McMillan[14]. Based on the approach first proposed by Armand, the peak-to-peak intensity fluctuations expected for a 230 GHz system under near standard conditions were calculated to be 1.16 dB, and the corresponding angle-of-arrival fluctuations were determined to be 0.3 mrad. In practice, observed intensity fluctuations at lower frequencies have occasionally been observed to be much larger, and little data are available for the angular fluctuations. Much work needs to be done before the effects of turbulence on NMMW systems have understood, but the meager results available to date indicate that it gives system degradation of a magnitude which must be considered.

The approximations discussed thus far demonstrate some of the atmospheric effects to be considered in systems trade-offs between the NMMW and IR/visible regions but do, in no way, describe the complexity that could occur at NMM wavelengths. Thus, when the limited experimental data for H_2O are compared with existing theories, the measured values in the window regions invariably exceed theoretical values. When measured values are compared with the monomer spectrum calculated with the Van Vleck-Weisskopf[15] or Gross[16] lineshape, the inadequacy of the theory is evident from Figure 13 in which the dashed curve B represents an empirical "continuum" absorption which must be added to bring the theoretical results into coincidence with the experimental results[4]. The empirical correction term has been given in the form[17]:

$$\Delta \alpha_{\nu} = 4.69 \times 10^{-6} \rho \left(\frac{300}{T}\right)^{2.1} \left(\frac{P}{1000}\right) \nu^2 \left(\frac{dB}{km}\right) \qquad (7)$$

where ρ is the water density (g/m^3), T is the atmospheric temperature, $^{\circ}K$, P is the pressure and ν the frequency. The discrepancy between measured and calculated water-vapor absorption closely follows this empirical correction term throughout the NMMW region. Various causes have been postulated for this excess or anomalous absorption, but, thus far, the source is not understood. Great anomalies have been observed in high humidity, cold conditions and in fog[18]. Further experimentation is needed in this area of atmospheric effects.

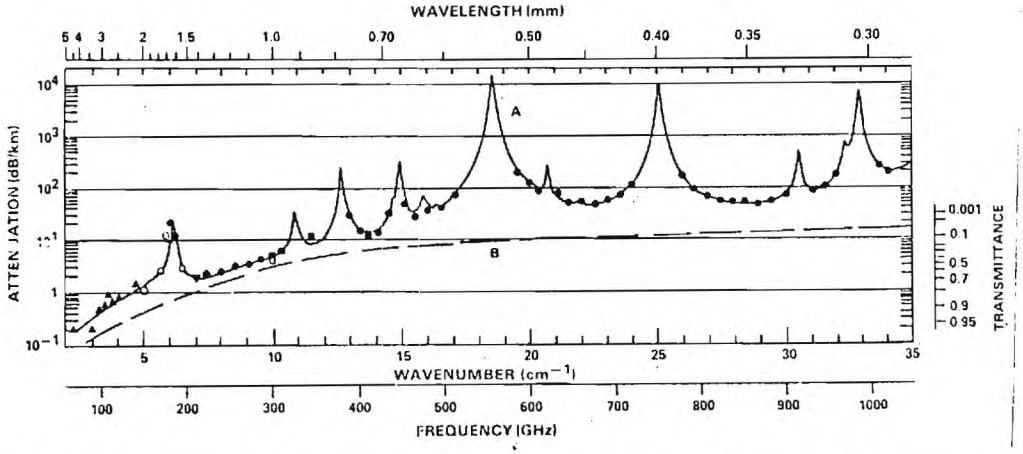

Figure 13. Spectral plots of the attenuation by atmospheric H_2O at sea level. Curve A represents a combination of theoretical and experimental results for an H_2O density of 5.91 g/m^3. At a fixed temperature and 1 atm total pressure, the attenuation is approximately proportional to the H_2O density. Curve B corresponds to an empirical continuum that is added to theoretical results to provide agreement with the experimental results. The transmittance scale on the right-hand side corresponds to a 1 km path[4].

Considerable space has been devoted in this paper to a discussion of atmospheric effects on propagation. However, it is just these effects which are the most important factors in determining the applicability of a particular military system in the NMM wavelength region.

Potential NMMW systems applications

Several NMMW military applications have been investigated in recent years. Of these, some have not shown advantages over the equivalent system operating in another spectral region, whereas some have sufficient promise to warrant initiation of experimental development of prototype systems. Among the potential systems applications which have been studied are the following[1-3]:

1. Beamrider systems
2. Terminal homing
3. Target designation and semi-active homing
4. Command guidance
5. Target surveillance and acquisition
6. Active NMMW quasi-imaging
7. Low angle tracking
8. IFF systems
9. Airborne passive imaging
10. Aircraft detection from satellites
11. Boost phase plume detection
12. Re-entry applications
13. Secure communications
14. Mine detection
15. Obstacle and terrain avoidance
16. Space object identification (SOI)
17. Fuzing
18. Hybrid (IR/NMMW) systems

The details of the investigation of most of these systems can be found in the references, and only a selected system, the NMMW beamrider, and brief statements on others will be discussed in this section.

Beamrider

A beamrider guidance system[19, 20, 21] is defined as a technique for guiding missiles which utilizes a beam directed into space, such that the beam axis forms a line along which it is desired to direct a missile. The missile contains equipment that can sense the direction and magnitude of the error when its path has deviated from the center of the beam, and that can generate guidance error signals which cause the missile to return toward the center of the beam. In principle, a beamrider system can be employed in surface-to-surface, surface-to-air, air-to-air, and air-to-surface roles, although it is potentially more effective against slowly moving targets. The basic elements of a beamrider system are the same for each of the roles but the stringency of the requirements placed on these elements will be determined by the particular applications. For the purposes of interest here, a surface-to-surface anti-armor role has been emphasized as an example of a credible application of NMMW guidance.

In the beamrider concept adopted as an example for this study, the target is acquired and tracked by a precision near millimeter wave (NMMW) radar with a conical scan antenna. The missile is launched toward the target along the conical scanning tracking beam, which is coded to provide information on the position of the missile relative to the scan axis which defines the line-of-sight (LOS) to the target. A receiver in the rear of the missile detects the scanning beam, decodes it to determine its position with respect to the scan axis, and generates the appropriate error signals to keep the missile in the center of the beam. In the conical scan mode, a relatively simple PRF coding scheme can be used to develop the required guidance error signals.

Figure 14 shows the NMMW beamrider guidance concept. The first and second beams are the capture beams which establish line-of-sight (LOS) guidance as quickly as possible. The basic functions of the beamrider system are target acquisition, target track, missile capture and missile guidance.

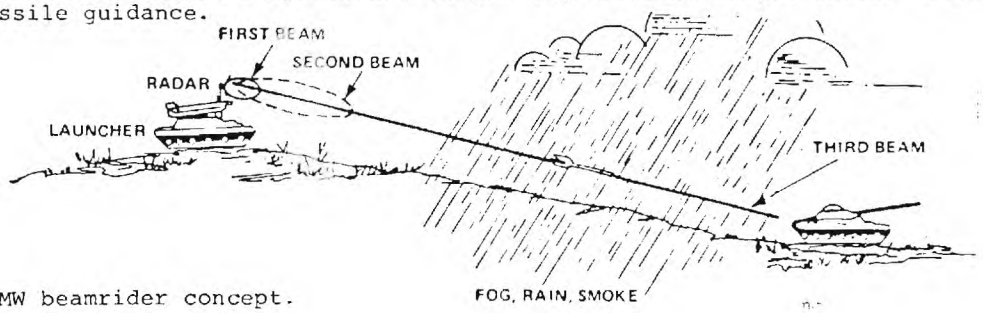

Figure 14. NMMW beamrider concept.

The basic system configuration considered to be most desirable for a ground-to-ground, anti-armor beamrider system requires that the entire system be a self-contained, crew-served and vehicle-mounted package with an antenna aperture diameter less than one meter. The candidate missile would be of the TOW or SHILLELAGH generic class, and would be tube-launched from the tracking/guidance platform. This concept would require an integrated target acquisition capability for performing target handover from a wide-area battlefield surveillance system, and for establishing an autonomous operating capability over a limited battlefield sector. The acquisition capability would of necessity require the development of suitable target recognition criteria based on the near millimeter wave target signature.

Nominal system parameters relating to these requirements have been given as the following[21]:

Operating Range	- Maximum: > 2 km; Minimum: < 0.5 km
Capture Range	- Maximum: $\leq$ 100 m
Weather and Environmental Extremes	- Rain: 4 mm/hr; Fog: 100 m vis. Temperature: 90 - 100°F; Relative Humidity: 80 - 100% Smoke: Battlefield-generated dust and aerosols; tactical screening agents
Acquisition	- Search Sector: 5° x 25°, movable scan sector; Search Time: < 10 sec.
Missile Data Rate	- 50 Hz

In addition to these characteristics, a NMMW system should also satisfy the general requirements of high reliability and maintainability, compatibility with existing equipment, capability for CM hardening, minimum operator interaction and training, rapid fire capability, and high first round probability of kill.

Based on these requirements, system concepts and estimated performance for a NMMW anti-armor beamrider system have been addressed[21]. However, the paucity of essential data for target and terrain reflectivity and atmospheric propagation may result in an altering of the performance calculations when those data become available.

The beamrider concept has been successfully implemented in the infrared, demonstrating good clear weather performance. Currently, there is an enthusiastic interest in the beamrider for the anti-armor application. The U. S. Army Ballistic Research Laboratory (BRL) has successfully carried out a feasibility demonstration of beamrider tracking and guidance at 140 GHz[20], and plans to repeat these experiments at 217 GHz. Efforts have also been initiated at U. S. Army MIRADCOM to define and verify a baseline beamrider missile system for anti-armor applications.

The critical performance parameters of any beamrider system are related to (1) high accuracy centroid tracking of the target, (2) a temporal and spatial beam structure such that the missile guidance is not biased by the terrain effects, and (3) a method of capturing the missile at a range close enough to insure adequate damping of the missile's angular deviations from LOS at the closest tactical range of interest.

The application of beamrider technology is most promising in the guided direct fire anti-tank role with the radar and launcher borne by a land vehicle. The system as presently envisioned requires a relatively large antenna ($\sim$ 0.6 m diameter), a precision tracking mount, and a dual beamwidth antenna configuration to accomplish missile capture. It is not feasible to consider a helicopter-borne weapon system at this time because of the size of the antenna/mount configuration; however, it may be possible to exploit optical scanning techniques which involve stabilization of scan components to obviate the requirement for a large precision tracking mount. The anti-helicopter role could be considered if the target exposure time is adequate to acquire and to accommodate the missile time-of-flight. In the anti-aircraft role the end game maneuverability requirements on the missile would be severe for crossing targets or for targets performing high G maneuvers; however, such a system appears to be feasible.

In considering why a beamrider system should be investigated as the initial concept for NMMW guidance feasibility rather than another scheme, the following factors are influential:

(1) The guidance link is one-way, so that relatively simple video receivers are potentially adequate for the missile link.

(2) Beamrider guidance has been demonstrated at IR and optical wavelengths in operational situations so that it is not necessary to go through a concept demonstration phase.

(3) Target cross section is high because the tracker looks at backscatter rather than at off-axis scatter.

(4) Since only the low cost missile receiver is expended in firing, the cost per round could be significantly less than that for a missile employing an active seeker.
(5) The missile is difficult to jam since the receiver looks back at friendly territory.
(6) It is possible to implement a multiple wavelength system so that wavelength optimization is possible for the acquisition, tracking and guidance functions.
(7) The airframe could be optimized aerodynamically since there is no seeker to complicate the warhead. Complexity of the on-board guidance and control is minimal.

The NMMW beamrider system must perform several functions in sequence, with the capability for continuity or rapid handover from one function to the next. This system must be capable of searching for and acquiring a target over a limited field-of-view (FOV), followed by the target tracking and missile guidance. Handover from the tracking to guidance modes must include a missile capture phase during which the missile is launched toward the target and LOS guidance along the tracking radar beam is established. For simplicity, it is desirable that one system at a single wavelength perform the entire beamrider operation; however, because of the complexity of these multiple operations (target acquisition, tracking, missile capture and guidance), the optimum configuration might require a multi-wavelength system.

Several approaches for implementation of the beamrider system have been investigated[21]. Performance in inclement weather is the most important consideration for a NMMW beamrider. For 94 GHz, 140 GHz and 220 GHz, an example of the transmitter power requirement for target acquisition as a function of range for rain rates of 4 and 16 mm/hr on a warm day is given in Figure 15. The following parameters are used in the calculations for source power:

	94 GHz	140 GHz	220 GHz
λ (m)	3.19×10^{-3}	2.14×10^{-3}	1.36×10^{-3}
G_T (dia. = 0.6 m; η = 0.5)	1.78×10^{5}	3.88×10^{5}	9.60×10^{5}
σ_T (m^2)	30	30	30
L_{RF}	0.5	0.40	0.16
S/N	3.1 (4.9 dB)	6.2 (7.9 dB)	38.9 (15.9 dB)
kTB (B = 10^7 Hz)	4.14×10^{-14}	4.14×10^{-14}	4.14×10^{-14}
N_f (dB)	4	7	15

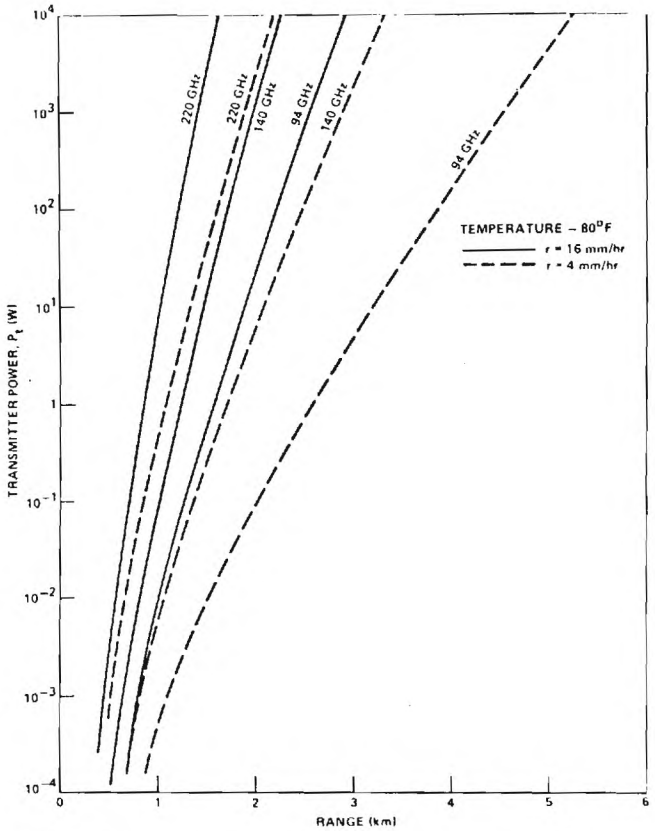

Figure 15. Power required for target acquisition on a warm day with moderate to heavy rain.

Trade-offs between search time, PRF, and antenna beamwidth must be considered in designing a beamrider system. If a separate acquisition system is employed, the required S/N for tracking will be considerably improved by the integration of additional pulses during the tracking interval which is long with respect to the acquisition target dwell time.

The curves of Figure 15 show that only the 94 GHz system is capable of a range of 3 km with a power of 1 kW in moderate rainfall. The transmitter power requirements for missile guidance are not as severe as those required for acquisition and tracking because the guidance link is a one-way path. It has been shown[21] that power levels required for acquisition are more than adequate for guidance.

For a five year projection of system performance, it would seem reasonable to anticipate improved noise figures and decreased RF losses at 140 and 220 GHz. These projections of improved performance are listed below:

Frequency (GHz)	State-of-the-art			5 Year Projection		
	L_{RF}	NEP	N_f	L_{RF}	NEP	N_f
140	4 dB	1.6×10^{-12}	7 dB	3 dB	10^{-12}	6 dB
220	8 dB	5×10^{-12}	15 dB	3 dB	10^{-12}	6 dB

The reason for projecting the same parameters for both frequencies is that quasi-optical components should show very little frequency dependence over the range, and the cutoff frequency of Schottky barrier mixers is presently about 3000 GHz.

Target acquisition, guidance with video detection and tracking have been calculated with the projected parameters. For tracking, it is assumed that the tracking error is

$$\sigma_m \approx \frac{CEP}{\sqrt{3R}} = \frac{0.35}{R(m)} ,$$

and a pulse integration gain of 17 dB is also assumed.

The projected performance levels for acquisition and tracking are shown in Figures 16 and 17 for each of the frequencies and a 1 kW source. Corresponding curves for guidance were not plotted because power adequate for the other two functions is more than adequate for guidance. These curves show some improvement over those of Figure 15; in particular, they show that it is possible to achieve tracking and guidance at a range of 3 km under more stringent conditions than before.

The calculations in the study show that, neglecting angle error due to multipath and glint, 94 GHz is the best frequency for a multifunctional tracking, acquisition and beamrider guidance system using state-of-the-art performance parameters. For a system dominated by multipath effects, either 140 or 220 GHz appears to be the preferred choice for operating frequency; whereas, without the presence of multipath effects, 94 GHz is a better choice for development of first generation millimeter guidance systems. This result is to be expected for performance dominated by propagation effects, since the absorption due to water vapor is much higher at 140 and 220 GHz than at 94 GHz. On the other hand, it would seem that tracking accuracy would favor 140 or 220 GHz in view of the reduced beam divergence at shorter wavelengths. For a conscan tracker, the tracking error due to thermal noise is $\approx \theta_B/\sqrt{S/N}$, and the $\sqrt{S/N}$ decreases faster than θ_B as the wavelength goes to 2.14 mm (140 GHz) and 1.36 mm (220 GHz) due to the increase in mixer noise figure and atmospheric attenuation coefficients at the shorter wavelengths. Even for projections based on extrapolation of available source power and improved performance of quasi-optical components, the 94 GHz window is still slightly preferable in terms of tracking accuracy for a system in which multipath is not a consideration.

On the other hand, if the multipath model adopted is valid, there are indications that 94 GHz will not provide adequate angle tracking error over typical types expected to be encountered in tactical operations in adverse environments. If the trend of these calculations is consistent with projected performance from realistic terrain models, operation at 220 GHz may also be necessary to insure an adequate accuracy for missile impact over the desired clear weather range of 3 km. If this is the case, a reduced low visibility operating range will be incurred. Thus, among the trade-offs to be considered will be that of adequate clear weather operation against maximum range of low visibility operation. A 94 GHz system, for example, might perform reasonably well over a 1.5 - 2 km range interval in a wide range of adverse meteorological and terrain conditions, whereas a 220 GHz system might extend the clear weather operating range to 2.5 - 3 km while restricting the adverse

weather range to < 1.5 km.

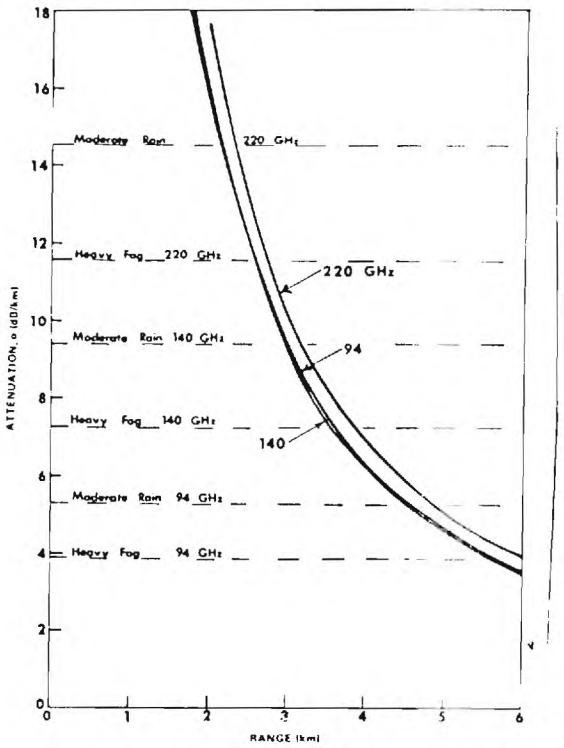

Figure 16. Projected performance levels for acquisition under different weather conditions for a 1 kW source. The conditions are: moderate rain 4 mm/hr, 80°F; heavy fog, 30 m visibility, 40°F.

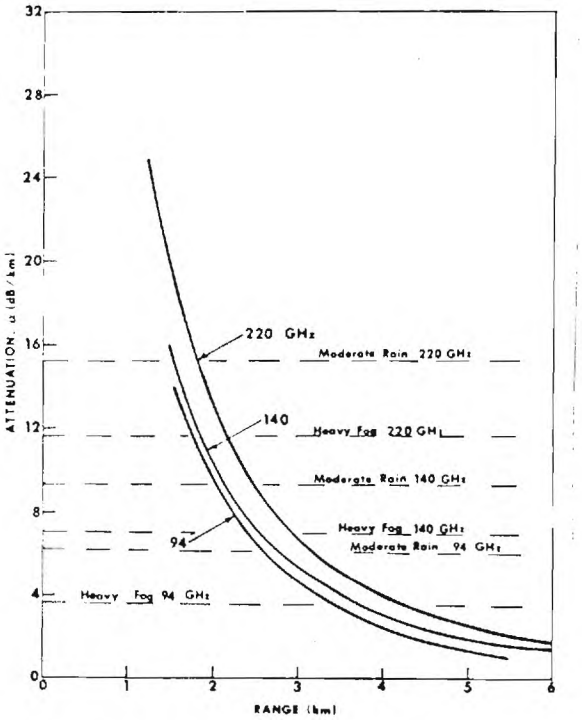

Figure 17. Projected performance levels for tracking under different weather conditions. The conditions are the same as those given in Figure 16.

Preliminary system studies have shown that millimeter guidance systems offer a potentially significant improvement in penetration of adverse environments which limit the visibility of electro-optical guidance systems. Further, there is the potential for improved accuracy with adequate penetration under adverse environmental conditions when compared to guidance systems operating in the microwave frequency band.

The state-of-the-art will currently support the development of operational breadboard beamrider or command guidance systems at 94 or 140 GHz. One such breadboard system has been developed at BRL[20], and tests performed at both BRL and MIRADCOM on tracking and guidance link operational simulations were found to be supportive of this millimeter guidance concept. MIRADCOM is also supporting several contractor-developed millimeter guidance systems which will involve development and testing of both differential guidance and beamrider concepts. As a part of these efforts, the evolutionary development of critical subsystems such as the tracking radar and guidance link will provide a means for performing operational tests to determine multipath effects, measure target signatures, and assess various schemes which have been proposed for missile capture; however, a very significant concern is the development of an appropriate target acquisition concept for an autonomous millimeter guidance system, and this and other critical technology issues are addressed in Table 9.

A basic deficiency in the current millimeter technology base is the lack of measured target, terrain and atmospheric data. Without these data, accurate quantitative estimates of system performance in realistic tactical environments cannot be made with any degree of confidence. Thus, the development of millimeter measurement systems operating in the windows at 94, 140 and 220 GHz is a critical step in establishing their operational limitations in terms of meteorological conditions and reduced visibility situations resulting from smokes and other battlefield-generated aerosols. The acquisition of these data should be a major part of a program to develop millimeter guidance systems.

Table 9. Critical Beamrider Technology Areas

ACTIVITY	RATIONALE	RESOURCES NEEDED
Multipath	Limits tracking accuracy; Degrades beam/guidance	mm λ radar/optical tracker; field problems - frequency and terrain dependence
Wavelength Selection	Potential of improved tracking vs λ; source and detector performance dependence; multipath dependence; optimum search/acquisition wavelength	Transmitter/receivers; accurate propagation measurements in smoke, rain, fog and high humidity; supporting meteorological measurements
Target Signatures	Reduce angle error and signal loss	Transmitters/receivers; Signal Processing; Pulse-to-Pulse target reflectivity data; function of target aspect
Target Acquisition	Prime system function	Coherent system measurements to feed computer simulation to determine signal processing required, e.g. MTI, vibrational signatures, and
Capture	Required for initiation of missile guidance	Determine required beam profile vs range for capture; near field measurement; determine concepts for multifunctional capture/track/guidance
Acceleration Hardened Schottky Diodes	Required for missile receiver	Trade-off video/superheterodyne for missile receivers; test diodes under shock, simulated flight conditions
Near mm wave Components	Required for low loss system	Quasi-Optical approach - circulators, isolators, modulators, antenna conscan schemes,diplexers, rotary joints, mixers, local oscillators
Transmitters	High Power Stable Sources Required	EIO's vs Impatts; develop stability techniques; chirp techniques; gyrotrons - long term source
Target Tracking Techniques	Need to provide high accuracy target coordinates and maintain good pointing accuracy	High precision tracking radar-spread spectrum techniques for decorrelation of target scatterers; coherent, frequency agile system
Clutter Characteristics	Information required for enhancement of target-to-clutter signals	Measurements of NMMW clutter characteristics terrain masking effects; establish discrimination schemes

Comments on other systems applications

The above discussion of the beamrider indicates some of the factors which can influence the design and operation of a NMMW system. The same type of considerations must be made for other potential NMMW systems. Only brief comments can be made here on some of these systems.

Target designator and semi-active seekers

Target designators have been successfully operated at 1.06 μm in clear atmosphere. However, during adverse propagation conditions (mainly fog and smoke), the IR designators are ineffective. The existing IR systems, operating at 1.06 μm, have the advantage of having all laser power incident upon the target. This is important since the reflectivity of terrain and vegetation exceeds that of the target at 1.06 μm. For NMM wavelengths, two techniques have been investigated [3]: the case in which the target fills the beam and the more general case for long wavelengths in which the beam size exceeds the target dimensions. Because target reflectivity is expected to exceed background reflectivity, a largest pulse logic is postulated for designation of the target in clutter.

Command guidance

The application of NMMW command guidance to anti-helicopter or anti-aircraft missions appears to be feasible. Command guidance is also applicable in a ground-to-ground anti-armor role, but no clear advantage over Beamrider guidance is evident at this time. The technology barriers associated with this guidance concept are similar to those for the Beamrider, and the general conclusions reached for the beamrider guidance concept apply to command guidance. The state-of-the-art can support breadboard system development at 94 and 140 GHz, and additionally, the window at 220 GHz appears to be applicable if source development evolves as projected by current technology.

Target surveillance and acquisition

For the successful operation of battlefield NMMW systems, it is important that target acquisition and surveillance techniques be applicable to NMMW systems. This would provide autonomous operation. For the optimum weapon system, several combinations of different wavelength sub-systems must be evaluated to obtain the optimum combination of surveillance,

acquisition, and guidance. Among the systems that have been identified as potential NMMW applications are:

battlefield ground-to-ground target acquisition;
airborne surveillance by RPV radars of land-based targets;
long-range surveillance and target acquisition;
target acquisition for NMMW airborne missile seeker systems;
horizon search radars;
shipboard surveillance radars;
track-while-scan systems for short-range self-defense systems (point defense);
restricted scan target acquisition for missile systems.

A large number of equipment and technique developments are necessary to ascertain the applicability of NMM waves. Techniques for search, recognition and classification have been identified [3] but more detailed investigations are needed to implement these techniques. Greater transmitter power, improved receiver sensitivity, new low-loss components and light-weight rapid-scan antennas are necessary. Source stability for coherent operation must be greatly improved. For implementation of the recognition/classification techniques, target characteristics, clutter effects and atmospheric effects are among the phenomenology that must be thoroughly documented.

Boost phase plume detection

Calculations have been performed to determine the feasibility of detecting missile plumes during the boost phase of the vehicle [22]. In the altitude regime of 30-100 km, it has been shown that, for a solid propellant system, molecular species, e. g. H_2O and H Cl, emit to permit radiometric detection from aircraft or satellites. Airborne radiometric observations are required to confirm predictions. The necessary passive technology is developing but must be extended to wavelengths as short as ~350 μm. Independent analysis of the bus stage indicate that spectral line opacity is sufficiently high to be detectable in occultation against the earth's radiation.

Conclusions

From the studies which have been performed, it can be concluded that the NMMW region offers a compromise for good resolution under adverse propagation conditions. Most systems, which have been investigated, profit from the narrow antenna beams available at NMM wavelengths, but are limited by atmospheric conditions. In some cases, the range limitations imposed by the atmosphere serve as an advantage for convert operation.

In order to utilize the NMMW spectral region properly, considerable technology must be developed. High-power sources, low loss components, precision antennas, sensitive receivers and stable local oscillators are priority devices to allow systems operations to be performed at NMM wavelengths. For many systems, highly coherent transmitters are required. This necessitates development of phase-locking and injection-locking technology for high-power sources. A driving force in extending military operation to NMM wavelengths is the prospect of small-size systems where space and antenna apertures are limited. Low cost, which is not a current characteristic of NMMW components, is expected to be an ultimate achievable goal.

One cannot expect to achieve everything that a system demands by employing NMM waves, and those working in the field are not doing this. Phenomenology in the form of atmospheric, terrain/clutter, target, and materials characteristics must be thoroughly developed for comparison with operation at other wavelengths. Thus far, studies have estimated certain characteristics and projected reasonable operational parameters for devices. From the considerations that have been made, optimum operation can be expected from hybrid IR/NMMW systems which will utilize the best of both spectral regions.

This work has been sponsored in part by the Harry Diamond Laboratories through the Army Research Office Contract No. DAAG29-77-C-0026.

References

1. 1974 Millimeter Wavelength Technical Conference, NELC/TD 308 Naval Electronics Laboratory Center, San Diego, CA 26-28, March 1974;

Proceedings of the DARPA/Tri-Service Millimeter Wave Conferences (8), Defense Advanced Research Projects Agency, Arlington, VA 22209

2. J. J. Gallagher, M. D. Blue, R. G. Shackelford, "Applications of Extreme Infrared to Missile Systems", Final Report on Basic Agreement DAHCO4-72-A0001, Task Order 76-8, Battelle Columbus Laboratories, January, 1976;

L. D. Strom, "Applications for Millimeter Radars", System Planning Corporation, Report No. 108, Contract No. DNA001-73-C-0098, ARPA Order No. 2353, December, 1973 AD529566;

"Low Probability of Intercept Multifunctional Tactical Sensors", Final Report, Contract F33615-76-C-1227, Raytheon Company, January, 1978;

Paul W. Kruse and Vitalij Garber, "Technology for Battlefield Target Recognition in Inclement Weather", Proceedings of the 23rd Annual IRIS Conference, 1976;

K. L. Koester, "Millimeter Wave Propagation", Norden Div. of United Technologies, Report 4392R005, 1972 (U);

A. M. Peterson, et al, "Low Angle Radar Tracking", Stanford Research Inst. Tech. Rept. JSR 74-7(U) February 1976, pages 53-57, 97-98;

J. J. Gallagher et al, "Applications of Submillimeter Wave Gigawatt Sources", Ga. Inst. of Technology, Engr. Experiment Station, Report GT/EES Project A-1717, DARPA Order 2840, 1975 (U);

R. LeLevier, "Applications of High Power Microwave/Millimeter Wave Technology" (U), R. and D Associates, Strategic Technology Final Report RDA-TR-4600-018, July 1975 (Report Secret);

Victor W. Richard, "Millimeter Wave Radar Applications to Weapons Systems", Ballistic Research Laboratories Memorandum Report No. 2631, June 1976 (U);

K. Evans, J. Dooley, R. Haraway, and H. Green, "Applications of Millimeter Wave Technology to Antiarmor Weapons Systems", Technical Report C-77-6, 22 February, 1977, U. S. Army Missile Research and Development Command, Redstone Arsenal, Alabama 35809

3. R. K. Parker, T. F. Godlove, and V. L. Granatstein, "Applications of High Power Microwave Sources - A Panel Study" (U), Vol. 1. NRL Memorandum Report 3339 (1976) (Report Secret);

"Interim Report on the Ad Hoc Study Group on the Military Applications of Millimeter Waves" Nato Document AC/243-D/332, AC/243(Panel III)D/115, June 1974 (U);

S. M. Kulpa and E. A. Brown, "DARCOM/DARPA Near-Millimeter Wave Technology Base Study", Harry Diamond Laboratories (1979);

4. S. M. Kulpa and E. A. Brown, "Propagation and Target/Background Characteristics", Volume 1 of Near-Millimeter Wave Technology Base Study, Harry Diamond Laboratories, October, 1979;

5. J. Preissner, "The Influence of the Atmosphere on Passive Radiometric Measurements", AGARD Conference Proceedings No. 245, Millimeter and Submillimeter Wave Propagation and Circuits, edited by E. Spitz, pp. 43-1 to 48-14, 4-8 September, 1978;

6. N. E. Feldman and S. J. Dudzinsky, Jr., "A New Approach to Millimeter-Wave Communications", R-1936-RC, April, 1977;

7. J. J. Gallagher, G. Loefer, J. L. Edwards, and J. P. Burns, "Microwave Instrumentation Applied to Aerosols and Smokes", Final Report, Contract No. DAA15-76-C-0087, 7 January 1979;

R. W. McMillan, R. Rogers, R. Platt, D. Guillory, J. J. Gallagher, and D. E. Snider, "Millimeter Wave Propagation through Battlefield Dust", Final Report, ASL-CR-79-0026-1, Contract DAAG29-77-C-0026, June, 1979;

J. J. Gallagher, R. C. Rogers, O. A. Simpson and J. H. Rainwater, "Millimeter Wave Propagation Through Smokes", Final Report, Contract No. DAAA11-77-C-0099, October, 1979;

8. G. D. Lukes, "Penetrability of Haze, Fog, Clouds and Precipitation by Radiant Energy Over the Spectral Range 0.1 Micron to 10 Centimeters", Naval Warfare Analysis Group of the Center for Naval Analysis, Study No. 61, under Contract N00014-68-A-0091, November, 1968;

9. H. J. Aufm Kampe, "Visibility and Liquid Water Content in Clouds in the Free Atmosphere", Journ. of Met 1, 54 (1970)

10. D. Deirmendjian, "Scattering and Polarization Properties of Water Clouds and Hazes in the Visible and Infrared", Applied Optics 3 , #2, 187-196, February 1964.

11. V. W. Richards and J. E. Kammerer, "Rain Backscatter Measurements and Theory at Millimeter Wavelengths", Ballistic Research Laboratories, Report No. 1838, October 1975.

12. See Reference 5.

13. N. A. Armand, A. O. Izyumov, and A. V. Sokolov, "Fluctuations of Submillimeter Waves in a Turbulent Atmosphere", Radio Engineering and Electronics Physics 16, 8, 1259 (August, 1971)

14. D. E. Snider, J. C. Wiltse, and R. W. McMillan, "The Effects of Atmospheric Turbulence and Adverse Weather on Near-Ground 94 and 140 GHz Systems", Workshop on Millimeter and Submillimeter Atmospheric Systems, Redstone Arsenal, Alabama, March, 1979.

15. J. H. Van Vleck and V. F. Weisskopf, Rev. Mod. Phys. 17, 227 (1945)

16. E. P. Gross, "Shape of Collision-broadened Spectral Line", Phys. Rev. 97, 394 (1955)

17. N. E. Gaut and E. C. Reifenstein, III, Environmental Research and Technology Report No. 13, NASA Contract NAS8-26275, Waltham, MA

18. R. A. Bohlander, et al, "Excess Absorption by Water Vapor and Comparison with Theoretical Dimer Absorption", D. T. Llewellyn-Jones, "Laboratory Measurements of Absorption by Water Vapor in the Frequency Range 100-1000 GHz", and H. A. Gebbie, "Observations of Anomalous Absorption in the Atmosphere", Proceedings of the Workshop on Atmospheric Water Vapor, Vail, Colorado, 11-13 September, 1979 (Institute for Atmospheric Optics and Remote Sensing, Hampton, Virginia 23666)

19. A. H. Green and F. King, "Preliminary Millimeter Beamrider Feasibility Assessment", Internal Technical Note RE-77-3, Advanced Sensors Directorate, U. S. Army Missile Research, Development and Engineering Laboratory, U. S. Army Missile Command, Redstone Arsenal, 1 October, 1976.

20. D. G. Bauerle, R. A. McGee, J. E. Knox and H. B. Wallace, "140 GHz Beamrider Feasibility Experiment", Interim Memorandum Report No. 538, Ballistic Research Laboratories, January, 1977.

21. R. G. Shackelford and J. J. Gallagher, "Millimeter Wave Beamrider System", Advanced Sensors Directorate, U. S. Army Missile Research and Development Command, Technical Report TE-CR-77-7, August, 1977.

22. J. J. Gallagher, P. B. Reinhart, R. W. McMillan and J. H. Rainwater, "The Investigation of the Feasibility of Airborne Detection of Submillimeter Missile Plume Radiation", Final Report, Contract No. DASG60-78-C-0031 (February 22, 1979).